



TEAM TAO



Science

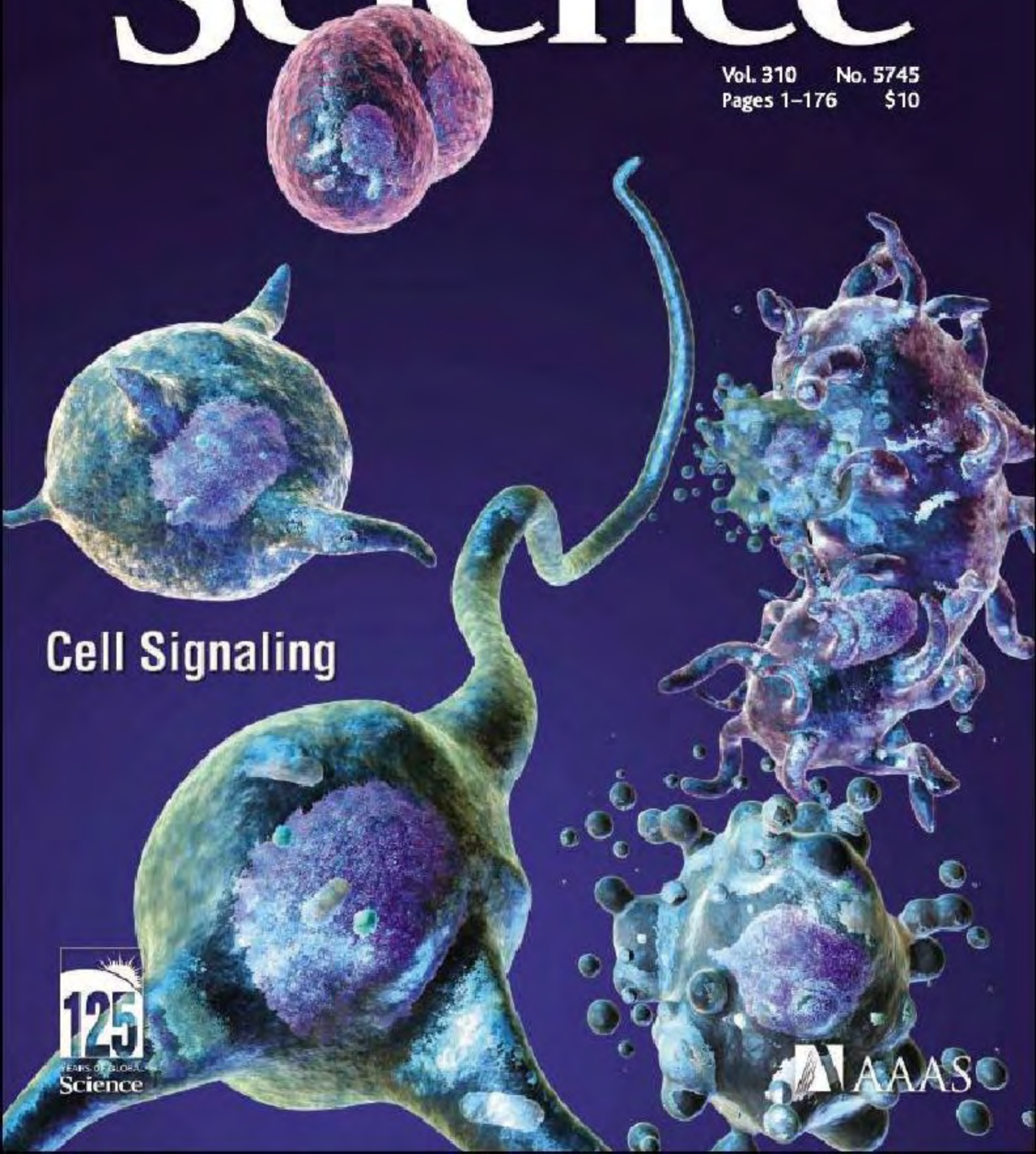
7 October 2005

Vol. 310 No. 5745
Pages 1-176 \$10

Cell Signaling

125
YEARS OF GLOBAL
Science

AAAS





SPECIAL ISSUE

CELL SIGNALING

A set of Viewpoints in this issue of *Science* highlights the signaling pathways that control the cellular life cycle, from undifferentiated stem cells to cell death by apoptosis. These signaling pathways are represented by canonical pathways, as well as pathways specific to rice, *Arabidopsis*, and humans, in the Connections Maps database at *Science's* STKE. [Illustration: Chris Bickel]

Volume 310
7 October 2005
Number 5745

INTRODUCTION

65 Signaling: From Stem Cells to Dead Cells

VIEWPOINTS

- 66 Connected to Death: The (Unexpurgated) Mitochondrial Pathway of Apoptosis
D. Spierings et al.
- 68 Transforming Growth Factor- β Signaling in Stem Cells and Cancer
L. Mishra, R. Derynck, B. Mishra

71 G Proteins Go Green: A Plant G Protein Signaling FAQ Sheet
S. M. Assmann

For related online content see page 11, or go to www.sciencemag.org/sciext/cellsignaling05/



DEPARTMENTS

- 11 SCIENCE ONLINE
13 THIS WEEK IN SCIENCE
17 EDITORIAL by Phillip A. Sharp
1918 Flu and Responsible Science
related News story page 28; Research Article page 77
- 19 EDITORS' CHOICE
24 CONTACT SCIENCE
27 NET WATCH
127 NEW PRODUCTS
128 SCIENCE CAREERS

NEWS OF THE WEEK

- 28 VIROLOGY
Resurrected Influenza Virus Yields Secrets of Deadly 1918 Pandemic
related Editorial page 17; Research Article page 77
- 29 U.S. BIOMEDICAL POLICY
Acting FDA Head Drops NCI Post
- 31 NEUROSCIENCE
Cancer Drugs May Help Injured Nerve Cells Regrow Their Axons
related Report page 106
- 31 SCIENCE SCOPE
- 32 ECOLOGY
Satellite Tracking Catches Sharks on the Move
related Reports pages 100 and 104
- 32 CONSERVATION POLICY
House Revises Endangered Species Act
- 33 FRANCE
Reform Law Fails to Impress Researchers
- 34 NOBEL PRIZE: PHYSIOLOGY OR MEDICINE
Triumph of the Ulcer-Bug Theory
- 34 SCIENTIFIC PUBLISHING
Withdrawn Parasite Paper Stirs Criticism of *Cell*
- 35 NOBEL PRIZE: PHYSICS
Quantum Optics Shines in the Photon's Centenary
- 37 ENDANGERED SPECIES
Ban on Beluga Caviar Points to Sturgeon's Worldwide Decline



41



55

37 ASTROPHYSICS
Short Gamma Ray Bursts: Mystery Solved

NEWS FOCUS

- 38 DRUG REGULATION
Plan B: A Collision of Science and Politics
- 41 CONSERVATION BIOLOGY
Premier Latin American Institute Loses Grants, Ponders Future
- 42 RUSSIAN SCIENCE
Academy Agrees to Post-Soviet Crash Diet
- 43 NEURODEGENERATION
Huntington's Disease Research Points to Possible New Therapies
- 46 RANDOM SAMPLES

LETTERS

- 49 Retraction *R. Alshire*. Benefits and Risks in Malaria Control *M. D. W. Ward and M. J. K. Selgrade*;
O. C. Hutchinson and A. A. Cunningham. Response *M. B. Thomas et al.*. Estrogen Receptors and Cell Signaling *R. J. Pietras et al.*. Response *E. R. Prossnitz et al.*. What Should We Call Pluto? *A. G. Fahn*
- 54 Corrections and Clarifications

BOOKS ET AL.

- 55 GEOSCIENCE
A Crack in the Edge of the World: America and the Great California Earthquake of 1906; A Crack in the Edge of the World: The Great American Earthquake of 1906.
S. Winchester, reviewed by *S. E. Hough*
- 56 SCIENCE AND POLITICS
The Republican War on Science
C. Mooney, reviewed by *N. Oreskes*

ESSAY

- 57 GLOBAL VOICES OF SCIENCE
Mangroves, Fishponds, and the Quest for Sustainability
J. H. Primavera



Contents continued

PERSPECTIVES

- 60 **PLANT BIOLOGY**
Growth by Auxin: When a Weed Needs Acid *M. Grebe* *related Report page 121*
- 61 **APPLIED PHYSICS**
Subsurface Imaging with Scanning Ultrasound Holography *A. C. Diebold* *related Report page 89*
- 62 **PSYCHOLOGY**
The Nature of Personality: Genes, Culture, and National Character *R. W. Robins* *related Report page 96*
- 63 **CHEMISTRY**
Inventing the Nanomolecular Wheel *J. Siegel* *related Report page 80*

SCIENCE EXPRESS www.sciencexpress.org

ATMOSPHERIC SCIENCE: The Radiative Signature of Upper Tropospheric Moistening

B. J. Soden, D. L. Jackson, V. Ramaswamy, M. D. Schwarzkopf, X. Huang

The relative humidity of the upper troposphere has increased as the atmosphere has warmed over the past two decades, increasing the greenhouse effect as predicted.

MATERIALS SCIENCE: Ordered Liquid Aluminum at the Interface with Sapphire

S. H. Oh, Y. Kauffmann, C. Scheu, W. D. Kaplan, M. Rühle

The crystalline ordering of a ceramic substrate influences the structure of molten metal droplets lying upon it.

PLANT SCIENCE: Stem-Cell Homeostasis and Growth Dynamics Can Be Uncoupled in the *Arabidopsis* Shoot Apex

G. V. Reddy and E. M. Meyerowitz

A single signaling factor regulates cells at the tip of the growing plant shoot, separately controlling their number and identities.

BREVIA

- 75 **PALEONTOLOGY:** Bottom-Feeding Plesiosaurs
C. R. McHenry, A. G. Cook, S. Wroe
Fossilized stomach contents from two plesiosaurs, long-necked predators in Mesozoic oceans, show that they feasted heavily on bottom-dwelling invertebrates, not just fish.

RESEARCH ARTICLE

- 77 **VIROLOGY:** Characterization of the Reconstructed 1918 Spanish Influenza Pandemic Virus
T. M. Tumpey et al.
A reconstituted, infectious virus has been made with the genes of the 1918 Spanish flu virus and used to investigate the cause of its extraordinary virulence. *related Editorial page 17; News story page 28*

REPORTS

- 80 **CHEMISTRY:** A Reversible, Unidirectional Molecular Rotary Motor Driven by Chemical Energy
S. P. Fletcher, F. Dumur, M. M. Pollard, B. L. Feringa
A sequence of reactions can induce a compound to rotate fully around a carbon-carbon single bond, and changing the chirality of the reagents changes the rotation direction. *related Perspective page 63*
- 83 **CHEMISTRY:** Sequential Proton Transfer Through Water Bridges in Acid-Base Reactions
O. F. Mohammed, D. Pines, J. Dreyer, E. Pines, E. T. J. Nibbering
An intermediate glimpsed for picoseconds during the transfer of a proton from acid to base in water has an infrared absorption consistent with the H_3O^+ cation.
- 86 **APPLIED PHYSICS:** PbSe Nanocrystal Solids for n- and p-Channel Thin Film Field-Effect Transistors
D. V. Talapin and C. B. Murray
Chemical treatment of PbSe nanoparticle arrays fabricated into thin film transistors can switch their charge carrier from predominantly electrons to predominantly positive holes.
- 89 **APPLIED PHYSICS:** Nanoscale Imaging of Buried Structures via Scanning Near-Field Ultrasound Holography
G. S. Shekawat and V. P. Dravid
Phase and amplitude information from ultrasonic waves are used to image subsurface features of materials and living cells at nanometer resolution. *related Perspective page 61*



86

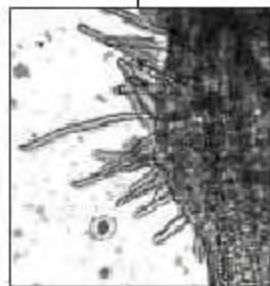
Contents continued

REPORTS CONTINUED

- 92 **PLANETARY SCIENCE:** A 5-Micron-Bright Spot on Titan: Evidence for Surface Diversity
J. W. Barnes et al.
 A large bright region on Saturn's moon Titan may be produced by methane fog or recent methane rainfall.
- 96 **PSYCHOLOGY:** National Character Does Not Reflect Mean Personality Trait Levels in 49 Cultures
A. Terracciano et al.
 Stereotyped personality traits defining "national character" differ from the actual personalities of that nation's citizens. *related Perspective page 62*
- ECOLOGY**
- 100 **Transoceanic Migration, Spatial Dynamics, and Population Linkages of White Sharks**
R. Bonfil et al.
- 104 **Satellite Tagging and Cardiac Physiology Reveal Niche Expansion in Salmon Sharks**
K. C. Weng et al.
 Satellite tracking of salmon sharks in the North Pacific and the white shark in the Indian Ocean show that individuals of each species have ranges approaching or exceeding 10,000 kilometers yearly. *related News story page 32*
- 106 **NEUROSCIENCE:** ECFR Activation Mediates Inhibition of Axon Regeneration by Myelin and Chondroitin Sulfate Proteoglycans
V. Koprivica et al.
 Small molecules that can prevent a common signaling molecule from inhibiting neuronal growth might be useful therapeutically to allow neuronal regeneration after injury. *related News story page 31*
- 111 **NEUROSCIENCE:** Retinoic Acid Signaling Affects Cortical Synchrony During Sleep
S. Maret et al.
 A receptor for a growth hormone unexpectedly is necessary for oscillations in brain activity during slow-wave sleep.
- 113 **NEUROBIOLOGY:** Astrocytic Purinergic Signaling Coordinates Synaptic Networks
O. Pascual et al.
 In the brain, astrocytes are the exclusive source of extracellular adenosine, which is generated by the hydrolysis of the extracellular ATP they release.
- 116 **NEUROSCIENCE:** Failure to Detect Mismatches Between Intention and Outcome in a Simple Decision Task
P. Johansson, L. Hall, S. Sikström, A. Olsson
 When an experimenter substitutes a different item for one previously chosen by a human subject, subjects who fail to notice the change offer sensible reasons for their false choice.
- 119 **EVOLUTION:** Sexual Selection Can Resolve Sex-Linked Sexual Antagonism
A. Y. K. Albert and S. P. Otto
 A model of sexual selection explains why male ornamentation may depend on the genetic mode of sex determination and sexual conflict.
- 121 **PLANT SCIENCE:** *Arabidopsis* H⁺-PPase AVP1 Regulates Auxin-Mediated Organ Development
J. Li et al.
 A transporter that maintains the acidity of intracellular compartments in plant cells is also necessary for growth control by the hormone auxin. *related Perspective page 60*



32,
100, &
104



60 &
121



ADVANCING SCIENCE. SERVING SOCIETY

SCIENCE (ISSN 0036-8075) is published weekly on Friday, except the last week in December, by the American Association for the Advancement of Science, 1200 New York Avenue, NW, Washington, DC 20005. Periodicals Mail postage: Publication No. 494490 postpaid at Washington, DC, and additional mailing offices. Copyright © 2005 by the American Association for the Advancement of Science. The title SCIENCE is a registered trademark of the AAAS. Domestic individual membership and subscription (\$1 issue) \$700 (\$74 allocated to subscription). Domestic institutional subscription (\$1 issue) \$2500. Foreign postage extra: Mexico, Caribbean (surface mail) \$50; other countries (air mail delivery) \$85. First class, airmail, student, and individual rates on request. Circulation: with GST available upon request, GST # R123456782. Publication Mail Agreement Number 1006968. Printed in the USA.

Change of address: allow 4 weeks; if vinyl label and new address and 8-digit account number Postmaster: Send change of address to Science, P.O. Box 18171, Danbury, CT 06813-1817. Single copy sales: \$10.00 per issue; prepaid individual surface postage; bulk rates on request. Authorization to photocopy items for internal or personal use, or the internal or personal use of specific clients, is granted by AAAS to libraries and other users registered with the Copyright Clearance Center (CCC) Transactional Reporting Service, provided that the fee of \$10.00 per article is paid directly to CCC, 222 Rosewood Drive, Danvers, MA 01923. The Alert Label on code for Science is 0036-8075/05 \$15.00. Science is indexed/abstracted in the Reader's Guide to Periodicals literature and in several specialist references.

Contents continued

Leading Lampreys by the Nose

Scientists isolate chemicals that tell migrating pests where to spawn.

Wild Gorillas Pick Up Tools

Two females use branches to test water depth, make bridges.

The Stress of Being Admired

Tourism may be bad for the health of Argentinean penguins.



Next Wave's 10th anniversary.

science's next wave www.nextwave.org CAREER RESOURCES FOR YOUNG SCIENTISTS

GLOBAL: 10th Anniversary Issue—Happy Birthday to Us *J. Austin*

Though many individual lives have changed over the last decade, much has stayed the same.

GLOBAL/US: Balance and Love *C. Parks*

Tyrone Hayes has become the youngest full professor at the University of California at Berkeley.

GLOBAL/US: Wearing Many Hats *R. Arnette*

A former University of Virginia biology doctoral student has since worn many professional hats.

GLOBAL/US: Surviving the Crash *J. Kling*

Three founders of high-tech companies share how they have fared since the early 1990s.

GLOBAL/CANADA: Reminiscences from the North *A. Fazekas*

Four past Canadian contributors share the life lessons they have learned along the way.

GLOBAL/UK: A Career Eureka Moment *A. Forde*

A 1996 Next Wave article inspired a scientist to change her career path to science editor.

GLOBAL/EUROPE: Keeping A Golden Paragraph in Mind *E. Pain*

An assistant professor from Spain says a "golden paragraph" in Next Wave never quite left him.

GLOBAL/POSTDOCNETWORK: What a Difference Ten Years Makes *B. Benderly*

Several early Next Wave contributors share the lessons of their first post-postdoc decade.

science's sage ke www.sageke.org SCIENCE OF AGING KNOWLEDGE ENVIRONMENT

PERSPECTIVE: Revising the Standard Wisdom of *C. elegans* Natural History—Ecology of Longevity *E. P. Caswell-Chen, J. Chen, E. E. Lewis, G. W. Douhan, S. A. Nadler, J. R. Carey*

A symbiotic relationship between *C. elegans* and snails provides a new context for understanding the evolution of the worm and its life history traits.

News Focus: Turning Back the Clock *R. J. Davenport*

Cancer drugs reverse nuclear defects of progeria.

News Focus: Cut the Fat *M. Leslie*

Enzyme restores lipid-damaged DNA.



Give and take between worms and snails.



New signaling connections.

science's stke www.stke.org SIGNAL TRANSDUCTION KNOWLEDGE ENVIRONMENT

Related Cell Signaling section page 65

- ▶ **EDITORIAL GUIDE: Cell Signaling—From Beginning to End** *N. R. Gough, E. M. Adler, L. B. Ray*
Ten new Connections Maps highlight cell signaling during the early stages of development to cell death by apoptosis.

Separate individual or institutional subscriptions to these products may be required for full-text access.

GrantsNet
www.grantsnet.org
RESEARCH FUNDING DATABASE

AIDScience
www.aidscience.com
HIV PREVENTION & VACCINE RESEARCH

Members Only!
www.AAASMember.org
AAAS ONLINE COMMUNITY

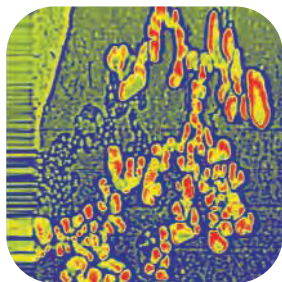
Functional Genomics
www.sciencegenomics.org
NEWS, RESEARCH, RESOURCES

Chemically Switching Transistors

Solution-based processing of inorganic semiconductors offers the potential of a high throughput and inexpensive fabrication alternative to conventional silicon-based technology. **Talapin and Murray** (p. 86) fabricated field-effect transistors with the conductive channels assembled from PbSe semiconductor nanocrystals via solution-phase processing. The nanocrystals form into ordered arrays and are initially insulating. Exposing the materials to hydrazine decreased the spacing between the nanocrystals, which increased their electronic coupling and resulted in n-type conduction. A mild heat treatment that desorbed the hydrazine switched the conduction back to p-type. The ability to readily switch reversibly between n- and p-transport will enable complementary metal oxide semiconductor circuitry to be fabricated with this technique.

A Molecular Turnstile

Progress in rational chemical synthesis has fostered the miniaturization of macroscopic engineering components, such as gears and ratchets, to the molecular scale. **Fletcher et al.** (p. 80; see the Perspective by **Siegel et al.**) have applied a sequence of reactions to a biaryl compound that effectively mimics the action of a turnstile. Through a succession of hydroxyl protection and deprotection steps, coupled with enantioselective lactone reductions, the authors achieve 360° rotation of one aryl ring about the other in a specific selected sense. The choice of reagents determines whether rotation about the carbon-carbon single bond axis is clockwise or counterclockwise.



Sounding Out Subsurface Nanofeatures

Nondestructive subsurface imaging in the size range from 10 to 100 nanometers is particularly challenging but would be valuable in applications ranging from device construction to cell biology. **Shekhawat and Dravid** (p. 89; see the Perspective by **Diebold**) have developed a

technique, scanning near-field ultrasound holography, that takes advantage of both the phase and amplitude of scattered ultrasound waves to produce nanoscale-resolution images of internal substructure. Examples include images of voids in polymer coatings of SiN shallow trench structures and malaria parasites in red blood cells.

The Blind Decision-Maker

What is the relation between intention, choice, and introspection? **Johansson et al.** (p. 116) used a card trick in a simple decision task to identify a dissociation between awareness of the initial choice and the outcome when this has been surreptitiously altered. Participants were given a choice to make in the attractiveness of two female faces shown on two cards, and then asked to justify their choice as they examined the card with the alternative they had allegedly chosen. In some trials, the experimenters covertly switched the cards. In the majority of such trials, participants failed to recognize the switch, and proceeded to justify their choice of the card they were handed, although it was not the one they had selected.



A Bright Spot in the Distance

Saturn's large moon Titan may have active exchange between its methane-rich lower atmosphere and surface. Cassini has recently studied one of the brightest surface features on Titan, which seems to have an unusual origin compared with other features that have been observed on the rest of the surface.

Barnes et al. (p. 92) present analyses of data from several instruments on the spacecraft, as well as from the Keck Observatory, which show that this feature probably is produced by a methane-rich ground fog or veneer of methane rainfall.

Tracking Marine Migrations

Satellite tracking techniques have been used by **Weng et al.** (p. 104) and **Bonfil et al.** (p. 100) to reveal the habits and movements of salmon shark in the North Pacific and white shark in the southern Indian Ocean, respectively (see the news story by **Pennisi**). The endothermic salmon shark's niche

extends from subtropical to subarctic waters. The white shark can rapidly cross distances in excess of 10,000 kilometers, from South Africa to Australia, in addition to regular migration along the southeastern South African coasts.

Doing Double Duty

A single gene in *Arabidopsis*, *AVP1*, encodes the pyrophosphatase that regulates acidity in the vacuole of the plant cell. **Li et al.** (p. 121; see the Perspective by **Grebe**) now report that this same enzyme also affects transport of the plant hormone auxin. Disruptions in auxin transport result in disruptions in shoot and root development. The effects of *AVP1* on auxin function are mediated through distribution of the auxin efflux facilitator.

Genes and Waves

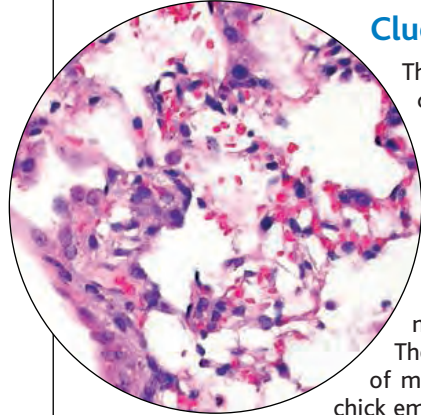
Slow electroencephalogram oscillations, or delta waves, represent one of the most important aspects of sleep and its regulation because they determine the depth of sleep, sleep consolidation, and sleep quality. Delta oscillations are also a direct measure of the need for sleep, and they are tightly regulated during development and aging. **Maret et al.** (p. 111) identified and functionally characterized a gene that codes for a vitamin A-activated ligand-dependent transcription factor, retinoic acid receptor beta (*Rarb*). This gene regulates slow-wave oscillations during sleep.

CONTINUED ON PAGE 15

Helping Neuronal Repair

Regeneration of axons in the central nervous system after injury is limited in part because of inhibitory signals derived from myelin and glia. **Koprivica *et al.*** (p. 106; see the news story by **Miller**) screened a bank of small molecules to identify molecules that might alleviate the inhibition. The results implicate the epidermal growth factor receptor (EGFR) in the endogenous signaling that allows myelin to block neurite outgrowth. Of about 400 small molecules screened, tyrphostin variants seemed particularly effective. Because EGFR inhibitors are already in clinical use for cancer patients, it is possible that these findings could be exploited rapidly in the treatment of neuronal injury.

Clues for the Origin of Killer Flu



The 1918 influenza pandemic killed more people than did the fighting in World War I, but the reasons for this virus's extraordinary virulence have remained enigmatic. **Tumpey *et al.*** (p. 77; see the news story by **Kaiser**) have used reverse genetics to generate an influenza virus bearing all eight gene segments of the pandemic virus. Subsequent pathogenicity studies in mice, chick embryos, and human lung cells show that the 1918 hemagglutinin and polymerase genes are responsible for the high virulence. The 1918 virus does not bear the molecular signatures of modern highly pathogenic strains, but it is lethal to chick embryos. The fully reconstructed virus kills mice rapidly and shows a high apical release from cultured human lung cells. The lung pathology in mice shows high viremia, destruction of the alveolar architecture, and distinct oedematous-hemorrhagic pathology. This work provides predictive insights for therapeutic options in case of a forthcoming influenza pandemic.

Challenging Preconceptions

Our knowledge of our own personalities comes from a long-standing familiarity with ourselves and, in a similar fashion, we often can gauge quite accurately the personalities of others whom we know well. In contrast, the stereotypes we hold may be based upon an amalgam of bits and pieces, gathered from public figures or celebrities and mixed with singular aspects of individuals whom we encounter casually or impersonally. **Terracciano *et al.*** (p. 96; see the Perspective by **Robins**) have compiled a well-established personality inventory to extract self-ratings, as well as observer ratings of specific people across roughly 50 nationalities, and a character survey to elicit the same sort of personality assessments of the mythic stereotypical native of these same nations. The first two sets of ratings based on specific ratings correlate well with each other when aggregated across the entire sample of each group; however, neither agrees with the common perception of the national character.

Battles of the Sexes

In mammals, the male gamete specifies male (XY) versus female (XX) offspring, but in birds, the female gamete determines male (ZZ) versus female (ZW) offspring. **Albert and Otto** (p. 119) develop a model that explores the evolution of display trait alleles that are expressed in both sexes, and considers how sexually antagonistic selection favors males or females depending on the mode of sex determination. Females evolve preferences to increase the fitness of daughters at the expense of sons in XY species, which results in less flashy male displays. In contrast, females are more likely to evolve preferences that increase the fitness of sons at the expense of daughters in ZW species, which leads directly to the evolution of exaggerated male displays. This model may explain why sexually selected characters are more commonly exaggerated in birds and butterflies, which both have ZW sex determination.

1918 Flu and Responsible Science

The influenza pandemic of 1918 is estimated to have caused 50 million deaths worldwide; 675,000 in the United States. The reconstruction of the 1918 virus by the synthesis of all eight subunits and the generation of infectious virus are described on p. 77 of this issue,* and the sequences of the final three gene segments of the virus are described in a concurrent *Nature* paper.† Predictably, but alarmingly, this virus is more lethal to mice than are other influenza strains, suggesting that this property of the 1918 virus has been recovered in the published sequence. The good news is that we now have the sequence of this virus, perhaps permitting the development of new therapies and vaccines to protect against another such pandemic. The concern is that a terrorist group or a careless investigator could convert this new knowledge into another pandemic.

Should the sequence of the 1918 virus have been published, given its potential use by terrorists? The dual-use nature of biological information has been debated widely since September 11, 2001. In 2003, a committee of the U.S. National Academies chaired by Gerald Fink considered this issue, weighing the benefits against the risks of restricting the publication of such biological information. They outlined the tradeoff between erring on the side of prudence, thus potentially hindering the progress of critical science, and erring on the side of disclosure, thus potentially aiding terrorists. The U.S. National Science Advisory Board for Biosecurity (NSABB) was established to advise governmental agencies and the scientific community on policies relative to public disclosure. This board has begun to deliberate, but the questions are complex, as typified by these papers on the 1918 virus. It is reassuring that the NSABB was asked to consider these papers before publication and concluded that the scientific benefit of the future use of this information far outweighs the potential risk of misuse. People may be reassured that the system is working, because agencies representing the public, the scientific community, and the publishing journals were involved in the decision.

I firmly believe that allowing the publication of this information was the correct decision in terms of both national security and public health. It is impossible to forecast how scientific observations might stimulate others to create new treatments or procedures to control future pandemics. For example, in the *Nature* article, sequence comparisons suggest that the 1918 virus was generated not by incremental changes in the polymerase genes, but by the movement of these genes, in total, from an avian source into a human influenza virus. The availability of these sequences will permit identification of their avian origin and should show why this particular set of genes was selected. Similarly, the results in the *Science* article suggest that the cleavage of a protein on the surface of the 1918 virus, a step critical for virulent infection, may occur by a previously unknown mechanism—a hint that could lead to new drugs for inhibiting this step and thus preventing future pandemic eruptions.

Influenza is highly infectious, and a new strain could spread around the world in a matter of months, if not weeks. The public needs confidence that the 1918 virus will not escape from research labs. All of the described experiments were done in a Biosafety Level 3 laboratory, a high-containment environment recommended by the U.S. Centers for Disease Control and Prevention and the National Institutes of Health on an interim basis, whose use should become a permanent requirement for such experiments. Current evidence suggests that some available drugs and possible future vaccines could suppress infections by the 1918 virus. Given the prospect of another natural influenza pandemic, the recent decision by the U.S. administration to stockpile antivirals for influenza treatment seems wise. Finally, although a sequence of the 1918 virus has been determined and is highly virulent in mice, this may not be the specific form of the virus that caused the pandemic of 1918. An article in the same issue of *Nature*‡ reports the existence of sequence variation in a natural population of influenza virus; yet we have only one sequence for the 1918 pandemic strain, and the reconstructed virus described in the *Science* article was built into the backbone of a laboratory strain. Because a pandemic infection is dependent on many unknown properties, there is no certainty that the reconstructed 1918 virus is capable of causing a pandemic.

Phillip A. Sharp

Phillip A. Sharp is Institute Professor at the Massachusetts Institute of Technology, 77 Massachusetts Avenue, Cambridge, MA 02139, USA.

10.1126/science.1120820

*T. M. Tumpey *et al.*, *Science* **310**, 77 (2005). †J. Taubenberger *et al.*, *Nature* **437**, 889 (2005). ‡S. Salzberg, *Nature* 10.1038/nature04239 (2005).



EDUCATION

Frog Film Fest

Instead of prolonging their breeding season over weeks or months as some amphibians do, wood frogs (right; *Rana sylvatica*) cram it into three or four frantic nights. To screen video showing tangles of mating frogs and other amphibian footage, click over to Frog Calls, hosted



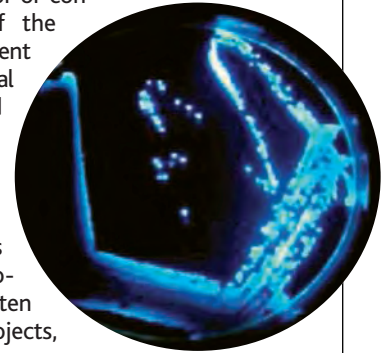
by documentary filmmaker David McGowan. The site focuses on Midwestern species, offering clips of a dozen kinds of frogs and toads singing their lungs out. In video interviews, herpetologists discuss topics such as the different calls males use to attract mates and rebuff rivals and the advantages of breeding early or late in the year. Researchers also touch on the problems of malformed and disappearing amphibians. For example, Michael Lannoo of Ball State University in Muncie, Indiana, explains that the once-common northern cricket frog (*Acris crepitans*) has vanished from Canada and much of the upper Midwest, possibly because roads and development prevent the amphibians from hopping to more suitable habitat.

www.midwestfrogs.com

LINKS

Home Base for Microbes

You'd expect microbes to be high on the research agenda at the National Institutes of Health, but many other federal agencies sponsor or conduct investigations of the bugs, from the Department of Defense to the National Institute of Standards and Technology. Visitors can discover more about these efforts at The Microbe Project. The new portal offers a synopsis of each agency's microbiological research, often providing links to projects, databases, and other resources.



The site also furnishes news and an education section, which includes information on fellowships and mentoring programs.

www.microbeproject.gov

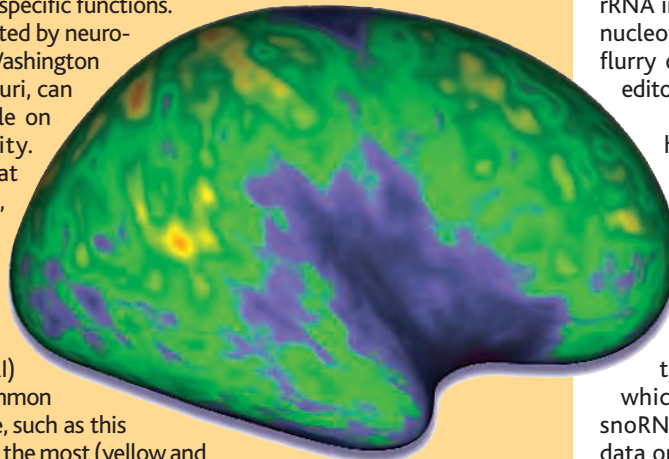
IMAGES

Cerebral Surveying

All human brains look pretty much alike in a jar of formaldehyde, but on closer inspection each person's sports a unique pattern of wrinkles and crevices. That's good news for individualists and bad news for neuroscientists striving to pin down what areas manage specific functions.

The new brain atlas PALS, created by neurobiologist David Van Essen of Washington University in St. Louis, Missouri, can help researchers get a handle on this geographical variability. Unlike previous atlases that relied on scans of one brain, PALS maps the contours of the cerebral cortex—which governs “higher functions” such as planning and problem solving—by averaging magnetic resonance imaging (MRI) scans of 12 people. You can summon

17 views of the brain's surface, such as this map showing which areas vary the most (yellow and orange) and the least (blue) among individuals. Controls let you rotate the images and view them from different angles. You can also superimpose data such as functional MRI measurements of activity. PALS is part of the neuroimaging database SumsDB that features similar atlases for the human cerebellum and for macaque, rat, and mouse brains.



sumsdb.wustl.edu/sums/index.jsp

DATABASES

Let It sno

Like the rough cut of a movie, a newly minted ribosomal RNA (rRNA) molecule needs fine-tuning before it's ready for release. Enter the small nucleolar RNAs, or snoRNAs, which team with proteins to snip rRNA into usable segments and modify its nucleotide bases. Researchers will find a flurry of information on these molecular editors at this pair of databases.

For profiles of more than 350 human snoRNAs, check out this clearinghouse* at the Laboratoire de Biologie Moléculaire Eucaryote in Toulouse, France. Search for a particular snoRNA to read a description of the molecule and find its sequence, size, and target.

You can also scan rRNA and other types of RNA molecules to learn which bases get modified and what snoRNA makes the revision. For similar data on *Arabidopsis thaliana* and 17 other plant and algae species, drop by this site† from the Scottish Crop Research Institute in Invergowrie.

* www-snorna.biotoul.fr

† bioinf.scri.sari.ac.uk/cgi-bin/plant_snorna/home

Send site suggestions to netwatch@aaas.org. Archive: www.sciencemag.org/netwatch



VIROLOGY

Resurrected Influenza Virus Yields Secrets of Deadly 1918 Pandemic

As worries about a new flu pandemic mount, researchers have figured out the traits that made the 1918 influenza virus, which killed between 20 million and 50 million people, so virulent. Although a study on page 77 sheds new light on these questions, it raises a host of others because the researchers reconstructed the complete virus, which no longer existed anywhere on Earth.

The team resurrected the 1918 pandemic virus by using gene sequences fished from preserved tissue from a 1918 victim. The virus is as lethal as expected, killing mice more quickly than any other human flu virus known. Recreating the 1918 strain “had to be done, and it’s produced some extremely interesting results,” comments flu researcher Robert Webster of St. Jude Children’s Research Hospital in Memphis, Tennessee.

Although a scientific triumph, the experiment has stirred debate over safety procedures for handling such a deadly virus. Moreover, a new federal biosecurity board gave the paper an unusual last-minute review to make sure the merits of its publication outweighed the risks of releasing potentially dangerous knowledge. The board’s green light is a relief to scientists who have worried about a clampdown on scientific information following the anthrax attacks 4 years ago. “The system is working,” suggests Massachusetts Institute of Technology molecular biologist Phillip Sharp, who wrote an accompanying editorial (p. 17).

The team, from the Centers for Disease Control and Prevention (CDC) in Atlanta, Georgia, the Armed Forces Institute of Pathology (AFIP) in Washington, D.C., Mount Sinai School of Medicine in New York City, and the U.S. Department of Agriculture, says its work will provide crucial knowledge for heading off the next influenza pandemic, which could be brewing in Asia, where the H5N1 bird flu has killed more than 60 people.

“This work has to be seen in a positive light,” says lead author Terrence Tumpey of CDC.

The research grows out of AFIP pathologist Jeffrey Taubenberger’s efforts, begun in 1995, to sequence the genome of the 1918 flu virus. Working mainly with tissue from a victim found in permafrost in Alaska, he and others have been piecing together the virus’s eight genes and characterizing their protein products.

Last year, this work revealed the structure of the 1918 hemagglutinin (HA), the cru-



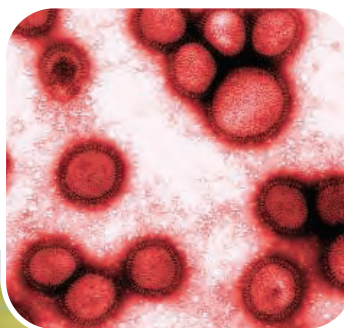
Handle with care. CDC’s Terrence Tumpey wore a respirator as part of BSL-3 procedures for studying the recreated 1918 influenza virus. (Inset) A regular flu virus.

cial surface protein that flu viruses use to latch onto host cells (*Science*, 19 March 2004, p. 1866); in a separate study, Yoshihiro Kawaoka’s group at the University of Wisconsin, Madison, showed that a virus containing this HA was unusually potent. This week in *Nature*, Taubenberger’s group publishes the sequences of the last three genes, which together encode the virus’s polymerase, the machinery for virus replication.

With those final sequences in hand, Peter Palese’s team at Mount Sinai then stitched the eight 1918 genes into a regular flu virus genome contained within bacterial DNA.

They shipped these inert plasmids to Tumpey at CDC, who inserted them into cells to make live virus.

In this issue of *Science*, Tumpey, Taubenberger, and collaborators report how the reconstructed 1918 virus behaves. In experiments at CDC, the virus killed mice in 3 to 5 days and caused severe lung inflammation reminiscent of that reported by doctors who examined 1918 flu victims. The team also studied viruses with various combinations of 1918 genes and regular flu genes, which showed that “without that HA, the virus was not virulent,” says Tumpey.



One is that the virus doesn’t need to rely on its host cells for the protease trypsin to cleave and activate the HA protein; instead, another surface protein, neuraminidase

(NA), appears to help cleave the HA. That suggests the 1918 virus, like some highly virulent bird flu strains, can grow in any cell type, not just trypsin-laden lung cells. In addition, the 1918 flu’s polymerase genes appear to allow it to replicate very efficiently in human bronchial cells. Probing these mechanisms may lead to the development of new antiviral drugs.

The virus also kills chicken embryos, unlike most human flu viruses. The polymerase genes are similar to those found in bird flu, including H5N1 in Asia, Taubenberger notes in the *Nature* paper. That means the 1918 flu likely

arose from a bird virus and did not need to combine with a flu strain already adapted to humans to become so deadly.

Because of the sensitive nature of the work, the CDC lab’s safety precautions received unusual scrutiny, says Tumpey, including review by several biosafety committees. Workers followed biosafety level 3 (BSL-3) practices, with additional enhancements, for instance, wearing battery-powered air purifiers with face shields and showering when leaving the lab. A year ago, Kawaoka’s team drew fire for doing experiments with partial 1918 viruses under similar enhanced BSL-3

CREDITS: DARRRELL KAPCZYNSKI; (INSET) YOSHIHIRO KAWAOKA/UNIVERSITY OF WISCONSIN, MADISON

38

Teen behavior and Plan B



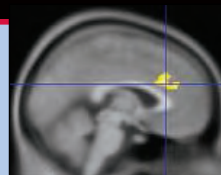
41

Conserving INBio



43

Hunting down Huntington's causes



conditions, as opposed to the more stringent BSL-4 (*Science*, 22 October 2004, p. 591).

Since then, the government has weighed in, recommending in a draft biosafety manual that researchers use BSL-3 with additional measures for 1918 flu experiments. One reason BSL-4 isn't necessary, says government adviser Robert Lamb of Northwestern University in Evanston, Illinois, is that antiviral drugs are effective against 1918-like flu viruses. (CDC is also treating 1918 flu virus as a select agent, which means access is tightly controlled.)

Both the authors and *Science's* editors acknowledge concerns that terrorists could, in theory, use the information to reconstruct the 1918 flu virus. Similar fears erupted 3 years

ago when *Science* published a paper on the reconstruction of a poliovirus. *Science* decided to publish the 1918 flu paper because it "could help prevent another global flu pandemic," says Editor-in-Chief Donald Kennedy. That benefit "far outweighs the risk of working with this virus," he says.

In addition to regular scientific review, *Science* required the authors to show that they had approval to publish from CDC Director Julie Gerberding and National Institute of Allergy and Infectious Diseases Director Anthony Fauci. After being briefed, Health and Human Services (HHS) Secretary Michael Leavitt also requested that his new National Science Advisory Board for Biosecurity (NSABB) review the *Science* and

Nature papers "to make sure we'd touched every possible base," said HHS spokesperson William Hall. After a flurry of e-mails and phone conferences last week, the panel suggested adding two sentences that underscore the stringent safeguards and the importance of the work in protecting public health.

The board's review surprised some scientists who expected NSABB to develop only general guidelines for journals. But Sam Kaplan of the University of Texas, Houston, publications chair for the American Society for Microbiology, says such reviews seem reasonable as long as they don't delay publication for months. "We certainly might turn to the NSABB" for a hot paper, he says.

—JOCELYN KAISER

U.S. BIOMEDICAL POLICY

Acting FDA Head Drops NCI Post

Trying to calm an uproar after he took a second job, the chief of the U.S. National Cancer Institute (NCI) declared last week that he would take a leave of absence while he serves as acting commissioner of the Food and Drug Administration (FDA).

President George W. Bush's appointment of NCI Director Andrew von Eschenbach on 23 September to succeed FDA's Lester Crawford drew an outcry from cancer researchers and several members of Congress, who argued that both agencies would suffer and that the two jobs posed conflicts of interests (*Science*, 30 September, p. 2142). Giving up the NCI job seems to allay at least some of those concerns.

The temporary NCI boss will be John Niederhuber, who came to the institute last month and this week became its deputy director for translational and clinical sciences. Niederhuber will also serve as "chief operating officer to handle the day-to-day management at NCI," according to memos von Eschenbach sent to FDA and NCI staff last Friday. Niederhuber, a surgical oncologist who has also studied cell signaling in tumors, most recently headed the department of surgery at the University of Wisconsin School of Medicine. Until July, he also was chair of NCI's National Cancer Advisory Board.

Niederhuber is "highly regarded in the oncology community," says David Korn, a senior vice-president at the Association of American Medical Colleges. As dean of Stanford University medical school, Korn hired

Niederhuber in 1991 to head the surgery department. "I think it's a terrific opportunity for him and for the NCI," Korn says. Cancer biologist Tom Curran of St. Jude Children's Research Hospital in Memphis, Tennessee, is pleased as well. "John is an excellent choice for a challenging but important position at this critical time," says Curran.

Speaking anonymously, some cancer researchers said they were not disappointed that von Eschenbach, a friend of the Bush family who came to NCI 3 years ago from the University of Texas M. D. Anderson Cancer Center, is stepping aside from the research institute for the moment. His plan to eliminate suffering and death from cancer by 2015 has been criticized as wildly unrealistic. And his proposals for achieving it—initiatives on nanotechnology, proteomics, and tissue banking—have drawn a lukewarm response from NCI advisers. Meanwhile, success rates for obtaining basic R01 research grants are steadily declining. "I'm not sure [his tenure] will be seen as a great period in the history of NCI," said one academic researcher.

Within NCI, morale has slipped as budgets for intramural research have been trimmed

and von Eschenbach built up a large personal staff that operated free of the established division directors, sources say. "It can't get much worse," said one senior scientist.

Even so, David Johnson, deputy director of the Vanderbilt-Ingram Cancer Center in Nashville, Tennessee, worries about how NCI will fare under an acting director, which "is about the most powerless position you can be in." Johnson wonders whether Niederhuber will "have the courage" to prioritize different NCI programs.

Von Eschenbach's memo says he "will not participate" in FDA matters involving NCI drug applications or clinical trials. But Johnson says that unless von Eschenbach resigns from NCI, his "residual interest" in the institution poses a potential conflict of interest. Another possible conflict, noted by

The Cancer Letter, involves von Eschenbach's unpaid role as vice-chair of the board of C-Change, a nonprofit cancer advocacy organization headed by the president's parents, George H. W. and Barbara Bush. Its board members include drug industry executives.

—JOCELYN KAISER

With reporting by Jennifer Couzin.



Fill-in. John Niederhuber will handle NCI's day-to-day business.

CREDIT: NCI

Cancer Drugs May Help Injured Nerve Cells Regrow Their Axons

The central nervous system in adult mammals is notoriously bad at healing itself. Once severed, the axons that connect one neuron to another can't regrow. That's why people regain little, if any, movement and sensation after a spinal cord injury. Neuroscientists are working hard on ways to coax adult neurons to regenerate axons, but progress so far has been slow.

On page 106, a Boston-based research team reports a surprising discovery that may be a substantial step forward. They identify a molecular signaling pathway that appears to prevent axon regeneration in rodent neurons and show that drugs that interfere with this pathway promote regeneration. "It's a really unexpected finding," says Marie Filbin, a neurobiologist at Hunter College in New York City. She and other experts say they never suspected that this signaling pathway, which involves a cell surface protein called the epi-

blockers had impressive effects, He says. To test the compounds on nerve injuries in live animals, the researchers crushed an optic nerve in adult mice and then packed the nerve with foam soaked with one of the EGFR blockers. Two weeks after the injury, the treated mice showed a ninefold increase in axon regeneration compared to untreated animals.

Until now, the primary role in the nervous system of epidermal growth factor, which activates EGFR, was thought to be signaling neural stem cells to divide. "Now it shows up in a very different context," says Martin Schwab, a neurobiologist at the University of Zürich in Switzerland.

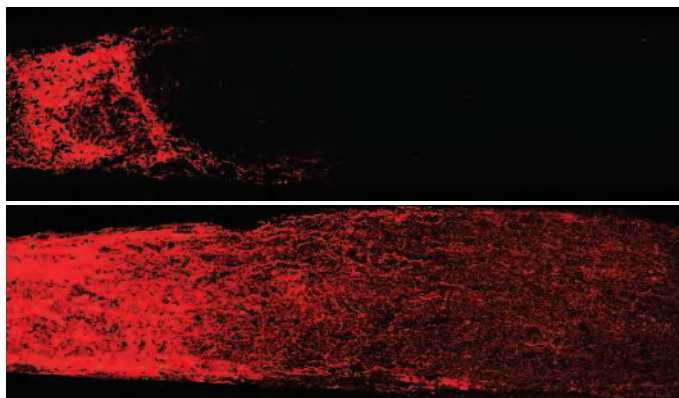
Additional work by He's team has provided clues about how EGFR blockers promote axon regeneration. Two types of molecular signals conspire to stymie regeneration in the adult nervous system: inhibitory molecules embedded in the myelin insulation on axons and inhibitory signals spewed out by astrocytes, support cells that form a scar around the site of injury. The team's experiments with cultured neurons suggest that EGFR signaling is necessary for both types of inhibition.

"To the extent to which we have to inhibit both pathways to get regrowth, this means that our chances

of inhibiting all the bad actors [with a single drug] is that much greater," says Marc Tessier-Lavigne, a neurobiologist at Genentech in South San Francisco, California, and collaborator on the current study. Genentech's drug Tarceva, which has FDA approval for treating non-small cell lung cancer, was one of the EGFR blockers tested on cultured neurons. Tessier-Lavigne says Genentech is now investigating the drug's effects on axon regeneration in a mouse model of spinal cord injury.

But even if those experiments yield good results, EGFR blockers alone may not be enough to heal spinal injuries, He cautions. Other research has suggested that compounds that actively promote axon regeneration may be needed as well. As with driving a car, He says, taking your foot off the brake only gets you so far—then you need to hit the gas.

—GREG MILLER



Growth potential. Axons (red) regrow in a crushed nerve treated with an EGFR blocker (bottom) but not in an untreated nerve (top).

dermal growth factor receptor (EGFR), might have a role in thwarting regeneration. The study "identifies a novel target for therapeutic interventions," Filbin says.

Even more exciting, says Ben Barres, a neurobiologist at Stanford University in California, drugs that inhibit EGFR signaling are already approved for treating lung cancer. "This raises the possibility of almost immediate application of EGFR antagonists in patients with spinal or other central nervous system injuries," he says.

The new study was led by Zhigang He and Vuk Koprivica of Children's Hospital in Boston, Massachusetts. They and colleagues tested about 400 small molecules on cultured rat neurons, hoping to identify those that promoted the growth of new axonlike extensions. Most of the compounds did nothing, but several EGFR

Nuclear Traffic Report

VIENNA—There's good news and bad news about illicit trafficking of radioactive materials, says the International Atomic Energy Agency in a new report. The good news is that the number of incidents involving uranium, plutonium, or thorium—ingredients for a "dirty bomb"—have remained low since peaking in the early 1990s. Perpetrators were caught with such materials 19 times in 2003 and 2004 combined, compared with 45 in 1994 alone.



The bad news is that the market is booming for less dangerous materials. There were a record 78 incidents last year involving isotopes such as cesium-137, which is used in hospitals as a source of x-rays. The most worrying was a 2003 incident in the Republic of Georgia, where an arrest netted 170 grams of weapons-grade uranium that seems to have been part of a larger cache for sale.

—JOHN BOHANNON

More Bang for the Buck?

BARCELONA—Spain plans to boost research spending next year by 33%, but scientists are unhappy that much of the increase will go toward building more military weapons.

The total research budget for FY 2006, which starts on 1 January, will be \$6.5 billion, including a 27% increase for military research. But funding for basic research in physics and chemistry, for example, would rise only marginally. The budget "reinforces the scientific militarization undertaken by previous governments over the last 10 years," says Jordi Armadans, director of a group of scientists against military research called Fundació per la Pau.

Researchers also object to the government's continued listing of military construction programs—tanks, ships, and the like—as research, despite a pledge this summer from Prime Minister José Luis Rodríguez Zapatero that such spending would not be part of the government's promised doubling of the research budget over the next 5 years. According to Fundació, more than 80% of the \$1.7 billion for military R&D will go toward construction.

—XAVIER BOSCH

ECOLOGY

Satellite Tracking Catches Sharks on the Move

With the speed of a tuna and the homing instinct of a salmon, the great white shark—once considered a homebody—is proving a transoceanic traveler. And not to be outdone, a less fearsome cousin called the salmon shark has now shown up in Hawaii, far away from its supposed home in Alaska.

Two studies in this week's issue document these unexpected sea trips. Two species “we have previously considered to be largely coastal in their movements have a much greater ecological link with the open ocean than previously thought,” says Barry Bruce, a marine biologist at the Commonwealth Scientific and Industrial Research Organisation in Hobart, Australia. These findings complicate conservation efforts, he adds, as multiple countries must take part in protecting the species.

Over the past decade, satellite technologies have enabled marine biologists to follow the oceanic travels of animals tagged with transmitters. On page 100, a team led by Ramón Bonfil of the Wildlife

Conservation Society in New York, New York, reports using such technologies and visual markings on fins to observe 32 great white sharks over 15 months. “These researchers have gone where others have feared to tread,” says Barbara Block of Stanford University Hopkins Marine Station in Pacific Grove, California, referring to the danger and challenges of tagging these beasts.

An electronic device attached to the dorsal fin sent data about geographical coordinates whenever a tagged shark surfaced, enabling Bonfil and his colleagues to plot a shark's journey. Another device, fastened

by a releasable pin, recorded depth and temperature. When the pin snapped as planned, the device surfaced and relayed these data “directly to the office,” says Bonfil. In addition, the researchers equipped the sharks with acoustic transmitters and tracked the animals' finer scale movements using microphones scattered in certain South African bays.

Bonfil's work extends earlier studies by Block's group, which found that great white sharks around the California coast periodically headed more out to sea. Bonfil's data showed just how far this species could travel.

One female sped across the Indian Ocean and back at 4.7 kilometers per hour, covering 20,000 kilometers in less than 9 months. Other tagged great whites, thought to be looking for prey, regularly took 2000-kilometer trips up and down South Africa and into the waters off Mozambique.

In a separate study, reported on page 104, Kevin Weng, working with Block and others, used remote-sensing satellites to track 48 tagged salmon sharks based in Prince William Sound, Alaska. The salmon sharks also migrated long distances. After wintering off Alaska, some headed south, ▶



Easy now. Researchers release a great white shark that now bears satellite tags much like those of this salmon shark (*inset*).



CONSERVATION POLICY

House Revises Endangered Species Act

Legislation that would remove a controversial provision of the U.S. Endangered Species Act (ESA) was passed last week by the House of Representatives. The bill, introduced by a longtime opponent, was pushed through at a whirlwind pace despite pleas by moderates for more time. Critics are now looking to the Senate to correct provisions that they say will weaken protection of species.

Representative Richard Pombo (R-CA) and other critics argue that the 1973 act, last amended in 1988, hurts landowners while not adequately helping endangered species. They say only 1% of 1268 species listed have ever been removed after recovering. But supporters say that the act's main achievement has been to prevent extinctions. As chair of the House Resources Committee, Pombo moved his bill through committee in just 4 days—a pace that some legislators and officials at the Fish and Wildlife Service (FWS) say precluded adequate analysis. On 29 September, the House approved it by a vote of 229 to 193.

The bill (H.R. 3824) would eliminate so-called critical habitat provisions, land or water that FWS designates as necessary for a species to recover. The designation brings several legal protections into place, but it also generates many lawsuits (*Science*, 30 September, p. 2150). FWS maintains that it's not necessary because those legal protections are redundant, but many environmentalists say that in practice critical habitat bolsters conservation efforts.

Pombo's bill would also require FWS to quickly evaluate any proposed projects that might harm an endangered species. If the agency doesn't finish within 180 days, the proposal would get an automatic green light. Environmentalists worry that FWS's long backlog will result in many harmful projects going forward. Finally, if FWS determines that land shouldn't be altered, then the agency must compensate landowners. The Congressional Budget Office estimated that amount at \$10 million per year initially, but critics say

it's likely to be much higher and could wind up bankrupting FWS's \$143-million-a-year endangered species program.

Representative Sherwood Boehlert (R-NY), chair of the House Science Committee, and several others proposed a floor amendment that would avoid these concerns by neither giving automatic approval to projects nor compensating landowners. The amendment would have abolished the critical habitat provisions and replaced them with a similar and enforceable type of habitat designation. Although he lost by a vote of 206 to 216, Boehlert said the slim margin of defeat “showed the Senate that the House would be willing to pursue moderate reforms of the Endangered Species Act.”

The Senate is unlikely to work on a companion bill until next spring. The subcommittee responsible for ESA is chaired by Senator Lincoln Chafee (R-RI), a moderate who has expressed reservations about making significant changes to the act. —ERIK STOKSTAD

sometimes going as far as Hawaii or Baja California before returning to Alaska. One covered 18,220 kilometers in just 640 days, Block's group reports. As with the great whites, the salmon sharks took multiple trips but always seemed to return to familiar territory. "[Both] sharks use entire ocean basins as home ranges and show remarkable fidelity to areas," she says. "These two papers represent great leaps in our understanding of how top predators utilize the world's oceans," says Andrew Martin, an evolutionary biologist at the University of Colorado, Boulder.

Block's group also discovered that two cardiac proteins may enable the salmon shark to withstand water temperatures cold enough to stop a polar bear's heart. She and her colleagues now report that salmon sharks have excess SERCA2 and Ryanodine receptors—proteins key to keeping

the heart beating—just as hibernating animals do. In the heart's muscle cells, these proteins help control the flow of calcium and consequently the rate of contraction. This result "advances Block's developing story about how physiological adaptations allow niche expansion," says Martin.

The unexpectedly large ranges for both sharks revealed by the new studies have a downside: The more spread out a species is, the harder it is to protect. Great whites are particularly vulnerable. For example, great whites protected by South Africa are fair game for Mozambique fishers. "They are so much more exposed to being caught because they cover a much wider area," says Andre Boustany of the Hopkins Marine Station. Thus, "conservation management of this species and other highly migratory species must occur on an international level."
—ELIZABETH PENNISI

FRANCE

Reform Law Fails to Impress Researchers

PARIS—French scientists will be more competitive, young scientists will be paid better, and the public and private sectors will work together more closely, say government officials, thanks to a long-awaited draft science reform law unveiled last week. But research leaders who have protested against current policies say the reforms don't go far enough, urging the government to do more to create jobs and improve prospects for young scientists. "The system is becoming more complex and more opaque," says chemist Jacques Fossey, head of the main research union SNCS.

In the reform bill, due to be published on 5 October, the government earmarks an extra \$23 billion in public funds for research between 2004 and 2010. It will award young researchers in public labs an 8% pay hike in both 2006 and 2007, allow university lecturers to spend fewer hours teaching, and provide incentives for companies to hire more postdocs. The government will also create a 24-member agency to evaluate labs, research teams, and individuals so as to improve the distribution of funds. Universities and government research agencies would be offered subsidies to join forces on projects from neuroscience to nanotechnology.

The draft law, which is expected to be adopted by Parliament in February, is "sym-

bolic" of the government's research reforms, says junior research minister François Goulard, because it has already set up the grant-giving National Research Agency this year (*Science*, 26 August, p. 1316) and will soon form a blue-ribbon council to advise the French president on research priorities. But Fossey says that the government must go further. France needs 9000 new public scientific posts and a \$6-billion-a-year jump in spending to reach the European Union goal of 3% of gross domestic product spent on research by 2010.



No guarantees. French research minister François Goulard.

Goulard won't make any guarantees, saying only that this figure is "accessible" and that "the weak link is the private sector." Even the government's commitment is short-term, however, given that national budgets are drawn up annually and presidential and parliamentary elections are due in 2007.

Cochin Institute biologist Alain Trautmann, a leader of the protest movement, wishes it were otherwise. "Governments can and should make long-term moral commitments beyond the next elections," he says.

—BARBARA CASASSUS

Barbara Casassus is a writer in Paris.

Baltimore Bids Adieu

Biologist David Baltimore will step down as president of the California Institute of Technology (Caltech) in Pasadena in June 2006 after 9 years on the job. The 67-year-old Nobel laureate plans to return to research and teaching as a faculty member.

"I analyzed a lot of things about myself and my position in the world and my age and where my satisfactions were, and I decided that, on a personal basis, this was a time to think about it," he said, announcing his decision last week. "And as I thought about Caltech, I recognized that we had a lot of things in place and had done a lot of things and it wasn't a bad time to have a transition."

Caltech has already raised \$1.1 billion in a \$1.4 billion capital campaign that it launched in 2002, and Baltimore was instrumental in creating the Broad Center for the Biological Sciences. He will go down in history "as one of the great presidents of Caltech," says Eli Broad, a trustee of the institute and namesake of the center.

—YUDHIJIT BHATTACHARJEE

Googling NASA

After years of casting about for a major industrial partner, NASA's vast Ames Research Center will take advantage of its Silicon Valley location and partner with Google.

The famous search-engine company will develop up to 93,000 square meters on an Ames research park for its research and development efforts. Ames Director G. Scott Hubbard predicts that Google's presence will provide advances in "new sensors and materials from collaborations on bio-info-nano convergence, improved analysis of engineering problems," as well as in supercomputing and data mining.

—ANDREW LAWLER

Annan Names U.N. "Flu Czar"

British public health expert David Nabarro has been picked to become the United Nations' point man for influenza. The 28 September appointment by U.N. Secretary-General Kofi Annan gives Nabarro, who has held various positions within the World Health Organization (WHO), a coordinating role in efforts against avian and human influenza across U.N. branches. WHO will remain the lead agency on flu.

Nabarro immediately made world headlines when he told reporters that a flu pandemic might claim as many as 150 million lives. The next day, a WHO spokesperson said that a more reasonable projection would range from 2 million to 7.1 million deaths.
—MARTIN ENSERINK

CREDIT: BEHROUZ MEHR/AP/GETTY IMAGES



Triumph of the Ulcer-Bug Theory

A simple but revolutionary finding, perseverance in the face of opposition, and scientific salesmanship were the ingredients enabling two Australians to win the 2005 Nobel Prize in physiology or medicine. On Monday, the Nobel Assembly at the Karolinska Institute in Stockholm, Sweden, announced that Robin Warren and Barry Marshall have been recognized for their discovery that an easily treatable bacterium called *Helicobacter pylori*—and not stress, spicy foods, or a host of other factors—causes most peptic ulcers. “With tenacity and a prepared mind,” the duo “challenged prevailing dogmas,” the assembly said in a press release.

“It’s fantastic,” says microbiologist Francis Mégraud of the Hôpital Pellegrin in Bordeaux, who heads France’s national reference center for *Helicobacter*. “Their work has made a huge difference in the lives of millions of people.” In the past, ulcer patients under-

went stomach operations or took medicines for life, he says; thanks to Warren and Marshall, a simple course of antibiotics is often enough to cure them completely. Warren says that he and Marshall had long hoped for a

Nobel but worried that “a bug in the stomach might not be romantic enough.”

Warren, 68, a pathologist who retired from the Royal Perth Hospital in 1999, first observed small, curved bacteria in biopsies from ulcer patients’ stomachs in the early 1980s. He also noticed that they appeared to cause inflammation. Marshall, now 54 and a researcher at the University of Western Australia in Nedlands, was a young clinical fellow at the time, looking for something interesting to do. He teamed up with Warren and managed to culture an unknown bacterium from the biopsies. In a 1984 paper in *The Lancet*, the two first suggested that the microbe, which they then classified as a new *Campylobacter* species, played a role in causing ulcers. ▶

PHYSIOLOGY OR MEDICINE



To your health. Robin Warren (left) and Barry Marshall celebrate after hearing they have won the Nobel Prize.

SCIENTIFIC PUBLISHING

Withdrawn Parasite Paper Stirs Criticism of *Cell*

Many biologists are protesting a decision by the editors of the journal *Cell* to retract a paper without the authors’ assent or any allegations of misconduct.

In July 2004, a group at the University of Brasilia published a widely noted paper claiming that experiments in chickens and rabbits showed that the parasite (*Trypanosoma cruzi*) responsible for Chagas disease actually transfers DNA to the host genome. They even reported that parasitic DNA integrated into DNA of patients with heart damage from the disease. The unexpected finding offered a possible way to explain why the disease, prevalent in

Latin America, can damage a person’s organs decades after the parasite is gone.

In June, *Cell* editor Emilie Marcus wrote the research team, headed by Antonio Teixeira of the Chagas Disease Multidisciplinary Research Laboratory, that “subsequent re-analyses” by a reviewer she did not name “do not support the claim” of DNA integration. Although the Brazilian team offered detailed rebuttals, *Cell* published a one-paragraph retraction in the 23 September issue. The retraction has generated a flurry of indignant correspondence, including a protest letter from the Brazilian Society of Protozoology. *Cell* editors so far have stayed mum.

Scientists agree that the paper, which was the first to claim integration of parasite DNA into a host genome, is controversial, and some doubted the finding from the start. Nonetheless, many biologists are alarmed at the failure of the journal to supply the evidence on which the retraction was based. “This is not the way science should be done,” says Roberto Docampo, a cellular biologist at the University of Georgia, Athens. “I am very concerned with the editor’s power to retract papers based on opinions without publishing the basis for the retraction. ... If an editor starts to do that, maybe half of the literature will start to disappear.”

Microbiologist David Engman of

Northwestern University School of Medicine in Chicago, Illinois, adds that he knows of “maybe a dozen” people in parasitology alone who have written *Cell* editors to protest. On the other hand, parasitologist Dmitri Maslov of the University of California, Riverside, says he “was not surprised at all” that the report’s “extraordinary” claim had been retracted. *Cell* editors “provided a compelling rationale, ... namely, that the integration sites’ sequences have not been properly characterized, and some other data did not support the integration unequivocally,” says Maslov.

Cell’s action appears to fall within policies Marcus explained in testimony submitted to the British House of Commons Committee on Science and Technology in March 2004: “Editor-instigated retractions occur when the Editor receives correspondence from a third party who cannot reproduce the original data.” In such a case, she wrote, “the authors are invited to respond in writing, and both sets of data are then evaluated by independent reviewers.” Teixeira claims, however, that he was never shown any experimental evidence to contradict his findings.

Teixeira says he’s not going to let the matter drop: “I shall fight back to show that the data in our paper is correct.” But regardless of how the matter is resolved, *Cell* may face repercussions. Engman says a colleague asked by *Cell* to review a paper is now wondering if he should bother because the paper “may be reversed postpublication.”

—CONSTANCE HOLDEN



Paper protest. The retraction of a *Cell* paper on the parasite (above) causing Chagas disease has caused a furor.

Most gastroenterologists rejected the idea out of hand, and it took a decade of many more studies, including treatment trials with antibiotics, to win over the field. “Many people had been spending a lot of time on all kinds of hypotheses, and all of a sudden there was a very simple answer,” says gastroenterologist Loren Laine of the University of Southern California’s Keck School of Medicine in Los Angeles. Although Warren was “a little bit shy,” Mégraud says, Marshall “fought very hard” to get the idea accepted. He traveled the world, pleaded his case endlessly, and even experimented on himself, swallowing a *Helicobacter* culture to show that it caused inflammation. Warren agrees that Marshall is the “better salesman” of the

two: “I just don’t think I would have been able to convince people on my own.”

H. pylori is also implicated in two types of stomach cancer, other researchers have discovered, and the microbe’s epidemiology is now much better understood. About half the world’s population may be infected permanently, even if only one in 10 hosts develops ulcers. Infection rates are highest in the developing world but have gone down in wealthier nations during the 20th century because of improved hygiene and increased antibiotic use. Several tests are now available for rapid diagnosis of *H. pylori* infection, including a 20-minute breath test co-developed by Marshall.

Not all debate about *H. pylori* has ended, though. A few researchers believe that the

bug may confer some benefits to its host along with the risks. New York University’s Martin Blaser, for instance, says there may be a causal relationship between declining *H. pylori* infection rates and the rising incidence of acid reflux disease and a deadly type of esophageal cancer. Doctors may one day reintroduce *Helicobacter* strains into some patients’ stomachs to take advantage of its protective effects, he predicts. The question is hotly debated among gastroenterologists, but “in a peculiar type of irony,” Blaser says, he finds himself in the same underdog position as Warren and Marshall 20 years ago. “I guess he could be right,” says Warren. “But I don’t think he has as much evidence as we did.”

—MARTIN ENSERINK

NOBEL PRIZE: PHYSICS



Quantum Optics Shines in the Photon’s Centenary

One hundred years ago, Albert Einstein hypothesized that although light behaves like a wave, it consists of particulate bits or “quanta.” On the centennial of Einstein’s revolutionary insight, the 2005 Nobel Prize in physics honors three researchers who have pioneered the frontier between the wave and particle views of light and laid the foundation for the field of “quantum optics.”

Theorist Roy Glauber, 80, will receive half the \$1.3 million prize for mapping out the conceptual connection between assemblages of individual photons and classical waves of light. Experimentalists Theodor Hänsch, 63, and John L. Hall, 71, will share the other half for developing exquisitely precise techniques to manipulate laser light, which is a quantum-mechanical torrent of photons. Their work has opened new avenues of research and led to the development of ultraprecise frequency standards.

“Hänsch, Hall, and Glauber—what a wonderful combination!” says physicist Marlan Scully of Texas A&M University in College Station and Princeton University in New Jersey. “I think it bodes well for quantum optics that these heroes are getting the recognition they deserve.”

In the early 1960s, Harvard University’s Glauber tackled a fundamental problem with the quantum theory of light: A randomly produced bunch of photons behaves more like a hail of bullets than a graceful “classical” light wave. To appear more wavelike, the individual photons must be coordinated or synchronized to create a so-called coherent state, in somewhat the same way that a pointillist painter

organizes colored dots into a complete image.

That much was already known. But Glauber studied in detail the properties of such coherent states and their interactions with detectors. Coherent states “were treated as a curiosity,” Glauber says. “Some [hints from experiments] gave me the thought that their role was much more fundamental.”

work they’ve done for a very long time,” says physicist Stephen Lea of the National Physical Laboratory in Teddington, U.K.

A laser produces a beam with a narrow range of frequencies by coaxing atoms to emit light in concert. But there is always some variation in frequency because of the inherent uncertainty in the emission of

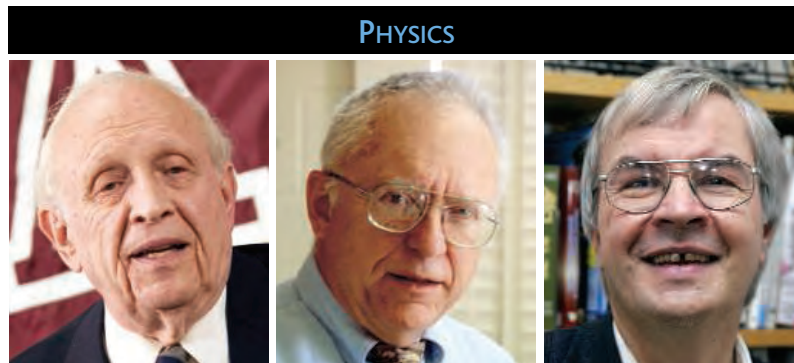
light by the atom and the mechanical instabilities of the laser. Hänsch and Hall independently developed techniques to greatly reduce that uncertainty by using a “resonant cavity”—essentially an optical bell that rings with light—to stabilize the laser.

These efforts led to the invention of the frequency comb, an ultraprecise frequency

standard that might someday replace the current atomic clock as the ultimate timekeeper. The comb consists of a highly stabilized laser locked into a cycle in which it spits out a regular stream of light pulses tens of femtoseconds long and separated by nanoseconds. The spacing of those pulses is constant to a few parts in a million billion. Hänsch had the idea for the frequency comb 25 years ago, Lea says, but Hall’s achievements were essential to making it work.

Einstein’s quantum hypothesis may be a century old, but the field of quantum optics is young and growing, Scully says. The likelihood of new applications, he adds, augurs well for more Nobels in the next 100 years.

—ADRIAN CHO



The light fantastic. Roy Glauber (left) charted the theoretical ground between waves and photons. John Hall (center) and Theodor Hänsch developed seminal laser techniques.

Glauber’s work explained surprising phenomena that occur only in experiments that probe the quantum nature of light. For instance, depending on the circumstances, individual photons can tend either to clump together or to avoid each other. Known as “bunching” and “antibunching,” those phenomena may be useful for conveying information in streams of individual photons.

This year’s prize also lauds Hänsch of the Max Planck Institute for Quantum Optics in Garching, Germany, and Hall of JILA, a research institution run jointly by the University of Colorado, Boulder, and the National Institute of Standards and Technology, for work on stabilizing and manipulating laser light. “It’s a very rich reward for the excellent

ENDANGERED SPECIES

Ban on Beluga Caviar Points to Sturgeon's Worldwide Decline

ALMATY, KAZAKHSTAN—Seeking to protect one of the oldest species of fish on Earth, the United States on 30 September banned importing caviar from the king of sturgeon, the beluga. That's good news for the sturgeon, but a bit late. A comprehensive study published last month found that all 25 species of sturgeon and two related paddlefish have been depleted worldwide.

"This is a case of the lessons not learned," says Ellen Pikitch, director of the Pew Institute of Ocean Science in New York City, the lead author with Phaedra Doukakis of the study in *Fish and Fisheries*. "For the first time, we're looking not just at the possible disappearance of a species but of a whole order, ... one of the oldest and most interesting ones in the world."

The study found local extinctions for 19 of 27 species. Belugas caught today usually weigh 150 kg—mere teenagers in a species that should include centenarians—and the study concluded that nearly all mature individuals, which can reach 6 meters in length, have been taken out. "It's no accident that the three species that are in the best shape are all in the States and are all completely protected," Pikitch says. "We need to extend the same protection to the other species, particularly the beluga, before it's too late."

Since 1997, the United Nations has



Endgame? Fishers haul sturgeon ashore from their breeding area in the Ural River in Kazakhstan.

tried to limit exports of the three commercially harvested species—the beluga, the Russian/Persian, and the stellate—through its regulatory body, the Convention on International Trade in Endangered Species of Wild Fauna and Flora (CITES). But this hasn't prevented widespread poaching. Three U.S. environmental organizations

5 years ago petitioned the U.S. Fish and Wildlife Service (FWS) to place the beluga on its threatened list and urged consumers to boycott beluga caviar (*Science*, 16 September, p. 1799).

As a result, the United States became the second nation, after Australia, to ban the importation of beluga. FWS Assistant Director for International Affairs Ken Stansell said in a telephone press conference that he hoped the U.S. measure would "encourage other nations to take a closer look at their imports." Stansell, the U.S. representative to CITES, said the 143 member states next meet in June 2007, the earliest date they could consider a proposal to ban the trade. But no such measure has yet been proffered.

In late July, Russia proposed a moratorium on fishing all three commercial species at a meeting of the Caspian Bioresources Commission, composed of the Caspian countries. The commission, which sets each country's yearly caviar export quotas, will take up the proposition at its next meeting, in November. If these countries adopt the moratorium, international trade will stop without CITES's intervention.

What a worldwide ban on the wild caviar trade would achieve is unclear, as illicit harvesting would likely continue. "Most of the poached caviar is consumed in the former Soviet Union," says Sabri Zain of Traffic International, an organization that tracks trade in endangered species. "As long as the producer countries don't control their domestic market, stopping exports will have very little effect."

—CHRISTOPHER PALA

Christopher Pala is a writer in Almaty, Kazakhstan

ASTROPHYSICS

Short Gamma Ray Bursts: Mystery Solved

The incredibly bright and extremely brief flashes of energy known as short gamma ray bursts have taunted astronomers for more than 3 decades, but it looks as if researchers have nailed their origin at last. According to a series of papers in this week's issue of *Nature*, these hugely powerful cosmic explosions that flood space with high-energy gamma rays are produced by merging neutron stars or black holes. Four international teams of astronomers reached that conclusion after observing two short gamma ray bursts earlier this year (*Science*, 13 May, p. 939). Detailed studies of three other short bursts support the merger scenario.

Gamma ray bursts were first detected by spy satellites in the 1960s. No one knew their source or even how distant they were until 1997, when the Italian-Dutch BeppoSAX satellite first detected a burst's afterglow, enabling researchers to determine its distance and prodigious energy output.

Since then, a wealth of new observations has convinced astrophysicists that the longer bursts—which last more than 2 seconds or so—are the death cries of rapidly rotating massive stars that explode as brilliant hypernovas while their cores collapse into black holes. However, a large and distinct population of very short bursts, lasting 0.3 seconds on average, remained mysterious.

Now, follow-up observations of the afterglows of two short bursts on 9 May and 9 July, detected by the Swift and HETE-II satellites, respectively, have settled the issue. The bursts, which occurred in relatively nearby galaxies, showed no hint of an underlying stellar explosion. Given their distances, they appear to have less than 1/100th the power of their long-lasting cousins. These observations agree perfectly with the merger model, in which two orbiting neutron stars—themselves compact remains of exploded giant stars—

slowly spiral toward each other and coalesce into a black hole, releasing huge amounts of energy.

Unpublished results from three more short gamma ray bursts support the conclusions, says Jochen Greiner of the Max Planck Institute for Extraterrestrial Physics in Garching, Germany. "The general feeling in the gamma ray burst community is that the issue has been settled," he says. "I am not aware of any remaining viable alternative explanations." Some riddles remain: Astronomers still wonder why the x-ray afterglows of short bursts appear so faint, and they still can't tell whether the merger involved two neutron stars or a neutron star and a black hole. As one team notes in its paper: "The stage is now set for detailed studies of these exotic cosmic explosions."

—GOVERT SCHILLING

Govert Schilling is an astronomy writer in Amersfoort, the Netherlands.

Studies of the emergency contraceptive in thousands of women have failed to assuage the concerns of abortion opponents and top drug regulators in the United States. Researchers see ideology trumping sound science

Plan B: A Collision of Science and Politics

The U.S. Food and Drug Administration (FDA) promised a decision on the emergency contraceptive Plan B early last summer. But on 26 August, after more than 2 years of deliberation, leaked memos, and a contentious advisory committee meeting, FDA ducked, putting off indefinitely a ruling on the application from Barr Laboratories in Woodcliff Lake, New Jersey, to move Plan B over the counter (OTC). The problem, agency officials said, was a dearth of information on whether the drug, approved for prescription use in 1999 and widely available in European pharmacies, would negatively influence the sexual behavior or health of adolescents. FDA was unsure how to restrict the drug's OTC status to older age groups.

That announcement, say critics of the non-decision, highlighted Plan B as the latest scientific issue—after climate change and evolution—to be taken ideological hostage by the Bush Administration. In late August, the head of FDA's Office of Women's Health, Susan Wood, resigned and publicly stated her disagreement with the Plan B decision. On 22 September, a *New England Journal of Medicine* editorial written by the journal's editor and two members of the two FDA advisory committees that voted in favor of the shift, citing the drug's safety, proclaimed that FDA's recent actions "have made a mockery of the process of evaluating scientific evidence."

Considered dead after the August announcement by then-FDA commissioner Lester Crawford, Plan B may yet rise again. Senators Hillary Clinton (D-NY) and Patty Murray (D-WA) had voted to confirm Crawford in July only after he promised a quick

decision on Plan B. Crawford failed to deliver. Two weeks ago, he resigned suddenly, and National Cancer Institute Director Andrew von Eschenbach was named FDA acting director (*Science*, 30 September, p. 2142). But a spokesperson for Murray says she would consider blocking the nomination of a new FDA head until the agency rules definitively on Plan B. Clinton, says a spokesperson, continues to press for a decision.

The furor stands in sharp contrast to how the issue has been handled in the rest of the world. Emergency contraception is available OTC or from a pharmacist in 39 countries. In France, it's provided by school nurses in every senior and junior high school, says James Trussell, director of the office of population research at Princeton University in New Jersey.

U.S. contraceptive researchers say the delay is inexplicable because of studies, some done years ago, that answered questions now being raised by Plan B opponents. Those studies involved thousands of young women from Scotland to San Francisco who were offered easy or more burdensome access to emergency contraception; it must be taken within 72 to 120 hours of intercourse to prevent pregnancy. They had been tested for sexually transmitted diseases and pregnancies. They'd been quizzed to determine whether keeping shrink-wrapped packs of Plan B in their nightstands made them likelier to engage in unprotected sex.

The results were unambiguous: Teenagers appeared to have no trouble understanding how to use Plan B, and its availability didn't change their behavior. Those results contributed to the near-unanimity among FDA

scientists and the scientific community that the drug ought to move from prescription-only status to OTC.

Plan B, or levonorgestrel, is a progestin-only pill that interferes with ovulation and perhaps with fertilization, explains Margaret Blythe, a pediatrician at Indiana University Medical Center in Indianapolis. Its effectiveness declines with time, which argues for making it rapidly available, say OTC supporters. Blythe spent 18 months reviewing studies of Plan B and helping write a statement for the American Academy of Pediatrics in support of OTC use. In her experience, politicians and the public often don't distinguish between Plan B and RU-486, a drug that chemically induces an abortion in the early weeks of pregnancy. Still, the difference between the two is often insufficient to appease opponents of abortion, including doctors. "We've had some physicians in the academy ... who are very, very upset" with its Plan B position, she says.

Two FDA advisory committees—on Reproductive Health Drugs and Nonprescription Drugs—together considered Barr's application in December 2003. Most members agreed that it met the OTC criteria. First, says Alastair Wood, an associate dean at Vanderbilt University in Nashville, Tennessee, and an advisory committee member who voted in favor of Barr's application, the drug is designed for an event (unprotected intercourse) that a patient can easily diagnose. Second, Plan B doesn't come with undue monitoring requirements, such as regular blood tests. And finally, side effects are few and can normally be managed without help from a doctor. The advisory committees voted unanimously that the drug was safe for OTC use.

This view is bolstered by a general belief among physicians that reproductive drugs work similarly in teenagers and adults. In the 1990s, oral contraceptive makers inquired at FDA about receiving "pediatric exclusivity": patent extensions on their products as a reward for conducting trials in a pediatric population. FDA turned down the request, says Lisa



Default strategy. If taken within a few days of unprotected sex, Plan B can prevent pregnancy.



Rarick, who spent 15 years at the agency, including as head of its reproductive drugs division, before leaving in 2003. “Reproductive-age women are reproductive-age women,” says Rarick. “The contraceptive drugs work the same in a 14-year-old [as in] a 20-year-old.” But now, with Plan B, she says, FDA is “saying kids are different.”

Opponents, including advisory committee members David Hager, an obstetrician-gynecologist at the University of Kentucky in Lexington, and Louis Cantilena, a clinical pharmacologist at the Uniformed Services University of the Health Sciences in Bethesda, Maryland, worry about how the drug might affect a teenager’s behavior. Will easier access to Plan B make teenagers more likely to engage in risky sexual behavior, and will they use the drug properly? Hager worries too about the safety of repeated use. “What happens when a young woman uses a medication three to four times a month for several months?” asks Hager of Plan B. “We just don’t know how it will affect her.” It’s true that such repetitive-use data are lacking, mainly because young women in virtually all the studies chose not to take emergency contraception very often, even if supplied it in advance.

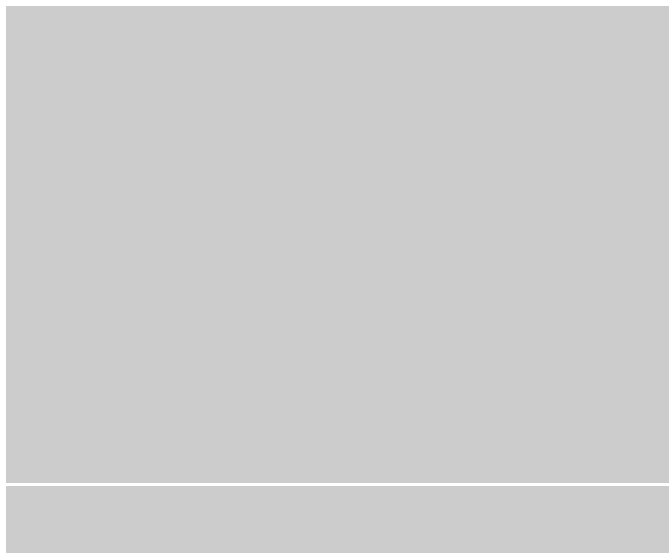
Cynthia Harper, a demographer at the University of California, San Francisco (UCSF), had some of the same questions. So in the late 1990s, she teamed up with UCSF ob-gyn Tina Raine, who runs a young women’s reproductive health clinic in San Francisco’s gritty Mission district, to follow up on a 1998 Scottish study of Plan B. That study of 1083 women (248 of them under age 20) found no difference in behavior among those offered easy access to emergency contraceptives and those who had to visit a doctor to get it. But Raine’s patients were poorer than those in the Scottish study, and at much higher risk of pregnancy. Would the results be the same?

The answer seems to be yes. In 2001, Raine and Harper began recruiting 2117 women aged 15 to 24 to follow up on a smaller pilot study they’d published in 2000. The large study, published last January in the *Journal of the American Medical Association (JAMA)*, assigned the young women to one of three groups: “advance provision” (receiving Plan B to keep at home), access to Plan B through a pharmacist, or access through a clinic.

The team found no differences in contraceptive use among the three. A similar outcome has been reported in other studies, including one of 15- to 20-year-olds in Pitts-

burgh, Pennsylvania. After 6 months, more than a third of women in the advance-provision group had used Plan B at least once, compared to a fifth of the controls. All three had similar rates of unprotected intercourse and sexually transmitted diseases. Oddly, however, despite more frequent use of Plan B among the advance-provision group, all three had similar pregnancy rates.

The comparable pregnancy figures—precisely what Plan B is designed to prevent—troubled some physicians. “Promoting easier access because it increases the use of a medication without any improvement in its desired outcome seems counterintuitive,” wrote family physician Stephen Wilson of the University of Pittsburgh Medical Center



St. Margaret Hospital and his former colleague Allen Last in a letter to *JAMA*.

The problem, Raine suspects, is that the drug was underused. “Only half the women who said they had unprotected sex” used Plan B in the *JAMA* study, she says. “Everyone’s worried that people are going to abuse it. The problem to me is that people don’t understand how easy it is to get pregnant.” Other emergency contraceptive studies have consistently found similar pregnancy rates regardless of the ease of Plan B access.

Why this is so is unclear, says Anna Glasier, an ob-gyn at the University of Edinburgh, U.K., who conducted the 1998 study as well as another on 18,000 women published last fall. She agrees that many women may not realize they’re at risk for pregnancy. Another possibility, she says, is that even at its best the drug works less well than thought, reducing the risk of pregnancy by perhaps 50% instead of 80% or more, as many believe. Still, says Glasier, who supports easy access to Plan B, “even if something is only 50% effective, it’s 100% better than doing nothing.”

David Grimes, an ob-gyn at Family Health International in Research Triangle Park, North

Carolina, distinguishes between the population effect seen in these studies and an individual woman’s need for Plan B access—“for example, a rape victim, or a woman who’s had sex with a man she does not wish to father a child with,” he says.

By 2004, the American Academy of Pediatrics, the Society for Adolescent Medicine, and the American College of Obstetricians and Gynecologists had all expressed their support for making Plan B available OTC. But at FDA, which had been reviewing data sometimes even before it was published, the effort to switch Plan B to OTC status “fell apart for nonscientific reasons,” says Grimes. “Everybody’s on board with this,” he says. “Everybody but the FDA.”

It’s unclear who made the decision to indefinitely postpone a ruling on Plan B. An internal memo in April 2004, from John Jenkins, head of FDA’s Office of New Drugs, notes that “both [FDA] divisions and offices responsible for this application have recommended approval.” Jenkins concurred with that assessment and added his own support for Barr’s application. Although FDA occasionally overrules its advisory committees—which in this case voted 23–4 in favor of OTC status—former FDA officials and those familiar with the agency say it almost never rejects the consensus of its own staff.

The FDA official who signed off on the delay—Steven Galson, head of the Center for Drug Evaluation and Research—declined through the press office to be interviewed. Susan Wood, who quit over Plan B last month, says she spoke with people below and above Galson prior to the August announcement, and “no one seemed to know what the answer was going to be. . . . The scientific staff were shut out of this decision,” including members of the commissioner’s office and the reviewing staff. Hager says that he was encouraged by someone at FDA to “write a minority opinion” on Plan B, which was submitted to the commissioner’s office. He declines to reveal who made the suggestion.

“I have never seen anything like this happen before,” says Rarick, now a consultant, who oversaw approval of both Plan B and RU-486 for prescription use. At the time, she says, FDA scientists were shielded from the politics of drug approval. “You had a buffer zone,” she says, which has since disappeared.

Now the question may be whether von Eschenbach will make a decision. “This will be [his] first test,” says Wood, “as to whether he can be independent and . . . can ensure that science drives the decision.”

—JENNIFER COUZIN

Premier Latin American Institute Loses Grants, Ponders Future

Layoffs hit Costa Rica's INBio, underscoring the difficulties of funding taxonomists

International biologists rejoiced when the National Biodiversity Institute (INBio) of Costa Rica was founded in 1989. Although the fledgling institute was modest—its first building was an idle warehouse for farm equipment—its vision was enormous: to inventory each and every species in Costa Rica, a country renowned for its biodiversity, and find sustainable ways to both preserve and use it. “We all thought: ‘There is an opportunity, there is hope’” for conservation in the tropics, says Arturo Gómez-Pompa, a botanist at the University of California, Riverside.

The cornerstone of INBio has been its pioneering species inventory. In a novel approach, the non-profit institute trained dozens of parataxonomists from local communities to collect specimens across the country. Soon INBio had amassed major collections, and from that core it started new ventures in bioprospecting, publishing, and ecotourism that were designed to provide revenues that could be invested in conservation.

“It takes your breath away to see what they’re doing there,” says Elizabeth Losos, a forest ecologist who heads the Organization for Tropical Studies.

But now, that flagship project is in serious trouble. Last month, INBio officials began the process of laying off a third of the 50 taxonomic staff. The proximate cause is that two major grants, which have funded most of the inventory work at INBio for the past 7 years, are running out. INBio officials play down the implications, saying that it’s just a temporary funding squeeze. But some outsiders worry that the problem extends beyond next year’s budget. They fear a depleted staff may curtail the organization’s critical survey work and compromise INBio’s broader goal of fostering biodiversity conservation. INBio’s shortfall also underscores the difficulty of raising money for taxonomy, they say, and the need to pursue more innovative funding mechanisms.

INBio led the way in showing scientists and policymakers that it makes economic sense to preserve biodiversity. “They were the first out of the gate in terms of trying to sell the idea of biodiversity,” says Losos. The institute

negotiated savvy deals with pharmaceutical companies to search for new molecules (*Science*, 22 May 1992, p. 1142), and the idea of nurturing native scientific talent in a developing country garnered broad appeal within the research community.



Pins and needles. INBio is looking for new ways to fund its taxonomic research, which it has cut as grants expire.

Although taxonomy was always a hard sell, international donors became more willing to open their wallets after the 1992 Convention on Biological Diversity. INBio won start-up grants to launch new operations that capitalized on biodiversity, such as tourism and education. Many projects now cover much of their own costs. A nongovernmental institution, INBio earns half its budget from revenue-producing activities including royalties from bioprospecting work and relies on grants for the other half.

Because grants for taxonomy are difficult to get, especially as donor interests have shifted, INBio has occasionally trimmed its inventory staff and scaled back the ambitious plans to survey absolutely everything. Last year, INBio decided to jettison its collections of mollusks and nematodes, which were shipped to Costa Rican universities, to focus on insects and plants. “It’s been really a struggle over the past decade to fund taxonomic inventories,” says Anne Larigauderie, head of Diversitas, a biodiversity network based in Paris.

Some 90% of the inventory program’s \$900,000 budget has come from two 7-year

awards, one from the World Bank’s Global Environment Facility (GEF) and the other from the Dutch government. But both grants will have expired by the end of the year. “They’re against the wall,” says Daniel Janzen, an ecologist at the University of Pennsylvania in Philadelphia and co-founder of INBio, who’s now an unofficial adviser.

Randall García, INBio’s associate director of conservation, says that about a year ago INBio was discouraged from reapplying for one of the grants because the Dutch are shifting their grant money from Costa Rica. Mario Ramos, GEF’s biodiversity program manager, says his organization’s grant was a one-time infusion to strengthen INBio’s capacity for the inventory of bees, wasps, beetles, vertebrate parasites, and fungi. “The idea is that the GEF is catalytic,” Ramos says. “We expect the follow-up won’t be by us.”

Critics inside and outside of INBio feel that managers weren’t very aggressive in seeking other sources of support. “The current leadership is not all that interested in inventory,” says Paul Hanson, an entomologist at the University of Costa Rica in San José, whose curator wife was given a pink slip. Not so, says García, who points to some \$250,000 the institute has raised in the last year from the Spanish government, the Nature Conservancy, and Conservation International.

But those grants don’t cover current inventory costs. So last month, 13 parataxonomists, curators, and technicians cleaned out their desks; about five more will be let go in December. The layoffs have been concentrated in entomology, the department that had received the lion’s share of support from the big grants. “It’s the best insect collection” in Latin America, says Hanson. “This is sending tremors through the taxonomic community.” INBio also shut down an ecological mapping division.

The layoffs will mean an end to field collecting, including the work of a team of five parataxonomists who provide information to the Costa Rican government for decisions on how to protect its lands. García hopes that INBio can rehire staff by 2007 if it can nail down more funding. But Janzen worries that well-trained staff members may not come back, taking with them their extensive knowledge of the collection. Even so, Janzen and others agree that INBio had no better alternatives.

Administrators say they are pursuing new grants from conservation organizations and other governments, as well as trying to spin grant applications toward donor interests such

as poverty alleviation. Longer term, they hope to further build INBio's revenue-generating operations, such as bioprospecting, and invest profits back into inventory.

Some observers are skeptical that INBio will ever be able to cover its own inventory costs. Gómez-Pompa thinks that winning

support from the Costa Rican government will be vital: "It's a dream to think that they will be able to survive for a long time without government support."

To Janzen, however, government support is a mixed blessing because of its unreliability. A major endowment—INBio's García

mentions \$21 million as a target for inventory—is the only permanent solution, he says. To that end, Janzen has agreed to help INBio pursue major donors. Despite the crowded playing field, Janzen is optimistic: "INBio is a first-class product."

—ERIK STOKSTAD

Russian Science

Academy Agrees to Post-Soviet Crash Diet

Faced with an aging membership and deteriorating infrastructure, the Russian Academy of Sciences accedes to government calls for reform

MOSCOW—It would turn out to be the most tumultuous meeting of the Russian Academy of Sciences (RAS) that anyone could remember. Many of the best scientific minds in Russia quietly seethed last May as science minister Andrei Fursenko told them how things were going to be different. The government would spend more on the sciences in return for a massive reorganization that would mean layoffs and many fewer research institutes.

But before Fursenko could finish, a shrill, stifling whistle pierced the air. Mathematician Yuri Osipov, the academy's president, immediately rose from his chair and said, "I demand that whoever whistled leave the hall." An elderly man with a thick, gray beard—a well-known specialist in artificial intelligence—stood and left. "The minister made my blood boil ... to such a degree that my fingers wound up in my mouth and a whistle came out," Vladimir Arlazarov later told the newspaper *Izvestia*.

Arlazarov wasn't alone in his outrage. But, in the end, RAS agreed to meet the government halfway in reconciling the scientific legacy of the Soviet Union with the realities of modern Russia. RAS plans by 2008 to close or reorganize dozens of its 452 research institutes and withhold funding from as much as 20% of its staff. Half of that workforce, some 56,000, are researchers. In return, the government has promised a 150% rise in state financing of the sciences, from \$1.6 billion to \$3.9 billion. That influx of cash would boost the average researcher's monthly salary from \$240 to \$1050, and annual per capita spending on labs and equipment would soar from \$3200 to \$26,000.

The academy comprises only 6% of Russia's state scientific workforce, but its roster of Nobel laureates and its commitment to basic research traditionally have made it the star of the country's scientific firmament.

Russia inherited the best institutes and infrastructure when the Soviet Union split up. Since then, however, the fortunes of its scientists have withered as government



Cost cutter. Science minister Andrei Fursenko persuaded the academy to accept cuts.

financing plummeted, and RAS members refused to countenance any downgrading of fundamental research. Yet many institutes can no longer afford to do any science and lease their premises to businesses. Many of those researchers who have remained at their posts hold second or third jobs.

Last year, government officials began to argue that a country as poor as Russia could not afford a system of 2670 scientific organizations with few ties to Russian businesses. The Ministry of Education and Science drew up a secret plan to reform and modernize the sciences that would have all but abolished

the academy, triggering protests nationwide by trade unions. Nobel laureate Zhores Alferov pronounced RAS akin to the Russian Orthodox Church: It neither could be, nor should be, reformed.

But hostility toward the plan began to soften as researchers realized that time was not on their side. With 69 as the average age of RAS members and only 5% under 35, "everyone came to the conclusion that reform is necessary and urgent, because any other way science will simply cease to exist," says RAS spokesperson Irina Presnyakova. Osipov and Fursenko began to talk seriously.

The final compromise preserves both the academy and basic science. But the brunt of the cuts will be borne by thousands of other scientific organizations—those engaged almost exclusively in applied research—largely under the control of state industries and various government ministries. Last month, Fursenko announced that, by 2010, the number of such organizations would be slashed to 1600. "Right now, the government is trying to restore control," says Aleksei Ananchenko, press secretary of the ministry's Federal Agency for Science and Innovation, who expects legislation spelling out the changes to be presented early next year in the State Duma, the lower house of Parliament.

The bulk of the institutes still left standing by 2010 will be compelled to compete for funds in seven priority areas including information technology, ecology, and research in security and counterterrorism. Ananchenko says that directors of these institutes would have to retire at 55, and heads of labs and departments at 60. Researchers would not be subject to age limits but would undergo annual reviews for the first 3 years beginning in 2006 instead of once every 5 years, as they do now. There will be special incentives for researchers between 30 and 35 years old, and inducements to return for those now working abroad.

After more than a decade spent defending their status and livelihood, the old warhorses of RAS are finally resigned to the inevitability of change. "Without science," says Presnyakova, "we'll become a Third World country with missiles."

—BRYON MACWILLIAMS

Bryon MacWilliams is a writer in Moscow.

Huntington's Research Points to Possible New Therapies

By studying the mutant protein made by the Huntington's gene, researchers have identified several candidate drugs that are starting clinical trials

The discovery of the gene that causes a life-threatening disease always sparks a wave of hope that it will lead to a cure. That certainly occurred in 1993 when researchers bagged the gene at fault in Huntington's disease, an inevitably fatal neurodegenerative condition that afflicts about 30,000 people in the United States alone. The gene hasn't so far provided a cure for Huntington's disease, let alone a therapy. But in the past few years, researchers have learned a great deal about how its product, a protein known as huntingtin (Htt), malfunctions and kills neurons when mutated—information that is suggesting therapeutic strategies.

Cell and animal studies have revealed that mutant Htt disrupts nerve cell function in several ways, all of which can contribute to neuronal death. Its actions range from disrupting normal gene activity patterns to interfering with the transport of proteins needed for nerve cell maintenance to overwhelming the cell with toxic amounts of calcium ions. "Talk to a dozen people, and you'll get a dozen different ideas" about what happens in Huntington's disease, says Christopher Ross of Johns Hopkins University School of Medicine in Baltimore, Maryland.

At present, no one knows whether any particular neuronal insult is primary, with the rest following as consequences, or whether they operate independently. "Some people believe there is a priming event you must find and address [for therapy], others that mutant Htt causes multiple problems," says Marian DiFiglia of Harvard's Massachusetts General Hospital in Boston.

Despite that uncertainty, researchers have already identified potential drugs that counteract some of the neuronal problems caused by mutant Htt and are beginning to move them into clinical trials. "It's an exciting time in this field. The pace is picking up, and things look brighter

than they did," says Steven Finkbeiner of the University of California, San Francisco.

Getting started

One of the first clues to how mutant Htt causes the brain degeneration of Huntington's disease came when researchers created a mouse model of the disease a few years after the responsible gene was discovered. The mutations causing the disease occur near the beginning of the gene, in a segment that codes for a repeating string of the amino acid glutamine. In the normal version of Htt, that string contains anywhere from six to 35 glutamines, but in Huntington's patients, the repeat contains 36 or more, with higher numbers producing earlier disease onset.

Over the years, researchers have identified

such polyglutamine expansions in the proteins encoded by about nine genes. In all cases, the gene mutations cause neurodegenerative diseases, none of which are completely understood.

Back in 1997, while trying to find out how glutamine expansions in Htt lead to the nerve cell death of Huntington's disease, Gillian Bates of King's College London and her colleagues introduced into mice the first (or N-terminal) coding segment of the human Htt gene bearing glutamine stretches of various lengths. Rodents with the longer expansions developed a fatal neurological disease with symptoms, such as abnormal movement coordination, similar to those of human Huntington's disease, the researchers reported.

They also saw abnormal deposits of the mutant Htt fragments, along with other proteins, in the animals' neurons, and these so-called inclusion bodies were present before symptoms developed. Subsequently, the Bates

team and others studied brain tissue taken during autopsies of Huntington's patients and found similar clumps in both the cell bodies of neurons and the long axonal projections through which they contact their target cells.

These findings suggested that Htt fragments containing extra glutamines cause at least some of the nerve damage of Huntington's disease and that their abnormal clumping contributes to this toxicity. Bolstering the idea that the fragments are toxic, researchers found that introducing them into cultured nerve cells leads both to clump formation and to the cells' death and that putting them in fruit flies produces a Huntington-like neurodegeneration in the small creatures.

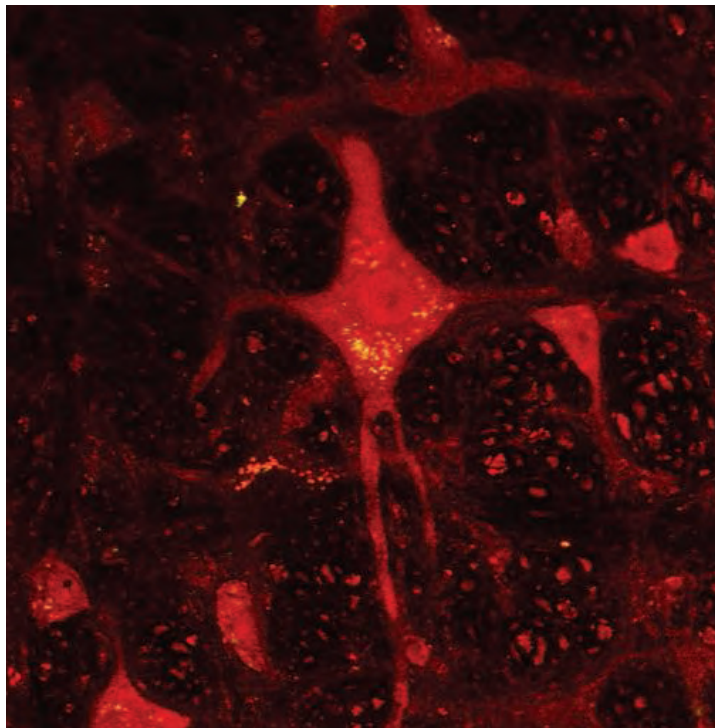
Researchers have also found that numerous protein-splitting enzymes, including certain caspases, can cleave Htt and release N-terminal fragments. As shown in 1996 by Michael Hayden's team at the University of British Columbia in Vancouver, Canada, this cleavage occurs in the brains of both normal humans and Huntington's patients, although only the mutant fragment is toxic.

If the pathology of Huntington's disease indeed depends on Htt being cleaved, then inhibitors

"It's an exciting time in this field. The pace is picking up, and things look brighter than they did."

—Steven Finkbeiner

University of California, San Francisco



Points of contention. Although Htt aggregates (bright dots) in brain neurons are a common pathological feature of Huntington's disease, it's currently unclear whether they kill the neurons or are protective.

Some Potential Huntington's Drugs

DRUG	ACTIONS	STATUS IN HUNTINGTON'S
Coenzyme Q10	Antioxidant; protects mitochondria	Late clinical trials
Creatine	Stabilizes mitochondria	Early clinical trials
Cystamine	Decreases Htt aggregation?	Early clinical trials
Geldanamycin	Decreases Htt aggregation	Preclinical
HDAC inhibitors (butyrates, SAHA)	Counters Htt's transcription effects	Early clinical trials
Memantine	Neurotransmission	Early clinical trials
Minocycline	Decreases cell death, Htt aggregation	Early clinical trials
Paroxetine	Protects neurons by increasing BDNF	Preclinical
Rapamycin	Decreases Htt aggregation by stimulating autophagy	Preclinical

of the enzymes responsible offer a potential therapy. In fact, researchers have found that treatments that inhibit or inactivate caspase activity decrease the toxicity of mutant Htt in both cultured cells and Huntington's mice.

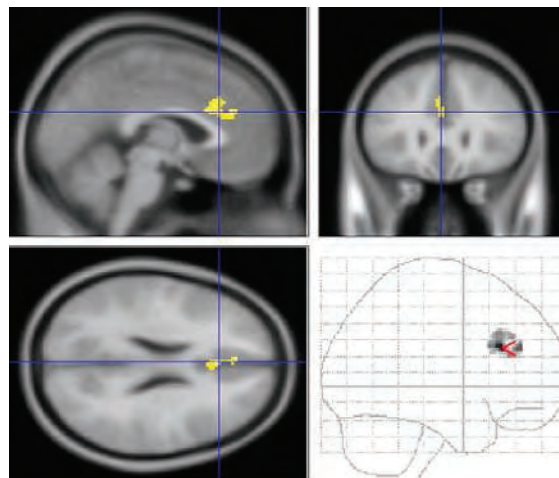
Although the idea that N-terminal fragments of mutant Htt are toxic has been gaining acceptance, the role of the aggregates remains controversial. Some evidence indicates that they contribute to Huntington's pathology, whereas other findings suggest that, far from causing harm, they serve to protect cells from mutant Htt's toxic effects. This debate mirrors a similar one in Alzheimer's disease in which researchers are wrestling to determine whether deposits of a protein fragment called β amyloid are toxic to brain neurons or are protective because they take the real culprit—soluble β amyloid—out of action.

The evidence that Htt aggregates are harmful includes demonstrations that inhibiting their formation reduces the toxicity of mutant Htt. For example, in the 18 January issue of the *Proceedings of the National Academy of Sciences*, a multi-institutional team led by Anne Young and Aleksey Kazantsev of Massachusetts General Hospital reported that feeding a compound, called C2-8, to fruit flies engineered to express mutant Htt prevents aggregate formation and reduces neurodegeneration in the insects' photoreceptor neurons.

David Rubinsztein of the Cambridge Institute for Medical Research in the United Kingdom and his colleagues have also found that the drug rapamycin suppresses Htt aggregate formation and decreases related toxicity in cultured neurons and in fruit fly and mouse models. The drug seems to work by enhancing a recycling process

called autophagy that cells use to destroy excess or damaged proteins. The process involves moving the proteins into small membranous sacs called lysosomes, which are essentially the cell's garbage-disposal units. The lysosomes are packed with enzymes that break down proteins and other cellular constituents. In the past few years, researchers, including DiFiglia and Rubinsztein, have found that autophagy helps clear Htt from nerve cells, thereby decreasing aggregate formation in the cells.

But autophagy apparently can't keep mutant Htt in check forever. The Rubinsztein team found that when rapamycin treatment began 33 hours after introducing DNA encoding the mutant N-terminal fragment of Htt into cultured neurons, it had no effect on aggregation or cell death, whereas it worked



Trouble sign. An area in the brain cortex (yellow) of people who are carrying a mutant Htt gene but have not yet developed Huntington's symptoms has lower activity during a cognitive task than it does in noncarriers.

just fine when introduced 15 hours after the gene transfer. "In the later stages [of Huntington's disease], autophagy might fail and allow the mutant protein to accumulate," DiFiglia says. These results suggest that if drugs such as rapamycin ever reach the clinic, they will have to be given before such a stage is reached.

Not all the researchers who have looked at Htt aggregation have found it harmful, however. In work described last fall in *Nature*, Finkbeiner and his colleagues found in lab cultures that many mouse neurons die even though they lack Htt inclusions. Indeed, the neurons with the inclusions survived better than those without, whereas neurons with lots of diffuse Htt had very poor survival. More recently, the Hayden group has confirmed this in mice, showing that animals with massive inclusions show no signs of neurodegeneration.

Work by Ross with Michelle Poirier and other Hopkins colleagues has shown that the inclusions develop in a stepwise process, with small, soluble aggregates forming first. The Finkbeiner and Hayden teams' results suggest that this diffuse Htt is the toxic form and that sequestering it in insoluble aggregates actually helps protect neurons. "At the moment, it looks like earlier forms of certain kinds of aggregates cause the problems," says Erich Wanker of the Max Delbrück Center for Molecular Medicine in Berlin, Germany, whose team has also looked at how the aggregates form.

Into the nucleus

No matter which form of mutant Htt is toxic, there is no doubt that the extra glutamines in the protein cause a raft of problems for nerve cells, including disruption of gene activity. Normal Htt binds to various transcription factors, proteins that control gene expression, and is thus part of the cell's gene regulatory machinery. Researchers, including Ross, Leslie Thompson of the University of California (UC), Irvine, and Dimitri Krainc of Massachusetts General Hospital, have found that the mutant N-terminal fragment of Htt disrupts this machinery. In some cases, it does this by binding to transcription factors and taking them out of action. This prevents the factors from turning on needed genes such as those encoding certain nerve cell growth factors.

Mutant Htt also indirectly alters gene expression by binding to and inhibiting a histone acetylase, an enzyme that marks genes for activity by tagging their associated histone proteins with acetyl

groups. This suggests another way of decreasing Htt's toxicity. "You can compensate for the decreased acetylation by using an inhibitor of the enzyme that removes the acetyl groups," says Thompson, who is one of the researchers who made the histone acetylase connection.

A few years ago, Thompson, working with Lawrence Marsh, also at UC Irvine, and colleagues, showed that this works in fruit fly models of Huntington's disease. Treating the animals with either sodium butyrate or a drug known as SAHA, both of which inhibit the enzyme that removes acetyl groups from histone, slowed down neurodegeneration in the flies. At about the same time, Bates and others obtained similar results with SAHA in Huntington's mice. Both of these deacetylation inhibitors are being explored for use in cancer therapy and are now also moving toward clinical trials for Huntington's disease.

Mutant Htt may also cause neuronal damage by increasing the activity of certain cell death-related genes, a new study suggests. Evidence has accumulated that the mitochondria, the small structures that produce most of the cell's energy, malfunction in animal Huntington's models and in human patients. In work reported in the 7 July issue of *Neuron*, Akira Sawa, working with Ross, Solomon Snyder, and colleagues at Johns Hopkins University School of Medicine, found that mutant Htt, but not the normal version, binds to a transcription factor called p53. Best known as one of the body's major tumor suppressors, p53 controls several genes, including some affecting mitochondria. Sawa's team found that the increase in p53 activity that occurs when it binds mutant Htt causes an abnormal flow of calcium ions across the mitochondrial membrane, thereby disrupting function of the organelles and leading to nerve cell death.

Sawa and his colleagues also showed that they could prevent the mitochondrial dysfunction by inactivating the *p53* gene in cultured mouse brain neurons carrying a toxic Htt N-terminal fragment. Similar *p53* inactivation suppresses neurodegeneration in Huntington's mice and flies, an indication that it might be another drug target. But Sawa cautions, "*p53* is so important for our life that complete *p53* suppression could be bad for us." Instead, he suggests,

scientists should look for molecules that either block the *p53*-mutant Htt interaction or inhibit the products of the mitochondrial genes activated as a result of that interaction.

A continuing mystery concerns the fact that the medium spiny neurons of the striatum of the brain are the first to degenerate in Huntington's disease. Hayden's team, working with that of Ilya Bezprozvanny at the University of Texas Southwestern Medical Center in Dallas and Lynn Raymond of the

Protective actions lost

Because the huntingtin mutation is dominant—causing disease if only one gene is inherited—researchers have focused mainly on the idea that the mutated protein has gained a toxic function. But recent work suggests that glutamine expansions can also contribute to neurodegeneration by reducing normal Htt's protective effects on neurons.

About a year ago, Frédéric Saudou of the Institut Curie in Paris and his colleagues found that normal Htt is part of the machinery that transports a nerve growth factor called brain-derived neurotrophic factor (BDNF) along their axons. Because of the structural changes caused by the additional glutamines, mutant Htt can't perform this transport function and in fact disrupts normal Htt interaction with the transport machinery.

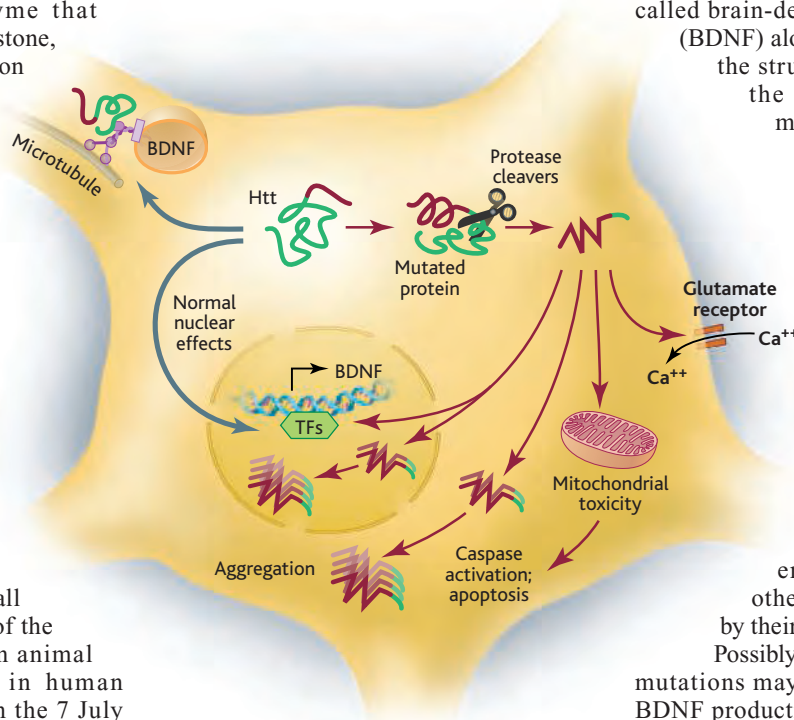
As a result, the neurons lose part of their supply of BDNF, which the cells need to survive. Saudou speculates that this may be one reason that medium spiny neurons are hit first in Huntington's disease. They're especially dependent on BDNF produced by other brain cells and taken up by their axons.

Possibly making matters worse, Htt mutations may also lead to a decline in BDNF production by medium spiny neurons. Elena Cattaneo and her colleagues at the University of Milan, Italy, have found that normal Htt helps turn up the activity of genes encoding BDNF and other proteins needed for neuronal maintenance. As a result, the BDNF supply will be further reduced when Htt is mutated, producing a double whammy for the cells.

If any of these revelations about the causes of Huntington's pathology ever generate effective treatments, they may have to be started early in life. Recent brain imaging studies from Ross's team, including Sarah Reading and Elizabeth Aylward, show that the degeneration in the striatum of the Huntington's brain is visible at least 11 years before a person develops symptoms, usually in their 40s.

Ross notes that this means there is a long time to try to halt the decline before a person gets sick. "What I've found most gratifying is that we've gone from a single gene to multiple possible mechanisms," he says. "Now we need to find which are most important and will lead to therapy."

—JEAN MARX



Many paths. The mutated Htt protein can disrupt neuronal functioning in several ways, some of which are shown in this diagram.

University of British Columbia, produced lab cultures of these neurons from mice carrying a full-length mutant Htt and compared the responses of those neurons to the excitatory neurotransmitter glutamate with those of neurons from normal mice. The modified medium spiny neurons experienced a much greater influx of calcium ions—and died—as a result, the researchers reported in the 15 February *Proceedings of the National Academy of Sciences*.

What's more, Hayden says, these changes occur very early. They were present in neurons studied just after the animals are born—well before disease symptoms develop. Hayden suggests that the receptors through which glutamate exerts its effects are possible targets for Huntington's therapies. In support of that idea, he and his colleagues found that drugs that block their activity suppressed the glutamate-induced death of cultured medium spiny neurons.

RANDOM SAMPLES

Edited by Constance Holden

Buried With Care

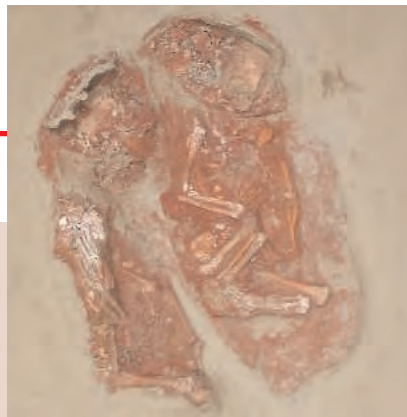
Austrian researchers have uncovered two baby human skeletons buried together at least 27,000 years ago. With red ochre and grave gifts, the site is "clearly ... a deliberate burial connected with a ritual," says lead scientist Christine Neugebauer-Maresch, a paleontologist at the Austrian Academy of Sciences.

In 1999, the academy set out to investigate Paleolithic settlements near the Austrian town of Krems. Extensive excavations hinted at rich settlements in an area where the Krems River flows into the Danube. Last month, the scientists found a thick cultural layer, 5 meters below the surface, harboring artifacts and animal remains including a shoulder blade of a mammoth.

The shoulder blade, supported by a large piece of mammoth ivory, protected a 5-centimeter-deep hollow where the two infants' bodies had been placed side by side covered by red ochre. More than 30 ivory beads were also with the bodies. Both babies' thighbones measured 71 mm, indicating that they were newborns. DNA and tooth-bud analyses may ascertain if they were also twins, says Neugebauer-Maresch.

The remains still need to be carbon-dated, but nearby remains have been dated to 40,000 to 27,000 years old, near the dawn of "modern" human behavior when our ancestors acquired hunting skills, rites, and customs. "This impressive result shows that, in this case, babies were already considered as full members of the glacial group of hunters and gatherers some 27,000 years ago," says Neugebauer-Maresch.

"This is an outstanding discovery that will contribute very much to our understanding of the evolution of human growth in a time when modern humans replaced Neandertals in Europe," says Antonio Rosas González of the National Museum of Natural Sciences in Madrid.



Giant Squid Snapshots

Forget Nessie and Big Foot. For the first time, scientists have captured pictures of a live giant squid (*Architeuthis*), answering some of the mysteries about the world's largest invertebrate.



Last year, in deep water off Japan's coast, a team led by Tsunemi Kubodera, a zoologist at the National Science Museum in Tokyo, suspended a camera, depth meter, light, and a rugged steel lure baited with a common squid and strong-smelling shrimp pulp. On 30 September 2004, enormous tentacles appeared out of the gloom 900 meters below the surface.

The beast is a fast and agile predator. Some scientists had proposed that the giant squid dangles its two longer feeding tentacles passively the way a jellyfish does, but this one grabbed the lure with its feeding tentacles and wrapped them into a ball to bring the lure to its beaked mouth, the team reports in the 28 September issue of the *Proceedings of the Royal Society of London B: Biological Sciences*. The 8-meter squid dragged the apparatus up 300 meters

and then back down again, finally breaking off a hooked tentacle after 4 hours.

"We are only left with a glimpse of the monster and more questions than before," such as which aspects of the apparatus actually attracted the squid, says William Gilly, a marine biologist at Stanford University in Palo Alto, California.

Roots of Hominid Evolution?

What caused the split between the first hominids and early apes 7 million years ago? According to a new hypothesis, the ability to survive on roots might have been the key.

Australopithecus, our earliest known ancestor, appeared in Africa more than 5 million years ago. Its teeth were larger

and thicker than those of modern humans or chimps, and the teeth became even bigger in later species. Such big teeth, with their broad, flat grinding surfaces and thick enamel, are useful for eating tough roots.



Chimp (l), *Australopithecus*, and human (r) teeth. (Inset) Efe pygmies use wild yams as fallback food.

Now, two anthropologists are proposing that this dental adaptation helped lead to the development of hominids, and eventually to modern humans.

In a paper in the October issue of the *Journal of Human Evolution*, Greg Laden of the University of Minnesota, Twin Cities, and Richard Wrangham of Harvard University propose that big teeth allowed australopiths to use roots, tubers, and other "underground storage organs" as fallback foods that kept them alive. This enabled them to leave the forest and spread out onto the savanna, where they could



live on roots when fruits, nuts, or game became scarce.

"I personally think it's one of the better [hypotheses] that we have now," says Leslie C. Aiello, a paleoanthropologist at the

Wenner-Gren Foundation for Anthropological Research in New York City. Modern hunter-gatherers, such as forest-dwelling African pygmies, also tend to use roots as a fallback food to get them through lean times, Laden says.

Edited by Yudhijit Bhattacharjee

FACE-OFFS

Not so fast. Breaking ranks with the Bush Administration and fellow Republicans on the issue of climate change, Senate energy committee chair Pete Domenici (R-NM) announced this summer that he supported capping U.S. greenhouse emissions. But a recent exchange with Senator Dianne Feinstein (D-CA) suggests that Domenici isn't too comfortable with his new allies, either.

Arguing in favor of a cap at a 20 September hearing, Feinstein pointed to research suggesting that global warming could be fueling storms like Hurricane Katrina. Her statement drew the ire of Domenici, who interrupted the next speaker to respond forcefully. "Certainly that's not the consensus opinion," he said. "All I did was quote from a study, Mr. Chairman," Feinstein protested. "I could

have had two of them" saying the opposite, Domenici responded. "Let's proceed."

Got any tips for this page? E-mail people@aaas.org

POLITICS

Cuban conundrum. To vaccine researchers, Vicente Várez-Bencomo is a stellar chemist at the University of Havana whose work on the first synthetic vaccine against *Haemophilus influenzae* type B, a deadly childhood disease, may someday save millions of lives (*Science*, 23 July 2004, pp. 460 and 522). But to the U.S. State Department, the 52-year-old Cuban is an unwelcome visitor whose presence would be "detrimental to the interests of the United States."

Next month, Várez-Bencomo had hoped to pick up an award from the Tech Museum in San Diego, California, and give a plenary lecture at the Society for Glycobiology meeting in Boston, Massachusetts. But that was before the U.S. government denied his visa request.

Várez-Bencomo finds that decision mystifying, because he received a visa earlier this year to attend a chemistry meeting. But his experience is by no means unique. Cuba's Center of Molecular Immunology (CIM), for example, once had no trouble sending five or so scientists a year to U.S. meetings. But since

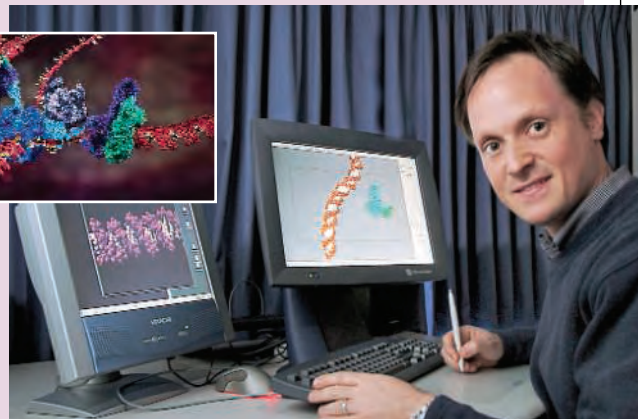
9/11, three-fourths of its visa requests have been denied, says a CIM official, and none of its scientists has been able to attend the American Society of Clinical Oncology annual conferences. The National Academies are looking into the problem, says the National Academy of Sciences' Wendy White.



TWO CULTURES

Animating life. Drew Berry provided the molecular representations for the television documentary *DNA*, which won an Emmy Award on 19 September. Berry, who works for the Walter and Eliza Hall Institute (WEHI), a medical research group in Melbourne, Australia, says he pored over journal articles to ensure that the depictions were accurate. It was hard to keep up: "Every week, papers were coming out that impacted the animation," he says.

Berry's interest in illustrating biological processes began at the University of Melbourne, where he filmed cells using time-lapse microscopy. After receiving a master's degree in cell biology, he left the lab and began working as a graphic artist, doing animations as a hobby. He later impressed WEHI researchers with a depiction of how the malaria-causing parasite invades blood cells. His next project involves a virtual trip through a pancreas cell.



JOB

Zoo's who. A career administrator with a background in conservation management took up his new job last week as director of the Smithsonian Institution's National Zoological Park in Washington, D.C. John Berry, 46, succeeds Lucy Spelman, who left in February 2004 in the wake of high-profile animal deaths and attempts to gut the zoo's conservation research programs (*Science*, 13 April 2001, p. 183).

Berry has been head of the National Fish and Wildlife Foundation, a nonprofit organization that works to protect U.S. native species. He has also been a congressional aide and directed government relations for the Smithsonian.

One challenge facing Berry is to strengthen links between zoo researchers and other Smithsonian scientists. "That has so much potential synergy," says anthropologist Jeremy Sabloff of the University of

Pennsylvania in Philadelphia, who led a 2001–03 review of the Smithsonian's scientific programs. But Kurt Benirschke, a pathologist at the University of California, San Diego, who served on a National Research Council panel that evaluated the zoo last year, thinks that improving research will take a back seat while Berry tackles needed capital repairs.



THEY SAID IT

"Here was the government putting this skinny 60-year-old guy into solitary confinement for nearly a year. I have come to realize that it was wrong, and I should have spoken out more."

—New Mexico Governor Bill Richardson, former energy secretary, on physicist Wen Ho Lee. Lee, then at Los Alamos National Laboratory, pled guilty in 2000 to a single charge of mishandling classified data.

CREDITS (TOP TO BOTTOM): DREW BERRY/WEHI; SMITHSONIAN NATIONAL ZOO; VICENTE VÁREZ-BENCOMO

4. J. F. A. Traniello *et al.*, *Proc. Natl. Acad. Sci. U.S.A.* **99**, 6838 (2002).
5. F. J. Genthner *et al.*, *Appl. Environ. Microbiol.* **58**, 2840 (1992).
6. R. A. Fromtling *et al.*, *J. Am. Vet. Med. Assoc.* **175**, 934 (1979).
7. J. F. Gonzalez-Cabo, *Mycoses* **38**, 167 (1995).
8. J. Lahr *et al.*, *Ecotox. Environ. Safety* **48**, 66 (2001).
9. D. L. Tucker *et al.*, *J. Clin. Microbiol.* **42**, 5412 (2004).
10. M. O. Henke *et al.*, *J. Clin. Microbiol.* **40**, 2698 (2002).

Response

ANY NOVEL ANTIMALARIA TECHNOLOGIES must be subject to rigorous public health cost-benefit evaluations. Given the magnitude of the malaria problem, and our current understanding of these insect pathogens, we are cautiously optimistic that the use of fungal biopesticides for malaria control will not be curtailed by their theoretical potential to impact on human or environmental health in malaria-endemic regions.

Any small protein-based particles can act as allergens. Such aeroallergens are ubiquitous (1). Similarly, common infectious fungal pathogens such as *Aspergillus* spp., *Fusarium* spp., and *Penicillium* spp. (2) are abundant and widespread. It seems unlikely that antimalaria fungal biopesticides would add significantly to this burden. The delivery systems we are investigating use spores formulated in oil. These oil formulations cause the spores to adhere to the substrate on which they are applied and so should not contribute substantially to spore load in the air. We expect the majority of infected mosquitoes to die in the external environment. Studies on the effects of *M. anisopliae* on grasshoppers in Africa indicate that >95% of infected individuals can be preyed upon before they ever have a chance to produce new spores (3). Some mosquitoes may, of course, die in houses, but spores only appear on insect cadavers when ambient relative humidity is very high, and by the time any spores could appear, scavengers such as ants will likely have removed any infected corpses that have evaded routine house cleaning.

Regarding broader environmental impact, possible nontarget species within houses, such as flies and other mosquito species, are frequently nuisance pests and sometimes also associated with health risks. Moreover, contrary to the suggestion of both sets of Letter writers, fungal host range is isolate-specific, not species-specific (4); thus, we as yet know little about host specificity of the individual fungal isolates we are investigating. Furthermore, infection also depends on ecological context. The study on the impacts of *M. anisopliae* on aquatic invertebrates cited by Hutchinson and Cunningham, for example, used a maximum challenge test exposing organisms to high doses of spore powder (of a completely

different isolate) mixed in water with detergent (5). Such an exposure route is of questionable relevance given our intended use strategy.

No interventions are risk-free, and it's important to evaluate what these risks are. Indeed, regulatory frameworks rightly demand it. However, risks should not be viewed in isolation or evaluated without proper appreciation of both the ecological and socioeconomic contexts.

MATT B. THOMAS,^{1*} SIMON BLANFORD,²
NINA E. JENKINS,³ GERRY F. KILLEEN,^{4,5}
BART G. J. KNOLS,^{6,7} ANDREW F. READ,²
ERNST-JAN SCHOLTE,⁷ WILLEM TAKKEN⁷

¹Imperial College London, Wye Campus, Wye, Kent TN25 5AH, UK. ²Institutes of Evolution, Immunology and Infection Research, University of Edinburgh, Edinburgh EH9 3JT, UK. ³CABI Bioscience at Department of Agricultural Sciences, Imperial College London, Wye Campus, Wye, Kent, TN25 5AH, UK. ⁴Ifakara Health Research and Development Centre, Post Office Box 53, Ifakara, Tanzania. ⁵Department of Public Health and Epidemiology, Swiss Tropical Institute, Socinstrasse 57, CH-4002 Basel, Switzerland. ⁶International Atomic Energy Agency (IAEA), A-2444 Seibersdorf, Austria. ⁷Laboratory of Entomology, Wageningen University and Research Centre, Post Office Box 8031, 6700 EH, Wageningen, The Netherlands.

*To whom correspondence should be addressed.
E-mail: m.thomas@imperial.ac.uk

References

1. J. Lacey, in *Pollens and Pollinosis: Current Problems*, R. Spiewak, Ed. (Institute of Agricultural Medicine, Lublin, Poland, 1995), pp. 11–15.
2. M. Ellis, *Mol. Immunol.* **38**, 947 (2001).
3. S. P. Arthurs, M. B. Thomas, J. Langewald, *Biol. Contrib.* **26**, 333 (2003).
4. S. Vestergaard *et al.*, in *Environmental Impacts of Microbial Insecticides*, H. M. T. Hokkanen, A. E. Hajek, Eds. (Kluwer Academic, Dordrecht, Netherlands, 2003), pp. 35–62.
5. J. Lahr *et al.*, *Ecotox. Environ. Safety* **48**, 66 (2001).

Estrogen Receptors and Cell Signaling

THE REPORT BY C. M. REVANKAR ET AL. (“A transmembrane intracellular estrogen receptor mediates rapid cell signaling,” 11 Mar., p. 1625) presents findings that the G protein-coupled receptor GPR30 localizes exclusively to endoplasmic reticulum and binds an estradiol-Alexa dye conjugate. As such, they suggest that it signals so-called estrogen-induced “rapid effects” in estrogen receptor (ER)-negative cells. In the accompanying Perspective (“A new mediator for an old hormone?,” 11 Mar., p. 1572), S. C. Hewitt *et al.* note that there are earlier reports of estrogen-induced GPR30 signaling, but in these studies, GPR30 was localized in the plasma membrane, not the endoplasmic reticulum; other work suggests GPR30-mediated estrogen effects

AAAS Travels

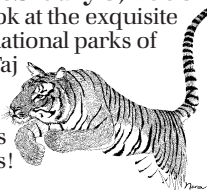
We invite you to travel with AAAS in the coming year. You will discover excellent itineraries and leaders, and congenial groups of like-minded travelers who share a love of learning and discovery.

December 27, 2005– Oaxaca January 2, 2006

Explore the rich cultural heritage from Mexico City to Oaxaca. Visit fascinating archaeological sites.
\$2,495 + air

India Wildlife Safari January 21–February 5, 2006

A magnificent look at the exquisite antiquities and national parks of India, from the Taj Mahal, Agra Fort & Khajuraho Temples to tigers and Sarus cranes!
\$3,595 + air.



Alaska Aurora Borealis March 2-8, 2006

Discover Alaska in winter including 20,320-ft Mt. McKinley. See ice sculptures in Fairbanks and the Aurora Borealis with lectures at the Geophysical Institute.
\$2,495 + air.



Turkey Eclipse Yacht Adventure March 21–April 1, 2006

Explore Greek and Roman sites from Dalaman to Antalya. See the Total Solar Eclipse March 29. \$4,995 + air.

China Feathered Dinosaur March 18–April 5, 2006

Explore highlights of Beijing, Xian and cruise the Yangtze River, plus the world's finest fossil sites of feathered dinosaurs, the species at the transition from reptile to bird.
\$5,990 + air.



Aegean Odyssey May 24–June 7, 2006

Our classic adventure to explore the history of Western Civilization in Athens, Delphi, Delos, Santorini, & Knossos.
\$3,695 plus 2-for-1 air + tax from JFK.



Call for trip brochures &
the Expedition Calendar
(800) 252-4910

AAAS Travels

17050 Montebello Road
Cupertino, California 95014
Email: AAASinfo@betchartexpeditions.com

LETTERS

but at μM levels of hormone (1), not the nM levels seen by Revankar *et al.* Further, the GPR30 gene may not be expressed in most ER-negative breast cancers (2). Also, Ahola *et al.* (3) find that estrogen induces growth in cells treated with GPR30 anti-sense oligonucleotides, indicating that GPR30 is not required for this action. The PI3K assay used by Revankar *et al.* addresses PIP3 accumulation in nuclei, but it is not clear if this means PI3K is activated at the plasma membrane by GRP30. There is no report of high-affinity, saturable estrogen binding to the endoplasmic reticulum. Another difficulty is the plethora of ER forms; some cells once considered ER-negative express ER β or variant ERs. Also, the biological significance of estrogen signaling in ER-negative breast cancers is unknown. Clinical findings on treatment of breast cancer patients show significant benefit of hormonal therapy in those with ER-positive tumors, but little in those with ER-negative tumors (4). Evidence suggests that ER associates with the plasma membrane and is required for rapid responses to estradiol (5, 6). No proof has yet been provided that GPR30 is relevant to estrogen action in ER-positive breast cancer. A role for GPR30 in cellular actions of estrogen, as emphasized by Revankar *et al.* in ER-negative breast cancer cells, remains to be demonstrated.

RICHARD J. PIETRAS,^{1*} ELLIS R. LEVIN,²
CLARA M. SZEGO³

¹Department of Medicine-Hematology/Oncology and Jonsson Comprehensive Cancer Center, University of California, Los Angeles School of Medicine, Los Angeles, CA 90095-1678, USA.

²Departments of Medicine, Biochemistry and Pharmacology, University of California, Irvine School of Medicine, Irvine, CA 92717, USA.

³Department of Molecular, Cell & Developmental Biology and Molecular Biology Institute, University of California, Los Angeles, Los Angeles, CA 90095-1606, USA.

*To whom correspondence should be addressed.
E-mail: rpietras@ucla.edu

References

1. M. Maggolini *et al.*, *J. Biol. Chem.* **279**, 27008 (2004).
2. C. Carmeci *et al.*, *Genomics* **45**, 607 (1997).
3. T. Ahola *et al.*, *Endocrinology* **143**, 3376 (2002).
4. Early Breast Cancer Trialists' Collaborative Group, *Lancet* **351**, 1451 (1998).
5. R. Pietras *et al.*, *Endocrine* **14**, 417 (2001).
6. E. Levin, *Mol. Endocrinol.* **19**, 1951 (2005).

Response

PIETRAS *ET AL.* SUGGEST THAT IN EARLIER reports of estrogen-induced signaling, GPR30 was shown to localize to the plasma membrane. However, the original description of GPR30 function (1) did not examine the receptor's localization; rather, it was assumed that it would be expressed in the plasma membrane. Furthermore, an

additional study (2) provided no markers by which to establish the subcellular localization of the diffuse cellular GPR30 staining. The use of membrane preparations, at times designated as plasma membranes, for binding and functional assays must also be viewed in light of the fact that the preparations were either crude (3) or at best enriched with marker distributions not presented to demonstrate purity (2). Our conclusion that GPR30 is expressed in the endoplasmic reticulum is supported by multiple independent approaches. Pietras and colleagues infer that other work (4) suggests that GPR30-mediated estrogen effects occur only at μM and not nM concentrations of estrogen. Robust GPR30-dependent cellular responses at 1 nM estradiol have been demonstrated [(1, 5–7); our Report]. In addition, the selectivity of 17β -estradiol over 17α -estradiol has been shown to be in excess of 10^3 to 10^4 [(2); our Report], revealing high selectivity for the physiological isomer of estradiol. Pietras *et al.* question whether the nuclear PIP3 accumulation is due to PI3K activation—our data demonstrate the de novo synthesis of PIP3 by PI3K. With respect to estradiol binding capacity, we demonstrated that binding of estradiol-Alexa633 to GPR30 is essentially equimolar with binding to ER α and ER β (Fig. 2E). Finally, competition binding studies with 17β -estradiol demonstrated a K_i of ~ 6 nM, within twofold the value recently reported by others using tritiated estradiol (2).

As Pietras *et al.* point out, some cells previously considered ER-negative may express ER β or other ER variants. For these reasons, we expressed GPR30 in cells that are otherwise unresponsive to estrogen stimulation and in addition, we depleted GPR30 in cells expressing endogenous GPR30 to confirm that the only estrogen-responsive receptor in the cells is GPR30. We agree that recent evidence suggests that the classical ER can associate with the plasma membrane and initiate rapid signaling, confirming the multiple mechanisms through which the classical estrogen receptor is likely to mediate the effects of this hormone. Such results, however, do not exclude a possible role for GPR30 in estrogen biology.

ERIC R. PROSSNITZ,^{1,2*} CHETANA M. REVANKAR,^{1,2}
JEFFREY B. ARTERBURN,⁴ LARRY A. SKLAR^{2,3}

1Department of Cell Biology and Physiology, 2Cancer Research and Treatment Center, 3Department of Pathology, University of New Mexico Health Sciences Center, Albuquerque, NM 87131, USA. 4Department of Chemistry and

Biochemistry, New Mexico State University, Las Cruces, NM 88003, USA.

*To whom correspondence should be addressed.

E-mail: eprossnitz@salud.unm.edu

References

1. E. J. Filardo, J. A. Quinn, K. I. Bland, A. R. Frackelton Jr., *Mol. Endocrinol.* **14**, 1649 (2000).
2. P. Thomas, Y. Pang, E. J. Filardo, J. Dong, *Endocrinology* **146**, 624 (2005).
3. E. J. Filardo, J. A. Quinn, A. R. Frackelton Jr., K. I. Bland, *Mol. Endocrinol.* **16**, 70 (2002).
4. M. Maggiolini *et al.*, *J. Biol. Chem.* **279**, 27008 (2004).
5. N. Kanda, S. Watanabe, *J. Invest. Dermatol.* **121**, 771 (2003).
6. N. Kanda, S. Watanabe, *J. Invest. Dermatol.* **121**, 1500 (2003).
7. N. Kanda, S. Watanabe, *J. Invest. Dermatol.* **123**, 319 (2004).

What Should We Call Pluto?

THE DISCOVERY OF 2003 UB313, AN OBJECT that is larger than and farther away from the sun than Pluto, has reopened the question of what is a planet (“Newfound ‘tenth planet’ puts Pluto behind the eight ball,” R. A. Kerr, *News of the Week*, 5 Aug., p. 859). The International Astronomical Union (IAU) has suggested the idea of calling both Pluto and the new object “Trans-Neptunian planets” (TNPs), including planet in the name but with a qualifier. This proposal is worth a try, but it raises some problems. Pluto, UB313, and other similar

bodies must be named as asteroids exclusively, not only because they are different from the other eight planets, but because of their similarity in origin, size, composition, and orbital parameters to hundreds of thousands of small rocky objects orbiting the sun at more than 30 AU, in a region called the Edgeworth-Kuiper Belt. If the term “planet” is still included in the name, then we could

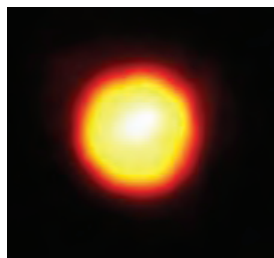


Image of Pluto taken by the European Space Agency's Faint Object Camera on 21 February 1994, when Pluto was 4.4 billion km from Earth.

have hundreds of this new kind of planet in the solar system in the future. If TNPs are a class roughly defined as “large objects that orbit the sun beyond Neptune,” what will be the name of similar small rocky objects that will eventually be discovered orbiting in the outer regions of stellar systems other than ours?

In planetary science, the tools for examining our cosmic neighborhood continue to be refined and extended, and so we are beginning to appreciate that the richness of our stellar system is much greater than it appeared to earlier explorers and name-givers, demanding revisions of

Power for your business



Hannover, 18–20 October 2005

Get your business moving by making the right contacts. BIOTECHNICA, the leading international trade fair for biotechnology, is the fast track to valuable business contacts. Europe's no. 1 showcase for the entire spectrum of life-science industries is a platform for applications in the food industry, agriculture, medicine/pharmaceuticals and the environment. An extensive supporting programme includes special presentations, conferences, congresses and seminars, plus the European BIOTECHNICA Award and the high-calibre international **Partnering Forum**, which makes its debut this year. For 1,000 exhibitors from Europe, Asia and the USA as well as for 13,000 visitors from all over the world, this event is a great opportunity to make new contacts and strengthen business. So don't get left behind! Register now at

www.biotechnica.de

BIOTECHNICA 2005

14th INTERNATIONAL TRADE FAIR FOR BIOTECHNOLOGY

For further information:

Deutsche Messe AG • Hannover, Germany
Phone: +49-511/89-321 28/36 • info@biotechnica.de

Travel, accommodation and admission tickets:

Travel2Fairs GmbH, Hannover, Germany
Phone: +49-511/33 64 45 10 • info@travel2fairs.com
www.travel2fairs.com

VIVASCIENCE
sartorius group

Adenovirus Purification
in only 2 hours

NEW

Vivapure®
AdenoPACK™ 500

Purification of up to
 3×10^{13} adenovirus
particles from
500 ml cell culture

Kits available for in-vitro
and small scale in-vivo
use

patented membrane
adsorber technology

Register for
15% discount!
www.vivascience.com/virus



Contact Vivascience

International	+49 511 524 875 60
Europe	+49 1802 84 82 01
USA	+1 877 452 2345
Email	info@vivascience.com
Web	www.vivascience.com

LETTERS

which Pluto is an excellent example. As Confucius said, "The beginning of wisdom is to call things by their right name."

ALBERTO G. FAIRÉN

Centro de Biología Molecular, Universidad Autónoma de Madrid, Facultad de Biología, Laboratorio C-101, Cantoblanco-Madrid 28049, Spain.

CORRECTIONS AND CLARIFICATIONS

Table of Contents: (2 Sept., p. 1447). The Brevia "Major biocontrol of plant tumors targets tRNA synthetase" by J. S. Reader *et al.* should have been listed with the overline of microbiology, and the one-sentence summary should have read, "A biocontrol agent for crown gall tumors acts by inactivating the transfer RNA synthetase for leucine, an approach that might be useful in targeting other plant diseases."

Reports: "Cladosporium Avr2 inhibits tomato Rcr3 protease required for Cf-2-dependent disease resistance" by H. C. E. Rooney *et al.* (17 June, p. 1783). Reference (28) was cited three times in the Fig. 1 legend, once in the Fig. 2 legend, and once in the Fig. 3 legend. All of these citations should have referred to reference (29), the Materials and Methods section of the Supporting Online Material. In addition, on p. 1786, *Pseudomonas syringae* p. *maculicola* should be *Pseudomonas syringae* pv. *maculicola*. The correct sentence should read, "In the case of RPM1- and RPS2-mediated resistance in *Arabidopsis*, the action of the Avr proteins AvrB, AvrRpm1, and AvrRpt2 on the guard cell RIN4 is thought to trigger the activation of the RPM1 (resistance to *Pseudomonas syringae* pv. *maculicola* expressing AvrRpm1) or RPS2 (resistance to *Pseudomonas syringae* pv. *tomato* expressing AvrRpt2) proteins (24–27)."

Reports: "The effects of artificial selection on the maize genome" by S. I. Wright *et al.* (27 May, p. 1310). In the first full paragraph of the third column on page 1312, the value of the likelihood ratio (LR) is incorrect. The sentence should read, "The LR provides statistically significant support for the presence of two gene classes (LR = 6.35, df = 2, $P < 0.05$)." This correction does not modify the results or the conclusions in any way. In addition, in the first column of page 1313, the LR statistic should read "(LR = 4.6, df = 2, $P = 0.10$, $\hat{k}_1 = 2.45$, $\hat{k}_2 = 0.001$)." With this correction, statistical support for the selection model with the reduced data set is borderline significant. However, the author's best estimate of f based on the reduced data remains 3.6%, and this correction does not substantially modify the results or the interpretation, since statistical support for selection was obtained from the full data set.

Letters to the Editor

Letters (~300 words) discuss material published in *Science* in the previous 6 months or issues of general interest. They can be submitted through the Web (www.submit2science.org) or by regular mail (1200 New York Ave., NW, Washington, DC 20005, USA). Letters are not acknowledged upon receipt, nor are authors generally consulted before publication. Whether published in full or in part, letters are subject to editing for clarity and space.

GEOSCIENCE

After the Earth Shook

Susan E. Hough

That *The Crack at the Edge of the World* is not in any simple sense of the phrase a “book about an earthquake” will not surprise readers familiar with Simon Winchester’s earlier works, such as *Krakatoa (1)*. More than half the book passes before the best-selling author begins substantive discussion of the 1906 San Francisco earthquake. Fundamentally, the story he tells is one of history rather than science: the history of the West in general and of San Francisco in particular, and the role of the 1906 earthquake in shaping that history.

To the task of presenting this tale, Winchester brings not only his formidable story-telling talents and his passion for history but also solid earth science credentials: an undergraduate degree in geology from Oxford University. Thus his treatment of history begins not with the earliest Spanish explorers or even with the earliest human inhabitants who presumably wandered in over the Bering Strait, but at the time when continents first coalesced out of the planetary stew. Along the way he explains how the present-day continents came to be; how supercontinents formed, broke apart, and formed again. The narrative journey across present-day North America follows Winchester’s own journey east to west, with stops along the way at several must-see attractions for any self-respecting geotourist, such as New Madrid, Missouri, and Yellowstone’s Old Faithful geyser. The book covers substantial ground scientifically as well as geographically, yet remains eminently readable and enjoyable.

Seismologists who read the book looking for nits to pick will find a handful, including the statement that the New Madrid seismic zone is an incipient (rather than a failed) rift, and a bit too much sympathy for the enduring myth that animals are sensitive to impending earthquakes. Given the sweeping scope of the book, I suspect that scholars in other fields may find additional inaccuracies. But the merit

The reviewer is at the U.S. Geological Survey, 525 South Wilson Avenue, Pasadena, CA 91106, USA. E-mail: hough@usgs.gov

**A Crack in the Edge of the World
America and the
Great California
Earthquake of 1906**
by Simon Winchester

HarperCollins, New York, 2005. 478 pp. \$27.95, C\$37.95. ISBN 0-06-057199-3.

**A Crack in the Edge of the World
The Great American
Earthquake of 1906**

Viking, London, 2005. £16.99. ISBN 0-670-91487-8.

of books like this is not that they teach science to scientists nor that they provide a detailed science education to nonscientists. Rather, the contribution of such books is that, by taking the reader on a grand and accessible adventure, writers like Winchester can make science palatable—even attractive—to readers who would never pick up even those more focused books on science that scientists would consider nontechnical.

Winchester’s latest offering is not only readable but also thought-provoking. After discussing in some detail the immediate response to the 1906 earthquake and subsequent

rebuilding efforts, he moves on to draw more sweeping conclusions about the long-term impact of the disaster. Winchester argues that the earthquake played a critical role in the emergence of the Pentecostal movement. He also concludes that the 1906 quake—and geological exigency more generally—caused San Francisco to cede its early stature as economic and cultural capital of the West to Los Angeles, where devastating earthquakes are (supposedly) less common.

The extent to which the earthquake provided a catalyst for the Pentecostal movement is debatable. The key hallmarks of Pentecostal faith, including charismata (speaking in tongues), have roots extending back at least into the late 18th century. Although the movement gained substantial momentum in the southern California town of Azusa in 1906, its growth was well under way by April 18. Nine days before the earthquake, the church had attracted enough followers for leaders to rent and start to fill a warehouse building in which the Apostolic Faith mission was born. And even though great earthquakes are known to strike terror in the hearts of sinners, as a rule this effect tends to be short-lived.

The role of the earthquake in shaping San Francisco’s fate is probably even more contentious. Many will balk at the notion that the city ever ceded anything to anyone.

Winchester laments that a proper San Francisco school of architecture never had a chance to develop because the city was patched back together so hastily in the aftermath of the earthquake. Yet, modern urban woes such as homelessness and AIDS notwithstanding, many regard San Francisco as one of America’s most livable, attractive, and romantic cities. If San Francisco’s growth has been checked, the earth scientist is tempted to blame geography rather than geology: compared to Los Angeles the city faced notably non-negotiable boundary conditions. Nonetheless, cities evolve into megacities, and even a confirmed Angeleno is hard-pressed to question the continuing economic and cultural importance of the powerhouse that is the modern greater San Francisco Bay Area. The city that was reduced to ashes 100 years ago grew into the metropolitan area that gave the world Silicon Valley.

Winchester concludes that human beings and their cities exist only by the sometimes ephemeral consent of a dynamic planet. Yet he also admits that great cities endure great tragedies, rebounding from hardship by virtue of the strategic amenities that led to



Shaken and burned. The U.S. Geological Survey described San Francisco’s City Hall as “a monument of bad design and poor materials and workmanship” (2).

their becoming great cities in the first place. Perhaps he underestimates another factor: the capacity for not only Earth but also its human inhabitants to rebound. (Cities do not rebuild themselves.)

Reasonable, informed people can debate such matters. And here we arrive at the other important contribution of books such as *A Crack in the Edge of the World*. Not only do they deliver science to a broad audience, but they can also bring a broader world to scientists. Whether or not we agree with Winchester’s conclusions, there is value as well as fun in going along for the ride.

CREDIT: BEAR PHOTO COLLECTION/COURTESY NATIONAL INFORMATION SERVICE FOR EARTHQUAKE ENGINEERING, UNIVERSITY OF CALIFORNIA, BERKELEY

References and Notes

1. S. Winchester, *Krakatoa: The Day the World Exploded: August 27, 1883* (Viking, London, 2003). [Reviewed by T. Simkin, R. S. Fiske, *Science* **301**, 50 (2003).]
2. G. K. Gilbert et al., *The San Francisco Earthquake and Fire of April 18, 1906, and Their Effects on Structures and Structural Materials* (U.S. Geological Survey, Washington, DC, 1907).

10.1126/science.1118551

SCIENCE AND POLITICS

Anti-Realism in Government

Naomi Oreskes

In the mid-1990s, a group of scientists led by Paul Gross and Norman Levitt made a grand fuss about attacks on science from the “academic left.” Most of these attacks originated in France and were linked to the philosophical question of how well human-constructed theories can map onto human-independent reality, an academic anxiety if ever there was one. But while Gross and his friends engaged in academic internecine warfare over postmodernist theory, a far more serious attack on science was building on the political right here in the United States, with serious consequences beyond the walls of academe. This attack is the subject of journalist Chris Mooney’s *The Republican War on Science*.

As Mooney recounts, for two decades, influential Republicans—initially in Congress and now also in the White House—in concert with determined allies in private industry and fundamentalist Christian organizations, have systematically denied, disparaged, and misrepresented scientific information on topics relevant to public policy. The list is long: acid rain, global warming, the efficacy of condoms in preventing the spread of sexually transmitted diseases, the health impacts of excess dietary sugar and fat, the alleged link between abortion and breast cancer, the status of endangered species, the efficacy of abstinence-only sex education programs, the therapeutic potential of adult stem cells, and more.

On these issues, a strange-bedfellows alliance has sought to mislead both the voting public and elected representatives about the scientific facts: misrepresenting real debates, exaggerating uncertainty, interfering with the activities of expert agencies, trumpeting the views of outlier scientists whose interpretations are rarely to be found

The reviewer is in the Department of History, University of California, San Diego, 9500 Gilman Drive, La Jolla, CA 92093-0104, USA. E-mail: noreskes@ucsd.edu

in the refereed literature, and attacking the integrity of genuine experts (1). In frighteningly Orwellian fashion, these actions are carried out in the name of “sound science.”

Much of this will be familiar to those who read the 2003 report prepared for California Congressman Henry Waxman, “Politics and Science in the Bush Administration” (2), or the 2004 report of the Union of Concerned Scientists, “Scientific Integrity in Policy-making: An Investigation into the Bush Administration’s Misuse of Science” (3). But Mooney goes further, documenting the roots of these abuses in the Reagan administration and the Congress of Newt Gingrich. Historically, Republicans have often been more sympathetic to scientific elites than populist-oriented Democrats, but the animus growing over the past 20 years has culminated in the present administration, which, being unable to control science, seems determined to undermine it.

Mooney points out that in many cases, the same groups and individuals have been involved in multiple misinformation campaigns. Consider global warming and ozone depletion. Two leading deniers of the reality or severity of anthropogenic global warming—S. Fred Singer and Sallie Baliunas—previously vociferously denied the link between chlorofluorocarbons (CFCs) and depletion of stratospheric ozone. Although his views lie well outside the mainstream of expert scientific opinion and it has been a long time since he regularly published in the refereed literature, Singer has been repeatedly invited to testify in Congress. Both he and Baliunas have links to the George C. Marshall Institute, founded in 1984 to defend Ronald Reagan’s Strategic Defense Initiative against the majority opinion of expert physicists that it was ill-conceived. Since then, the institute has claimed to support “sound science” in public policy while promoting positions that run against the mainstream of scientific opinion but are consistent with an uncompromisingly anti-regulatory ideology. In recent years, it has received funding from ExxonMobil, presumably not coincidentally linked to its efforts to deny global warming (4). The plot thickens further. One of the institute’s founders and its current chairman of the board, Robert Jastrow, has written books promoting intelligent design (5–7). Frederick Seitz, its chair emeritus, is well known in the scientific community as a past president of the National Academy of Sciences. Less well known is his role in the 1980s as a principal adviser to the R. J. Reynolds Tobacco Company in its support of biomedical research that might cast doubt on the links between tobacco and cancer (8).

The Republican War on Science

by Chris Mooney

Basic Books, New York, 2005. 338 pp. \$24.95, C\$32.95. ISBN 0-465-04675-4.

How are denials of global warming, the impact of CFCs on stratospheric ozone, and the link between tobacco and cancer; support of missile defense; and advocacy of creationism related? On the face of it, scarcely. But they all involve the promotion of a right-wing political agenda, and they all involve grotesque misrepresentations of scientific evidence. “Doubt is our product” was the slogan of an internal memorandum from the Brown and Williamson Corporation as it set out to deny the scientific evidence linking smoking to cancer well after

the epidemiological evidence was clear, and the same strategy underlines anti-scientific campaigns today (9, 10). The connections Mooney discusses are crucial, because they provide proof that these actions are politically and economically motivated, rather than based on principled scientific worries.

The same people are repeatedly involved in the same obfuscations.

Scientists have traditionally been loath to foray into politics for fear of politicizing science, but Mooney’s book makes it clear that when sensible people stand on the sidelines, a great deal of nonsense can be spread. Scientists and scientific societies have tried in recent years to correct misrepresentations and clarify misunderstandings, but the efforts have been too few and far between. Those who would attack science for political gain are organized, persistent, and well-financed. *The Republican War on Science* makes clear that scientists need to do more to present their knowledge to the rest of society, because there is no shortage of people willing to misrepresent it.

References and Notes

1. To these activities documented by Mooney, add the harassment of researchers by punitive demands for documentation of work already published in peer-reviewed journals. See Donald Kennedy’s Editorial, *Science* **309**, 1301 (26 August 2005).
2. http://democrats.reform.house.gov/features/politics_and_science/pdfs/pdf_politics_and_science_rep.pdf.
3. www.ucsusa.org/scientific_integrity/interference/reports-scientific-integrity-in-policy-making.html.
4. ExxonMobil’s contributions to the Marshall Institute are documented in their annual reports. See www.exxonsecrets.org/html/orgfactsheet.php?id=36 or www.environmentaldefense.org/article.cfm?contentid=3804&CFID=21084385&CFTOKEN=29888831.
5. R. Jastrow, *God and the Astronomers* (Norton, New York, 1978).
6. R. Jastrow, *The Enchanted Loom: The Mind in the Universe* (Simon and Schuster, New York, 1981).
7. www.godandscience.org/love/sld014.html.
8. S. A. Glantz, J. Slade, L. A. Bero, P. Hanauer, D. E. Barnes, Eds., *The Cigarette Papers* (Univ. California Press, Berkeley, CA, 1996).
9. D. Michaels, *Sci. Am.* **292**, 96 (June 2005).
10. On the misrepresentation of science in legal and regulatory settings, see also *Am. J. Public Health (Suppl.)* **95**, S1–S150 (2005).

10.1126/science.1115765

Mangroves, Fishponds, and the Quest for Sustainability

Jurgenne H. Primavera

As I write on this late June afternoon, my heart grieves amid news that a young couple, dearly loved former research colleagues living in the north of Panay Island in the Philippines where I work, had been shot over a fishpond dispute. The owner, it seems, did not want them to use a shortcut on his property that led to the pond the couple was renting from him. Bullets shattered the jaw, collarbone, and colon of the husband, a marine biologist who miraculously survived, but they proved fatal to his wife, an aquaculture nutritionist and university instructor.

The incident takes me back decades to my home island of Mindanao when rifle bullets strafed our campus cottage during a short-lived rebellion. My family and a neighbor crouched inside the bathroom, while the battle between rebels and government soldiers raged for 4 long hours. The growing insurgency forced me to give up my teaching job at Mindanao State University and flee to the quiet of the Visayas, in the central Philippines, where I accepted a research position with the Aquaculture Department of the Southeast Asian Fisheries Development Center (SEAFDEC/AQD).

Fast forward to the present, to another potential conflict elsewhere in northern Panay. This one is centered on the small-scale cutting

of trees in and near a magnificent mangrove stand of *Avicennia rumphiana* trees, some of them up to 8 m in circumference. This location has been among our study sites since 1997. But to make an official complaint would place my colleagues and me in harm's way from those who earn income by planting the cleared area with *Nypa* palm or converting it to ponds.

This yearlong essay series celebrates 125 years of *Science* by inviting researchers from around the world to provide a regional view of the scientific enterprise. Series editor, Ivan Amato

Troubles like these come with the mission of protecting the world's mangroves—the lushly forested environmental buffer zones by which the sea meets land in so many places around the world—even as these areas become ever more exploited for aquaculture and other uses. It is a mission that teeters on the always-difficult negotiation by which ecological and environmental goals, on the one hand, and economic, social, and immediate human needs, on the other, are adjudicated.

I have observed this difficult dynamic firsthand since the mid-1970s when the field of aquaculture, the farming of aquatic and marine plants and animals, was getting started. Indeed, my first studies in this area—on the growth and survival of shrimp in earthen ponds and production of breeders for hatcheries—contributed to the foundation on which increasingly efficient shrimp farming developed, so often, as it has turned out, to

the detriment of mangrove habitats.

Mangroves at Risk

Aquaculture ranks as a phenomenal success story in global food production. In 1975, when I joined the SEAFDEC/AQD, aquaculture contributed 8% to the overall yield of the world's fish harvest; now it provides more than one-third of the yield of the world's fisheries. Total aquaculture production in 2003 was 54.8 million metric tons, valued at \$67.3 billion in U.S. dollars. More than 90% of this output comes from Asia, where aquaculture has its origins.

As with land-based agriculture, all of this aquatic food production and economic activity has come with environmental problems and social conflicts. Foremost among these is the loss or modification of habitat in places where aquafarmers clear mangroves for ponds and where they install cages or pens above seagrass beds and coral reefs. Other environmental effects include the loss of bycatch (unwanted fish and invertebrate species) during the collection of wild “seed” used for stocking in ponds and of adult broodstock for hatcheries, introduction of exotic species, spread of parasites and diseases, interactions of escapees from ponds or pens with wild populations, misuse of chemicals and antibiotics, salinization of soil and water, and coastal pollution. Many of these ecological impacts of shrimp aquaculture have brought



Jurgenne H. Primavera
Philippines

Jurgenne H. Primavera, senior scientist of the Aquaculture Department of the Southeast Asian Fisheries Development Center based in Iloilo, central Philippines, for more than two decades has been a tireless champion of replacing unsustainable aquaculture practices with sustainable ones. In her early research career, in the 1970s, her studies of the early phases of the shrimp life cycle contributed to aquaculture know-how and practice, enabling this food-producing strategy to flourish in the world's mangrove areas, including some in her own country. As she learned first-hand about the environmental and socioeconomic perils that poorly managed and overextended aquaculture can bring, she began to investigate and develop mangrove-friendly aquafarming methods in order to move toward a sustainable industry that provides food and jobs while also preserving the environment. Trained in zoology and marine science, Primavera has published and lectured extensively on aquaculture and mangrove issues. Among her numerous awards and honors are her induction as a foreign member into the Swedish Royal Academy of Agriculture and Forestry and an honorary doctoral degree from Stockholm University. Earlier this year, she was chosen as a Pew Fellow in that organization's program in marine conservation.

All essays and interactive features appearing in this series can be found online at www.sciencemag.org/sciext/globalvoices/



along social problems, among them privatization of public lands and waterways, the decline of open-sea fisheries, rural unemployment, and social disruption.

Even the seemingly reasonable assumption that aquaculture is an efficient way to produce new protein is undermined by the dependence of shrimp, salmon, and other cultured aquatic carnivores on raw fish and on fish meal and oil in pelleted feeds. Careful calculations indicate that some cultured species actually are net consumers of fish.

In the 1980s, I began to ring warning bells about the perils of runaway shrimp farming.



Vanishing mangroves. The expanse of fish and shrimp pens in the foreground of this aerial view of Dagupan in the Philippine province of Pangasinan used to be filled with mangroves.

At the time, aquaculture was perceived as the coming Blue Revolution that would help solve world hunger, provide jobs, and fight poverty. Because of my cautionary views, I became marginalized in aquaculture circles. At some meetings I was ostracized and my research papers sometimes seemed harder to get through editorial decision-makers than the reviewers' comments would have suggested. Even so, other researchers would subsequently confirm my conclusions on, for example, the boom-and-bust nature of unplanned and poorly managed shrimp culture. And in recent years, momentum to develop sustainable aquaculture practices has been building.

For my part, I have received invitations from foreign groups, including the Global Wetlands Economics Network and the International Foundation for Science, to expose the plight of mangroves and share my ideas about aquaculture sustainability. At times, I have done so in high-profile media outlets, such as a BBC documentary in 2002. Although I had always been confident that even my early alarmist attitude was justified, I received my final peer vindication last year when Stockholm University presented me with a Ph.D. in science *honoris causa* for showing "... that mangroves are key areas for

recruitment of fish and shrimp and that development of conventional shrimp farming may have far-reaching negative economic and social implications... ?

For greater sustainability, the aquaculture industry must acknowledge its interdependence with fisheries and other stakeholders. Ecologically damaging practices need to be replaced with ecologically sound ones, such as locating culture ponds outside mangroves where possible, using native species whose inevitable escapes into nearby waters would be relatively innocuous, and stocking hatchery fry rather than wild seed whose collection entails the loss of bycatch.

Because surrounding waterways can be the source as well as recipient of contaminants and pathogens, systems of low water exchange between ponds and the surrounding environment can minimize such risks. Levels of suspended solids or sediment are reduced if pipes that provide aeration are set on the pond bottom, rather than on the surface, and also by means of settling ponds. Water quality can be maintained with natural biofilters such as clams and other bivalves. Probiotics are commercial suspensions of appropriate types of bacteria added to the pond that operate on the principle of competitive exclusion (of harmful bacteria). The so-called greenwater technique enhances shrimp growth and survival by means of a combination of phytoplankton and the presence of herbivorous fish in the pond. Finally, lower stocking densities of shrimp and their polyculture with suitable fish species can minimize waste levels and produce synergistic benefits.

Already, the culture of seaweeds and fish in cages in subtidal bays and rivers is compatible with adjoining mangroves and suitable for family-level operations.

But there remains a need for mangrove-friendly aquaculture technology in intertidal forests, in which mangrove trees spend high tides with their roots submerged and low tides with their roots exposed. That's why one of my current projects, funded by the European Commission, is to develop sustainable so-called aquasilviculture. An approach I have developed, which combines the rearing of mud crabs inside

intertidal pen enclosures, has been replicated by local people's organizations in the Philippines. Meanwhile, several studies have shown that mangrove estuaries can process nutrients, such as those from fertilizers, in aquaculture pond effluents at least over short spatial and temporal scales. That opens up the possibilities of integrating intensive aquaculture with natural or constructed mangrove wetlands in a way that could be sustainable through careful management and planning.

A Menagerie of Mangroves

My earliest training was in zoology, and when I began studying the taxonomy of mangroves, I found the diversity of these habitats challenging. On a trip to the Mai Po, Hong Kong, mangroves in 1993, experts from Thailand and Vietnam effortlessly called off the scientific names of mangrove species—*Avicennia marina*, *Kandelia candel*, *Aegiceras corniculatum*, etc. Feeling ignorant, I vowed to master the Indo-Pacific species of mangroves. Indeed it took me 10 years to write and publish, with UNESCO support, the *Handbook of Mangroves in the Philippines—Panay*, which came out last year. The diversity of mangroves and their wide distribution in the archipelago in the past are reflected in the names of many coastal towns and villages. The name of the country's premier city, Manila, derives from *Maynilad*, meaning there is *nilad*, referring to the mangrove *Scyphiphora hydrophyllacea*, which grew profusely along Manila Bay in pre-Hispanic times.

Mangroves, seagrass beds, and coral reefs bordering the 7150 Philippine islands have contributed appreciably to the livelihood and well-being of coastal communities over the centuries through their provision of various goods and services. Foremost among mangrove products are fish, shellfish, and other invertebrates that provide the most available and inexpensive protein in the Filipino diet. Other natural benefits afforded by mangroves include coastal protection, erosion control, sediment trapping, and recycling of nutrients from terrestrial run-off and river discharges.

Latest estimates, as of 2000, have placed the global coverage of mangroves at 15 million hectares (ha), a drastic decline from 18 million ha in the 1990s. The losses have been particularly heavy in Southeast Asia, which hosts a third of total mangrove area. The anthropogenic causes of such losses



Water world. Boys swim in this creek by a healthy intertidal mangrove during high tide.

include overexploitation of mangroves and conversion of mangroves to settlements, rice fields, salt beds, tourist resorts, and industrial facilities. But brackishwater pond culture, which dates back to 1400 in Java, has also taken its toll. Many thousands of hectares of culture ponds in the Philippines and Indonesia were carved out of mangrove swamps because these habitats were considered ideal for growing milkfish (*Chanos chanos*), a food fish favored by local people. Around half of the 279,000 ha of Philippine mangroves that disappeared between 1951 and 1988 were converted into ponds mainly for milkfish, but also for shrimp.

Aggressive mangrove and wetlands development became national policy in the Philippines in the 1950s. Some of these policies supported aquaculture development by enforcing a form of rent control on the mangroves. The original fee for leasing a pond was PhP50, or about \$2/ha per year. This fee was way out of line with the estimated values of \$538/ha per year and \$42 to \$156/ha per year, respectively, for fish and wood harvests from Philippine mangroves. By underpricing the rights to harvest public forests and by not penalizing low pond productivity, these policies and practices encouraged rampant conversion of mangroves to aquaculture ponds.

Both a 1991 decree and one in 1992 mandated an increase in the rental to PhP1000, or about \$20/ha per year, but its implementation was delayed indefinitely on both occasions by a strong fishpond industry lobby. In the past 2 years, the government presented a series of expert witnesses, including myself, who cited published valuations from the mangrove literature and aquaculture studies of mangroves and fishponds to justify the pond rental increase. The court is expected to rule within the year.

Actually, numerous laws, decrees, and ordinances aim to protect remaining mangrove areas. These include guidelines for mangrove-pond conversion and reversion of abandoned ponds to forest. Ownership policies, such as the Mangrove Stewardship Agreement that legitimizes de facto claims of local communities over coastal resources, improve the success rate of replanting programs. Even so, coordination is lacking between the national forestry and fisheries agencies tasked to administer mangroves and ponds. Legislation to conserve, protect, and rehabilitate Philippine mangroves has not been wanting—it is their implementation that is generally weak, hampered by inadequate manpower and resources, and overall lack of political will to enforce the laws.



Postharvest portrait. Milkfish, and perhaps some shrimp and crabs, have just been harvested from this drained milkfish pond in Iloilo Province, central Philippines. With mangrove stumps now visible, it will be dried, filled, and restocked with “seed” organisms for the next crop.

the coastline are no match for rampaging waters. It is time to enforce these greenbelt and other mangrove-preserving laws, because only a solid wall of trees can slow down a moving wall of water. More than ever, there is a need to preserve or rehabilitate mangrove-beach forests and coral reefs to serve as natural barriers that diminish the tremendous wave energy generated by tsunamis, as well as by typhoons. Tsunamis appear every 20 to 50 years in the Philippines, but in a single year 20 typhoons may devastate the country by inflicting massive losses of life and property.

Mangrove Sense

Only a fifth of the 500,000 ha of Philippine mangroves at the turn of the 20th century remain, whereas brackishwater ponds have increased almost fourfold, from 61,000 ha in 1940 to 230,000 ha at present. Many of these ponds have no associated legal papers—either the lease has expired or the application is pending. Often single families own up to hundreds of hectares of pond area. Twenty hectares is the most that a Filipino pond operator can realistically manage by himself, so many ponds are underutilized or abandoned, and productivity is low compared to that of Thai shrimp farms, which average 2 ha or less. By reducing farm sizes, Filipino aquaculturists can increase pond yields and afford to pay the still modest lease fee of PhP1000/ha per year. The remaining areas, especially those facing waterways, could be reverted to greenbelts, finally coming into compliance with Philippine laws. Also, by redressing

the present imbalance between the respective areas of mangroves and ponds, aquaculturists can embrace the more holistic approach, known as Integrated Coastal Zone Management, which incorporates an understanding of the complementary rather than competing roles of aquaculture and more traditional open-sea fisheries.

My environmental bias goes back to a childhood imprinted with mangoes, avocados, and a dozen other tropical species of backyard fruit trees, as well as yearly floods due to rampant logging that had denuded the forests in my home province. The floods were particularly bad and had downed many bridges in 1961 when, as a high school student, I took the government science examinations. To travel to the testing center in the next province, my father and I had to cross rivers on coconut trunks or bamboo poles. A decade later, my passion to work for a sustainable environment was greatly reinforced by my participation in the historic 1972 U.N. Conference on the Human Environment in Stockholm.

I am determined to continue mentoring younger researchers in sustainable aquaculture and mangroves. Sadly, most Filipino students of marine biology prefer the “glamorous” coral reefs and seagrass beds to muddy, mosquito-infested mangroves. This is unfortunate because, given a chance, mangroves can be thoroughly enchanting, the mud and insects notwithstanding. Imagine numerous white filaments of *Sonneratia alba* flowers gently falling from the canopy in the early morning breeze, or the unspeakable beauty of thousands of fireflies lighting up *Sonneratia caseolaris* trees on a moonless night.

We scientists in developing countries need to come down from the Ivory Tower and disseminate results not only in peer-reviewed journals but also through advocacy and the popular media. We must not forget our hearts even as we apply our minds. We do science not in a vacuum but against the grinding poverty and environment-unfriendly character of modern times, and we can use our scientific knowledge to reduce suffering and make life more full for fellow humans and creatures. With a Pew Fellows grant in marine conservation, I will pursue initiatives in mangrove management and rehabilitation through education and local governance. Success will be had on the day my grandchildren walk with me through these habitats, understanding their importance, appreciating their diversity, and captivated by their magic.

The author is with the Aquaculture Department, Southeast Asian Fisheries Development Center, Tigbauan, Iloilo 5021, Philippines. E-mail: jhprima@aqd.saefdec.org.ph

10.1126/science.1115179

www.sciencemag.org SCIENCE VOL 310 7 OCTOBER 2005

Published by AAAS

59

Growth by Auxin: When a Weed Needs Acid

Markus Grebe

The acid growth theory describes how the plant hormone auxin (indole acetic acid, or IAA) stimulates elongation of cells. Auxin triggers excretion of protons into the plant cell wall. This acidification loosens the wall, allowing the cell to expand [see the figure; (1)]. Apart from this certainly

Enhanced online at www.sciencemag.org/cgi/content/full/310/5745/60

not exclusive mode of auxin action, many aspects of plant development such as leaf differentiation, root formation, and organ development require directed auxin transport (2). That is, the hormone must get transported across plant tissue to where it can stimulate cell growth and proliferation when needed. Here, another “acid” aspect considered by the chemiosmotic model of auxin transport comes into play [see the figure; (3)]. In the rather acidic cell wall, part of the auxin resides in its protonated, lipophilic form. Once auxin exits the cell wall, crosses the plasma membrane, and enters the cytosol, it becomes deprotonated and this more hydrophilic anion gets trapped inside the cell. To export auxin in a directed manner, plants have been proposed to use efflux carrier proteins that are situated in the plasma membrane in a polar manner. Indeed, such efflux carriers have been identified through genetic approaches in the weed and model plant *Arabidopsis thaliana* (2, 4, 5). However, despite decades of acid growth research (1) and *Arabidopsis* genetics, functional genetic evidence for a proton pump that regulates auxin transport or cell wall acidity has been lacking.

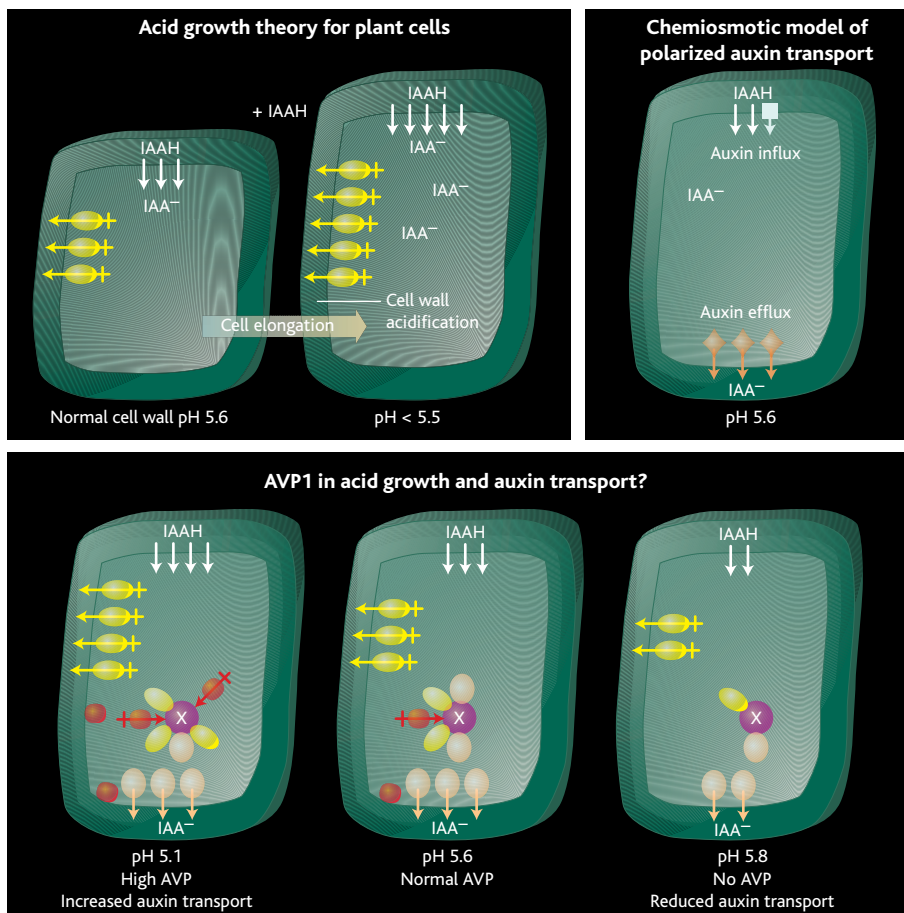
On page 121 of this issue, Li *et al.* (6) report that the *Arabidopsis* proton pump AVP1 regulates auxin transport and cell wall acidification. These findings are surprising because AVP1 is thought to act as a proton pump that is driven by pyrophosphate (V-PPase) to acidify intracellular membrane compartments in plant cells (7). It has generally been assumed that a plasma membrane-localized proton pump fueled by adenosine triphosphate (P-ATPase) is involved in cell wall acidification and possi-

bly in auxin transport. What evidence leads the authors to conclude that AVP1 contributes to auxin-mediated organ development? The absence of AVP1 in *avp1* mutants drastically affects plant development. A loss-of-function *avp1* mutation causes organ fusions and other defects that have also been observed in plants treated with inhibitors of polar auxin transport (8) and in mutants defective in multiple auxin

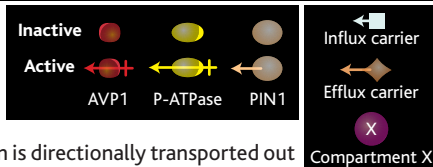
efflux components (5, 9). More informatively, *avp1* mutant roots display lower levels of the auxin efflux carrier PIN-FORMED1 (PIN1) and reduced polar auxin transport. Consistently, overexpression of AVP1 enhances polar auxin transport in root tips. This intracellular proton pump somehow modulates the directed transport of auxin.

Moreover, elevated expression of AVP1 increases leaf and root system size, consistent with impaired leaf and root development in *avp1* mutants. These opposite phenotypes observed with changes in AVP1 expression suggest that a threshold amount of AVP1 is critical for its function. Thus, AVP1 may play a regulatory role during plant growth and development by modulating polar auxin transport.

Some of the authors’ observations are not



An intracellular proton pump contributes to auxin-mediated plant development. According to acid growth theory, auxin (IAA) triggers plant cell elongation by stimulating acidification of the cell wall by a proton pump, P-ATPase. In the chemiosmotic model of polar auxin transport, auxin is directionally transported out of the cell by an efflux carrier protein. The intracellular proton pump AVP1 regulates the amount of P-ATPase and the efflux carrier protein PIN1 at the plasma membrane, presumably by acidifying an unknown shared intracellular transport compartment X. The nature of X and a potential contribution of AVP1 to “classical” acid growth remain open.



The author is at the Umeå Plant Science Centre, Department of Forest Genetics and Plant Physiology, Swedish University of Agricultural Sciences, 90 183 Umeå, Sweden. E-mail: markus.grebe@genfys.slu.se

yet easy to comprehend. For example, PIN1 protein expression is low in *avp1* mutants, yet plants overexpressing AVP1 do not really show the opposite phenotype. Similarly, it is difficult to explain why auxin transport is enhanced in the root tip but reduced at the root-shoot junction upon increased AVP1 expression. Despite these discrepancies, the authors' findings clearly support the notion that AVP1 affects auxin transport. Future studies may help to explain differences at the level of specific cell or tissue types.

In light of its unexpected role in auxin transport regulation, Li *et al.* (6) also address a potential function of AVP1 in cell wall acidification. Intriguingly, absence of AVP1 increases the cell wall pH, whereas overexpression of AVP1 lowers pH. Control of cell wall pH has been attributed to the plasma membrane proton pump, P-ATPase. Indeed, *avp1* mutants display reduced P-ATPase activity, whereas plants overexpressing AVP1 have increased P-ATPase activity and density at the plasma membrane. Thus, Li *et al.* uncover an unexpected role for AVP1 in the regulation of cell wall acidification by modulating P-ATPase levels—"acid growth" revisited?

Li *et al.* demonstrate AVP1 action on polar auxin transport and P-ATPase-mediated cell wall acidification. In addition, their study raises exciting questions. The authors report elongation defects in root cells versus reduced leaf cell numbers in *avp1* mutants (6). Does this indicate that AVP1-regulated cell wall acidification mediates cell expansion according to the acid growth theory in roots but not in leaves? Or does AVP1-mediated regulation of cell wall pH mostly feed back on auxin transport, taking into account the chemiosmotic model? Whichever of the two processes may be primarily affected by AVP1, it will be interesting to see how cell wall acidification and auxin transport are connected. The authors hypothesize that AVP1 somehow regulates transport of both P-ATPase and PIN1 to the plasma membrane by acidifying an unknown subcellular compartment along a common transport route. This idea can now be tested by extending the loss- and gain-of-function approaches (6) to detailed cell biological analyses. These should clarify to what extent AVP1, PIN1, and P-ATPase take common routes and whether AVP1 regulates vesicle transport. A hint of where this V-PPase could act comes

from studies on cauliflower where a V-PPase pump resides at the trans-Golgi network, in multivesicular bodies, the vacuole, and at the plasma membrane (10). Thus, there are several options as to where AVP1, PIN1, and P-ATPase could meet along the secretory or endocytic pathway. Undoubtedly, the work of Li *et al.* (6) opens new views on the regulation of auxin transport and proton pump action during plant development. Further detailed understanding of AVP1 subcellular function will help to merge or distinguish different concepts of auxin transport and action.

References

1. A. Hager, *J. Plant Res.* **116**, 483 (2003).
2. O. Leyser, *Cell* **121**, 819 (2005).
3. T. L. Lomax, G. K. Muday, P. H. Rubery, *Plant Hormones: Physiology, Biochemistry and Molecular Biology*, P. J. Davies, Ed. (Kluwer Academic, Dordrecht, Netherlands, 1995), pp. 509–530.
4. L. Gälweiler *et al.*, *Science* **282**, 2226 (1998).
5. J. Friml *et al.*, *Nature* **426**, 147 (2003).
6. J. Li *et al.*, *Science* **310**, 121 (2005).
7. E. J. Kim, R. G. Zhen, P. A. Rea, *Proc. Natl. Acad. Sci. U.S.A.* **91**, 6128 (1994).
8. C. Liu, Z. Xu, N. H. Chua, *Plant Cell* **5**, 621 (1993).
9. I. Blilou *et al.*, *Nature* **433**, 39 (2005).
10. R. Ratajczak, G. Hinz, D. G. Robinson, *Planta* **208**, 205 (1999).

10.1126/science.1119735

APPLIED PHYSICS

Subsurface Imaging with Scanning Ultrasound Holography

Alain C. Diebold

Characterization of subsurface structure is critical to almost every area of science and engineering (1). In biology, for example, imaging the structure of cells has always been a fundamental means of understanding the relationship between structure and function. Moreover, every innovative microscopy technique seems to highlight new or difficult-to-observe features in biological systems. But some problems, such as finding life-threatening arterial blockages, require much better spatial resolution (1).

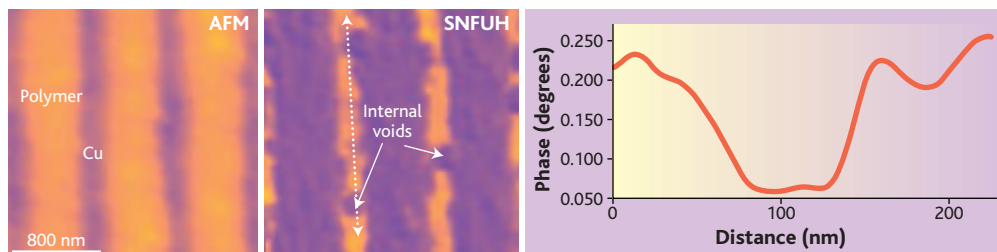
Some key microscopic imaging methods rely on sound waves rather than light. Perhaps the most prevalent application of acoustic microscopes is for imaging subsurface features in packaged electronic parts. Subsurface voids can be the root cause of coating delamination or can result in the fracture of a critical structure

under stress. As Shekhawat and Dravid report on page 89 of this issue, a novel form of acoustic holography has now extended the spatial resolution of this technique, thus enabling the imaging of subsurface features in a wide range of applications (2).

A conventional scanning acoustic microscope focuses acoustic waves under the surface of a sample by means of a transducer (often made from sapphire) and scans the sample under the transducer. The sample is immersed in water. The spatial resolution

is given by an equation similar to the Rayleigh criterion for a light microscope, namely $\omega = 0.51\lambda_0/NA$, where $\lambda_0 = v_0/f$, v_0 is the velocity of sound in the fluid, f is the frequency of the acoustic wave, and NA is the numerical aperture. For typical acoustic microscopes, the spatial resolution is close to 100 μm . Recently, scanning probe microscopy has extended the spatial resolution to the nanometer scale (3).

To obtain images of integrated circuit technology, however, much greater spatial resolution will be required. The width of metal lines is quickly approaching 60 nm, and by the year 2008 memory chips will have so-called dense metal lines 60 nm wide with spaces of 60 nm between them. Previous efforts had already pushed acoustic imaging resolution well below the limits of the scanning acoustic microscope. Geer *et al.* have demonstrated that the ultrasonic



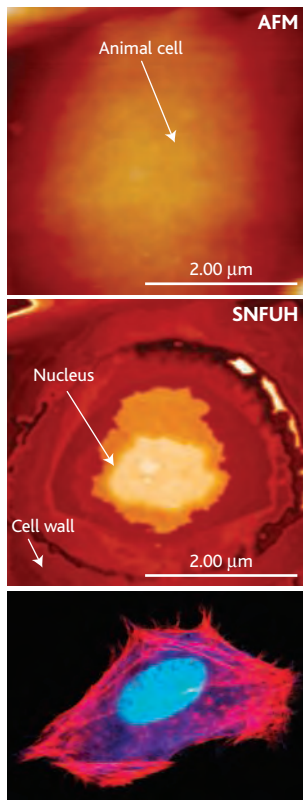
Fine lines. SNFUH imaging of a copper low-dielectric interconnect system. (Left) Typical AFM (topography) image shows periodic polymer and copper features. The copper lines are about 60 nm wide and the polymer one around 200 nm. (Middle) Phase image of SNFUH that clearly reveals the surface elastic contrast and subsurface voiding in the copper lines. (Right) Line profile across the voids.

The author is with SEMATECH, Austin, TX 78741, USA. E-mail: alain.diebold@sematech.org

PERSPECTIVES

force microscope can image changes in the elastic modulus with a resolution of <10 nm (3). This group ultrasonically vibrated the sample at 2.2 MHz while scanning the surface with an atomic force microscope (AFM). The apparatus is similar to that previously reported by Dinelli *et al.* (4). The spatial resolution was good enough to observe differences in the low dielectric constant film caused by variations in the processing (3).

Now, Shekhawat and Dravid have shown how scanning near-field ultrasound holography (SNFUH) can further improve spatial resolution and depth information (2). In SNFUH, acoustic waves are launched on both the probe tip and the sample at slightly different megahertz frequencies. The interference of these two waves forms a surface acoustic standing wave. This wave is altered by subsurface features such as voids, and the change in its frequency



Better bioimages. (Top) Image of mouse cell taken with conventional AFM technology. (Middle) SNFUH image of the same cell. (Bottom) Micrograph of mouse fibroblast cell for comparison (nucleus is blue, actin protein in cell's skeleton is shown in red).

is monitored by the AFM cantilever. Shekhawat and Dravid operate the AFM in the contact mode for hard materials and the noncontact mode for biological materials. The next step for this approach will be to develop the modeling to determine the depth dependence of the response from buried features turning two-dimensional maps into three-dimensional tomography maps.

Shekhawat and Dravid have also applied their technology to copper damascene structures and observed voids in copper lines (see the first figure). The direct, non-destructive observation of a void in an opaque material had previously seemed to be a nearly impossible task.

But semiconductor structures are not the only application of near-field acoustic microscopy. Shekhawat and Dravid have

illustrated the imaging capability of SNFUH for biological samples. In the top panel of the second figure, a typical AFM (topography) image shows a mouse cell on a cover slip, which was treated with phosphate buffer solution. It only shows the overall outer morphology of the cell. In the middle panel of the second figure, however, the SNFUH image appears to reveal the internal substructure of the cell, including the nucleus. It is instructive to compare the SNFUH image with a typical micrograph of an animal cell (the bottom panel of the second figure). Extra structure is observed with this additional resolution. With further research and development, SNFUH should be able to provide even more information, such as the depth of buried features and further quantification of elastic properties.

References

1. J. Ouellette, *Indus. Phys.* **10**(1), 14 (2004).
2. G. S. Shekhawat, V. P. Dravid, *Science* **310**, 89 (2005).
3. R. E. Geer, O. V. Kolosov, G. A. D. Briggs, G. S. Shekhawat, *J. Appl. Phys.* **91**, 4549 (2002).
4. F. Dinelli, S. K. Biswas, G. A. D. Briggs, O. V. Kolosov, *Phys. Rev. B* **61**, 13995 (2000).

10.1126/science.1119259

PSYCHOLOGY

The Nature of Personality: Genes, Culture, and National Character

Richard W. Robins

I recently had the opportunity to conduct research in a remote village in the West African nation of Burkina Faso, one of the countries whose national character was studied by Terracciano *et al.* in a report on page 96 of this issue (1). While there, I was struck by the degree to which everyone seemed so different yet so familiar at the same time. Despite dramatic differences in cultural customs and practices, the Burkinabe people seemed to fall in love, hate their neighbors, and care for their children in much the same way, and for many of the same reasons, as people in other parts of the world. Indeed, there is a core to human mentality and social behavior that cuts across nations, cultures, and ethnic groups. Even such profoundly different countries as Burkina Faso and the United States do not

differ substantially in the average personality tendencies of their people, as Terracciano and colleagues have shown (1, 2).

Against this backdrop of human universals, it is quite clear that individual variability exists: Some Burkinabe (or Americans) are shy and others sociable, some friendly and others disagreeable, and some driven to attain high status in their community while others lack the same drive. Of the vast array of human personality traits, the majority can be subsumed within five broad domains: extraversion-introversion, antagonism-agreeableness, conscientiousness, neuroticism, and openness to experience. Collectively, these five dimensions predict most of the outcomes that truly matter in life—health and mortality, academic success, job performance, the capacity to have a successful and lasting romantic relationship, and a wide range of personal and societal problems, including drug abuse and criminality (3, 4). Moreover, personality traits predict such outcomes with

as much precision as many biomedical measures predict diseases, including the prediction of heart disease by electrocardiogram stress tests, pregnancy outcomes by ultrasound exams, and breast cancer by screening mammograms (5).

What accounts for individual variability on the five primary dimensions of personality? Tensions exist in the scientific literature between explaining this variability in terms of basic physiological and genetic processes, and in terms of situational, social, and cultural contingencies that vary both within and across sociocultural groups. An eminent psychologist, John Watson, once famously claimed, "Give me a dozen healthy infants . . . and my own specified world to bring them up and I'll guarantee to take any one at random and train him to become any type of specialist I might select—doctor, lawyer, merchant-chief, and yes, even beggar-man and thief, regardless of his talents, penchants, tendencies, abilities, vocations, and race of his ancestors" (6). We now know that Watson was wrong. Genetic factors provide constraints on the way a child develops, and they account for about half of the variability in personality (in typical populations and environments). Identical twins separated at birth tend to have remarkably similar personalities, despite vastly different upbringings (7). In short, people are not blank slates upon which culture-

The author is in the Department of Psychology, University of California, 1 Shields Avenue, Davis, CA 95616, USA. E-mail: rwrubins@ucdavis.edu

CREDIT: (BOTTOM PANEL) DAVID BECKER/PHOTO RESEARCHERS, INC.



Expressions of human emotion are universal. Individuals from Burkina Faso receiving rice in compensation for participating in a study of emotion recognition. Cross-cultural research suggests that expressions of sadness, anger, happiness, pride, and other emotions are universally recognized, despite cultural differences in the conditions under which they are elicited and displayed.

specific experiences inscribe our personalities; rather, we all come into the world with a preprogrammed set of innate mechanisms and personal proclivities (8). Using a diverse array of methods, including survey research, computer simulations, brain imaging, and population and molecular genetics, researchers have shown that personality traits are highly heritable, replicable across a wide range of cultures and even species, largely stable across the life span, and linked (albeit weakly) to specific genes, hormones, neurotransmitters, and brain activation patterns (1–4, 7, 9).

The fact that individual differences in personality have a strong genetic foundation does not imply that cultural or national differences in aggregate personality levels have any genetic basis. These group differences may be, and most likely are, the result of environmental forces. And the results of Terracciano *et al.* effectively pull the plug on all claims that perceived differences in national character reflect genetic differences between ethnic or cultural groups. That mistaken belief has served as the basis for discrimination, intergroup conflict, and, in some tragic cases, genocide. In contrast to personality traits—which reflect actual differences in the way people think, feel, and behave—stereotypes about national character seem to be social constructions designed to serve specific societal purposes. This juxtaposition reveals a paradox at the heart of Terracciano *et al.*'s findings: People are capable of providing reliable and valid assessments of a particular individ-

ual's personality (including their own), but they are unable to judge accurately the aggregate, or national, character of the people around them—at least not in the 49 countries studied by Terracciano *et al.*

Why are stereotypes about national character inaccurate? One possibility is that national stereotypes are historically accurate but no longer apply because of cultural changes or systematic migration patterns. A second possibility is that national stereotypes grow out of historical conflicts between groups in which one was dominant and the other subordinate. A third possibility is that national stereotypes are accurate at a more specific level of analysis (e.g., amount of gesturing or the distance people typically establish in social interactions) but not at the level of broad personality dimensions such as extraversion. A fourth possibility is that stereotypes about the character of other nations are accurate, but the stereotypes people hold about their own nation—the stereotypes studied by Terracciano *et al.*—are not. Finally, a large body of research indicates that a host of cognitive processes maintain inaccurate stereotypes (10). We are less likely to notice, encode deeply, and remember information that violates our stereotypes. For the most part,

when we encounter people who contradict a stereotype, we perceive them as unique individuals rather than representatives of their national or cultural group. Further research is needed to explore these possibilities. A deeper understanding of the links among personality, culture, and national stereotypes is particularly critical at this time, as countries around the world adapt to globalization, experience a “clash of civilizations,” and cope with other social changes related to intercultural understanding (and misunderstanding).

References

1. A. Terracciano *et al.*, *Science* **310**, 96 (2005).
2. R. R. McCrae *et al.*, *J. Pers. Soc. Psychol.*, in press.
3. A. Caspi, B. W. Roberts, R. L. Shiner, *Annu. Rev. Psychol.* **56**, 453 (2005).
4. D. J. Ozer, V. Benet-Martinez, *Annu. Rev. Psychol.*, in press.
5. G. J. Meyer *et al.*, *Am. Psychol.* **56**, 128 (2001).
6. J. B. Watson, *Behaviorism* (Norton, New York, ed. 2, 1930).
7. T. J. Bouchard, *Science* **264**, 1700 (1994).
8. S. Pinker, *The Blank Slate* (Viking, New York, 2002).
9. S. D. Gosling, O. P. John, *Curr. Direct. Psychol. Sci.* **8**, 69 (1999).
10. D. L. Hamilton, J. W. Sherman, in *Handbook of Social Cognition*, R. S. Wyer Jr., T. K. Srull, Eds. (Erlbaum, Hillsdale, NJ, ed. 2, 1994), vol. 2, pp. 1–68.

10.1126/science.1119736

CHEMISTRY

Inventing the Nanomolecular Wheel

Jay Siegel

At the turn of the millennium, pop surveys placed the wheel as the most important invention (1). Upon the foundation of this basic mechanical unit, many types of macromachines have been developed. By analogy, some researchers hope that directable nanoscale wheels will spawn nanoscale machines. Within such a mechanism the counterpart to a wheel is a molecular rotor, capable of specific directed rotation. On the molecular level, random rotors abound, but coupling specific chemical reactions to control directional rotation is rare. On page 80 of this issue, Fletcher *et al.* report such a system and muse upon its implications for the development of molecular motors (2).

The directed rotor synthesized by Fletcher *et al.* rotates among four “stations”—two open-ring forms and two closed-ring forms (see the figure). It relies on a well-known stereoselective ring-opening

reaction to bias the conformational preference toward one open atropisomer (that is, a nonrotating form) of a chiral biaryl system (3). A series of well-established protection/deprotection steps ensures the selective reconnection of the ring in an orientation internally rotated by 180°. Another stereoselective ring opening and protection/deprotection sequence brings one back to the start in a directed sense. The hallmark of this work is not the novelty of its individual pieces but the molecular mechanical engineering of the whole (4, 5). This work begins to confront issues that arise from the idea that molecular engineers will soon rebuild the mechanical world in nanoscale effigy (6).

How does this belief in the molecular engineering analogy of the wheel arise? Why are some scientists so quick to believe in such direct parallels between macro- and nanomachinery? What paradigm could engender such a devout following? Perhaps it is the classical handheld molecular model and its crystallographic and computer-based legacy (7).

The success of van 't Hoff's tetrahedral

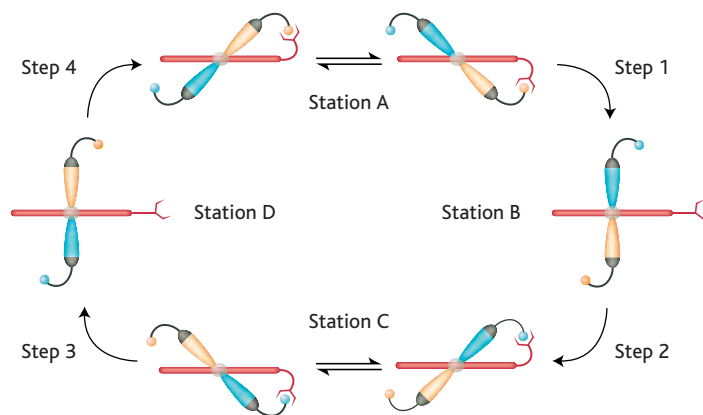
The author is at the Organic Chemistry Institute, University of Zürich, Winterthurerstr. 190, Zürich CH-8006, Switzerland. E-mail: jss@oci.unizh.ch

model of carbon, Watson and Crick's framework for DNA, and the colorful Corey-Pauling-Koltun space-filling chemical sphere models has lulled chemists into believing that these metaphors of molecules are accurate predictors for the nanoscience of the future. Without question, molecular models are useful tools for the chemist, but every model has limits and bounds to be respected. Symmetry even in the absence of specific shape accounts for many observations rationalized by models, and a quantum mechanical definition of molecular shape is at best ambiguous. What are the metaphorical infidelities of the classical molecular model, and what is their impact on Fletcher *et al.*'s molecular rotor and the dream of nanomachines?

Molecular cognates for the structural components of machines develop liberally from physical or computer-generated molecular models and become very seductive targets for chemical synthesis. Molecular-scale gears, turnstiles (rotors), springs, propellers, etc., have been proposed in molecular-model effigy, fabricated through creative synthetic strategies, and substantiated statically by x-ray crystallography (7). All stages of this structural mimicry are beholden to the physical molecular model, whether skeletal, ball-and-stick, or space-filling. But parallels of form need not be parallels of function, and the dynamic aspects are the true test of a molecular machine (8).

Pioneering work on the stereochemistry of molecular-scale gears realized the idea of phase-restricted molecular motion by demonstrating distinguishable dynamic gearing structures (9). Unlike their macro counterparts, molecular-scale gears have a rich dynamic motion owing to their $3n - 6$ internal normal modes (where n is the number of atoms). The amplitude of these motions is often comparable to that of envisioned "mechanical modes" that lead to gear slippage. These studies made clear the importance of tight gear meshing and good shape (tooth/notch) recognition if gear slipping due to the thermal background motion was to be avoided, as well as the fact that a comparable amount of energy is being distributed into mechanically nonproductive molecular motion; the systems exist in a background of high thermal noise (10).

Despite the time-averaged correlated motion of these gears, their motion is essentially Brownian and without capacity to do



Chemical rotor. The nanomachine created by Fletcher *et al.* (2) relies on a four-step cycle that pivots the rotor (yellow and blue) attached by a single carbon-carbon bond to the stator (red). In step 1, the rotor and stator begin connected by a second bond that holds the conformation in place. This second bond breaks to allow the initial stage of rotation to take place. Step 2 involves the creation of a new bond that directs the rotor to the next station. Step 3 is another bond breaking and step 4 another bond making, each driving the rotor to the successive stations. Random motion is prevented by structural and steric constraints. [Adapted from (2)]

work (11, 12). An asymmetry or directional character to the motion is needed, which can be achieved by a Brownian ratchet or Brownian motor (13). Brownian motors operate through the cyclic application of a periodic asymmetric potential to bias an otherwise symmetrically diffusing system of particles. Application of a periodic asymmetric potential focuses the particles to local minimum N of the potential. Removal of the potential allows natural diffusion to ensue via Brownian motion in a symmetrical way with respect to the focus point. Reapplication of the periodic asymmetric potential traps the particle in wells $N - 1$, N , or $N + 1$ unequally. Over multiple cycles, the position of the particle is moved in a bias direction. In effect, motors operating by these mechanisms do work by using enthalpy to corral entropy, something clearly different from their macroscale counterparts.

In contrast, macroscopic machines use heat flow and momentum as common design elements, which in principle could desymmetrize the environment. On the molecular level, however, thermal gradients are rapidly dissipated through the internal normal modes and collisions with solvent molecules. As such, momentum-based mechanisms for machines capable of doing work are unlikely to be feasible on the molecular scale. The molecular machine must harness thermal fluctuations to produce directed motion (14).

Chemical gradients have been used to create asymmetry in the environment, as in the case of proton pumps to couple chemical energy with molecular motion. Fletcher *et al.* define the use of a chemical ligation as a "power stroke" that provides

the bias necessary to surmount the barrier in a directional way. Thus, the rotor's asymmetry stems from the coupling of the molecule's potential energy surface, the sequence of the reactions, and the chemical energy of reaction (15). A related scheme to create directional cyclic ring motion by selective protection/deprotection in a polycatenane system has also been developed (16).

Unidirectional rotation is but one of various oscillatory motions that are nonsymmetrical in time (e.g., flexible paddle, flapping wing, or reptating flagella) (13). Controlled motions of this type should also lead to directional molecular motion and the chance to do mechanical work with chemical energy on the molecular scale.

Numerous possibilities exist for designing molecular-scale machines. The appeal of direct molecular analogs to macroscopic machines makes paying attention to the distinctions between macro- and nanoscopic mechanisms all the more crucial. Taming randomness requires more than turning a molecular crank, and in the development of molecular machines it is important to keep in mind that the "room at the bottom" is not simply a miniaturization of what we see on top (17).

References

1. See, for example, <http://archive.thisisoxfordshire.co.uk/2002/02/18/44419.html>.
2. S. P. Fletcher, R. Dumur, M. M. Pollard, B. L. Feringa, *Science* **310**, 80 (2005).
3. G. Bringmann *et al.*, *J. Organomet. Chem.* **661**, 31 (2002).
4. B. J. Dahl, B. P. Branchaud, *Tetrahedron Lett.* **45**, 9599 (2004).
5. T. R. Kelly, R. A. Silva, H. De Silva, S. Jasmin, Y. J. Zhao, *J. Am. Chem. Soc.* **122**, 6935 (2000).
6. K. E. Drexler, *Nanosystems: Molecular Machinery, Manufacturing and Computation* (Wiley, New York, 1992).
7. K. Mislow, *Chemtracts Org. Chem.* **2**, 151 (1989).
8. M. A. Garcia-Garibay, *Proc. Natl. Acad. Sci. U.S.A.* **102**, 10771 (2005).
9. H. Iwamura, K. Mislow, *Acc. Chem. Res.* **21**, 175 (1988).
10. P. Reimann, *Phys. Rep.* **361**, 57 (2002).
11. M. von Smoluchowski, *Phys. Z.* **13**, 1069 (1912).
12. R. P. Feynman, R. B. Leighton, M. Sands, *The Feynman Lectures on Physics* (Addison-Wesley, Reading, MA, 1963), vol. 1, chap. 46.
13. R. D. Astumian, *Science* **276**, 917 (1997).
14. H. Linke, M. T. Downton, M. J. Zuckerman, *Chaos* **15**, 026111 (2005).
15. C. Bustamante, D. Keller, G. Oster, *Acc. Chem. Res.* **34**, 412 (2001).
16. J. V. Hernández, E. R. Kay, D. A. Leigh, *Science* **306**, 1532 (2004).
17. R. P. Feynman, "There's Plenty of Room at the Bottom: An Invitation to Enter a New World of Physics," *Engineering and Science*, May 1960 (available at www.zyvex.com/nanotech/feynman.html).

INTRODUCTION

Signaling: From Stem Cells to Dead Cells

This special section on cell signaling features Viewpoints from contributing authorities who have provided annotated signaling pathways for *Science's* Signal Transduction Knowledge Environment (STKE) Connections Maps database. These overviews provide a snapshot of the current understanding of signaling pathways that influence a broad range of biological processes, from the birth of proliferating stem cells through cellular destruction by apoptosis. Detailed information on the components that make up these pathways, and on their relations with one another, can be viewed in the STKE Connections Map database, a resource available free of charge (with registration) to the entire scientific community through the Web interface at *Science's* STKE.

Many scientists are optimistic that the manipulation of stem cells will allow marked advances in the treatment of currently intractable diseases. Realizing the promise of these versatile cells will require understanding of their native control mechanisms. Members of the transforming growth factor- β (TGF- β) family have emerged as critical regulators of multiple stages in the life of various stem cells (Mishra *et al.*, p. 68). TGF- β family members initiate signals that can

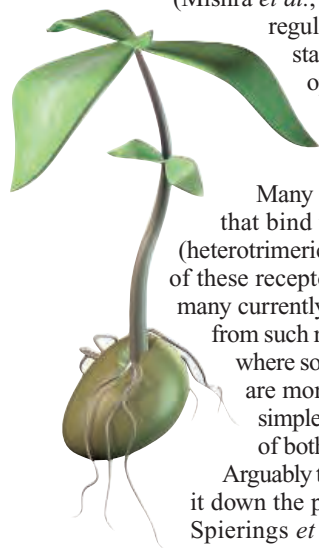
regulate the proliferation of stem cells in an undifferentiated state, specification of or commitment to a particular developmental lineage, and, in some cases, later differentiation into mature cells. Analogous effects of TGF- β family members on proliferation and differentiation are thought to account for their effects on cancer cells.

Many processes in differentiated cells are regulated by ligands that bind to receptors coupled to signal-transducing G proteins (heterotrimeric guanine nucleotide-binding proteins). The vast family of these receptors in mammals is under intense study, in part because many currently prescribed therapeutic agents act by modifying signals from such receptors. Assmann (p. 71) surveys the situation in plants, where so far just one G protein subunit has been identified (there are more than 20 in humans). She asks whether analysis of the simpler plant systems might provide new insights to investigators of both the plant and animal systems.

Arguably the most serious signal a cell will ever face is one that sends it down the path of organized self-destruction known as apoptosis. Spierings *et al.* (p. 66) have created a group of large pathways at the STKE Connections Maps that annotate some of the more than 150

components that are implicated in the signals that result in the disruption of mitochondrial function and the activation of caspases (proteases that chew up cellular substrates and lead to cell death). The summary poses the philosophical question of where this regulatory pathway starts and ends—a matter complicated by the fact that many if not all cell functions may contribute to signals that ultimately influence the cell's choice to live or die.

L. BRYAN RAY, NANCY R. GOUGH, ELIZABETH M. ADLER



PAGE 71

CONTENTS

VIEWPOINTS

- 66 **Connected to Death: The (Unexpurgated) Mitochondrial Pathway of Apoptosis**
D. Spierings *et al.*
- 68 **Transforming Growth Factor- β Signaling in Stem Cells and Cancer**
L. Mishra, R. Derynck, B. Mishra
- 71 **G Proteins Go Green: A Plant G Protein Signaling FAQ Sheet**
S. M. Assmann

S. M. Assmann G protein signaling in the regulation of *Arabidopsis* seed germination. *Sci. STKE* (Connections Map, as seen October 2005), http://stke.sciencemag.org/cgi/cm/stkecm;CMP_18476.

S. M. Assmann G protein signaling in the regulation of rice seed germination. *Sci. STKE* (Connections Map, as seen October 2005), http://stke.sciencemag.org/cgi/cm/stkecm;CMP_18492.

S. M. Assmann G protein regulation of disease resistance during infection of rice with rice blast fungus. *Sci. STKE* (Connections Map, as seen October 2005), http://stke.sciencemag.org/cgi/cm/stkecm;CMP_18511.

C. Bender *et al.* Mitochondrial pathway of apoptosis: BH3-only Bcl-2 family. *Sci. STKE* (Connections Map, as seen October 2005), http://stke.sciencemag.org/cgi/cm/stkecm;CMP_18017.

C. Bender *et al.* Mitochondrial pathway of apoptosis: Multidomain Bcl-2 family. *Sci. STKE* (Connections Map, as seen October 2005), http://stke.sciencemag.org/cgi/cm/stkecm;CMP_18015.

C. Bender *et al.* Mitochondrial pathway of apoptosis: Antiapoptotic Bcl-2 family. *Sci. STKE* (Connections Map, as seen October 2005), http://stke.sciencemag.org/cgi/cm/stkecm;CMP_17525.

C. Bender *et al.* Mitochondrial pathway of apoptosis: Caspases. *Sci. STKE* (Connections Map, as seen October 2005), http://stke.sciencemag.org/cgi/cm/stkecm;CMP_18019.

T. Blake *et al.* TGF- β signaling in development. *Sci. STKE* (Connections Map, as seen October 2005), http://stke.sciencemag.org/cgi/cm/stkecm;CMP_18196.

K. Kitisin *et al.* BMP signaling pathway in stem cells. *Sci. STKE* (Connections Map, as seen October 2005), http://stke.sciencemag.org/cgi/cm/stkecm;CMP_18170.

K. Kitisin *et al.* TGF beta signaling in gastrointestinal stem cells. *Sci. STKE* (Connections Map, as seen October 2005), http://stke.sciencemag.org/cgi/cm/stkecm;CMP_17699.

See also related STKE material on p. 11 or at www.sciencemag.org/sciext/cellsignaling05/

Science

Connected to Death: The (Unexpurgated) Mitochondrial Pathway of Apoptosis

Diana Spierings, Gavin McStay, Maya Saleh,* Cheryl Bender, Jerry Chipuk, Uli Maurer, Douglas R. Green†‡

The mitochondrial pathway of apoptosis in vertebrates is dependent on the process of mitochondrial outer membrane permeabilization (MOMP), which leads to the release of proteins from the mitochondrial intermembrane space into the cytosol. "Upstairs" of this event are the Bcl-2 family proteins that regulate and mediate MOMP; "downstairs" is the activation of caspases that orchestrate the dismantling of the cell. In the Connections Map database at *Science's* Signal Transduction Knowledge Environment (STKE), the pathways that define the mitochondrial pathway of apoptosis are illustrated, with the bulk of control occurring "upstairs" of MOMP.

Cell death is a fundamental fact of life, and in multicellular organisms it can be critically important for the organization of cells and tissues in the body. In animals, the preeminent mechanism of most (but not all) physiological cell deaths is by apoptosis, and in the vertebrates, most (but not all) apoptosis proceeds through the mitochondrial pathway, illustrated in the Connections Map database (1–4) at *Science's* STKE. These pathways present current information on the key elements of the mitochondrial pathway of apoptosis as they are understood in vertebrate systems, along with many of the molecules that may regulate elements of the pathway. The extent to which this pathway, as we define it below, is represented in other animals is controversial. The pathway is "unexpurgated" in that most of the protein functions and protein-protein interactions that have been described as regulating this process are included, regardless of whether they have been confirmed, challenged, or viewed skeptically (1–4). In this overview, only the best documented elements are discussed, although these too are not without controversy.

The mitochondrial pathway of apoptosis in vertebrate cells centers on and is defined by a pivotal event in the cell death process: mitochondrial outer membrane permeabilization (MOMP) (Fig. 1). Proteins sequestered in the mitochondrial intermembrane space, between the inner and outer mitochondrial membranes (IMM and OMM, respectively), gain access to other proteins in the cytosol, and this results in apoptosis. The mitochondrial pathway concerns the causes and conse-

quences of MOMP. In describing this pathway in simplified form, we have an "upstairs/downstairs" situation where, at first pass, most of the aristocratic decisions are made before MOMP (upstairs) and the workmanlike consequences occur thereafter (downstairs). As in entitled households, of course, this is only an approximation.

Upstairs of MOMP are the members of the Bcl-2 family, divided between those that are antiapoptotic (prevent MOMP) and those that are proapoptotic (promote MOMP). These proteins share up to four Bcl-2 homology domains (BH1 to BH4). The proapoptotic "multidomain" proteins (sharing BH1, 2, and 3), Bax and Bak, appear to be prerequisite for MOMP and are likely to directly mediate it by forming size-indeterminate openings in the OMM (1, 5). They are present in most cells in inactive form, and their activation to cause MOMP is triggered by other proteins, including a subset of the "BH3-only" proteins (Bcl-2 family members sharing only the BH3 domain), but perhaps other non-Bcl-2 proteins as well (2). This poorly understood activation event is inhibited by the antiapoptotic Bcl-2 proteins that sequester the activating proteins and probably also the active multidomain proteins (3). This inhibition can be reversed by several other BH3-only proteins ("derepressors" or "sensitizers"), as well as by protein modifications (such as phosphorylation or deamidation) of the antiapoptotic proteins to control MOMP. The BH3-only proteins, both "activators" and "derepressors," are regulated in various ways—only some of which are fully understood—and their regulation is likely to represent many of the major portals through which different signaling events converge on the mitochondrial pathway of apoptosis (3).

Once MOMP occurs, proteins of the intermembrane space are released to the cytosol (4). One is holocytochrome c, which binds to cytosolic, monomeric apoptotic protease activating factor-1 (APAF-1). The interaction with cytochrome c permits a 2'-deoxyadenosine 5'-triphosphate (dATP)-mediated conforma-

tional change in APAF-1, promoting APAF-1 oligomerization to form an "apoptosome." The apoptosome then binds the proform of a protease, caspase-9. The oligomerization of caspase-9 on the apoptosome activates the protease; initiator caspases such as caspase-9 can only be activated by dimerization (6). The active caspase-9 cleaves two other caspases, caspase-3 and caspase-7. These are "executioner" caspases, and, unlike initiator caspases, these can only be activated by cleavage at specific sites, which are targeted by initiator caspases. Once activated, the executioner caspases orchestrate apoptosis through the cleavage of key substrates within the cell, resulting in demolition and packaging of the dying cell for removal by phagocytic cells.

The process of apoptosis "downstairs" of MOMP is regulated at the apoptosome and each of the caspases. The latter are controlled by inhibitor of apoptosis proteins (IAPs) that bind and ubiquitinate the caspases for proteasomal degradation. The function of the IAPs, in turn, is blocked by IAP inhibitors. These include Smac (also known as DIABLO) and Omi (also known as HtrA2), which compete with caspases for IAP binding. Like cytochrome c, Smac and Omi are sequestered in the mitochondrial intermembrane space and are only available to regulate the cytosolic IAPs upon MOMP.

Cell death can also proceed downstairs of MOMP independently of caspase activation. This may occur through the action of lethal factors released upon MOMP [for example, apoptosis-inducing factor (AIF) and endonuclease G have been suggested to have this function] or through irreparable loss of essential mitochondrial functions. Such "caspase-independent" death remains poorly understood (7).

What, then, is connected to death? The mitochondrial pathway of apoptosis can be triggered by a bewildering array of conditions, including virtually anything that contributes to cellular stress or loss of housekeeping functions (such as nutrient deprivation, unfolded proteins, cytoskeletal disruption, DNA damage, ion imbalance, and toxins), as well as developmental signals (such as cytokines, steroids, and lipid mediators) and immunologic effector processes (such as cytotoxic effector cells and some cytokines). One important model of tumor suppression holds that all signals to enter the cell cycle simultaneously engage the mitochondrial pathway of apoptosis as a checkpoint on tissue expansion (8). With about 100,000 citations to "apoptosis" in the scientific litera-

La Jolla Institute for Allergy and Immunology, 10355 Science Center Drive, San Diego, CA 92121, USA.

*Present address: Department of Medicine, McGill University, 687 Pine Avenue West, Montreal, Quebec H3A 1A1, Canada.

†Present address: Department of Immunology, St. Jude Children's Research Hospital, 332 North Lauderdale, Memphis, TN 38105, USA.

‡To whom correspondence should be addressed. E-mail: dgreen5240@aol.com

ture, one might be tempted to answer the above question, "everything."

Survival versus death of a cell is a binary decision, and as most deaths of vertebrate cells involve in some way the mitochondrial pathway of apoptosis, the Connections Map of this pathway might eventually extend to most of the proteins in the cell. At first this may seem far-fetched, but a simple model experiment shows the feasibility of this idea.

The "button experiment" of Kauffman (9) illustrates the principle. Start with 500 buttons and at random tie two together with thread. Now pick up a button at random and count how many are tied to it. Repeat. At first the answer will be one or two, but at some point a "phase transition" occurs in which most randomly selected buttons are tied to large numbers of other buttons. In our example, this happens when there are about half as many threads as buttons. By extension to molecules in a cell, we do not need many connections to "tie" all signaling pathways to one another. Many inputs will therefore influence the mitochondrial pathway of apoptosis, and because the outcome is control of cell life and death, the effects can be obvious and potentially overinterpreted.

This, then, is our problem. Simply showing that a molecule (or process, agent, condition, etc.) influences apoptosis does not prove that it directly acts on any of the key players in the pathway. And even if a connection with a protein in the pathway is shown, it need not be pivotal in the outcome for the cell. The challenge for understanding how the mitochondrial pathway of apoptosis is engaged and controlled is to identify the most important interactions dictating cell life or death in a given setting, and to extend the pathway toward those key events. A rigorous investigation of the most relevant relationships is needed. We have tried to provide a map of the many roads to cellular ruin through the mito-

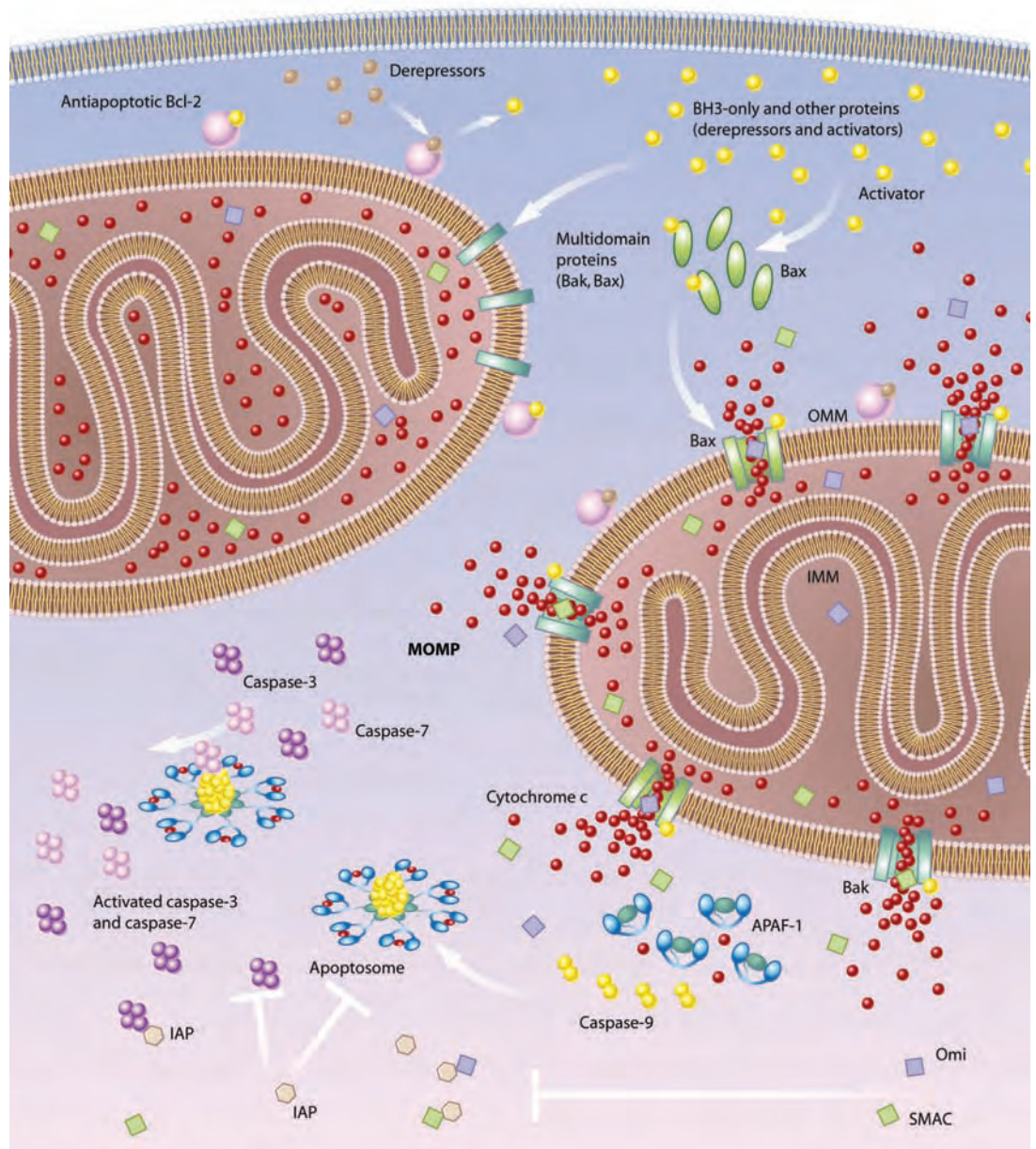


Fig. 1. The vertebrate mitochondrial pathway of apoptosis. At the core of this pathway is the process of mitochondrial outer membrane permeabilization (MOMP). This is mediated predominantly by the proapoptotic Bcl-2 family members, Bax and Bak, and inhibited by the antiapoptotic Bcl-2 family proteins. The BH3-only proteins of this family regulate MOMP either by activating Bax and Bak (activators) or by antagonizing the antiapoptotic Bcl-2 proteins (derepressors). MOMP allows proteins of the mitochondrial intermembrane space to gain access to the cytosol. Cytochrome c triggers the activation of APAF-1, leading to formation of the apoptosome followed by recruitment and activation of caspase-9. Caspase-9, in turn, cleaves and activates the executioner caspases 3 and 7 to orchestrate apoptosis by the cleavage of key substrates. IAP inhibits caspase activation, and this inhibition can be reversed by IAP antagonists (for example, Smac and Omi) released from the mitochondria upon MOMP.

chondrial pathway; the ones most traveled in apoptotic cell death remain to be determined.

References

1. C. Bender *et al.*, *Sci. STKE* (Connections Map, as seen October 2005), http://stke.sciencemag.org/cgi/cm/stkecm;CMP_18017.
2. Mitochondrial Pathway of Apoptosis: Multidomain Bcl-2 Family. *Sci. STKE* (Connections Map, as seen October 2005), http://stke.sciencemag.org/cgi/cm/stkecm;CMP_18015.
3. C. Bender *et al.*, *Sci. STKE* (Connections Map, as seen October 2005), http://stke.sciencemag.org/cgi/cm/stkecm;CMP_17525.
4. C. Bender *et al.*, *Sci. STKE* (Connections Map, as seen October 2005), http://stke.sciencemag.org/cgi/cm/stkecm;CMP_18019.
5. N. N. Danial, S. J. Korsmeyer, *Cell* **116**, 205 (2004).
6. K. M. Boaright, G. S. Salvesen, *Curr. Opin. Cell Biol.* **15**, 725 (2003).
7. J. E. Chipuk, D. R. Green, *Nat. Rev. Mol. Cell Biol.* **6**, 268 (2005).
8. D. R. Green, G. I. Evan, *Cancer Cell* **1**, 19 (2002).
9. S. Kauffman, *At Home in the Universe: The Search for the Laws of Self-Organization and Complexity* (Oxford Univ. Press, New York, 1995).

10.1126/science.1117105

Transforming Growth Factor- β Signaling in Stem Cells and Cancer

Lopa Mishra,^{1,3*} Rik Derynck,⁴ Bibhuti Mishra²

Transforming growth factor- β (TGF- β) and TGF- β -related proteins, such as the bone morphogenetic proteins, have emerged as key regulators of stem cell renewal and differentiation. These proteins have disparate roles in regulating the biology of embryonic stem cells and tumor suppression, and they help define the selection of cell fate and the progression of differentiation along a lineage. Here we illustrate their roles in embryonic stem cells and in the differentiation of neural, hematopoietic, mesenchymal, and gastrointestinal epithelial stem cells.

Stem cells are characterized by their undifferentiated state, their ability to give rise to fully differentiated cells, and their capacity for self-renewal. Embryonic stem (ES) cells are pluripotent cells derived from the inner cell mass of a blastocyst. They contribute to all three germ layers: ectoderm, mesoderm, and endoderm. A defining feature of ES cells is their ability to undergo prolonged symmetrical cell division in culture to produce identical pluripotent progeny. ES cells have evoked great interest, given their expected capacity to self-renew—thus resulting in an expansion of the cell population—and to differentiate into desired cell types—thus representing new sources for cell replacement therapy. Stem cells share some characteristics of cancer cells, including their ability to proliferate by a similar self-renewal process and the loss of contact inhibition. Furthermore, tumor growth and cancer progression are, at least in some cases, thought to be driven by a cancer stem cell population. Thus, studies of stem cells may provide guidance for our understanding of cancer development, and vice versa.

Multiple signaling networks orchestrate the development and differentiation of ES and somatic stem cells into functional neuronal, hematopoietic, mesenchymal, and epithelial lineages. Among these, the signaling mechanisms activated by TGF- β -family proteins have emerged as key players in the self-renewal and maintenance of stem cells in their undifferentiated state, the selection of a differentiation lineage, and the progression of differentiation along an individual lineage. Through gene knockout

experiments and observations with ES cells, TGF- β -family proteins have emerged as bifunctional regulators of the maturation of cells in each of the lineages mentioned above and as suppressors of carcinogenesis (1). Gradients of signaling, activated by the TGF- β -related bone morphogenetic proteins (BMPs), often lead to the selection of a defined differentiation pathway. TGF- β -family signaling then further drives differentiation along the lineage and maintains the differentiated phenotype of epithelial, mesenchymal, and other cell types, thereby interacting with other growth factors that help promote expansion of the cell population. When TGF- β signaling is disrupted, the imbalance can result in an undifferentiated phenotype, and cancer may ensue (2).

The TGF- β family contains about 30 structurally related growth and differentiation factors that include TGF- β s, activins, nodal and BMPs (1–3). TGF- β -family signals are conveyed through two types (type I and type II) of transmembrane receptor serine-threonine kinases, which form a complex at the cell surface (1, 3). Ligand binding to this complex induces a conformational change that induces phosphorylation and activation of type I receptors by type II receptors. Activation of Smad transcription factors ensues and results in their nuclear translocation and activation or repression of gene expression. The Smad activation and activity are modulated by various receptor- or Smad-interacting proteins that include ubiquitin and SUMO (small ubiquitin-related modifier) ligases, as well as multiple proteins in the transcription complexes (4). Depending on the differentiation stage of the target cell, the local environment, and the identity and dosage of the ligand, TGF- β proteins promote or inhibit cell proliferation, apoptosis, and differentiation. The diverse and often seemingly contradictory TGF- β functions can be understood by gene dosage; cross-talk of TGF- β -family signaling through Smads with other signaling pathways, such as Wnt and Hedgehog signaling and receptor tyrosine kinase signaling; and interac-

tions of Smads with a multitude of DNA binding transcription factors, which themselves are targeted by signaling pathways (1–5).

TGF- β -Family Signaling in ES Cells

Although human and mouse ES cells show substantial differences in their requirements for factors in the growth medium, TGF- β -family proteins play a role in both the maintenance of the cells in their undifferentiated state and in the initiation of differentiation. Nodal and activin, two TGF- β -related proteins that share the same receptors and Smads, are thought to have a role in human ES cell maintenance; accordingly, their receptors are expressed and their Smads are activated in undifferentiated ES cells (6). The activated Smad pathway downstream from these ligands is thus likely to cooperate with Wnt signaling in keeping the ES cells undifferentiated and pluripotent. BMP signals, in cooperation with leukemia-inhibiting factor (LIF), a member of the interleukin-6 (IL-6) cytokine family, are required to maintain mouse ES cells in an undifferentiated state. Apparently, the BMPs act through activation of BMP Smads, which in turn activate Id protein expression (6) transcription.

TGF- β -family signals mediate key decisions that specify germ layer differentiation. Thus, activin induces ventral or dorsal mesoderm and endoderm in *Xenopus* explants, depending on the dosage. In mammals, this signaling pathway is presumably activated by nodal or related factors. Conversely, inhibition of activin or TGF- β , as well as BMP signaling, gives rise to neuroectoderm formation in *Xenopus*, whereas the absence of these factors also allows neuroectoderm formation from mouse ES cells in culture. Activin or TGF- β also induces mesoderm differentiation, whereas BMP signals confer ectodermal and mesodermal differentiation, of human ES cells (7). Activin signaling also leads ES cells to differentiate into endoderm. Thus, the presence or absence of TGF- β -family signals is a determinant of both maintenance and initial specification of ES cells and of the primary cell fate decision in early embryogenesis that will give rise to multiple cell lineages and cell fates.

Roles of TGF- β Family Members in Neural Stem Cells

Neural differentiation from uncommitted ES cells is thought to occur in the absence of

¹Cancer Genetics and Digestive Diseases, ²Laboratory of CNS Development, Department of Surgery, Medicine & Lombardi Cancer Center, Georgetown University, Washington, DC 20007, USA. ³Department of Veterans Affairs, Washington, DC 20049, USA. ⁴Departments of Cell and Tissue Biology and Anatomy, Programs in Cell Biology and Developmental Biology, University of California, San Francisco, CA 94143, USA.

*To whom correspondence should be addressed at Georgetown University Medical/Dental Building, NW 212, 3900 Reservoir Road, N.W., Washington DC 20007, USA. E-mail: lm229@georgetown.edu; lopamishra@yahoo.com

exogenous TGF- β -family factors, yet it is also regulated by other inhibitory factors and cell adhesion proteins (8). Furthermore, BMPs inhibit neural differentiation and promote epidermal differentiation in *Xenopus* embryo explants; however, a gradient of BMP signaling does define the dorsoventral patterning of the neural tube (6). BMPs inhibit proliferation of ventricular zone progenitor cells at embryonic day 13 but enhance astroglial and neural crest cell differentiation at day 16; at higher doses, inducing apoptosis (9). Intriguingly, BMP-2 suppresses Sonic Hedgehog (Shh)-induced proliferation of medulloblastoma granule precursor cells, displaying a tumor-suppressive role. Additionally, the loss of Cripto, a functional Nodal receptor complex, also enhances neurogenesis (10), whereas the addition of Nodal suppresses neural differentiation.

Later in development, TGF- β promotes differentiation and lineage expansion of established progenitors; for example, by inducing autonomic gangliogenesis or olfactory neuron proliferation (11). There is a decrease of cerebellar Purkinje cells in *Smad4*^{-/-} mice and a proliferation of precursor cells in the developing cortex of mice lacking the Smad adaptor protein ELF (12, 13). Once a precursor lineage is established, TGF- β signaling appears to accelerate the differentiation and lineage commitment of precursor cells. Once cells are fully differentiated, TGF- β inhibits the growth of normal glial cells, setting the stage for malignant transformation into gliomas, if the growth-inhibitory and tumor-suppressor role of TGF- β is inactivated. At later stages of tumorigenesis, in gliomas, when the growth-inhibitory function of TGF- β is lost, TGF- β stimulates tumor progression and invasiveness, concomitantly with the angiogenic and immunomodulating activities of increased TGF- β expression by these cells (12, 14) (Fig. 1).

Roles of TGF- β Signaling in Hematopoietic Stem Cells

TGF- β -family proteins and their downstream signaling effectors, the Smads, also have key roles in hematopoietic differentiation (15, 16). TGF- β itself inhibits the proliferation of early multipotent hematopoietic stem cells but not that of later progenitors. The effects of TGF- β on more mature progenitor cells are complex and depend on the presence of other growth factors (17). In contrast to TGF- β , BMPs, in combination with cytokines, promote hematopoietic specification, differentiation, and proliferation of human ES cells (18). Although TGF- β acts as a negative regulator of hematopoietic progenitor and stem cells in vitro, impaired TGF- β signaling in vivo does not affect hematopoietic lineage selection (17). Indeed, the absence of a functional type I TGF- β receptor allows for normal development of hematopoietic progenitors and functional hema-

topoiesis in mouse embryos (19). The absence of Smad5, an effector of BMP and TGF- β signaling, enhances the efficiency of hematopoietic progenitor cell generation in embryoid bodies derived from ES cells (20), supporting the notion that TGF- β accelerates the differentiation and proliferation of committed precursors (Fig. 2). Signaling by TGF- β -family proteins through Smads may also regulate cell fate commitment decisions of myeloid versus lymphoid precursors. Enhanced myeloid differentiation at the expense of lymphoid commitment is observed when Smad7, which inhibits Smad activation, is overexpressed (21). To add to the complexity, the activation of feedback loops by TGF- β -family signaling further defines the regulation of hematopoietic stem cell differentiation. For example, BMPs activate the expression of the homeobox transcription factor *Dlx1*, which in turn blocks activin-induced differentiation of a hematopoietic cell line by interacting with Smad4 through its homeodomain (22).

Thus, TGF- β -family signaling through Smads exerts multiple effects that are dependent on the nature of the activating ligand and activated Smad pathway, as well as the nature and differentiation state of the targeted cell. Plenty of cross-talk of TGF- β -family signaling with other signaling pathways also occurs. Again, deregulation of TGF- β -family signaling may lead to malignant transformation and cancer progression. For example, expression of an AML1/EVI-1 chimeric gene that results from fusion of a segment of the protooncogene *Evi-1* to the N-terminal half of AML1, blocks the antiproliferative activity of TGF- β (23). This is achieved by the association of EVI-1 with Smad3, resulting in inactivation of the transcription function of TGF- β -activated Smad3.

TGF- β in Mesenchymal Stem Cells

Although mesenchymal stem cells are found predominantly in bone marrow, they are also interspersed in muscle, adipose, and connec-

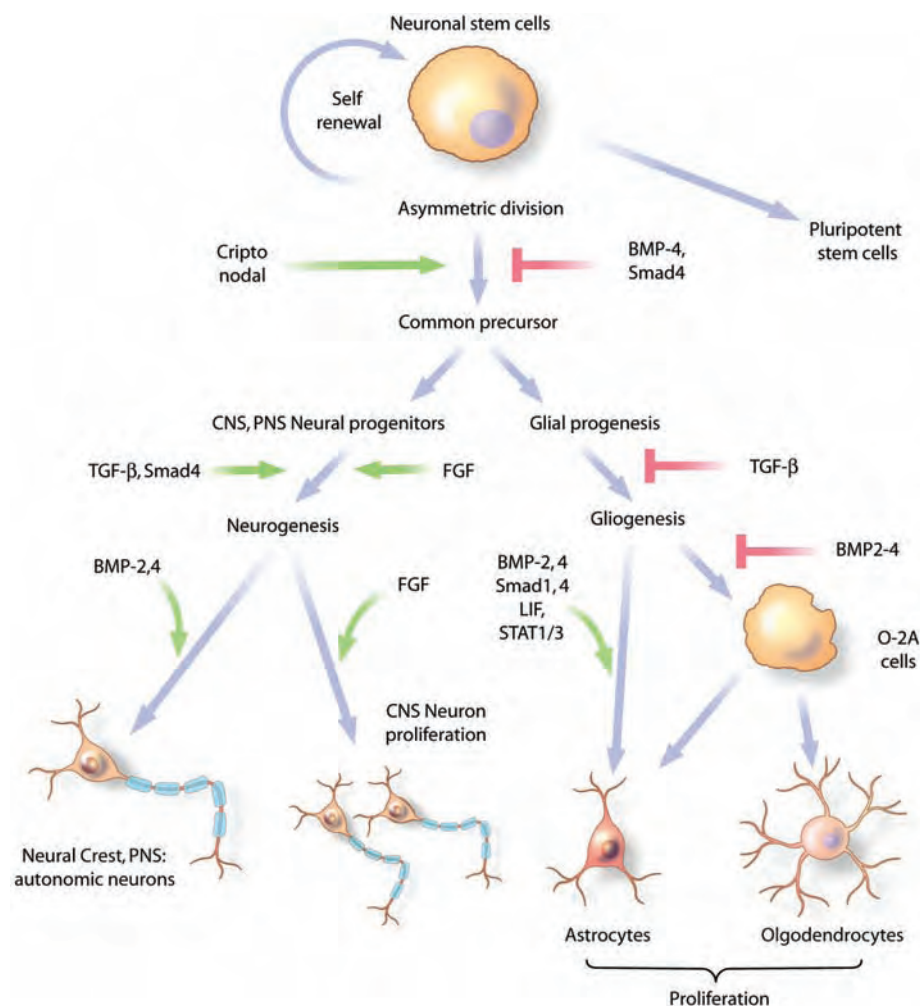


Fig. 1. Regulation of neural and neuronal differentiation by TGF- β -family signaling. The neural crest originates from the dorsal neural tube during the early stages of embryogenesis in vertebrates. Neural crest cells migrate to give rise to diverse cell types, including neurons and glia of the peripheral nervous system, smooth muscle cells, osteoblasts, and melanocytes. CNS, central nervous system; PNS, peripheral nervous system.

tive tissues, which are all of mesenchymal origin. The differentiation of mesenchymal stem cells into adipose, muscle, bone, or cartilage cells is defined by select TGF- β family members, often in cooperation with other signaling pathways. Although it is stimulatory for embryonic myoblasts, TGF- β itself inhibits the progression of differentiation and maturation of myoblasts, osteoblasts, and adipocytes. Combined with its stimulatory effect on mesenchymal cell proliferation, TGF- β signaling thus allows for an expansion of the mesenchymal stem cell population and of the progenitors of these different mesenchymal lineages (24). Because TGF- β expression and signaling are activated in response to injury, this response may be at the basis of efficient wound repair in mesenchymal tissues. Myostatin, a TGF- β -related factor that acts through the same type I receptor as TGF- β , is also emerging as a key regulator of myogenesis and possibly of fat differentiation. Inactivation of the myostatin gene confers a phenotype with excessive muscle mass (25). Conversely, BMPs drive mesenchymal cells into the osteoblast lineage yet can also stimulate fat cell differentiation under some culture conditions while antagonizing adipose maturation under others. BMP signaling may also allow mesenchymal cells to switch from an immature phenotype in one lineage to differentiation into another lineage. Indeed, BMPs activate early steps of osteoblast differentiation in myoblasts and pre-adipocytes, whereas BMP signaling in combination with retinoic acid signaling allows pre-adipocytes to differentiate into mature osteoblasts (26). The potent effects of BMPs on the differentiation of mesenchymal cells are at the basis of BMPs' ability to induce ectopic osteoblast

differentiation and bone deposition after administration into muscle or connective tissue. At such sites, BMPs mobilize mesenchymal cells to differentiate into bone-depositing osteoblasts.

TGF- β Signals in Gastrointestinal Tissues and Cancers

TGF- β -family signaling is most prominent at the interface between development and cancer in gut epithelial cells. Several TGF- β signaling components are bona fide tumor suppressors, with the ability to constrain cell growth and inhibit cancer development at its early stages. Inactivation of at least one of these components (such as the TGF- β receptors, Smad2, or Smad4) occurs in almost all gastrointestinal tumors (2, 27). Also, *Smad4*^{+/-} mice develop gastric tumors, and intercrossing of the *Smad4*^{+/-} genotype into mice with a mutation in the adenomatous polyposis coli tumor suppressor APC^{A716} results in the development of larger and more invasive colorectal tumors than those observed in the presence of the two *Smad4* alleles (28). These findings are consistent with the role of Smad4 in normal gut endoderm development. Support from genetic studies in the mouse has been crucial for identifying biologically significant proteins regulated by TGF- β in cancer suppression. Thus, genetic data demonstrate that only ELF, of the many adaptor proteins, is a TGF- β stem cell/differentiating factor, without which cancer ensues. Defects in gastrointestinal epithelial cell shape and polarity are also seen in *Smad2*^{+/-}/*Smad3*^{+/-} double heterozygous and *elf*^{-/-} homozygous mice, further arguing for a role of TGF- β signaling in normal gastrointestinal epithelial development (29).

BMP signaling may also play an active role in the stem cell compartments of the colon, presumably by suppressing the effects of Wnt signaling and consequently limiting stem cell renewal. Mutations in the BMP receptor BMPRI1A and in Smad4 contribute to juvenile intestinal polyposis and Cowden disease, respectively. Furthermore, inactivation of the gene for one of the type I BMP receptors in mice allows for an expansion of the stem and progenitor cell populations, eventually leading to intestinal polyposis resembling the human juvenile polyposis syndrome (2, 3).

Finally, TGF- β signaling also appears to be important for the transition of stem cells to a progenitor and fully differentiated phenotype in the liver and biliary system. Accordingly, *Smad2*^{+/-}/*Smad3*^{+/-} double heterozygous and *elf*^{-/-} homozygous mice all show defective liver development, with *elf*^{+/-} mice developing hepatocellular carcinoma (27, 30). Moreover, the TGF- β - and BMP-regulated protein PRAJA is expressed in hepatoblasts and modulates ELF and Smad3 (3, 31). The absence of this drive to normal epithelial differentiation may thus favor the formation of human hepatocellular carcinoma (Fig. 2).

As illustrated in this overview, TGF- β -family proteins and their signaling pathways play key roles in the self-renewal and maintenance of stem cells in their undifferentiated state, whereas changes in TGF- β -family signals drive the selection of defined differentiation pathways and their progression of differentiation. When deregulated, changes in TGF- β -family signaling may contribute to impaired differentiation and allow for the development of cancers, thus linking the differentiation of stem cells with the suppression of carcinogenesis.

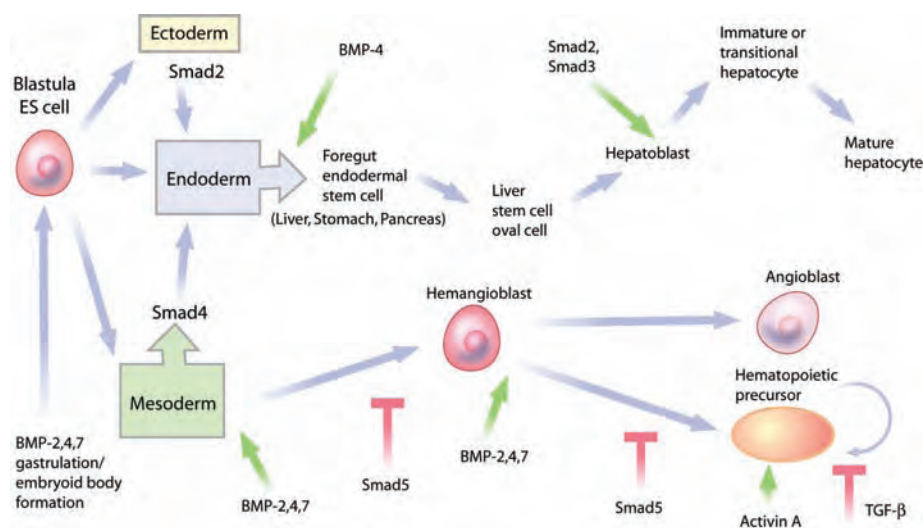


Fig. 2. Regulation of endodermal stem cells and differentiation into hepatocytes by TGF- β -family signaling. Ventral foregut endoderm cells develop into bipotential hepatoblasts that are committed to fetal hepatocytes. In hepatocarcinogenesis, human hepatic progenitor cells most likely give rise to hepatocellular carcinoma as well as cholangiocarcinomas. The lower part of the figure shows the role of TGF- β -family signaling in mesoderm and hematopoietic precursor differentiation.

References and Notes

1. J. Massague, S. W. Blain, R. S. Lo, *Cell* **103**, 295 (2000).
2. L. Mishra, A. Roberts, *Oncogene* **24**, 5667 (2005).
3. R. Derynck, Y. E. Zhang, *Nature* **425**, 577 (2003).
4. X.-H. Feng, R. Derynck, *Annu. Rev. Cell Dev. Biol.* **21**, 659 (2005).
5. A. K. Kitisin *et al.*, *Sci. STKE* (Connections Map, as seen September 2005), http://stke.sciencemag.org/cgi/cm/stkecm;CMP_18196.
6. Q. L. Ying, J. Nichols, I. Chambers, A. Smith, *Cell* **115**, 281 (2003).
7. M. Schuldiner, O. Yanuka, J. Itskovitz-Elder, D. A. Melton, N. Benvenisty, *Proc. Natl. Acad. Sci. U.S.A.* **97**, 11307 (2000).
8. I. Munoz-Sanjuan, A. H. Brivanlou, *Nat. Rev. Neurosci.* **3**, 271 (2002).
9. M. P. Fogarty, J. D. Kessler, R. J. Wechsler-Reya, *J. Neurobiol.* **64**, 458 (2005).
10. S. Parisi *et al.*, *J. Cell Biol.* **163**, 303 (2003).
11. R. M. Gangemi, M. Perera, G. Corte, *J. Neurochem.* **89**, 286 (2004).
12. Y. X. Zhou *et al.*, *J. Biol. Chem.* **278**, 42313 (2003).
13. Y. Tang *et al.*, *Science* **299**, 574 (2003).
14. N. Golestaneh *et al.*, *Sci. STKE* (Connections Map, as seen September 2005), http://stke.sciencemag.org/cgi/cm/stkecm;CMP_18170.
15. F. W. Ruscetti, S. Akel, S. H. Bartelmez, *Oncogene* **24**, 5751 (2005).
16. J. M. Scandura, P. Bocconi, J. Massague, S. D. Nimer, *Proc. Natl. Acad. Sci. U.S.A.* **101**, 15231 (2004).
17. J. Larsson, S. Karlsson, *Oncogene* **24**, 5676 (2005).

18. C. Park *et al.*, *Development* **131**, 2749 (2004).
 19. J. Larsson *et al.*, *EMBO J.* **20**, 1663 (2001).
 20. B. Liu *et al.*, *Blood* **101**, 124 (2003).
 21. K. Chadwick, F. Shojaei, L. Gallacher, M. Bhatia, *Blood* **105**, 1905 (2005).
 22. S. Chiba *et al.*, *Proc. Natl. Acad. Sci. U.S.A.* **100**, 15577 (2003).
 23. H. K. Lin, S. Bergmann, P. P. Pandolfi, *Oncogene* **24**, 5693 (2005).
 24. D. Chen, M. Zhao, G. R. Mundy, *Growth Factors* **22**, 233 (2004).
 25. S. J. Lee, *Annu. Rev. Cell Dev. Biol.* **20**, 61 (2004).
 26. J. Skillington, L. Choy, R. Derynck, *J. Cell Biol.* **159**, 135 (2002).
 27. M. Weinstein, X. Yang, C. Deng, *Cytokine Growth Factor Rev.* **11**, 49 (2000).
 28. K. Takaku *et al.*, *Cell* **92**, 645 (1998).
 29. Y. Tang *et al.*, *Cancer Res.* **65**, 4228 (2005).
 30. T. Blake, N. Ganesan, K. Shetty, L. Mishra, *Sci. STKE* (Connections Map, as seen September 2005), http://stke.sciencemag.org/cgi/cm/stkcm;CMP_17699.
 31. L. Mishra *et al.*, *Cancer Biol. Ther.* **4**, 694 (2005).
 32. Supported by NIH grants RO1 DK56111 (L.M.), RO1 CA106614A (L.M.), RO1 DK58637 (B.M.), RO1 CA63101 (R.D.), and P60 DE 13058 (R.D.), and by a Veterans' Administration Merit Award (L.M.). L.M. is a R Robert and Sally D. Funderburg Research Scholar. We thank M. Zasloff, D. Haines, N. Golestaneh, V. Muregesan, and T. Blake for critical review of the manuscript.

10.1126/science.1118389

VIEWPOINT

G Proteins Go Green: A Plant G Protein Signaling FAQ Sheet

Sarah M. Assmann

Plants, like animals, use signal transduction pathways based on heterotrimeric guanine nucleotide-binding proteins (G proteins) to regulate many aspects of development and cell signaling. Some components of G protein signaling are highly conserved between plants and animals and some are not. This Viewpoint compares key aspects of G protein signal transduction in plants and animals and describes the current knowledge of this system in plants, the questions that still await exploration, and the value of research on plant G proteins to scientists who do not study plants. Pathways in *Science's* Signal Transduction Knowledge Environment Connections Maps database provide details about the emerging roles of G proteins in several cellular processes of plants.

The turn of the 21st century, accompanied by completion of the sequencing of the genome of the model plant species, *Arabidopsis thaliana*, and the identification of G protein mutants in *Arabidopsis* and rice (*Oryza sativa*), has marked the start of a minirevolution in our understanding of G protein signaling in plants. This Viewpoint highlights the components, mechanisms, and functions of G protein signaling in plants as compared with metazoans (1–4).

Heterotrimeric G proteins are secondary messengers composed of three dissimilar subunits: $G\alpha$, $G\beta$, and $G\gamma$. $G\alpha$ and the nondissociable $G\beta\gamma$ dimer link signals emanating from altered activation states of G protein-coupled receptors (GPCRs) that contain seven transmembrane (7TM) domains to multitudinous intracellular effectors (Fig. 1). In humans, there are 20-some $G\alpha$ subunits, five $G\beta$ subunits, and about a dozen $G\gamma$ subunits. G proteins mediate vision, olfaction, and some aspects of gustation, and they are intimately involved in numerous neuroendocrine signaling pathways (5, 6). Thus, it is not surprising that G protein-centered signaling cascades are targets of an estimated one-third to one-half of the pharmaceuticals currently marketed (7, 8).

1) Do plants have heterotrimeric G proteins and are they essential? The genomes of diploid plant species encode single canonical G protein α subunit and G protein

β subunit proteins: GPA1 and AGB1 in *Arabidopsis* and RGA1 and RGB1 in rice (1, 2). Two *Arabidopsis* proteins, AGG1 and AGG2, are likely $G\gamma$ subunits on the basis of their ability to interact with plant $G\beta$ subunits, stretches of sequence similarity with known $G\gamma$ proteins including a predicted C-terminal prenylation site, and structural modeling (9–11). The corresponding rice homologs are RGG1 and RGG2 (12).

Knockout mutants of *GPA1*, *AGB1*, and the likely plant GPCR, *GCR1*, as well as their double- and triple-mutant combinations, are viable and healthy, although not phenotypically identical to wild-type plants, under standard laboratory conditions (Fig. 1, inset) (4). However, the extent to which such mutations would confer reduced fitness in the natural environment awaits assessment (13).

2) Do plants have any noncanonical G protein subunits? This viability of the G protein knockouts leads one to ask whether there are noncanonical G protein subunits in plants. Indeed, identified in plant genomes are the “extra large G protein” genes (*XLGs*) (2). The three *XLG* proteins of *Arabidopsis* and the four rice *XLGs* are twice as large as the typical metazoan $G\alpha$ protein and are typified by the presence of a carboxy half, with ~50% similarity to the plant $G\alpha$ subunit GPA1, and a unique amino half, with a cysteine-rich region and a nuclear localization site. *Arabidopsis* *XLG1* has been verified biochemically as a guanosine 5'-triphosphate (GTP)-binding protein. The plant *XLG* proteins have no se-

quence similarity outside of the $G\alpha$ domain with mammalian $XL\alpha$ proteins, which are $G\alpha_s$ splice variants (14) and, thus, are unlikely to be evolutionarily or functionally related.

A group of plant proteins, the *RACK1s* or *Arcs*, with three family members in *Arabidopsis*, has a predicted three-dimensional structure similar to that of $G\beta$ s (15). However, to date, there is no evidence that the *XLGs* or the *RACKs* interact with the canonical G protein subunits (that is *XLGs* with $G\beta\gamma$ and *RACKs* with $G\alpha$ or $G\gamma$), so their role as nonconventional subunits remains hypothetical.

3) Do plant genomes encode G protein regulatory proteins commonly found in metazoans? In known plant genomes, there are no obvious homologs of genes encoding arrestins or GRKs (G protein-coupled receptor kinase) (3). Plant genomes are rich in kinase-encoding genes (16), and another class of kinases may act as GRKs in plants. The *Arabidopsis* genome contains one *RGS* (regulator of G protein signaling) gene, *RGS1*, which encodes a protein with a predicted 7TM domain structure, followed by a domain containing an *RGS* box. On the basis of its unique structure, it is intriguing to speculate that *RGS1* may have dual function as a receptor and a guanosine triphosphatase (GTPase)-activating (GAP) protein (17).

4) Do plants have GPCRs, and do they share ligands with mammalian GPCRs? *GCR1* and *RGS1* are good candidates for plant GPCRs because they physically interact with GPA1 in planta, and because their genetic elimination affects plant processes, such as hormone sensitivity and cell division, known to be regulated by GPA1 (17, 18). The *Arabidopsis* protein *GCR1* has limited similarity within its predicted 7TM region to the slime mold cyclic AMP receptor, *CAR1* (18, 19). Because the 800 to 1000 metazoan GPCRs (20) are typified not by sequence conservation but rather by their 7TM structure, the absence in plant genomes of additional genes with

Biology Department, Pennsylvania State University, 208 Mueller Laboratory, University Park, PA 16802, USA. E-mail: sma3@psu.edu

sequence similarity to metazoan GPCRs does not necessarily lead to the conclusion that plants are deficient in these receptors. Indeed, plants have many predicted 7TM proteins (21). For one plant 7TM family, the MLO proteins, the 7TM structure of a family member from barley has been experimentally confirmed (22); whether any of the MLOs couple with $G\alpha$ awaits evaluation (23). Another question is whether dimerization, which is recognized for maturation and signaling of some metazoan GPCRs (24), is also important for the activity of plant 7TM proteins.

No ligands of GCR1 or RGS1 have yet been identified by ligand-binding experiments. However, *gpa1* knockout mutants have reduced sensitivity to sphingosine-1-phosphate (S1P), the ligand of the five mammalian S1P [previously referred to as the protein product of the endothelial differentiation gene (EDG)] GPCRs (25), as well as to the related metabolite, phytosphingosine-1-phosphate (26, 27); rice mutants in the $G\alpha$ subunit gene, *RGAI*, also show decreased responsiveness to sphingolipid compounds (28, 29). In addition, *rgs1* mutants exhibit altered sensitivity to glucose (17), and sugars are ligands for both yeast and mammalian GPCRs (30). Thus, there is evidence to suggest that some molecules act as GPCR ligands in both animals and plants.

5) Do plants exhibit signaling by GPCRs through G protein-independent pathways?

In *Arabidopsis*, knockout mutation of *GCR1* results in reduced sensitivity of seed germination to the germination-promotive hormones gibberellin (GA) and brassinolide. However, the double mutants *gcr1 gpa1* and *gcr1 agb1* have even less sensitivity to these hormones than the single *gcr1* mutants. Epistasis analysis predicts that, if GCR1 signals only through the G protein, then these single and double mutants should exhibit identical phenotypes, but they do not.

Thus, GCR1 may have a signaling role independent of the G protein (19), as has also been observed for some metazoan GPCR-mediated responses and has been termed "signaling at zero G" (31).

6) Do plant G proteins exhibit a G protein cycle of guanine nucleotide exchange and GTP hydrolysis?

In the classical paradigm, agonist activation of G protein signaling is initiated when GTP binds with $G\alpha$ and signaling is terminated by the intrinsic GTPase activity of $G\alpha$. Recombinant plant $G\alpha$ subunits also exhibit GTPase activity, although

rates are lower than for typical mammalian $G\alpha$ subunits (2, 32, 33). Moreover, GTPase activity of recombinant GPA1 is accelerated when assayed in the presence of the C4 domain of *Arabidopsis* RGS1, which includes the RGS box (17). Localization of the rice heterotrimer in the plasma membrane has been verified, and the α , β , and γ subunits cofractionate in gel filtration experiments (12). This cofractionation is disrupted when membranes are treated with the G protein activator, guanosine 5'-O-(3'-thiotriphosphate) (GTP- γ -S), or when a constitutively active version of the $G\alpha$ protein

of the subunit (34). There is no experimental evidence addressing this possibility in plants, but it is tantalizing that $G\alpha$ and $G\beta$ knockout mutants both exhibit alterations in cell division (11, 35).

7) Do plants and animals share similar G protein effector proteins?

Several plant effector proteins have been uncovered, and more are likely to be identified, especially because, to date, only two direct interaction partners have been identified for GPA1 and none for RGA1 or the $G\beta\gamma$ dimers. In vitro pull-down and yeast two-hybrid assays, *Arabidopsis* Pirin1, which is a postulated transcriptional cofactor, and phospholipase D $\alpha 1$ directly bind to GPA1 (36, 37). Increased phospholipase C (PLC) activity in tobacco cell lines overexpressing *GCR1* or *GPA1* also implicates this class of lipases as plant G protein targets (38). In addition, the TUBBY protein (39), which in mammalian cells exhibits PLC- β and $G\alpha_{q/11}$ -dependent translocation from the plasma membrane to the nucleus, has plant homologs (40). Through phenotypic analysis of *gpa1* knockout plants, inwardly rectifying K^+ channels and anion channels have been identified as targets of G protein signaling in *Arabidopsis* (26, 41), and application of recombinant tomato $G\alpha$ protein to excised plasma membrane patches increases the open probability of Ca^{2+} -permeable channels (32). Thus, there is some commonality between plant and animal G protein effectors.

8) Do G proteins regulate similar cellular and developmental processes in plants and animals?

Cell division, ion channel regulation, and disease response are processes regulated by G proteins in both plants and animals. *Arabidopsis gpa1* mutants exhibit decreased cell division in the hypocotyl (the seedling stem) and in leaves, and exhibit a rounded leaf shape (35). *agb1* mutants exhibit proliferation of lateral roots, a phenomenon linked to differential sensitivity to the phytohormone auxin (11).

An example of ion channel regulation by G proteins in plants can be seen in guard cells, in which the responses to another plant hormone, abscisic acid (ABA), are altered in *gpa1* mutants. Guard cells are specialized pairs of cells in the plant epidermis in which osmotically driven cell swelling or shrinkage regulates the width of the stomatal pore found between each guard cell pair, thereby controlling both carbon dioxide uptake and water vapor loss through

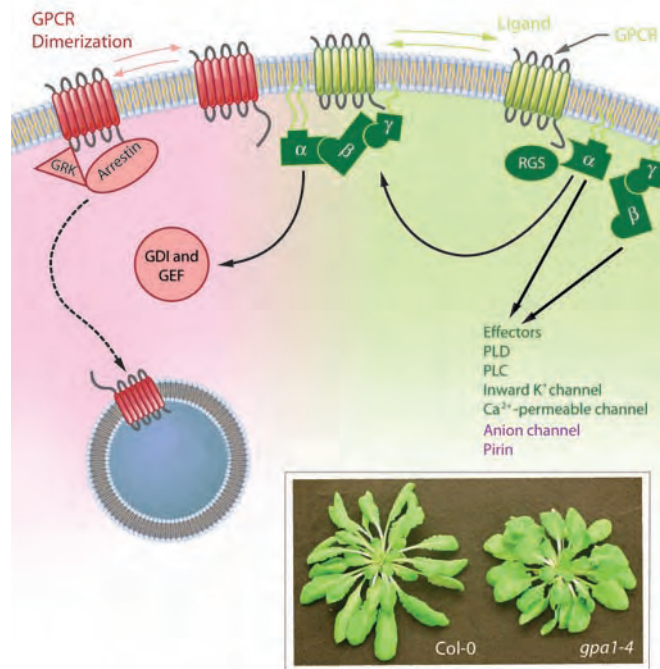


Fig. 1. The G protein cycle. Components and processes found in both plants and animals are indicated in green, with darker green indicating more definitive evidence (in plants) than lighter green. Those components and processes to date reported only for plants are in purple and those reported only for animals are indicated in red. GEF (guanine nucleotide exchange factor) and GDI (guanine nucleotide dissociation inhibitor) are two $G\alpha$ binding proteins so far only identified in animals. In addition to desensitization and internalization, arrestins also act as adapter proteins in the regulation of intracellular signaling. (inset) The round-leaf phenotype exhibited by $G\alpha$ (*gpa1*) knockout plants of *Arabidopsis* (right), in this case, a plant with the mutant allele *gpa1-4*, in comparison with a wild-type plant of the Columbia-0 ecotype (Col-0) (left).

is expressed (12). In addition, *gpa1* and *agb1* knockout plants share a subset of phenotypes (4). Thus, the classical mode of G protein signaling is likely to operate in plants, although the possibility also exists for unique modes of action, as suggested by the novel bipartite structure of the *Arabidopsis* RGS1 protein.

We are learning that "inactive," guanosine diphosphate (GDP)-bound $G\alpha$ subunits also can play an active role, e.g., in the regulation of mammalian cell division through interaction of GDP-bound $G\alpha$ with proteins that bind the GDP-bound but not the GTP-bound form

the pore. ABA inhibits inwardly rectifying K⁺ channels and activates anion channels in wild-type guard cells, but channels of *gpa1* guard cells show decreased ABA responsiveness (26, 41).

G proteins have been implicated in many aspects of human disease (6–8). In plants, rice *Gα* mutants exhibit reduced disease resistance responses to the highly destructive rice blast fungus and to fungal sphingolipid elicitors (28, 29), as described in the Connections Map (42).

9) What is the evidence for species-specificity in plant G protein function?

Arabidopsis gpa1 knockout plants are within the normal size range, and the most obvious phenotype of the mature vegetative plant is that the rosette leaves are rounded, rather than lanceolate (Fig. 1, inset). By contrast, rice plants harboring a nonfunctional *RGAI* gene are dwarfs (3, 4). The dwarfing in rice has been traced, at least in part, to reduced sensitivity of the *Gα* mutant stems to the plant hormone GA, which promotes cell elongation (43). With regard to seed germination, pharmacological and biochemical studies have shown that the *Gα* subunit of barley is involved in transducing the effects of ABA, whereas *Arabidopsis gpa1* mutant seeds exhibit hypersensitivity to this hormone, rather than the insensitivity predicted by the results from barley (36, 44, 45).

However, not enough is known yet about the complete signaling pathways to conclude that these phenotypic differences necessarily result from fundamentally different G protein signaling mechanisms in the different species. It is also important to note that the *Gα* mutants of rice and *Arabidopsis* also show some phenotypic similarities, such as reduced sensitivity of seed metabolism to GA (19, 43, 44). The Connections Maps for rice and *Arabidopsis* G protein signaling in seed germination should prove useful tools for exploring these comparisons (46, 47).

10) Do plants have some pathways that signal through *Gα* and other pathways that signal through *Gβγ*? Some phenotypes, such as rounded rosette leaves, are exhibited similarly by both *gpa1* and *agb1* knockout mutants (35, 48). Plausibly, these phenotypes are mediated by *Gα*, and loss of *Gβ* confers the same phenotype because, in the absence of *Gβ*, *Gα* cannot couple appropriately with its GPCRs, effectors, or both.

For pathways signaling through *Gβγ*, one might predict that knockout of *Gα*, which may increase the availability of free *Gβγ* to interact with its effectors, would lead to the opposite phenotype than knockout of *Gβ*, which would

eliminate *Gβγ*-effector coupling. Lateral root production appears to be one process that is regulated in this manner: Compared with wild type, *agb1* mutants exhibit increased numbers of lateral roots while *gpa1* mutants show decreased lateral root production. These results suggest that *AGB1* acts as a negative regulator of lateral root production (11). *agb1* mutants also exhibit more damage following acute O₃ treatment, whereas *gpa1* mutants exhibit more resistance than wild type (49). Thus, genetic evidence indicates that plants, like animals, have some pathways that signal through *Gα* and other pathways that signal through *Gβγ*.

11) What are the advantages to researchers studying nonplant systems of research on plant G protein signaling?

Plants afford several advantages to the study of heterotrimeric G proteins over those offered by other systems. Because of the plethora of G protein subunits in animals, it is not possible to create knockout mammals in which the effects of complete abrogation of G protein signaling can be assessed. By contrast, because plants have few G protein subunits, it is feasible to create knockout plants in which G protein signaling has been genetically eliminated. Plants and mammals share multicellularity, and some human disease-related genes are actually more similar to *Arabidopsis* genes than to counterpart genes in other model systems, such as yeast and *C. elegans* (16). Because plants and mammals also share some G protein effectors, changes in cellular processes detected in G protein knockout plants may also inform our knowledge of mammalian G protein signaling. A second advantage of such knockout plants is that they can be used as heterologous expression systems for the study of mammalian G protein signaling, in the absence of the “native” G protein subunits that complicate data interpretation when mammalian subunits are heterologously expressed in mammalian cell lines. Moreover, the cost and regulatory burden of maintaining transgenic plants as seeds is minimal.

Finally, it is worth pointing out that some exogenous ligands of human GPCRs, including key analgesics, are plant metabolites. One can anticipate that with the growth of the field of plant metabolomics, more plant-based GPCR ligands of pharmaceutical interest will be identified.

References and Notes

1. H. Ma, *Plant Mol. Biol.* **26**, 1611 (1994).
2. S. M. Assmann, *Plant Cell* **14**, (Suppl.), S355 (2002).
3. A. M. Jones, S. M. Assmann, *EMBO Rep.* **5**, 572 (2004).
4. L. Perfus-Barbeoch, A. M. Jones, S. M. Assmann, *Curr. Opin. Plant Biol.* **7**, 719 (2004).
5. A. J. Morris, C. C. Malbon, *Physiol. Rev.* **79**, 1373 (1999).

6. A. M. Spiegel, L. S. Weinstein, *Annu. Rev. Med.* **55**, 27 (2004).
7. A. Wise, S. C. Jupe, S. Rees, *Annu. Rev. Pharmacol. Toxicol.* **44**, 43 (2004).
8. Editorial, *Nat. Rev. Drug Discov.* **3**, 539 (2004).
9. M. G. Mason, J. R. Botella, *Biochim. Biophys. Acta* **1520**, 147 (2001).
10. M. G. Mason, J. R. Botella, *Proc. Natl. Acad. Sci. U.S.A.* **97**, 14784 (2000).
11. H. Ullah et al., *Plant Cell* **15**, 393 (2003).
12. C. Kato et al., *Plant J.* **38**, 320 (2004).
13. S. Assmann, *Sci. STKE*, re20 (2004).
14. J. Abramowitz, D. Grenet, M. Birnbaumer, H. N. Torres, L. Birnbaumer, *Proc. Natl. Acad. Sci. U.S.A.* **101**, 8366 (2004).
15. S. Ishida, Y. Takahashi, T. Nagata, *Proc. Natl. Acad. Sci. U.S.A.* **90**, 11152 (1993).
16. *Arabidopsis* Genome Initiative, *Nature* **408**, 796 (2000).
17. J. G. Chen et al., *Science* **301**, 1728 (2003).
18. S. Pandey, S. M. Assmann, *Plant Cell* **16**, 1616 (2004).
19. J. G. Chen et al., *Plant Physiol.* **135**, 907 (2004).
20. K. Kristiansen, *Pharmacol. Ther.* **103**, 21 (2004).
21. R. Schwacke et al., *Plant Physiol.* **131**, 16 (2003).
22. A. Devoto et al., *J. Biol. Chem.* **274**, 34993 (1999).
23. M. C. Kim et al., *Nature* **416**, 447 (2002).
24. S. Bulenger, S. Marullo, M. Bouvier, *Trends Pharmacol. Sci.* **26**, 131 (2005).
25. T. Sanchez, T. Hla, *J. Cell. Biochem.* **92**, 913 (2004).
26. S. Coursol et al., *Nature* **423**, 651 (2003).
27. S. Coursol et al., *Plant Physiol.* **137**, 724 (2005).
28. U. Suharsono et al., *Proc. Natl. Acad. Sci. U.S.A.* **99**, 13307 (2002).
29. D. Lieberherr et al., *Plant Physiol.* **138**, 1644 (2005).
30. I. Holsbeeks, O. Lagatie, A. Van Nuland, S. Van de Velde, J. M. Thevelein, *Trends Biochem. Sci.* **29**, 556 (2004).
31. J. A. Brzostowski, A. R. Kimmel, *Trends Biochem. Sci.* **26**, 291 (2001).
32. G. S. Aharon, A. Gelli, W. A. Snedden, E. Blumwald, *FEBS Lett.* **424**, 17 (1998).
33. F. S. Willard, D. P. Siderovski, *Methods Enzymol.* **389**, 320 (2004).
34. C. R. McCudden, M. D. Hains, R. J. Kimple, D. P. Siderovski, F. S. Willard, *Cell. Mol. Life Sci.* **62**, 551 (2005).
35. H. Ullah et al., *Science* **292**, 2066 (2001).
36. Y. R. Lapid, L. S. Kaufman, *Plant Cell* **15**, 1578 (2003).
37. J. Zhao, X. Wang, *J. Biol. Chem.* **279**, 1794 (2004).
38. F. Apone et al., *Plant Physiol.* **133**, 571 (2003).
39. K. Carroll, C. Gomez, L. Shapiro, *Nat. Rev. Mol. Cell Biol.* **5**, 55 (2004).
40. C. P. Lai et al., *Plant Physiol.* **134**, 1586 (2004).
41. X. Q. Wang, H. Ullah, A. M. Jones, S. M. Assmann, *Science* **292**, 2070 (2001).
42. S. M. Assmann, *Sci. STKE* (Connections Map, as seen October 2005), http://stke.sciencemag.org/cgi/cm/stkcm;CMP_18511.
43. M. Ueguchi-Tanaka et al., *Proc. Natl. Acad. Sci. U.S.A.* **97**, 11638 (2000).
44. H. Ullah, J. G. Chen, S. Wang, A. M. Jones, *Plant Physiol.* **129**, 897 (2002).
45. S. Ritchie, S. Gilroy, *Plant Physiol.* **124**, 693 (2000).
46. S. M. Assmann, *Sci. STKE* (Connections Map, as seen October 2005), http://stke.sciencemag.org/cgi/cm/stkcm;CMP_18476.
47. S. M. Assmann, *Sci. STKE* (Connections Map, as seen October 2005), http://stke.sciencemag.org/cgi/cm/stkcm;CMP_18492.
48. K. A. Lease et al., *Plant Cell* **13**, 2631 (2001).
49. J. H. Joo, S. Wang, J. G. Chen, A. M. Jones, N. V. Fedoroff, *Plant Cell* (2005).
50. Research on G proteins in the author's laboratory is supported by NSF (MCB 02-09694) and U.S. Department of Agriculture (2003-35304-13924). L. Wilson assisted with figure preparation.

10.1126/science.1118580

Bottom-Feeding Plesiosaurs

Colin R. McHenry,^{1*} Alex. G. Cook,² Stephen Wroe³

Long-necked, small-headed elasmosaurid plesiosaurs were distinctive predators of the Mesozoic oceans. Historically, on the basis of morphology and gut contents, they have been considered specialist hunters of agile fish and cephalopods (1, 2). Here, we report that the fossilized stomach contents of two Australian elasmosaurids are dominated by bottom-dwelling invertebrates.

The specimens were collected by the Queensland Museum (QM) from Early Cretaceous marine deposits of the Great Artesian Superbasin. Each was ~5 to 6 m long and weighed ~1000 kg.

Specimen QMF33037 is a partially articulated torso with associated limb elements from the late Aptian Doncaster Formation. Within the stomach cavity are the remains of many benthic invertebrates, predominantly bivalve shell fragments but also the remains of gastropods and pieces of crinoid (Fig. 1A). Two bivalve shells

are referable to *Macoyella*. Free-swimming taxa are represented by belemnite endoskeletons and a single teleost plate. Thirty-five gastroliths are also present, as is an 18-cm-long bromalite (3), digested material preserved within the animal's alimentary canal or defecated at the time of death (Fig. 1, B and C). From analysis of a cross section of the bromalite, we estimate that it comprises 92% gastropod and bivalve shell and 8% belemnite guards, similar to the proportions found in the stomach contents. Because belemnite endoskeletons represent a smaller fraction of the prey animals' live weight than do the shells of the benthic mollusks, these figures underestimate the proportion of nekton in the diet; however, gastropods and bivalves were clearly a major component of the predator's last meal. There is no evidence of action by stomach acids on material in the bromalite or the stomach cavity.

The second specimen (QMF2100) is an articulated torso from the late Albian Allaru

Formation. The stomach cavity contains an intact decapod carapace, several crustacean fragments, and a fish scale. There are also ~135 gastroliths, the lithology of which is predominantly acid to intermediate volcanic. The nearest source for the gastroliths was at least 300 km away from the burial site.

The long elasmosaurid neck has been understood as a specialization for the capture of free-swimming prey (4), but a large proportion of epibenthic prey in these specimens suggests that some individuals were not nekton specialists. Elasmosaurid teeth were conical, as in modern fish- and squid-eaters (5). The gastroliths present in the QM specimens were probably useful for crushing the calcareous shells of their prey, as has been suggested for specimens containing mollusks as minor components of gut content (6, 7). However, unbroken shells in the bromalite indicate that not all material was pulverized (Fig. 1C). Gastroliths with exotic provenance are common in elasmosaurid fossils (1, 8) and have been interpreted as evidence of deliberate ingestion (6), a behavior noted in crocodylians (9) that may be related to buoyancy control or digestion (1, 10, 11).

Stratigraphic analysis of Late Cretaceous elasmosaurid gut contents suggests that dietary preferences shifted from nektonic cephalopods to teleosts (1). Diet may have also varied with ontogeny (12). Our data raise the possibility that a more fundamental dietary shift occurred earlier in the family's history and suggest that even structures as apparently specialized as the elasmosaurid neck do not necessarily indicate narrow ecology. The success of long-necked plesiosaurs during the Mesozoic may have been partly due to a versatile feeding apparatus (Fig. 1D).

References

1. D. J. Cicimurri, M. J. Everhart, *Trans. Kans. Acad. Sci.* **104**, 129 (2001).
2. R. T. Bakker, *Geol. Assoc. Can. Spec. Pap.* **39**, 641 (1993).
3. C. Northwood, *Palaeontology* **48**, 49 (2005).
4. T. Thulborn, S. Turner, *Mod. Geol.* **18**, 489 (1993).
5. J. A. Massare, *J. Vertebr. Paleontol.* **7**, 121 (1987).
6. B. Brown, *Science* **20**, 184 (1904).
7. S. W. Williston, *Field Columb. Mus. Publ. Geol. Ser.* **2**, 1 (1903).
8. S. W. Williston, *Science* **20**, 565 (1904).
9. D. G. Darby, R. W. Ojakangas, *J. Paleontol.* **54**, 548 (1980).
10. D. M. Henderson, *Can. J. Zool.* **81**, 1346 (2003).
11. M. A. Taylor, *Nature* **290**, 628 (1981).
12. J. Wiffen, V. de Buffrenil, A. de Ricqlès, J.-M. Mazin, *Geobios* **28**, 625 (1995).

11 July 2005; accepted 7 September 2005
10.1126/science.1117241

¹School of Environmental and Life Sciences (Geology) University of Newcastle, New South Wales 2308, Australia. ²Geology, Queensland Museum, Post Office Box 3300, South Bank, Queensland 4101, Australia. ³Key Centre for Microscopy and Microanalysis, Electron Microscope Unit, F09, University of Sydney, New South Wales 2006, Australia.

*To whom correspondence should be addressed.
E-mail: colin.mchenry@newcastle.edu.au

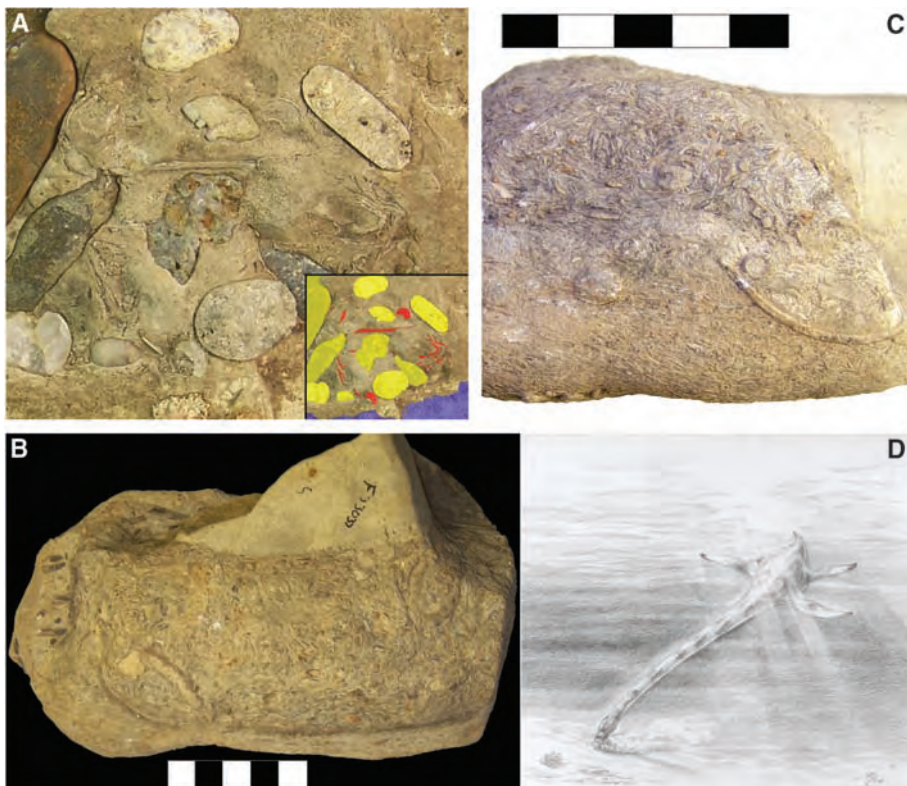


Fig. 1. (A) Close-up of a block containing stomach content from QMF33037. Inset: Interpretation of the block, showing gastroliths (yellow), molluscan shell (red), and parts of the elasmosaurid's ribs (blue). The field of view is 49.8 mm across. (B) Bromalite found in association with QMF33037, composed mainly of compacted, crushed mollusk shell. Belemnite guards are preserved on the left end of the bromalite. Scale bar, 5 cm. (C) End-on view of the QMF33037 bromalite; intact bivalve shell is visible to the lower right of the image. Scale bar, 5 cm. (D) Reconstruction of a Queensland elasmosaurid feeding on the benthos (Credit: Chris Glen).

Characterization of the Reconstructed 1918 Spanish Influenza Pandemic Virus

Terrence M. Tumpey,^{1*} Christopher F. Basler,²
 Patricia V. Aguilar,² Hui Zeng,¹ Alicia Solórzano,²
 David E. Swayne,⁴ Nancy J. Cox,¹ Jacqueline M. Katz,¹
 Jeffery K. Taubenberger,³ Peter Palese,² Adolfo García-Sastre²

The pandemic influenza virus of 1918–1919 killed an estimated 20 to 50 million people worldwide. With the recent availability of the complete 1918 influenza virus coding sequence, we used reverse genetics to generate an influenza virus bearing all eight gene segments of the pandemic virus to study the properties associated with its extraordinary virulence. In stark contrast to contemporary human influenza H1N1 viruses, the 1918 pandemic virus had the ability to replicate in the absence of trypsin, caused death in mice and embryonated chicken eggs, and displayed a high-growth phenotype in human bronchial epithelial cells. Moreover, the coordinated expression of the 1918 virus genes most certainly confers the unique high-virulence phenotype observed with this pandemic virus.

The influenza pandemic of 1918 was exceptional, resulting in the deaths of up to 50 million people worldwide, including an estimated 675,000 deaths in the United States (1, 2). The pandemic's most striking feature was the unusually high death rate among healthy adults aged 15 to 34 years, which consequently lowered the average life expectancy in the United States by more than 10 years (3). A similarly high death rate has not occurred in this age group in either prior or subsequent influenza A pandemics or epidemics (4).

Genomic RNA of the 1918 virus was recovered from archived formalin-fixed lung autopsy materials and from frozen, unfixed lung tissues from an Alaskan influenza victim who was buried in permafrost in November of 1918 (5, 6). The complete coding sequences of all eight viral RNA segments have now been determined, and analysis of these sequences has provided insights into the nature and origin of this pathogen (5–11). Plasmid-based reverse genetics has allowed for the generation of recombinant viruses containing 1918 hemagglutinin (HA) with or without the 1918 neuraminidase (NA) rescued in the genetic background of contemporary

human H1N1 or H3N2 influenza viruses. The resulting strains were demonstrated to cause mortality in mice only at high infection doses (12, 13); however, the virulence of the complete 1918 virus has not been evaluated.

In the present study, we generated a virus containing the complete coding sequences of the eight viral gene segments from the 1918 virus in an effort to understand the molecular basis of virulence of this pandemic virus. Genes encoding the 1918 influenza virus were reconstructed from deoxyoligonucleotides and corresponded to the reported coding sequences of the 1918 virus as previously described (5–11). Because the 1918 5' and 3' noncoding regions have not been sequenced, the genes were constructed such that they had the noncoding regions corresponding to the closely related influenza A/WSN/33 (H1N1) virus. The 1918 virus and recombinant H1N1 influenza viruses were generated using the previously described reverse genetics system (8, 14). All viruses containing one or more gene segments from the 1918 influenza virus were generated and handled under high-containment [biosafety level 3 enhanced (BSL3)] laboratory conditions in accordance with guidelines of the National Institutes of Health and the Centers for Disease Control and Prevention (15). Viruses were grown in Madin-Darby canine kidney cells (MDCK) cells and/or the allantoic cavity of 10-day-old embryonated hens' eggs (table S1). The control viruses included an avian A/duck/Alberta/35/76 H1N1 virus, two contemporary human H1N1 influenza viruses, the wild-type A/New Caledonia/20/99 (N. Cal/99, H1N1) virus and A/Texas/36/91 (Tx/91, H1N1) virus generated by reverse genetics. The other recombinant viruses used were a virus having only

the HA from the Tx/91 virus with the remaining seven genes from the 1918 virus (Tx/91 HA:1918); a virus having the NA from 1918 with the remaining seven genes from the Tx/91 virus (1918 NA:Tx/91); and recombinant viruses having two 1918 (1918 HA/NA:Tx/91) or five 1918 genes (1918 HA/NA/NP/NS:Tx/91) with the remaining genes derived from the Tx/91 virus. The HA of the 1918 viruses used throughout these studies was derived from A/South Carolina/1/18 strain that was shown to preferentially bind the α 2,6 sialic acid (human) cellular receptor (16). The identity of the 1918 and Tx/91 influenza virus genes in the rescued viruses was confirmed by reverse transcription polymerase chain reaction and sequence analysis.

The infectivity of the 1918 virus and the ability to form plaques in the presence and in the absence of the protease trypsin were assayed in MDCK cells by the plaque method. The proteolytic cleavage of the HA molecule is a prerequisite for multicycle replication, and the ability of an influenza virus to replicate in the absence of trypsin has been thought to be an important determinant of influenza virus pathogenicity in mammals (17–20). In contrast to the contemporary human Tx/91 and N. Cal/99 H1N1 viruses, which require an exogenous protease source for their multicycle replication and plaque formation (Table 1), the 1918 virus and a recombinant influenza virus bearing the 1918 HA and NA segments only (1918 HA/NA:Tx/91) formed visible plaques without the addition of trypsin (Table 1). Furthermore, a virus having only the 1918 NA with the remaining genes, including the HA, from Tx/91 virus (1918 NA:Tx/91) also replicated in the absence of trypsin, which suggests that the 1918 NA activity facilitates HA cleavage. However, the 1918 HA and NA gene sequences lack the obvious genetic features that have previously been associated with the ability

Table 1. Plaque formation of the 1918 virus in MDCK cells with or without trypsin. Serial 10-fold dilutions of virus stocks were prepared before a standard plaque assay. Duplicate monolayers of MDCK cells were washed extensively (7 times) before and after adsorption of virus. An agar overlay was added with or without trypsin (1 μ g/ml, Sigma) and incubated at 37°C with 5% CO₂ for 48 hours. 1918 (1) and (2) represent two independently rescued viruses.

Virus	Infectivity titer (PFU/ml)	
	Trypsin (+)	Trypsin (–)
N. Cal/99	3.6×10^7	–*
Tx/91	1.4×10^7	–
1918 HA/NA:Tx/91	2.4×10^7	2.1×10^7
1918 NA:Tx/91	3.4×10^7	2.5×10^7
1918 (1)	4.8×10^7	4.2×10^7
1918 (2)	1.4×10^8	1.1×10^8

*No visible plaques were formed at the lowest dilution (1:10) tested.

¹Influenza Branch, Mailstop G-16, Division of Viral and Rickettsial Diseases (DVRD), National Center for Infectious Diseases, Centers for Disease Control and Prevention, 1600 Clifton Road, NE, Atlanta, GA 30333, USA. ²Department of Microbiology, Mount Sinai School of Medicine, New York, NY 10029, USA. ³Department of Molecular Pathology, Armed Forces Institute of Pathology, Rockville, MD 20850, USA. ⁴Southeast Poultry Research Laboratory, Agricultural Research Laboratory (ARS), U.S. Department of Agriculture (USDA), 934 College Station Road, Athens, GA 30606, USA.

*To whom correspondence should be addressed. E-mail: tft9@cdc.gov

to replicate in the absence of trypsin; that is, the 1918 virus has neither a series of basic amino acids at the HA cleavage site (as seen in highly pathogenic avian H5 or H7 influenza viruses) nor mutations (N146R or N146Y) in the NA that lead to the loss of a glycosylation site like those that allow the A/WSN/33 virus NA to sequester plasminogen (6, 7, 17, 18, 20). We will need to consider other mechanisms of NA-mediated HA cleavability that may be relevant to the replication and virulence of the 1918 virus.

To evaluate the pathogenicity of the 1918 virus in a mammalian species, we intranasally inoculated BALB/c mice with two independently generated 1918 viruses and then determined morbidity (measured by weight loss), virus replication, and 50% lethal dose (LD_{50}) titers (21, 22). For comparison, groups of mice were infected with a recombinant influenza virus containing five 1918 genes with the remaining three polymerase genes from Tx/91 (1918 HA/NA/M/NP/NS:Tx/91) virus or a recombinant 1918 virus (Tx/91 HA:1918), in which the HA has been replaced with that of Tx/91 virus. Infection of mice with the 1918 virus resulted in lung virus titers, on day 4 post inoculation (p.i.), that were at least 125 and 39,000 times those of mice infected with the Tx/91 HA:1918 and Tx/91 viruses, respectively (Fig. 1A). The 1918 HA/NA/M/NP/NS:Tx/91 virus also replicated efficiently in the mouse lung, but virus titers were markedly lower than those for mice infected with the 1918 virus, and the lethality of the 1918 virus ($LD_{50} = 10^{3.25-3.5}$) was at least 100 times that for the 1918 HA/NA/M/NP/NS:Tx/91 virus ($LD_{50} = 10^{5.5}$). Strikingly, the mice infected with 10^6 PFU (plaque-forming units) of the 1918 virus succumbed to infection as early as 3 days p.i. (Fig. 1B), and they lost up to 13% of their body weight 2 days after infection (Fig. 1C). In contrast to the lethal outcome of the 1918 virus infection, the Tx/91 HA:1918 virus, like the

wild-type Tx/91 virus, did not kill mice ($LD_{50} = 10^{>6}$) (Fig. 1B) and displayed only transient weight reduction (Fig. 1C). To determine whether the 1918 virus replicated systemically in the mouse after intranasal infection with 10^6 PFU of virus, we harvested brain, heart, liver, and spleen tissues from four mice each on days 4 and 5 p.i. All eight mice infected with the 1918 virus or the Tx/91 control viruses had undetectable levels [$\leq 10^{0.8}$ of the 50% egg infectious dose (EID_{50})/ml determined by serial titration in chicken eggs] of virus in these tissues (fig. S1), which indicated that the 1918 virus did not spread systemically to other organs in the mouse.

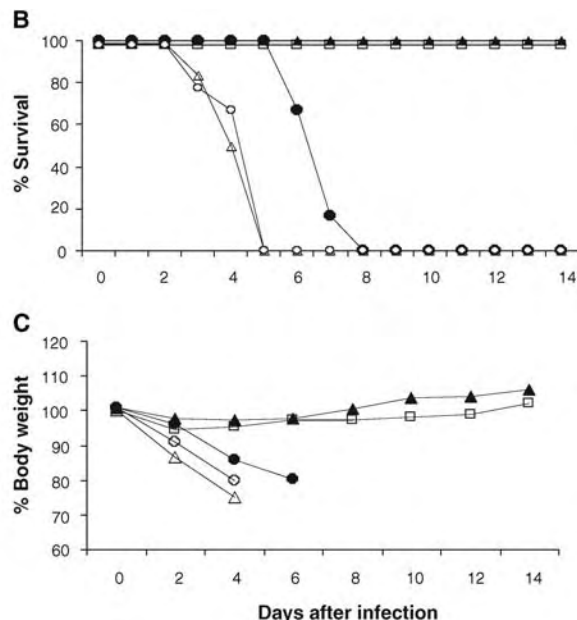
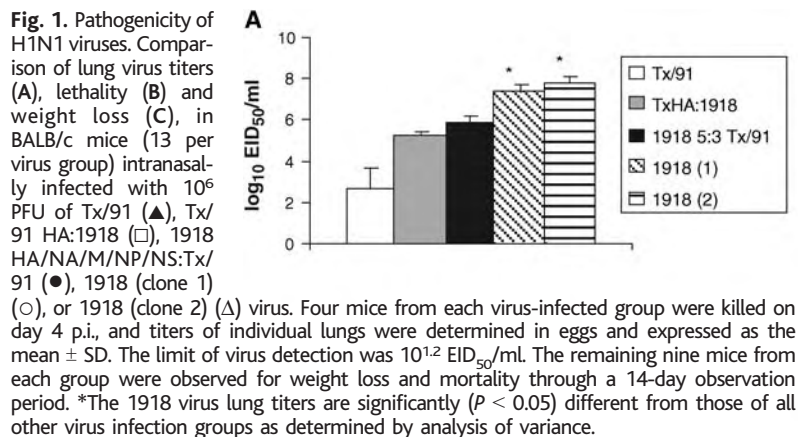
Histopathological analysis of lung tissues from individuals who died from primary influenza pneumonia in 1918 frequently showed acute pulmonary edema and/or hemorrhage with acute bronchiolitis, alveolitis, and bronchopneumonia (23). In mice, the most severe lung lesions were observed after infection with the 1918 virus (21). On day 4 p.i., mice infected with the pandemic strain had necrotizing bronchitis and bronchiolitis and moderate to severe alveolitis (Fig. 2A). The alveolitis varied from peribron-

chial to diffuse in distribution and was composed of neutrophils and macrophages. Accompanying the inflammation was moderate-to-severe peribronchial and alveolar edema (Fig. 2B) and alveolar hemorrhage. Neutrophils were the predominant inflammatory cells, but alveolar macrophages were also prominent (Fig. 2C). As in autopsy studies performed in 1918, there was no histological evidence of systemic infection such as necrosis or inflammation in the liver, kidney, spleen, heart, and brain tissues of mice infected with the 1918 virus. In general, the 1918 HA/NA/M/NP/NS:Tx/91 virus induced less severe pathology; however, mild-to-moderate peribronchial alveolitis with some mild-to-moderate alveolar edema was observed (Fig. 2D). The 1918 HA gene was essential for severe pulmonary lesion development, because the Tx/91 HA:1918 virus produced very mild pulmonary lesions characterized by minimal, diffuse alveolitis and mild focal lymphocytic-histiocytic peribronchitis (Fig. 2E). The Tx/91-inoculated mice lacked noteworthy lesions in the lungs (Fig. 2E).

Since 1918 virus gene sequences are related more closely to avian H1N1 viruses than any

Table 2. Lethality of the 1918 influenza virus for 10-day-old embryonated chicken eggs. Fifty percent egg infectious dose (EID_{50}) and egg lethal dose (ELD_{50}) titers were determined as described in the text. For ELD_{50} titers, embryo viability was visually determined by daily candling. EID_{50} and ELD_{50} titers were determined simultaneously and calculated by the method of Reed and Muench (27). The mean death time (MDT) of embryo death was calculated by examining embryo viability daily for 7 days. The MDT is the mean time in days for the minimum lethal dose to kill embryos.

Virus	$\log_{10} EID_{50}/ml$	$\log_{10} ELD_{50}/ml$	MDT (day)
N. Cal/99	8.5	≤ 1.2	-
Tx/91	8.7	≤ 1.2	-
Tx/91 HA:1918	9.0	≤ 1.2	-
1918 HA/NA:Tx/91	9.0	≤ 1.2	-
1918 HA/NA/M/NP/NS:Tx/91	8.7	≤ 1.2	-
1918 (1)	9.0	7.2	4.5
1918 (2)	9.5	8.2	4.5
A/duck/Alberta/35/76	9.0	8.5	2



other mammalian H1N1 strains (5–11), it was of interest to determine whether the 1918 strain would be lethal for fertile chicken eggs, a pathogenic feature of avian H1N1 viruses. After serial titration in 10-day-old embryonated chicken eggs, the 1918 virus was lethal for chicken embryos: 50% egg lethal dose (ELD₅₀) titers

were similar to those for an avian H1N1 representative, A/duck/Alberta/35/76 virus (Table 2). By contrast, neither contemporary human H1N1 viruses nor any of the 1918 recombinant viruses containing two, five, or seven genes from the 1918 virus caused mortality of embryos by day 7 p.i., which indicated that the 1918 HA

and 1918 polymerase genes were associated with virulence of chicken embryos.

We evaluated growth and release of the virus in polarized Calu-3 cells, a human lung epithelial cell line, grown on membrane inserts (24). Culture medium was collected from the apical and basolateral chambers at different times after inoculation and examined for virus production in the presence or absence of trypsin. With all viruses tested, titers of progeny virus progressively increased during the first 24 hours p.i., and virus was detected almost exclusively in the apical supernatant (Fig. 3). Regardless of the presence or absence of trypsin, infectivity titers of the 1918 virus were significantly higher than virus titers released in the Tx/91 HA:1918 and 1918 HA/NA/M/NP/NS:Tx/91 virus-infected cultures at 12, 16 and 24 hours p.i., which suggests that the 1918 HA and 1918 polymerase genes are essential for maximal replication of the virus in human bronchial epithelial cells. At 16 and 24 hours p.i., 1918 virus release was at least 50 times that observed in Tx/91 virus-infected cultures. The evidence of significantly higher apical release of 1918 progeny virus after an apical infection supports the hypothesis of an increase in the amount of virus present in the infected lung and may provide important insight into the virulence of this virus.

Until now, the exceptional virulence of the 1918 pandemic influenza virus has been a question of historical curiosity. Herein, we demonstrate the successful reconstruction of the 1918 pandemic virus in order to understand more fully the virulence of this virus and possibly of other human influenza pandemic viruses. Because the emergence of another pandemic virus is considered likely, if not inevitable (25), characterization of the 1918 virus may enable us to recognize the potential threat posed by new influenza virus strains, and it will shed light on the prophylactic and therapeutic countermeasures that will be needed to control pandemic viruses. A number of biological properties associated with this unusually virulent influenza virus were found. Comparison of the 1918 virus with recombinant viruses expressing one or more 1918 virus genes demonstrated that the 1918 HA and polymerase genes are essential for optimal virulence

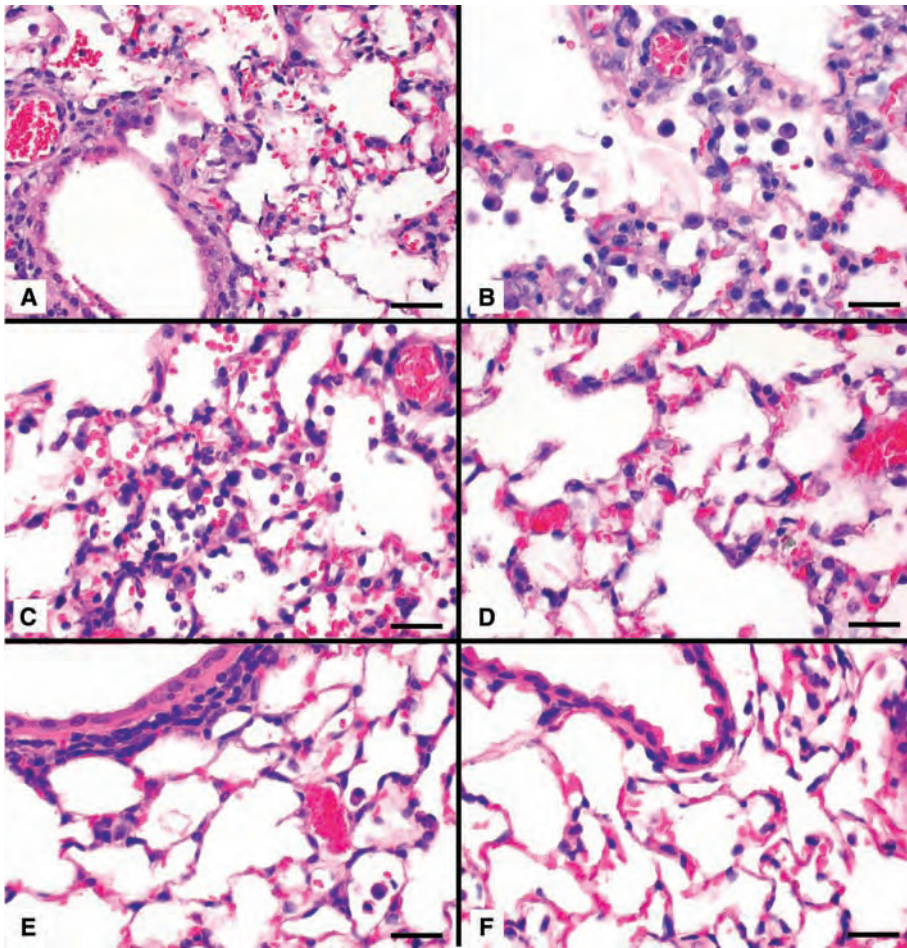
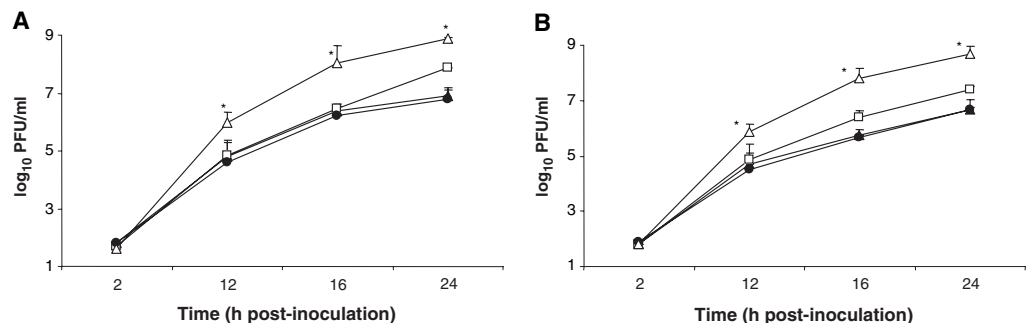


Fig. 2. Photomicrographs of hematoxylin and eosin–stained lung sections. (A to C), lungs from mice infected with the 1918 influenza virus: (A) necrotizing bronchiolitis and severe alveolitis, (B) severe alveolar edema and histiocytic alveolitis with scattered neutrophils, and (C) alveolitis, predominantly neutrophilic, and associated hemorrhage. (D) Moderate alveolitis and edema in lungs from a mouse infected with 1918 HA/NA/M/NP/NS:Tx/91 virus. (E) Mild peribronchial inflammation with adjacent minimal alveolitis in a mouse infected with Tx/91 HA:1918 virus. (F) Lung tissue from a Tx/91-infected mouse showing the paucity of lesions. Scale bars, 25 μm (A) and 15 μm (B to F).

Fig. 3. Release of 1918 influenza virus from apically infected human bronchial epithelial cells. Calu-3 cells were grown to confluency on transwell inserts as previously described (24). Cells were infected with Tx/91 (\blacktriangle), Tx/91 HA:1918 (\square), 1918 HA/NA/M/NP/NS:Tx/91 (\bullet), or 1918 (\triangle) virus at an MOI of 0.01 for 1 hour at 37°C. Unbound virus was removed by washing the cells 3 times, and infected cells were cultured in Dulbecco's modified Eagle's medium (DMEM) medium supplemented with 0.3% bovine serum albumin in the presence (A) or absence (B) of trypsin (1 $\mu\text{g}/\text{ml}$; Sigma, St. Louis, MO). Apical and basolateral (not shown) supernatants were collected at the indicated times and virus content was determined in a standard plaque assay.



The values shown represent the mean virus titer of fluids from three replicate infected cultures. *The 1918 virus titers are significantly ($P < 0.05$) different from those of all other virus infection groups as determined by analysis of variance.

and that the constellation of all eight genes together make an exceptionally virulent virus in the model systems examined. In fact, no other human influenza viruses that have been tested show a similar pathogenicity for mice 3 to 4 days after infection. This information provides a partial explanation for what made this virus so lethal. In this regard, it should be noted that the U.S. Food and Drug Administration (FDA)-approved antiviral drugs, oseltamivir and amantadine, have been shown to be effective against viruses carrying the 1918 NA and the 1918 M gene, respectively (22). Furthermore, vaccines containing the 1918 HA and NA were protective in mice (26).

Note added in proof: This research was done by staff taking antiviral prophylaxis and using stringent biosafety precautions (15) to protect the researchers, the environment, and the public. The fundamental purpose of this work was to provide information critical to protect public health and to develop measures effective against future influenza pandemics.

References and Notes

1. A. Crosby, *America's Forgotten Pandemic* (Cambridge Univ. Press, Cambridge, 1989).
2. N. P. Johnson, J. Mueller, *Bull. Hist. Med.* **76**, 105 (2002).
3. W. P. Glezen, *Epidemiol. Rev.* **18**, 64 (1996).
4. E. D. Kilbourne, in *The Influenza Viruses and Influenza*, E. D. Kilbourne, Ed. (Academic Press, New York, 1975), pp. 483–538.
5. J. K. Taubenberger et al., *Science* **275**, 1793 (1997).
6. A. H. Reid et al., *Proc. Natl. Acad. Sci. U.S.A.* **96**, 1651 (1999).
7. A. H. Reid et al., *Proc. Natl. Acad. Sci. U.S.A.* **97**, 6785 (2000).
8. C. Basler et al., *Proc. Natl. Acad. Sci. U.S.A.* **98**, 2746 (2001).
9. A. H. Reid et al., *J. Virol.* **76**, 10717 (2002).
10. A. H. Reid et al., *J. Virol.* **78**, 12462 (2004).
11. J. K. Taubenberger et al., *Nature* **437**, 889 (2005).
12. D. Kobasa et al., *Nature* **431**, 703 (2004).
13. T. M. Tumpey et al., *J. Virol.*, in press.
14. E. Fodor et al., *J. Virol.* **73**, 9679 (1999).
15. Interim CDC-NIH Recommendation (www.cdc.gov/flu/h2n2bs13.htm).
16. L. Glaser et al., *J. Virol.* **79**, 11533 (2005).
17. H. Goto, Y. Kawaoka, *Proc. Natl. Acad. Sci. U.S.A.* **95**, 10224 (1998).
18. H. Goto et al., *J. Virol.* **75**, 9297 (2001).
19. M. Hatta, P. Gao, P. Halfmann, Y. Kawaoka, *Science* **293**, 1840 (2001).
20. S. Li et al., *J. Virol.* **67**, 6667 (1993).
21. Materials and methods are available as supporting material on Science Online.

22. T. M. Tumpey et al., *Proc. Natl. Acad. Sci. U.S.A.* **99**, 13849 (2002).
23. M. C. Wintemitz, I. M. Wason, F. P. McNamara, *The Pathology of Influenza* (Yale Univ. Press, New Haven, CT, 1920).
24. C.-T. K. Tseng et al., *J. Virol.* **79**, 9470 (2005).
25. R. J. Webby, R. G. Webster, *Science* **302**, 1519 (2003).
26. T. M. Tumpey et al., *Proc. Natl. Acad. Sci. U.S.A.* **101**, 3166 (2004).
27. L. J. Reed, H. Muench, *Am. J. Hyg.* **27**, 493 (1938).
28. This work was partially supported by grants from the NIH to P.P., A.G.-S., C.F.B., and J.K.T. In the Ellison Medical Foundation Program in Global Infectious Diseases, P.P. is a Senior Fellow and C.F.B. is a New Scholar. This work was partially supported by USDA/ARS Current Research Information System (CRIS) project number 6612-32000-039-00D and by National Institute of Allergy and Infectious Diseases (NIAID) cooperative agreements with the Northeastern Biodefense Center (U54 AI57158) and with the Center for Investigating Viral Immunity and Antagonism (CIVIA) (U19 AI62623), as well as by NIAID grant P01 AI058113-01.

Supporting Online Material

www.sciencemag.org/cgi/content/full/310/5745/77/DC1

Materials and Methods

Fig. S1

Table S1

References and Notes

26 August 2005; accepted 20 September 2005

10.1126/science.1119392

REPORTS

A Reversible, Unidirectional Molecular Rotary Motor Driven by Chemical Energy

Stephen P. Fletcher, Frédéric Dumur, Michael M. Pollard, Ben L. Feringa*

With the long-term goal of producing nanometer-scale machines, we describe here the unidirectional rotary motion of a synthetic molecular structure fueled by chemical conversions. The basis of the rotation is the movement of a phenyl rotor relative to a naphthyl stator about a single bond axle. The sense of rotation is governed by the choice of chemical reagents that power the motor through four chemically distinct stations. Within the stations, the rotor is held in place by structural features that limit the extent of the rotor's Brownian motion relative to the stator.

One of the most challenging components required for the fabrication of molecular machines (1–5) is the rotary motor (6, 7): the element that converts energy into controlled rotational motion (8). Natural systems often use adenosine triphosphate (ATP) as an energy source. Rotation in these systems is powered by the energy released upon the hydrolytic conversion of ATP to the diphosphate ADP (6, 9, 10). The system introduced here analogously uses exothermic chemical reactions to power unidirectional rotary motion.

Previous synthetic molecular motor designs have often relied on external light or voltage as an energy source. Recent reports include repetitive, light-driven unidirectional motion about double bonds (11–13), as well as multistep reaction sequences that induce unidirectional (14) and reversible (15) mechanical motion in interlocked molecular rings, partly through photochemistry. A nanometer-scale rotational actuator based on multiwalled carbon nanotubes has also been demonstrated (16). Theory further predicts the feasibility of inducing unidirectional rotation about a single bond in a chiral system by applying linearly polarized laser pulses within optimized electric fields (17, 18), and inducing mechanical motion in a double-walled carbon nanotube by applying axially varying electrical voltage (19).

Purely chemical strategies have been scarcer (7, 20, 21). Limited unidirectional (120°) rotation about a single bond in a helically shaped molecule (22, 23) has been achieved with a modified molecular ratchet (24–26). Here, we report a system that uses chemical energy to achieve unidirectional 360° rotation of one half of the molecule relative to the other half (Fig. 1). The rotation is driven by a combination of chemical reactions and random thermal (Brownian) motion. Understanding these processes may be relevant to natural molecular motors, which work on similar principles.

Our system consists of a rotor half and a stator half, connected by a single carbon-carbon bond which acts as the axis of rotation (Fig. 1). Chemical reactions control movement of the rotor through four structurally distinct stations, with the net effect of turning the rotor 360° relative to the stator. Bonding and steric constraints limit the extent of the rotor's uncontrolled Brownian motion. In two of the stations (Fig. 1, stations A and C) the rotor's position is restricted by the action of additional chemical bonds, although helix inversion can occur. In stations B and D (Fig. 1), the rotor and stator cannot pass each other due to nonbonding interactions. Movement between the stations is guided by four power strokes, or chemically induced rotational events. The complete cycle involves two bond-breaking steps (step 1 and step 3) and two bond-making steps (step 2 and step 4), each of which provides the driving force for approximately 90° unidirectional rotation to the next station.

Two general mechanisms (27) for the conversion of energy into mechanical motion have

Department of Organic and Molecular Inorganic Chemistry, Stratingh Institute, University of Groningen, Nijenborgh 4, 9747 AG Groningen, Netherlands.

*To whom correspondence should be addressed. E-mail: b.l.feringa@chem.rug.nl

been identified: the power stroke (28, 29) and the Brownian motor (30, 31). The present motor relies on a power stroke mechanism to achieve unidirectional motion, the sense of which is solely dependent on chemical reactivity and not on inherent asymmetry within the motor itself. In a power stroke mechanism, the chemical reaction is mechanically coupled to movement and force is directly generated to move the motor forward (28, 29).

The locking of the upper rotor and lower stator was achieved by the presence of a lactone unit (structures **1a** and **1c** in Fig. 2). The *ortho* substituents on the aryl rings in structures **1b** and **1d** (Fig. 2) block free axial rotation for steric reasons and thereby prevent thermal helix inversion in the unlocked states.

Key to the overall unidirectional motion of the rotor are asymmetric reductive ring opening reactions of lactones **1a** and **1c** (32–34). The use of (*S*)-2-methyl-oxazaborolidine [(*S*)-CBS reagent] (32) resulted in an excellent enantioselectivity (ratio of 96.8:3.2 and 90.3:9.7 starting from **1a** and **1c**, respectively) and high preference for the rotor to move in the clockwise direction (Fig. 2). The sense of rotation induced in breaking the lactone bond (Fig. 2, step 1, **1a** → **1b** and step 3, **1c** → **1d**) is determined solely by the chirality of the fuel—i.e., the chiral reducing agent. Thus (*R*)-CBS could be used to drive counterclockwise rotation instead. Similarly, the sense in steps 2 and 4 is also controlled by the choice of chemical reagents, in this case the order of deprotection of the rotor's enantiotopic hydroxyl groups. After deprotection, the selectively released phenol group undergoes lactonization to return the rotor to **1c** or **1a**.

The order of the chemical transformations is essential (Fig. 2). The phenolic alcohols, which are the initial reduction products of **1a** and **1c**, must first be protected at the phenol position. After protection of the phenol moieties, the alcohols must be oxidized to the acids **1b** and **1d** before the opposite (orthogonally protected) phenol group is deprotected (in subsequent steps 2 and 4). Oxidation of an unprotected hydroxy phenol would form a lactol in situ. The rotational barriers of such biphenolic lactols are expected to be low (34), so the rotor would cross the plane of the stator and wide-angle oscillation would occur. When the rotor moves from **1b** → **1c** and **1d** → **1a**, complete unidirectionality is achieved by selectively unmasking only one of the phenolic hydroxyl groups.

Sterically congested 1-(4-methoxybenzyloxy)-6*H*-naphth[2,1-*c*]chromen-6-one (**1a**) was prepared from 1-bromo-2-naphthoic acid (35). Step 1 entailed first the asymmetric reduction of the lactone moiety in **1a** to a configurationally stable diol intermediate (34, 36) with a phenol on the rotor and a benzylic alcohol on the stator. Subsequent orthogonal protection of the phenol with an allyl group, then oxidation of the benzylic alcohol provided carboxylic acid **1b** (35). In step 2, removal of the *para*-methoxybenzyl (PMB)

protecting group induced spontaneous cyclization to lactone **1c**. Step 3, like step 1, involved asymmetric reduction of lactone **1c**, protection of the phenol with a PMB group, and alcohol oxidation to provide carboxylic acid **1d**. Finally, in step 4, removal of the allyl protecting group is followed by lactonization to regenerate **1a**. The whole reaction sequence produces a net unidirectional rotation of the rotor about the stator. Not all of the chemical manipulations in this cycle actually produce motion; however, each chemical conversion is currently a necessary component of the motor's design. These reac-

tions are used either to interconvert functionality so that motion is energetically favorable, or to ensure that the entire 360° rotational process occurs exclusively in one direction.

Although the lactone bond locks the rotor in place in **1a** and **1c**, these species are configurationally unstable and have a low barrier to racemization of the atropisomers (Fig. 3) (33, 34). Because the rotor and stator can pass through coplanarity by means of limited partial rotation (shown for **1a** in Fig. 3), the lactones exist as a racemic mixture of rapidly inverting helices. From this dynamic equilibrium, a stereoselective

Fig. 1. Schematic illustration for the operation of unidirectional power stroke motor **1**. A rotor (yellow and blue) is driven, about an axis, in the clockwise direction relative to the position of a stator (red). Four stations A to D are involved. Directionally selective bond breaking processes (step 1 and step 3) drive movement between stations.

These steps alternate with directionally selective bond-making chemical reactions (step 2 and step 4). The bond-breaking processes rely on chiral nonracemic chemical fuel that discriminates between the two dynamically equilibrating helical forms of A or C. The bond-making processes between the rotor and the stator use the principle of orthogonal chemical reactivity to achieve unidirectionality: Either the yellow or the blue end of the rotor can be selectively bound to the stator to form A or C.

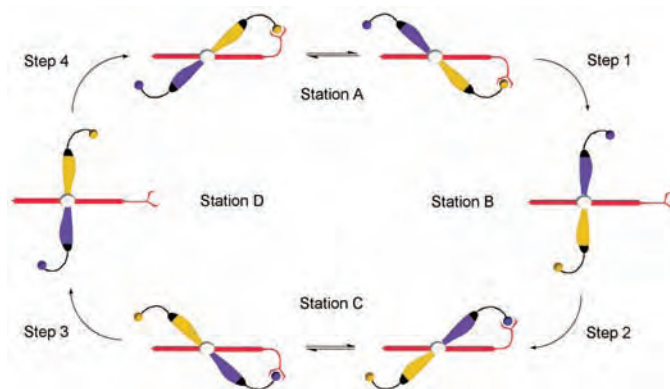
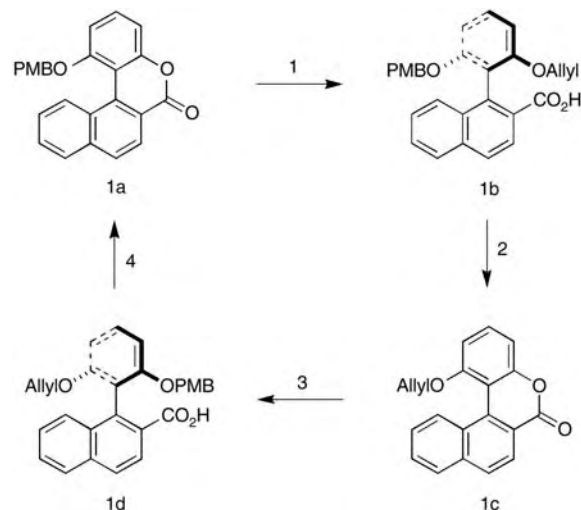


Fig. 2. Chemical structures and reaction scheme for unidirectional chemically driven rotary motor **1**. The rotary cycle had four steps employing the following reagents and conditions (unless otherwise stated, reactions were carried out at room temperature, and the percentage yields refer to preparatively isolated compounds).

Step 1 had two parts: (i) First, **1a** was reduced with (*S*)-2-methyl-CBS-oxazaborolidine and $\text{BH}_3\cdot\text{THF}$ in toluene and THF at 0°C for 25 min to give a 92% yield of a diol (bearing a phenol and an alcohol). The ratio of molecules that have undergone rotation in the indicated direction was 96.8 to 3.2. (ii) The phenol moiety was then alkylated by allyl bromide in a suspension of K_2CO_3 in DMF over 20 hours. Next, the alcohol moiety was oxidized to an aldehyde by $\text{CrO}_3\cdot\text{H}_2\text{SO}_4\cdot\text{H}_2\text{O}$ in acetone for 2 hours, and then to an acid by NaClO_2 in the presence of 2-methyl-2-butene in AcOH , H_2O , and THF over 1 hour to give **1b** in 76% overall yield. In **Step 2**, the PMB ether was cleaved by $\text{Ce}(\text{OTf})_3$ in MeNO_2 in the presence of 1,3-dimethoxybenzene at 60°C for 25 min to give **1c** in 76% yield. **Step 3** had three parts: (i) First, the lactone was reduced by (*S*)-2-methyl-CBS-oxazaborolidine and $\text{BH}_3\cdot\text{THF}$ in a solution of toluene and THF at 0°C for 7 min to give the diol (again bearing one phenol, one alcohol) in 56% yield. The ratio of molecules that underwent rotation in the indicated direction was 90.3 to 9.7. (ii) The phenol moiety was then alkylated by *p*-methoxybenzyl chloride in a suspension of K_2CO_3 and NaI in refluxing acetone over 30 hours to give the product in 87% yield. (iii) The alcohol moiety was oxidized first to the aldehyde by MnO_2 in CH_2Cl_2 for 48 hours, then to the acid by NaClO_2 in a solution of 2-methyl-2-butene, AcOH , H_2O , and THF for 1 hour to give **1d** in 82% overall yield. In **Step 4**, deprotection of the phenol by removing the allyl group was achieved with $\text{Pd}(\text{PPh}_3)_4$ and HCO_2H in refluxing THF over 24 hours and the product cyclized with *N,N'*-dicyclohexylcarbodiimide over 15 min to give the lactone **1a** in 99% overall yield. [The complete cycle including all intermediates is provided (35).]



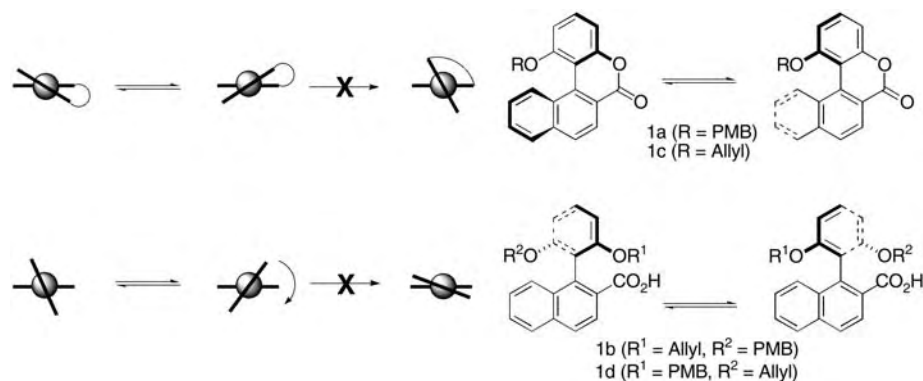


Fig. 3. Dynamic processes due to thermal rotary motion around the biaryl single bond in **1**. Projections are along biaryl single bond axis. In station A the lactone moiety locks the rotor in place relative to the stator. The lactone **1a** is configurationally unstable and limited movement in the form of dynamic helix inversion (biaryl rotation) occurs. In the open form of the motor **1b** partial rotation of the rotor relative to the stator can occur, but for steric reasons the rotor and the stator cannot pass each other. The same dynamic stereochemistry applies to **1c** and **1d**.

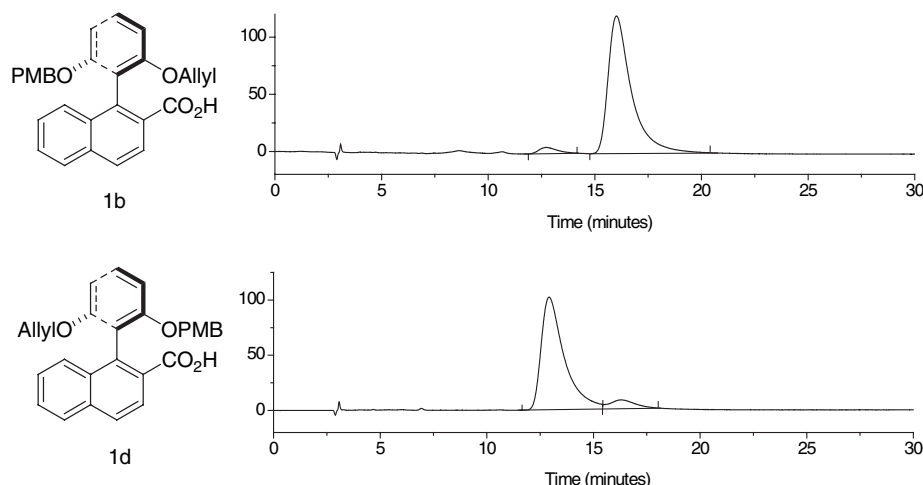


Fig. 4. Chiral HPLC chromatograms of **1b** and **1d** obtained from step 1 and step 3 (Fig. 2), respectively. Conditions: chiralpak AD column (0.46 × 15 cm); eluant 75:25 heptane-isopropanol; flow rate 0.6 ml/min; detection at 225 nm, temperature 40°C. The use of achiral NaBH_4 instead of (S)-2-methyl-CBS-oxazaborolidine produces two peaks of equal intensity (racemic **1b/1d**).

ring opening reaction with homochiral CBS reagents leads to unidirectional 90° rotation. In the open forms **1b** and **1d**, only partial rotation around the biaryl single bond can occur (shown for **1b** in Fig. 3); racemization is sterically precluded at room temperature (34, 36, 37).

The degree to which the rotation was unidirectional was determined by analyzing compounds **1b** and **1d** with the use of high-performance liquid chromatography (HPLC) with a chiral nonracemic stationary phase (Fig. 4 and supporting online material text). To confirm the location of the rotor relative to the stator, a mixture of **1b** and **1d** was prepared independently by performing the ring opening sequence of **1a** with racemic fuel (sodium borohydride). As expected, ring opening of **1a** occurred in both directions to generate an equal mixture of **1b** and **1d**. These species are enantiomers and have identical spectral data. Comparison of the HPLC traces of the racemic mixture with the HPLC traces of **1b** and **1d** generated by asym-

metric opening in our motor system revealed >90% directional selectivity for the motor sequence (Fig. 4). Thus, although motor **1** does require a number of synthetic steps, the absolute control in directionality for each of the four rotational events is between 90 and 100%.

The combination of reactions, purifications, and the time scale involved for the motor's function make it less practical than previously reported light-driven synthetic motors (11–13). However, this reversible rotary motor does establish that chemically driven 360° unidirectional rotation is feasible. The rotation is controlled, because the chemical events driving rotation are highly selective for a specific direction. Furthermore, each of the four stations provides a deep enough thermodynamic well to restrict thermal randomization of the rotational sense.

References and Notes

1. R. P. Feynman, in *Miniaturization*, H. D. Gilbert, Ed. (Reinhold, New York, 1961).

2. K. E. Drexler, *Nanosystems: Molecular Machinery, Manufacturing and Computation* (Wiley, New York, 1992).
3. K. Kinbara, T. Aida, *Chem. Rev.* **105**, 1377 (2005).
4. V. Balzani, A. Credi, F. M. Raymo, J. F. Stoddart, *Angew. Chem. Int. Ed. Engl.* **39**, 3349 (2000).
5. V. Balzani, M. Venturi, A. Credi, *Molecular Devices and Machines, A Journey into the Nano World* (Wiley-VCH, Weinheim, Germany, 2003).
6. M. Schliwa, Ed., *Molecular Motors* (Wiley-VCH, Weinheim, Germany, 2002).
7. C. P. Mandl, B. König, *Angew. Chem. Int. Ed. Engl.* **43**, 1622 (2004).
8. G. S. Kottas, L. I. Clarke, D. Horinek, J. Michl, *Chem. Rev.* **105**, 1281 (2005).
9. J. E. Walker, *Angew. Chem. Int. Ed. Engl.* **37**, 2308 (1998).
10. P. D. Boyer, *Angew. Chem. Int. Ed. Engl.* **37**, 2296 (1998).
11. N. Koumura, R. W. J. Zijlstra, R. A. van Delden, N. Harada, B. L. Feringa, *Nature* **401**, 152 (1999).
12. N. Koumura, E. M. Geertsema, M. B. van Gelder, A. Meetsma, B. L. Feringa, *J. Am. Chem. Soc.* **124**, 5037 (2002).
13. M. K. J. ter Wiel, R. A. van Delden, A. Meetsma, B. L. Feringa, *J. Am. Chem. Soc.* **125**, 15076 (2003).
14. D. A. Leigh, J. K. Y. Wong, F. Dehez, F. Zerbetto, *Nature* **424**, 174 (2003).
15. J. V. Hernández, E. R. Kay, D. A. Leigh, *Science* **306**, 1532 (2004).
16. A. M. Fennimore et al., *Nature* **424**, 408 (2003).
17. K. Hoki, M. Yamaki, Y. Fujimura, *Angew. Chem. Int. Ed. Engl.* **42**, 2976 (2003).
18. M. Yamaki, K. Hoki, Y. Ohtsuki, H. Kono, Y. Fujimura, *J. Am. Chem. Soc.* **127**, 7300 (2005).
19. Z. C. Tu, X. Hu, *Phys. Rev. B* **72**, 033404 (2005) (preprint available at <http://arxiv.org/abs/cond-mat/0501062>).
20. M. F. Hawthorne et al., *Science* **303**, 1849 (2004).
21. B. J. Dahl, B. P. Branchaud, *Tetrahedron Lett.* **45**, 9599 (2004).
22. T. R. Kelly, H. De Silva, R. A. Silva, *Nature* **401**, 150 (1999).
23. T. R. Kelly, R. A. Silva, H. De Silva, S. Jasmin, Y. J. Zhao, *J. Am. Chem. Soc.* **122**, 6935 (2000).
24. T. R. Kelly, I. Tellitu, J. P. Sestelo, *Angew. Chem. Int. Ed. Engl.* **36**, 1866 (1997).
25. For a related system see R. P. Feynman, R. B. Leighton, M. Sands, *The Feynman Lectures on Physics* (Addison-Wesley, Reading, MA, 1963), vol. 1, chap. 46.
26. A. P. Davis, *Angew. Chem. Int. Ed. Engl.* **37**, 909 (1998).
27. C. Bustamante, D. Keller, G. Oster, *Acc. Chem. Res.* **34**, 412 (2001).
28. H. Wang, G. Oster, *Nature* **396**, 279 (1998).
29. G. Oster, H. Wang, *Biochim. Biophys. Acta* **482**, 1458 (2000).
30. T. Elston, H. Wang, G. Oster, *Nature* **391**, 510 (1998).
31. R. Astumian, *Science* **276**, 917 (1997).
32. E. J. Corey, C. J. Helal, *Angew. Chem. Int. Ed. Engl.* **37**, 1986 (1998).
33. G. Bringmann, T. Hartung, *Angew. Chem.* **104**, 782 (1992), *Angew. Chem. Int. Ed. Engl.* **31**, 761 (1992).
34. G. Bringmann et al., *J. Organomet. Chem.* **661**, 31 (2002).
35. Materials and methods are available as supporting material on Science Online.
36. The configurational stability of the open forms was confirmed by chiral HPLC analysis, which showed no change in the enantiomeric ratio of the open forms throughout the chemical transformations.
37. The configurational stability of **1b** and **1d** was also verified by following its circular dichroism with respect to time. No change was observed after monitoring for 2 hours at 100°C.
38. We thank the Netherlands Organization for Scientific Research (NWO-CW), the Natural Sciences and Engineering Research Council of Canada (NSERC) (a postdoctoral fellowship to S.P.F.), and the Materials Science Centre (a postdoctoral fellowship to M.M.P.) for financial support. We thank M. Walko for performing the molecular modeling calculations.

Supporting Online Material

www.sciencemag.org/cgi/content/full/310/5745/80/DC1
Materials and Methods

SOM Text

Figs. S1 to S3

References

7 July 2005; accepted 24 August 2005
10.1126/science.1117090

Sequential Proton Transfer Through Water Bridges in Acid-Base Reactions

Omar F. Mohammed,¹ Dina Pines,² Jens Dreyer,¹ Ehud Pines,^{2*}
Erik T. J. Nibbering^{1*}

The proton transfer mechanism between aqueous Brønsted acids and bases, forming an encounter pair, has been studied in real time with ultrafast infrared spectroscopy. The transient intermediacy of a hydrated proton, formed by ultrafast dissociation from an optically triggered photoacid proton donor ROH, is implicated by the appearance of an infrared absorption marker band before protonation of the base, B⁻. Thus, proton exchange between an acid and a base in aqueous solution is shown to proceed by a sequential, von Grothuss-type, proton-hopping mechanism through water bridges. The spectra suggest a hydronium cation H₃O⁺ structure for the intermediate, stabilized in the Eigen configuration in the ionic complex RO⁻⋯H₃O⁺⋯B⁻.

Although aqueous proton transfer is one of the most fundamental chemical reactions (1), many molecular details remain elusive. Water mediates the transfer of a proton through membrane protein proton channels (2–4) and in the photosensor green fluorescent protein (5, 6). These proton channels function by a sequential hopping of protons through proton wires consisting of amino acid side groups and water molecules. A sequential proton transfer is also at the heart of the von Grothuss mechanism of anomalously high proton mobility in water (7). Water is considered to play a key role in aqueous acid-base neutralization reactions, where a proton is exchanged between an acid and a base, forming the conjugate base and conjugate acid, respectively. Theory suggests that water facilitates an efficient charge separation when the proton leaves the acid (8–10). Here, we show compelling experimental evidence that water also functions as a proton transfer bridge between an acid and a base, thereby stabilizing both acid and base while moving the proton along.

Infrared (IR) spectroscopy has been a useful tool to determine the structures of acids and bases in liquid solution from characteristic vibrational marker modes. However, it remains challenging to identify the hydrated proton in room-temperature aqueous acidic solutions, even at low pH (11), because the steady-state infrared spectrum is the result of hydrated proton species with strongly varying configurations. In particular, two different structures for hydrated proton species have been pro-

posed for aqueous solutions, the Zundel cation H₅O₂⁺ and the Eigen cation H₉O₄⁺. In the Zundel cation the proton resides in between two water molecules, H₂O⋯H⁺⋯OH₂ (11), whereas the Eigen cation H₉O₄⁺ consists of a H₃O⁺ core symmetrically solvated by three additional water molecules [H₃O⁺(H₂O)₃] (12). Even in the gas phase, a theoretical analysis of vibrational band patterns of hydrated proton clusters is not trivial (13–17). Experimentally, a recent study of such clusters has clarified how the hydration environment influences the infrared-active vibrational resonances of the hydrated proton (18). In liquid solutions at room temperature, on the other hand, a continuous dynamical exchange between all configurations exists (19–21). As a result, the description of the extremely broadened steady-state IR spectrum of concentrated acid solutions (11, 22, 23) and the possible underlying microscopic structures of the hydrated protons in solution phase remain debated subjects.

Proton transfer dynamics between acids and bases in aqueous solution may involve different reaction pathways and dynamics, depending on the absolute and relative reactivities and the geometries of the reactants and the number of water molecules in between acid and base and their relative orientations. The inherent complexity of aqueous acid-base reactions has been analyzed by Rini *et al.* (24, 25), who reported on three different types of acid-base reaction pathways in aqueous solution: In the case of tight acid-base complexes, where proton donating and accepting groups are directly linked, transfer of a proton is ultrafast, accompanied by only modest rearrangements of surrounding solvent shells. For loose (solvent-separated) complexes, where proton donating and accepting groups are linked by an intermediate water bridge, proton transfer may be largely controlled by the sol-

vent. Substantial reorganization of solvent shells either produces a tight complex or else stabilizes the charge transport over larger distances when the proton is channeled through a water bridge. In the third type, at low base concentrations, the acid and base molecules are initially separated by a substantial distance and must diffuse together, forming an encounter pair, before proton transfer can occur. In this case, the diffusion step is rate-limiting.

Use of a photoacid enables study of these different proton transfer pathways in real time. An optical trigger, the pump pulse tuned at the electronic transition of the photoacid, causes a pK_a (where K_a is the acid dissociation constant) jump of 6 to 7 units in the photoacid, initiating the proton transfer reaction. A probe pulse tuned in the mid-infrared then monitors the reaction progress of both proton-donating and proton-accepting molecules (24, 25).

For the aqueous neutralization reaction between pyranine (8-hydroxy-1,3,6-trisulfonate-pyrene or HPTS) and acetate (OAc⁻) in D₂O, Rini *et al.* have found that tight HPTS⋯OAc complexes transfer the deuteron within 150 fs (time resolution in the experiments), whereas encounter complexes formed after mutual diffusion react with an effective first-order time constant of about 7 ps (24, 25). A more detailed analysis of the kinetics of the proton transfer reaction to the acetate base at 1 to 4 M base concentration (25) has suggested the existence of an additional population (about 7% at 1 M) of preformed solvent-separated (loose) acid-base complexes that transfer the proton with a 6-ps time constant, similar to the proton transfer rate of encounter complexes formed by diffusion. Therefore Rini *et al.* inferred that the encounter reaction pairs must consist of loose water complexes of the type HPTS⋯(D₂O)_n⋯OAc without being able to specify the number *n* of water molecules linking HPTS and OAc or to elucidate details of the transfer dynamics of this complex.

To reveal finer details on aqueous acid-base reactions and in particular to elucidate the nature of these loose complexes, we have explored the carboxylic base family ⁻OOC-CH_(3-x)Cl_x because it offers a simple way to tune reactivity: with increasing number *x* of chlorine atoms, the basicity decreases [pK_a = 4.75 for acetic acid and pK_a = 2.7 for monochloroacetic acid (*x* = 1)]. Lower basicity results in a decrease in reaction exothermicity and slower proton transfer rates, opening the possibility of observing intermediates during the reaction. Here, we present results obtained for the reaction of HPTS with monochloroacetate (⁻OOC-CH₂Cl, abbreviated as ⁻OAc-Cl) (26). The advantage of the base ⁻OAc-Cl over ⁻OAc in solutions with molar base concentrations is threefold: The fraction of water-separated loose complexes is larger,

¹Max Born Institut für Nichtlineare Optik und Kurzzeitspektroskopie, Max Born Strasse 2A, D-12489 Berlin, Germany. ²Department of Chemistry, Ben-Gurion University of the Negev, Post Office Box 653, Beer-Sheva 84125, Israel.

*To whom correspondence should be addressed. E-mail: epines@bgumail.bgu.ac.il (E.P.); nibberin@mbi-berlin.de (E.T.J.N.)

the IR transmission for frequencies near 1435 cm^{-1} is sufficient for detection of the onset and the rise of a HPTS photobase marker band (Fig. 1), and slower proton transfer rates offer a longer window of observation.

We monitored a sequential proton-hopping mechanism in the loose complexes of $\text{HPTS}\cdots(\text{H}_2\text{O})\cdots^-\text{OAc-Cl}$ by following specific vibrational marker modes with femtosecond IR spectroscopy. In particular, we detected the transient IR-active absorption band of the hydrated proton and found it to be the marker band of the intermediate species in contact acid-base reactions: The transient appearance of the absorption of the hydrated proton is sequentially correlated with the transient disappearance of reactant and the appearance of product bands.

For solutions in D_2O , we observed the following IR-active vibrational marker bands of HPTS in the electronically excited state (Fig. 1): The decay of the photoacid (HPTS) band at 1486 cm^{-1} and the simultaneous rise of the conjugate photobase (HPTS⁻) band at 1435 cm^{-1} indicate when the deuteron leaves the photoacid (27). The electronically excited states of HPTS and HPTS⁻ decay with lifetimes of 4.8 and 5.3 ns, respectively, and thus have no influence on the dynamics discussed here. The rise of the carbonyl stretching band of chloroacetic acid (HOAc-Cl) at 1725 cm^{-1} marks the arrival of the deuteron at the base. Importantly, a previously unobserved transient absorption band located at 1850 cm^{-1} revealed the presence of an intermediate hydrated deuteron when the deuteron was channeled through the water bridge (Fig. 2B). This observation was corroborated by the detection of the corresponding, isotope-shifted, hydrated proton band at 2570 cm^{-1} in H_2O solutions (Fig. 2A).

We observed the decay of the photoacid band at 1486 cm^{-1} and the rise of the conjugate photobase band at 1435 cm^{-1} on multiple time scales (Fig. 1, B to D). In contrast to the situation in pure D_2O (no base added, Fig. 1A), about $20 \pm 5\%$ of the photobase signal appears for $1\text{ M}^-\text{OAc-Cl}$ within our time resolution of 150 fs (Fig. 3A), indicating prompt deuteron dissociation for this fraction of HPTS molecules. Because uncomplexed HPTS does not dissociate on this time scale in D_2O (28), the dissociation should be caused by nearby base molecules. However, unlike the case with the stronger ⁻OAc base (24, 25), no significant signal from the C=O stretching vibration of chloroacetic acid is detected for $1\text{ M}^-\text{OAc-Cl}$ base concentration until pulse delays of several picoseconds (Fig. 1, C and D, and Fig. 2B). It appears that the deuterons already dissociated from HPTS within 1 ps after excitation are located on water molecules: Concomitant with the initial rise of the photobase, we observe a

broad and well-defined band appearing within time resolution at 1850 cm^{-1} , indicating the transient existence of hydrated deuterons. We compare the location of this band with $1\text{ M}^-\text{OAc-Cl}$ measurements in H_2O (Fig. 2A). The appearance of a transient band at 2570 cm^{-1} is in full accordance with a H-D isotope effect of the hydrated proton or deuteron band, revealing that the band is likely due to an O-H or O-D stretching transition.

We exclude the possibility of a transient response of the O-H stretching band of HPTS in its photoacid form, because in D_2O we did not observe a signal within signal-to-noise around 1850 cm^{-1} and in H_2O we have detected a weaker featureless response with different transient dynamics (29). Moreover, we measured the neutralization dynamics of HPTS with acetate (⁻OAc) in D_2O with improved sensitivity (Fig. 2C). Consistent with previous estimations (25), the C=O stretching band of acetic acid reveals two types of acid-base complexes: 24% of the HPTS population form tight complexes that promptly transfer the deuteron to the acetate base, and a small fraction ($\sim 7\%$) of the HPTS population form loose $\text{HPTS}\cdots(\text{D}_2\text{O})\cdots^-\text{OAc}$ complexes. These loose complexes also give rise to the hydrated deuteron band at 1850 cm^{-1} , although it decays much more rapidly than the corresponding hydrated deuteron band we monitor with the ⁻OAc-Cl base.

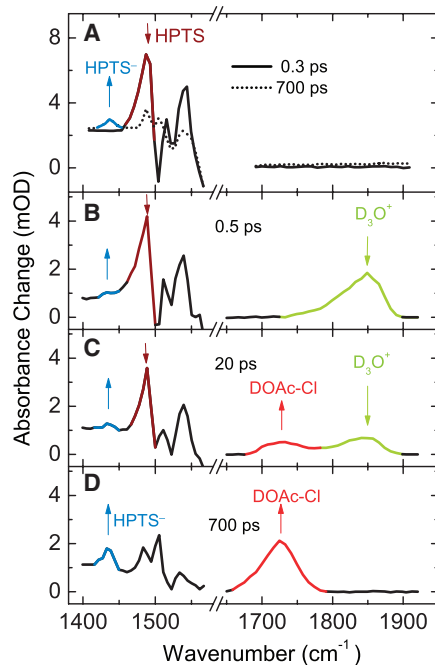


Fig. 1. Transient spectra showing the response of HPTS photoacid (brown, 1486 cm^{-1}) and HPTS⁻ photobase (blue, 1435 cm^{-1}) marker modes in the electronically excited state in the fingerprint region and the DOAc-Cl (red, 1725 cm^{-1}) and D_3O^+ (green, 1850 cm^{-1}) bands for the case of HPTS only (no base) (A) and for HPTS with $1\text{ M}^-\text{OAc-Cl}$ (B to D) in D_2O . OD, optical density.

Because the base-induced dissociation of the excited photoacid occurs within 150 fs, the proton-accepting base must be close to the photoacid, implying a limited number of water molecules in between acid and base (i.e., $n \sim 1$). Comparison with previously reported IR spectra of hydrated proton species in well-defined surroundings (18, 30–34) strongly suggests that the hydrated deuteron exists as the hydronium ion, D_3O^+ (and the hydrated proton as H_3O^+). In particular the position of the hydrated proton band observed here for the ionic complex $\text{HPTS}\cdots\text{H}_3\text{O}^+\cdots^-\text{OAc-Cl}$ is very similar to that observed for the Eigen cation $\text{H}_3\text{O}^+(\text{H}_2\text{O})_3$ as recently measured in spectra of hydrated proton clusters (18) and calculated for the Eigen cation in the proton wire of bacteriorhodopsin (34). Thus, our results are consistent with the hydrated proton in an Eigen solvation core with a symmetric hydrogen bonding configuration, i.e., $(\text{H}_3\text{O}^+)\text{L}_3$, with L representing hydrogen-accepting groups. We can exclude a role in the proton transfer dynamics of the Zundel cation H_5O_2^+ under our experimental conditions, because its vibrational transitions are located at other frequency positions (13, 18, 34). An intermediate complex of the type $\text{HPTS}\cdots\text{H}_3\text{O}^+(\text{H}_2\text{O})\cdots^-\text{OAc-Cl}$, where the hydronium ion is hydrogen bonded

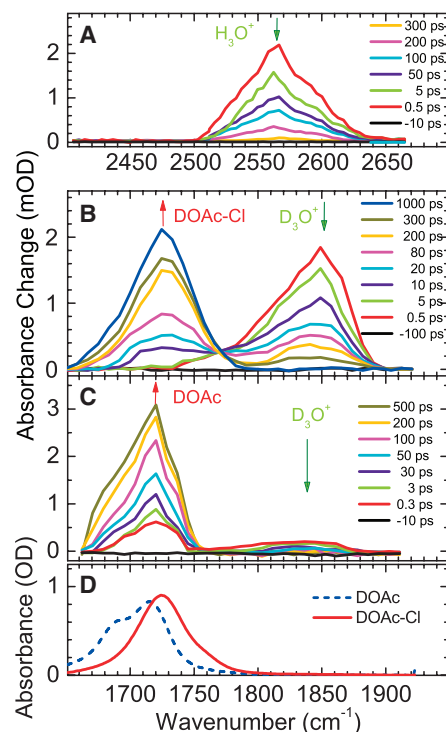


Fig. 2. Transient response of the hydronium O-H stretching band at 2570 cm^{-1} measured with $1\text{ M}^-\text{OAc-Cl}$ in H_2O (A), the C=O stretching band of DOAc-Cl at 1725 cm^{-1} , and the hydronium O-D stretching band at 1850 cm^{-1} for $1\text{ M}^-\text{OAc-Cl}$ in D_2O (B). For comparison, the transient response of a solution with $1\text{ M}^-\text{OAc}$ in D_2O is shown in (C), as well as the steady-state spectra of DOAc and DOAc-Cl also measured in D_2O (D).

to HPTS^- , $^- \text{OAc-Cl}$, and an additional H_2O , also seems unlikely, because such a complex would rearrange into $\text{HPTS}^- \cdots \text{H}_2\text{O}_2 \cdots \text{OAc-Cl}$. We propose that the intermediate complex has a hydronium ion with an almost symmetrically hydrogen-bonded Eigen core, where H_3O^+ connects to HPTS^- with a single hydrogen bond and in addition links to both oxygen atoms of $^- \text{OAc-Cl}$. With an approximate negative charge of $\sim 0.5e$ on all three oxygen atoms linked to the hydronium ion for both the electronically excited HPTS^- anion and for the delocalized unit charge over two oxygen atoms on $^- \text{OAc-Cl}$, the intermediate complex may acquire relative stability.

After the initial sub-time-resolution appearance of the hydrated deuteron (D_3O^+), we observe a picosecond decay of the D_3O^+ and a rise of the C=O band of DOAc-Cl. The fastest decay components of the D_3O^+ band (up to 5 ps), however, are not accompanied by an equally fast rising C=O DOAc-Cl band (Fig. 2B). We explain this discrepancy by a solvent rearrangement around D_3O^+ affecting the IR cross section (29, 35). These solvent rearrangements also enable the hydronium ion to transfer the deuteron in a second step to the base $^- \text{OAc-Cl}$. When comparing the magnitude of the D_3O^+ band at early delays with the final value reached by the C=O stretching mode, we can calculate the extinction co-

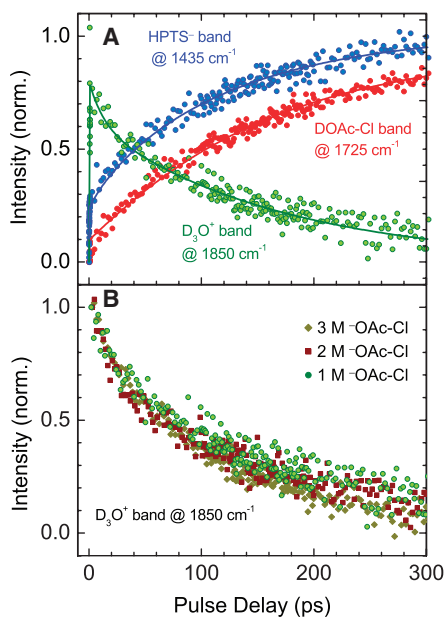
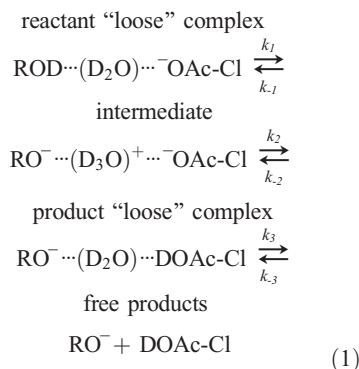


Fig. 3. (A) Normalized transient response for the HPTS^- photobase (blue), monochloroacetic acid (red), and hydronium marker bands (green) as a function of pulse delay (dots) for 1 M $^- \text{OAc-Cl}$ in D_2O . The fits (solid lines) have been obtained by using a reaction dynamics model implementing contributions from loose and tight acid-base complexes and initially uncomplexed HPTS^- (26). (B) Comparison of the normalized transient response of the hydronium band in the intermediate complex $\text{HPTS}^- \cdots \text{D}_3\text{O}^+ \cdots \text{OAc-Cl}$ showing no dependence on base concentration.

efficient of the D_3O^+ band to be $\epsilon_{\text{max}} \sim 900 \text{ M}^{-1} \text{ cm}^{-1}$. Such a value lies in the typical range for O-H or O-D stretching vibrations, even when taking into account the initial decrease in magnitude by a factor of 2 due to solvent reorganization.

On longer time scales, the D_3O^+ band disappears completely, whereas the C=O stretching band of DOAc-Cl as well as the conjugate photobase band at 1435 cm^{-1} reach their full magnitude. Because the observed dynamics are determined by different species in solution, we can obtain a consistent interpretation only by analyzing the dependence on base concentration. While keeping the HPTS^- concentration fixed at 20 mM, we varied the concentration of the base $^- \text{OAc-Cl}$ in the range from 0.5 to 3 M. In this concentration regime, we adjusted the relative concentration of the loose $\text{HPTS}^- \cdots (\text{H}_2\text{O}) \cdots \text{OAc-Cl}$ or $\text{HPTS}^- \cdots (\text{D}_2\text{O}) \cdots \text{OAc-Cl}$ complexes. The most important outcome of the concentration-dependent measurements is the finding that the dynamics of the hydrated proton band of these complexes are independent of base concentration, whereas the amplitude of the signal scales linearly with base concentration (Fig. 3B). At the highest concentrations, we also observed significant signal contributions of tight $\text{HPTS}^- \cdots \text{OAc-Cl}$ complexes, whereas at the lowest base concentrations the signal contributions are dominated by the fully separated HPTS^- and base and the acid-base population then shows diffusion-controlled reaction dynamics.

We have modeled the reaction dynamics of the intermediate species with a kinetic mechanism of acid-base proton transfer by using the reacting model in Eq. 1 (26), which is a variant of the Eigen kinetic scheme for general acid-base reactions (12):



We calculate a time constant for the initial photoacid dissociation step, when $\text{HPTS}^- \cdots (\text{D}_3\text{O}^+) \cdots \text{OAc-Cl}$ is formed faster than 150 fs, limited by our experimental resolution. The second transfer, generating $\text{HPTS}^- \cdots (\text{D}_2\text{O}) \cdots \text{DOAc-Cl}$, has a much slower time constant of 25 ps. The observed isotope H-D effect on the decay constant of the intermediate ionic complex $\text{HPTS}^- \cdots (\text{D}_3\text{O}^+) \cdots \text{OAc-Cl}$ is governed by the square root of the ratio of the isotope

masses ($m_{\text{H}}/m_{\text{D}})^{1/2}$, $k_{\text{H}}/k_{\text{D}} \sim 1.45$. With a diffusion-controlled time constant of 50 ps, the product complex $\text{HPTS}^- \cdots (\text{D}_2\text{O}) \cdots \text{DOAc-Cl}$ separates into the bulk solution, thus completing the acid-base proton transfer reaction.

The proton and deuteron transfer dynamics we observe for the $\text{HPTS}^- \cdots (\text{H}_2\text{O}/\text{D}_2\text{O}) \cdots \text{OAc-Cl}$ complex exhibit a von Grothuss-type sequential hopping mechanism reminiscent of the results of a theoretical study of acid dissociation of hydrogen halides in water (8, 9). For comparison, the proton transmission through water also occurs by sequential hopping to neighboring water molecules (7, 19, 21, 36). Both for proton transmission in neat water and for hydrogen halide dissociation, the primary and secondary accepting sites are water molecules. In our experiment we have chemically distinct reaction partners on the primary (water) and secondary (base) accepting sites. Optically triggering the proton transfer in our experiment reveals the time scales of these sequential stages of aqueous proton transfer. Whereas the first proton or deuteron transfer step is faster than 150 fs, indicating a preexisting reaction coordinate with an almost barrierless reaction dynamics, the second transfer takes much longer. The $\text{HPTS}^- \cdots (\text{D}_3\text{O}^+) \cdots \text{OAc-Cl}$ complex is relatively long lived, with lifetimes of several tens of picoseconds (37) contrasting with the ~ 1 ps lifetimes of the hydrated proton H_3O^+ in liquid water (4) as estimated from nuclear magnetic resonance studies (38) and from theoretical investigations (20, 21).

References and Notes

- J. T. Hynes, *Nature* **397**, 565 (1999).
- H. Luecke, H.-T. Richter, J. K. Lanyi, *Science* **280**, 1934 (1998).
- W. Kühlbrandt, *Nature* **406**, 569 (2000).
- T. E. Decoursey, *Physiol. Rev.* **83**, 475 (2003).
- M. Zimmer, *Chem. Rev.* **102**, 759 (2002).
- D. Stoner-Ma et al., *J. Am. Chem. Soc.* **127**, 2864 (2005).
- C. J. T. de Groot, *Ann. Chim. Phys.* **LVIII**, 54 (1806).
- K. Ando, J. T. Hynes, *J. Phys. Chem. B* **101**, 10464 (1997).
- K. Ando, J. T. Hynes, *J. Phys. Chem. A* **103**, 10398 (1999).
- P. L. Geissler, C. Dellago, D. Chandler, J. Hutter, M. Parrinello, *Science* **291**, 2121 (2001).
- G. Zundel, *Adv. Chem. Phys.* **111**, 1 (2000).
- M. Eigen, *Angew. Chem. Int. Ed.* **3**, 1 (1964).
- K. R. Asmis et al., *Science* **299**, 1375 (2003).
- M. Miyazaki, A. Fujii, T. Ebata, N. Mikami, *Science* **304**, 1134 (2004); published online 29 April 2004 (10.1126/science.1096037).
- J. W. Shin et al., *Science* **304**, 1137 (2004); published online 29 April 2004 (10.1126/science.1096466).
- T. D. Fridgen, T. B. McMahon, L. MacAleese, J. Lemaire, P. Maitre, *J. Phys. Chem. A* **108**, 9008 (2004).
- J. M. Headrick, J. C. Bopp, M. A. Johnson, *J. Chem. Phys.* **121**, 11523 (2004).
- J. M. Headrick et al., *Science* **308**, 1765 (2005).
- D. Marx, M. E. Tuckerman, J. Hutter, M. Parrinello, *Nature* **397**, 601 (1999).
- R. Vuilleumier, D. Borgis, *J. Chem. Phys.* **111**, 4251 (1999).
- H. Lapid, U. W. Schmitt, M. K. Petersen, G. A. Voth, *J. Chem. Phys.* **122**, 014506 (2005).
- M. V. Vener, O. Kühn, J. Sauer, *J. Chem. Phys.* **114**, 240 (2001).
- J. Kim, U. W. Schmitt, J. A. Gruetzmacher, G. A. Voth, N. E. Scherer, *J. Chem. Phys.* **116**, 737 (2002).
- M. Rini, B.-Z. Magnes, E. Pines, E. T. J. Nibbering, *Science* **301**, 349 (2003).

25. M. Rini, D. Pines, B.-Z. Magnes, E. Pines, E. T. J. Nibbering, *J. Chem. Phys.* **121**, 9593 (2004).
26. Details of the experimental methods and modeling can be found on *Science* Online.
27. Because the photobase band at 1503 cm^{-1} strongly overlaps with two transitions of HPTS in the photoacid state, its magnitude at early pulse delays cannot be determined accurately.
28. E. Pines, D. Huppert, N. Agmon, *J. Chem. Phys.* **88**, 5620 (1988).
29. O. F. Mohammed, J. Dreyer, B.-Z. Magnes, E. Pines, E. T. J. Nibbering, *ChemPhysChem* **6**, 625 (2005).
30. B. S. Ault, G. C. Pimentel, *J. Phys. Chem.* **77**, 57 (1973).
31. J. M. Williams, in *The Hydrogen Bond: Recent Developments in Theory and Experiments*, vol. 2, *Structure and Spectroscopy*, P. Schuster, G. Zundel, C. Sandorfy, Eds. (North Holland, Amsterdam, 1976), pp. 655.
32. L. Delzeit, B. Rowland, J. P. Devlin, *J. Phys. Chem.* **97**, 10312 (1993).
33. M. Okumura, L. I. Yeh, J. D. Myers, Y. T. Lee, *J. Phys. Chem.* **94**, 3416 (1990).
34. R. Rousseau, V. Kleinschmidt, U. W. Schmitt, D. Marx, *Angew. Chem. Int. Ed.* **43**, 4804 (2004).
35. S. A. Corcelli, J. L. Skinner, *J. Phys. Chem. A* **109**, 6154 (2005).
36. N. Agmon, *Chem. Phys. Lett.* **244**, 456 (1995).
37. We also performed experiments with dichloro- and trichloroacetate as bases. The results show similar behavior to that of monochloroacetate but with even longer lifetimes of the intermediate ionic complexes.

38. S. Meiboom, *J. Chem. Phys.* **34**, 375 (1961).
39. This research has been supported by the German-Israeli Foundation for Scientific Research and Development (project GIF 722/01) and a long-term mission fellowship of the Egyptian government for O.F.M.

Supporting Online Material

www.sciencemag.org/cgi/content/full/310/5745/83/DC1
Materials and Methods
Figs. S1 to S3
Table S1

21 July 2005; accepted 26 August 2005
10.1126/science.1117756

PbSe Nanocrystal Solids for n- and p-Channel Thin Film Field-Effect Transistors

Dmitri V. Talapin* and Christopher B. Murray

Initially poorly conducting PbSe nanocrystal solids (quantum dot arrays or superlattices) can be chemically "activated" to fabricate n- and p-channel field effect transistors with electron and hole mobilities of 0.9 and 0.2 square centimeters per volt-second, respectively; with current modulations of about 10^3 to 10^4 ; and with current density approaching 3×10^4 amperes per square centimeter. Chemical treatments engineer the interparticle spacing, electronic coupling, and doping while passivating electronic traps. These nanocrystal field-effect transistors allow reversible switching between n- and p-transport, providing options for complementary metal oxide semiconductor circuits and enabling a range of low-cost, large-area electronic, optoelectronic, thermoelectric, and sensing applications.

Solution-based processes such as spin coating, dip coating, and inkjet printing offer substantial cost reductions for the fabrication of electronic and optoelectronic devices when combined with materials such as organic semiconductors (1), carbon nanotubes (2), nanowires (3), soluble precursors for inorganic semiconductors (4), and hybrid organic-inorganic films (5). However, none of these approaches can yet enable devices with performance comparable to that of conventional inorganic crystalline semiconductors. Improvement of the electronic performance in these systems comes at the price of high-precision and low-throughput fabrication techniques (3) or else requires high-temperature anneals that limit compatibility with flexible plastic substrates. The trade-off between device performance and fabrication costs motivates the search for new classes of materials for low-cost electronics. Here, we report the assembly of solid-state field-effect transistors (FETs) from solution-processable semiconductor nanocrystals.

Charge transport in an array of nanocrystals separated by insulating capping ligands (a "nanocrystal solid") depends on matching of the energy levels of neighboring nanocrystals (site energies, α), on the exchange coupling energy between the nanocrystals (β), and on the Coulomb charging energy of the nanocrystal array (E_c) (6, 7). For efficient charge transport, the dispersion of site energies $\Delta\alpha$ should not exceed β , or Anderson localization will dominate. If $\beta < E_c$, the nanocrystal array can behave as a Mott insulator (8).

Past studies have revealed low electronic conductivity in semiconductor nanocrystal arrays because of poor exchange coupling and large concentrations of surface dangling bonds that trap carriers in mid-gap states (9–12). Sintering individual nanocrystals into a polycrystalline film increases film conductance but leaves structural defects that limit the device switching speeds (13). Another approach to enhance electron mobility in a nanocrystal solid is based on cross-linking of the nanocrystals by conjugated organic molecules (e.g., 1,4-phenylenediamine) followed by electrochemical charging with several additional electrons per nanocrystal (14–16). Charge screening by the electrolyte's mobile ions substantially reduces E_c , facilitating the nanocrystal charging (12). The mobility increases

because of a combination of trap filling and the participation of multiple quantum confined electronic states (1S, 1P, etc.) in charge transport (12, 14). However, technological implementations require FETs with insulated gates capacitively coupled to the transistor channel.

We selected PbSe nanocrystals because they allow smaller $\Delta\alpha$ and E_c and larger β values, compared to the extensively studied CdSe and ZnO nanocrystal solids. In an ensemble of strongly confined semiconductor nanocrystals, charge transport occurs between electronic quantum confined orbitals (12), and $\Delta\alpha$ can be estimated from the linewidth of the first excitonic ($1S_h$ - $1S_e$) transition (15). We optimized the synthesis (16) to obtain monodisperse (<5% SD) PbSe nanocrystals, with the full width at half maximum of the $1S_h$ - $1S_e$ transition below 40 meV (Fig. 1, A and B). The 1S quantum confined orbitals in rock-salt PbSe nanocrystals are eight-fold degenerated (17) versus the two-fold spin degeneracy in II-VI nanocrystals. Higher degeneracy and narrower linewidth provide a higher density of electronic states (DOS) available for the charge transport. In a close-packed array of 8-nm PbSe nanocrystals, the densities of $1S_h$ and $1S_e$ states are each $\sim 5 \times 10^{20}\text{ eV}^{-1}\text{ cm}^{-3}$, an order of magnitude higher than the DOS in arrays of CdSe or ZnO nanocrystals of the same size and ~ 330 times the DOS in amorphous germanium (15).

The exchange coupling energy scales approximately as $\beta \sim \exp[-\kappa(d + \delta)]$, where d is the nanocrystal diameter, δ is the interparticle spacing, and κ^{-1} describes the length scale of the wave function leakage outside the nanocrystal (6, 7). The large Bohr radius of electrons and holes in PbSe ($\sim 23\text{ nm}$ in both) suggests that their wave functions spill far outside the volume of the nanocrystal, facilitating exchange interactions.

The charging energy E_c of a spherical nanocrystal can be estimated as $E_c = e^2/(4\pi\epsilon_m\epsilon_0d)$ where ϵ_m is the dielectric constant of the surrounding medium. The dielectric constant for bulk PbSe is very high ($\epsilon \sim 250$, as compared to $\epsilon \sim 6.2$ for CdSe), with $\epsilon > 100$ measured for individual 12-nm PbSe nanocrystals (18). This predicts an E_c of $<4\text{ meV}$ for a three-

IBM Research Division, T. J. Watson Research Center, 1101 Kitchawan Road, Yorktown Heights, NY 10598, USA.

*To whom correspondence should be addressed.
E-mail: dmitrit@us.ibm.com

dimensional array of 8-nm PbSe nanocrystals, which is a small fraction of thermal energy at room temperature ($k_B T$, where k_B is the Boltzmann constant and T is the temperature) and an order of magnitude smaller than E_c for analogous CdSe nanocrystal arrays (16).

For electronic studies, close-packed PbSe nanocrystal films, 35 ± 10 nm thick, were deposited on highly doped Si wafers with 100-nm-thick SiO_2 thermal gate oxide. Source and drain Ti/Au (75/375 Å) electrodes spaced from 4 μm to 40 μm apart were patterned on the SiO_2 surface before nanocrystal deposition (16).

Small angle x-ray scattering at grazing incidence (GISAXS) from 8-nm PbSe nanocrystals assembled in the channel between parallel electrodes showed well-resolved reflections (Fig. 1C), confirming both in-plane and vertical particle ordering in a film that was drop-cast from a hexane:octane (9:1 by volume) solution. The parallel source and drain electrodes directed the crystallographic orientation of growing superlattices (fig. S1). Moreover, close-packed PbSe nanocrystals showed strong preferential orientation of their atomic lattices, favorable for charge transport through P-quantized states (figs. S2 and S3)

As-deposited PbSe nanocrystal arrays were insulating, with a conductance (G) less than 10^{-11} S cm^{-1} , because of ~ 1.5 -nm interparticle spacing maintained by insulating oleic acid molecules (Fig. 1B). Thorough washing of the nanocrystal colloids (16) removed a fraction of the native capping groups, reducing interparticle spacing to ~ 1.1 nm and yielding a higher conductance of $G \sim 3 \times 10^{-10}$ S cm^{-1} . However, the removal of capping groups introduced pronounced hysteresis in the current-voltage (I - V) scans (Fig. 2A), probably due to filling of traps associated with surface dangling bonds. No gate modulation was observed in the native nanocrystal films.

The conductance of PbSe nanocrystal solids increased by ~ 10 orders of magnitude after treatment with a 1.0 M solution of hydrazine in acetonitrile (Fig. 2B) (16). The current through the nanocrystal film can be modulated by application of a potential to the back gate electrode, producing an n-FET (I) (Fig. 2C). Figure 3A shows a current modulation $I_{\text{on}}/I_{\text{off}}$ of $\sim 2.5 \times 10^3$ for a PbSe nanocrystal n-FET, with minor hysteresis between gate voltage (V_G) scans in the forward and reverse directions (fig. S4). In the “on” state, low-field conductance of PbSe nanocrystal film was ~ 0.82 S cm^{-2} ($V_G = 40$ V), and the current density in the saturation regime approached 2.7×10^4 A cm^{-2} . Extracting field-effect electron mobilities (μ) from a series of devices yielded $\mu_{\text{lin}} \sim 0.4$ $\text{cm}^2 \text{V}^{-1} \text{s}^{-1}$ in the linear regime and $\mu_{\text{sat}} \sim 0.7$ $\text{cm}^2 \text{V}^{-1} \text{s}^{-1}$ in the saturation regime (16). The μ_{sat} values increased with nanocrystal size. The highest mobility, $\mu_{\text{sat}} = 0.95$ $\text{cm}^2 \text{V}^{-1} \text{s}^{-1}$, was observed for 9.2-nm PbSe nanocrystals.

Vacuum treatment or mild heating (to $\sim 100^\circ\text{C}$) of activated PbSe nanocrystal films switched their conductivity from n-type (Fig. 3A) to ambipolar (Fig. 3B) and, finally, to p-type (Fig. 3, C and D) as the hydrazine desorbed. The resulting p-FETs showed room-temperature hole mobilities μ_{sat} of 0.12 to 0.18 $\text{cm}^2 \text{V}^{-1} \text{s}^{-1}$, current modulations of $\sim 10^2$ (Fig. 3D), and “on” state current densities approaching $\sim 3 \times 10^3$ A cm^{-2} . At 120 K, current modulation increased to $\sim 1.6 \times 10^4$, whereas the hole mobility decreased to $\mu_{\text{sat}} = 0.09$ $\text{cm}^2 \text{V}^{-1} \text{s}^{-1}$ and was almost independent of the gate voltage (Fig. 3C). The hole transport in PbSe nanocrystal solids most probably occurs through the $1S_h$ orbitals (19). Switching between electron and hole transport was reversible upon re-exposure to hydrazine, allowing fabrication of complementary metal oxide semiconductor circuits.

Scanning and transmission electron microscopy (SEM and TEM) and x-ray diffraction studies showed that the hydrazine treatment did not change nanocrystal size or shape but markedly reduced the interparticle spacing (Fig. 4A and fig. S3). The reflections in GISAXS patterns shifted to higher scattering (2θ) angles, showing that interparticle spacing decreased by 0.8 nm, i.e., from ~ 1.1 nm to ~ 0.3 nm (Fig. 4B) (16). Once hydrazine-treated, films neither dissolved nor swelled on re-exposure to nonpolar solvents. This allowed us to pattern PbSe nanocrystal films. Local exposure to hydrazine solutions rendered the regions conductive, whereas unexposed film could be lifted off in hexane. Sequential layer-by-layer deposition would allow different material combinations, e.g., p- and n-conducting layers for designing nanocrystal-based photovoltaic cells.

The absorption spectra of the conductive PbSe nanocrystal films show excitonic peaks

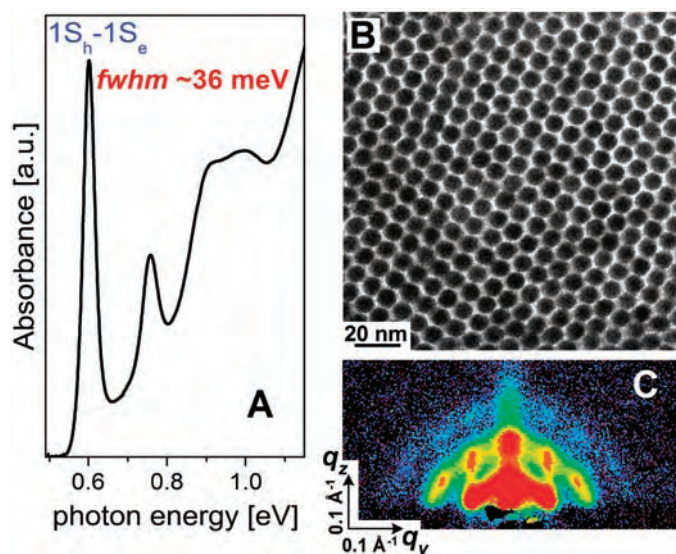


Fig. 1. (A) Optical absorption spectrum of a colloidal solution of 8-nm PbSe nanocrystals in tetrachloroethylene. a.u., arbitrary units; fwhm, full width at half-maximum. (B) TEM image of an array of 8-nm PbSe nanocrystals. q_y and q_z are the lateral and vertical components of the momentum transfer, respectively. (C) GISAXS pattern of PbSe nanocrystal film (16).

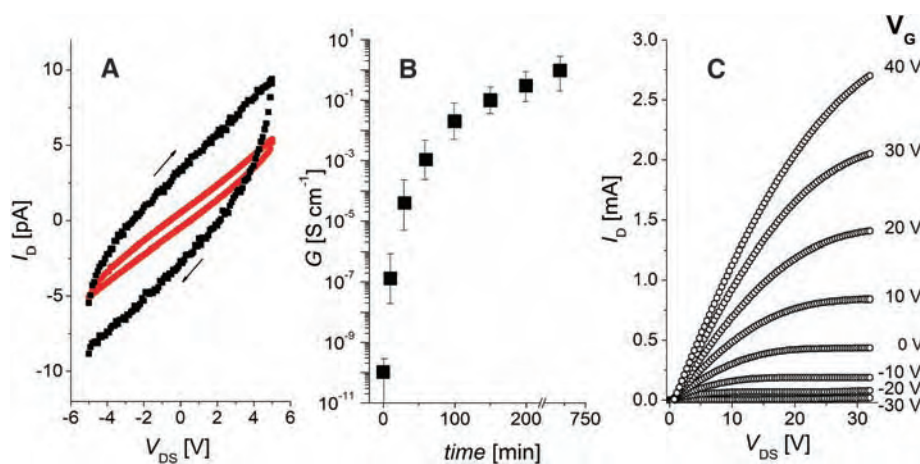


Fig. 2. (A) I - V scans for a film of 8-nm oleic acid capped PbSe nanocrystals in which the voltage scan rate is 0.5 V s^{-1} (black) and 0.025 V s^{-1} (red) and the channel length L and width W are 6 μm and 5000 μm , respectively. (B) Conductance G of a PbSe nanocrystal film versus time of exposure to a 1 M solution of N_2H_4 in acetonitrile. The error bars show the spread in data from five samples. (C) Plot of drain current I_D versus drain-source voltage V_{DS} , as a function of V_G for a nanocrystal FET with a channel composed of 8-nm PbSe nanocrystals treated with hydrazine solution for 12 hours ($L = 10 \mu\text{m}$, $W = 2000 \mu\text{m}$, with a 100-nm-thick SiO_2 gate dielectric).

that shifted by ~ 20 meV to lower energy relative to native insulating films (Fig. 4C). The persistence of excitonic peaks implies the electron and hole wave functions either remain localized on the individual PbSe nanocrystals or form narrow minibands due to exchange coupling (20). At low temperatures, charge transport in PbSe nanocrystal solids occurred through variable range hopping, as confirmed by linearization of low-field conductance in the Mott coordinates ($\ln G \sim T^{-3/4}$) (8) (fig. S5).

The hydrazine treatment can simultaneously tune β , E_c , trap density, and the doping level

of a PbSe nanocrystal solid. Hydrazine is a Brønsted base and can gently react to remove and replace the bulky oleic acid capping ligands from the nanocrystal surface, reducing the interparticle spacing and increasing β . Hydrazine is also a strong Lewis base with lone pairs of electrons that can saturate dangling bonds at the nanocrystal surface in analogy to primary amines (21). We might also speculate about linking PbSe nanocrystals by bidentate hydrazine molecules, as the mean interparticle spacing is close to the length of a hydrazine molecule. Hydrazine is a reducing agent, pre-

venting oxidation of PbSe nanocrystals and “repairing” any oxidized selenium surface sites that might generate mid-gap levels (22). Replacement of oleic acid ($\epsilon \sim 2$) with hydrazine ($\epsilon \sim 52$) also substantially reduces E_c . The increase of β and decrease of E_c helps to close the Hubbard gap (8), enabling the insulator-metal Mott transition in the nanocrystal solid. Finally, hydrazine behaves as a charge-transfer n-type dopant, as has been observed for PbSe nanowires (23) and carbon nanotubes (24).

Annealing the activated PbSe nanocrystal films at $\sim 200^\circ\text{C}$ for 1 hour and re-exposing them to a hydrazine solution allowed us to achieve degenerate doping and metallic conductivity ($G \sim 8.5 \text{ S cm}^{-2}$) (fig. S6). The semiconductor-metal transition was reversible, as partial stripping of the hydrazine (6 hours at 40°C under nitrogen) yielded n-type semiconducting films with high electron mobility ($\mu_{\text{lin}} \sim 2.5 \text{ cm}^2 \text{ V}^{-1} \text{ s}^{-1}$) (fig. S7), thus demonstrating that tailoring of β and the doping density allows controllable switching between insulating, semiconducting, and metallic states in PbSe nanocrystal solids.

Colloidal nanocrystals can now enable room-temperature fabrication of n- and p-channel field effect devices by inexpensive and high-throughput solution-based processes. We observed good performance for PbSe nanocrystal FETs, even for long (e.g., $40 \mu\text{m}$) channels (fig. S8). Such device dimensions are easily accessible by stamping or inkjet-printing. The observed field-effect mobilities in PbSe nanocrystal films are comparable to the hole mobility in pentacene films (2), although lower than the electron mobility in the best solution-processed inorganic semiconductors (4).

The hydrazine treatment is a general technique for increasing conductance in nanocrystal solids. In addition to PbSe FETs, we have assembled operational solid-state FETs from PbS, PbTe, CdSe, and InP nanocrystals and CdSe nanorods, thus demonstrating the applicability of our approach to different materials.

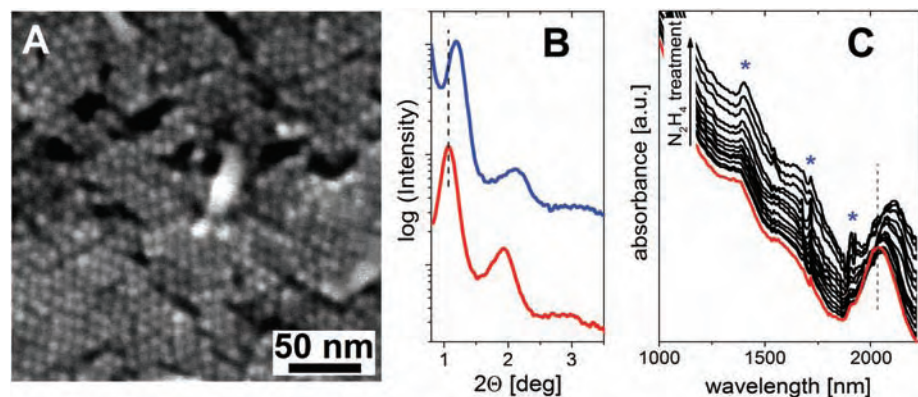
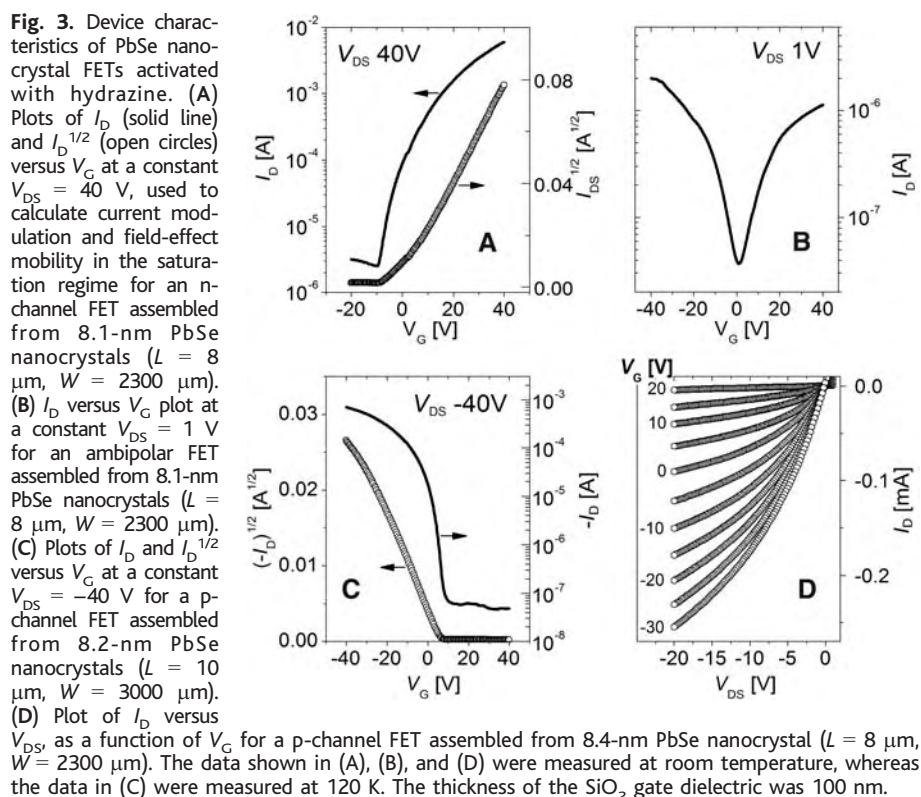


Fig. 4. (A) High-resolution SEM image of a PbSe nanocrystal film treated with a 1 M N_2H_4 solution for 12 hours. (B) Small-angle x-ray scattering from an array of 8.1-nm PbSe nanocrystals before (red) and after (blue) the hydrazine treatment. 2θ , scattering angle. (C) Evolution of the absorption spectrum of the 7.5-nm PbSe nanocrystal film with time during a 4-hour hydrazine treatment (16). The initial absorption spectrum is shown in red. The infrared absorption bands from the solvent are marked by blue asterisks, and the dashed line indicates the position of the $1S_n-1S_e$ excitonic transition in the initial, insulating nanocrystal film.

References and Notes

- C. R. Kagan, P. Andry, Eds., *Thin Film Transistors* (Marcel Dekker, New York, 2003).
- E. Artukovic, M. Kaemppgen, D. S. Hecht, S. Roth, G. Gruner, *Nano Lett.* **5**, 841 (2005).
- X. Duan et al., *Nature* **425**, 274 (2003).
- D. B. Mitzi, L. L. Kosbar, C. E. Murray, M. Copel, A. Afzali, *Nature* **428**, 299 (2004).
- C. R. Kagan, D. B. Mitzi, C. D. Dimitrakopoulos, *Science* **286**, 945 (1999).
- F. Remacle, K. C. Beverly, J. R. Heath, R. D. Levine, *J. Phys. Chem. B* **107**, 13892 (2003).
- C. P. Collier, R. J. Saykally, J. J. Shiang, S. E. Henrichs, J. R. Heath, *Science* **277**, 1978 (1997).
- N. F. Mott, *Conduction in Non-Crystalline Materials* (Clarendon, Oxford, 1993), ed 2.
- N. Y. Morgan et al., *Phys. Rev. B* **66**, 075339 (2002).
- M. B. Jarosz, V. J. Porter, B. R. Fisher, M. A. Kastner, M. G. Bawendi, *Phys. Rev. B* **70**, 195327 (2004).
- D. S. Ginger, N. C. Greenham, *J. Appl. Phys.* **87**, 1361 (2000).
- D. Vanmaekelbergh, P. Liljeroth, *Chem. Soc. Rev.* **34**, 299 (2005).
- B. R. Ridley, B. Nivi, J. M. Jacobson, *Science* **286**, 746 (1999).

14. D. Yu, C. Wang, P. Guyot-Sionnest, *Science* **300**, 1277 (2003).
15. D. Yu, C. Wang, B. L. Wehrenberg, P. Guyot-Sionnest, *Phys. Rev. Lett.* **92**, 216802 (2004).
16. Materials and methods are available as supporting material on Science Online.
17. G. Allan, C. Dellerue, *Phys. Rev. B* **70**, 245321 (2004).
18. C. H. Ben-Porat, O. Chernyavskaya, L. Brus, K.-S. Cho, C. B. Murray, *J. Phys. Chem. B* **108**, 7814 (2004).
19. The possibility of hole injection into the $1S_n$ state of a semiconductor nanocrystal has been demonstrated by Wehrenberg and Guyot-Sionnest (25).
20. O. L. Lazarenkova, A. A. Balandin, *J. Appl. Phys.* **89**, 5509 (2001).
21. D. V. Talapin, A. L. Rogach, A. Kornowski, M. Haase, H. Weller, *Nano Lett.* **1**, 207 (2001).
22. J. S. Steckel, S. Coe-Sullivan, V. Bulović, M. B. Bawendi, *Adv. Mater.* **15**, 1862 (2003).
23. D. V. Talapin, unpublished data.
24. C. Klinke, J. Chen, A. Afzali, Ph. Avouris, *Nano Lett.* **5**, 555 (2005).
25. B. L. Wehrenberg, P. Guyot-Sionnest, *J. Am. Chem. Soc.* **125**, 7806 (2003).
26. We thank C. T. Black, C. R. Kagan, J. J. Urban, E. V.

Shevchenko, V. Perebeinos, R. L. Sandstrom, and A. Afzali for helpful comments, suggestions, and stimulating discussions.

Supporting Online Material
www.sciencemag.org/cgi/content/full/310/5745/86/DC1
 Materials and Methods
 Figs. S1 to S8

28 June 2005; accepted 1 September 2005
 10.1126/science.1116703

Nanoscale Imaging of Buried Structures via Scanning Near-Field Ultrasound Holography

Gajendra S. Shekhawat^{1,2} and Vinayak P. Dravid^{1,2,3*}

A nondestructive imaging method, scanning near-field ultrasound holography (SNFUH), has been developed that provides depth information as well as spatial resolution at the 10- to 100-nanometer scale. In SNFUH, the phase and amplitude of the scattered specimen ultrasound wave, reflected in perturbation to the surface acoustic standing wave, are mapped with a scanning probe microscopy platform to provide nanoscale-resolution images of the internal substructure of diverse materials. We have used SNFUH to image buried nanostructures, to perform subsurface metrology in microelectronic structures, and to image malaria parasites in red blood cells.

Nondestructive real-space imaging of deeply buried or embedded structures and features with lateral resolution below ~ 100 nm is a formidable challenge (1–5). Conventional imaging with noninvasive radiation, such as light and acoustic waves, cannot achieve useful resolution below 100 nm because of the classical diffraction limit (6–8). Scanning probe microscopy (SPM) and its analogs offer superb spatial resolution but are sensitive only to surface or shallow subsurface features (9, 10). Near-field scanning optical microscopy offers sub-wavelength resolution but is unable to image optically opaque and deeply buried structures (11, 12). Thus, with respect to nondestructive real-space imaging, there is a clear void between the two ranges of length scales offered by confocal/photon or acoustic/sonography techniques (micrometer scale) (13–16) and SPM (nano- and subnanometer scale) (9, 10), particularly if the features of interest are buried deeper into the material, beyond the interaction range of proximal probes.

The need for nondestructive nanoscale imaging of buried and embedded structures is critical for numerous materials, structures, and phenomena as the scale of fabrication continues to shrink and the micro/nanofabrication paradigm moves from planar to three-dimensional

(3D) or stacked platforms. In microelectronics, for example, such metrology challenges are well articulated in the International Technology Roadmap for Semiconductors (17). The need for a higher resolution, nondestructive, real-space imaging approach is equally critical in biological systems for noninvasive monitoring of signal pathways, cellular transfection, and other subcellular phenomena.

In conventional nondestructive imaging approaches based on acoustic and light microscopy, classical diffraction limits the spatial resolution in the far-field regime. For example, the spatial resolution, δ , in an acoustic microscope is given by

$$\delta = 0.51(v_o/fNA) \quad (1)$$

(7, 8), where v_o is the speed of sound in the coupling medium, f is the frequency of the acoustic/ultrasonic wave, and NA is the numerical aperture of the lens. Conventional far-field approaches are also limited by the need for liquid lenses and coupling fluid, among other considerations.

Several SPM-based techniques have been introduced in recent years with mixed results in the context of sensitivity to surface nanomechanical variations, ability to probe deeply buried or embedded features, or quantitative extraction of nanomechanical contrast. Force modulation microscopy (also called ultrasonic force microscopy) (18–23) and heterodyne force microscopy (24) are notable SPM-based techniques that have enjoyed some success in nanomechanical mapping of elastic and visco-

elastic properties of soft and hard surfaces. However, a wider deployment of these techniques is generally marred by lack of reproducibility, unpredictable environmental effects in the usual contact mode of imaging, and lack of compelling evidence for demonstrated sensitivity to buried and embedded structure. Moreover, these techniques use nonlinear tip-sample interactions, where the origin of the dominant mechanical contrast in the images is mainly from differential surface mechanical properties with a large physical contact between the cantilever and sample; such methods are therefore not well suited for imaging of soft materials such as polymers and biological structures.

Here we introduce an imaging approach, scanning near-field ultrasound holography (SNFUH), that is sensitive to deeply buried features, offers nanoscale lateral resolution with depth sensitivity, and is equally amenable to hard (engineered systems), soft (polymers and biological structures), and hybrid materials. In SNFUH, a high-frequency acoustic wave (on the order of megahertz or higher, substantially greater than the resonance frequency of the typical cantilever, $f_0 \sim 10$ to 100 kHz) is launched from the bottom of the specimen while another wave is launched on the SPM cantilever, albeit at a slightly different frequency (Fig. 1). The interference of these two waves would nominally form a surface acoustic standing wave, which is analogous to, for example, x-ray standing waves that result from interference of scattered and reference x-ray waves (25, 26). The perturbations to the phase and amplitude of the surface acoustic standing wave are locally monitored by the SPM acoustic antenna via the lock-in approach and a SNFUH electronic module. As the specimen acoustic wave is perturbed by buried features, the resultant alteration in the surface acoustic standing wave, especially its phase, is effectively monitored by the SPM cantilever. Thus, within the near-field regime (which enjoys superb spatial resolution), the acoustic wave (which is nondestructive and sensitive to mechanical and/or elastic variation along its path) is fully analyzed, point-by-point, by the SPM acoustic antenna in terms of its phase and amplitude. Thus, as the specimen is scanned, a pictorial representation of its acoustic wave perturbation is recorded and displayed that offers a quantitative account of the internal features of the specimen.

¹Institute for Nanotechnology, ²NUANCE Center, ³Department of Materials Science and Engineering, Northwestern University, Evanston, IL 60208, USA.

*To whom correspondence should be addressed.
 E-mail: v-dravid@northwestern.edu

The SNFUH approach, especially its implementation, is quite different from prior approaches (18–24) that make use of launching ultrasound frequency on the specimen, the cantilever, or both. The difference is in the collective combination of near-field, noncontact, and holography mode for detection, with noninvasive acoustic waves for depth sensitivity, as demonstrated below.

A conventional JEOL SPM 5200 scanning probe microscope system with a modified stage and cantilever holder system was used to develop the SNFUH mode. The feedback electronics of the system were also modified, and an electronic module developed in-house was implemented together with a radio frequency (RF) lock-in approach to extract the phase and amplitude of the acoustic standing wave perturbed by buried features. Commercial piezoelectric ceramics were used to provide ultrasonic vibrations to the sample and the cantilever, with out-of-plane resonances of ~ 2.1 and ~ 2.3 MHz, respectively. The images were acquired using soft-contact mode (for hard structures) and near-contact mode (for biological structures). In soft-contact mode, the SNFUH feedback controller is used to bring the cantilever toward the surface, and the contact force is monitored by the system software. In near-contact mode, optical feedback is used to lift the tip by a small amount (2 to 5 nm) after it touches the surface.

The SNFUH controller and cantilever monitor the perturbation to the surface acoustic standing waves, especially their phase, which

carries information about buried structures reflected in the scattering of specimen acoustic waves due to the difference in elastic moduli, for example. The use of near-contact mode is particularly suitable for imaging and monitoring soft and biological structures in vitro. Matching piezoceramics were used to keep the frequency difference below the cutoff frequency of the SPM photodiode (~ 1 MHz). The SPM differential photodiode signal constitutes an input to the SNFUH electronic module, which enables simultaneous extraction of all image data: the topography, amplitude, and phase of the acoustic standing wave.

Experimentally, the two acoustic oscillations are applied to the tip and the sample by two matching piezocrystals attached to the cantilever and at the base of the sample. Each piezocrystal is driven by a separate sinusoidal waveform generated by arbitrary waveform generators. The SNFUH electronic module monitors the difference frequency input to an RF lock-in amplifier as a reference for the extraction of the amplitude phase of the acoustic standing wave.

We used a model polymer-nanoparticle composite to demonstrate the high lateral spatial resolution and depth sensitivity of the SNFUH approach. A specimen consisting of gold nanoparticles buried deep beneath a polymer cover layer was prepared by dispersing colloidal gold nanoparticles on a silicon substrate coated with poly(2-vinylpyridine) (PVP). Nanoparticle coverage was measured by Rutherford backscattering spectrometry as described (27). The gold nanoparticles had an average diameter of 15 nm and were well dispersed on the film surface, as observed previously by transmission

electron microscopy (TEM) (27). The nanoparticles were then fully covered with another polymer film about 500 nm thick (Fig. 2A). The normal atomic force microscopy (AFM) topography scan (Fig. 2B) shows a smooth featureless surface of top polymeric layer with surface roughness of ~ 0.5 nm. However, the phase image of SNFUH (Fig. 2C) clearly shows well-dispersed gold nanoparticles buried ~ 500 nm deep from the top surface. The contrast in the phase image of SNFUH arises from the difference in elastic modulus between the polymer and the gold nanoparticles, which induces the time-dependent phase delay of the acoustic waves reaching the sample surface.

As shown schematically in Fig. 2, D and E, the buried scattering features (the nanoparticles) perturb the specimen acoustic wave, resulting in local change in the phase and amplitude of the acoustic standing wave, which is detected by the SPM cantilever “antenna.” At the operating frequency of 2.1 MHz, the wavelength of the specimen acoustic wave is greater than a few hundred micrometers. Thus, the experimental conditions are well within the near-field regime, resulting in minimal diffraction or wide-angle scattering of the acoustic waves reaching the top surface. The degradation of spatial resolution and the depth sensitivity of SNFUH beyond the near-field regime requires additional experimental and modeling studies.

The mechanism of the formation of the acoustic standing wave and the origin of the contrast and high subsurface sensitivity of the SNFUH approach can be conceptually understood as follows (Fig. 2, D and E): In SNFUH mode, the perturbation to the surface acoustic standing wave resulting from specimen

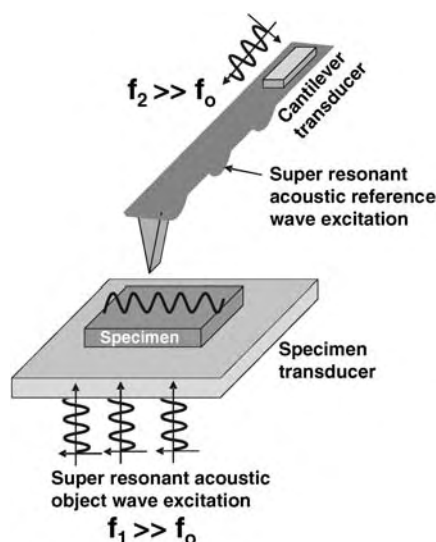


Fig. 1. Schematic illustration of the SNFUH approach. A high-frequency acoustic wave is launched from below the specimen while another high-frequency acoustic wave (at a slightly different frequency) is launched on the SPM cantilever. The SNFUH electronic module is used to spatially monitor the phase perturbation to the surface acoustic standing wave that results from the scattered specimen acoustic wave. The resonant frequency of the typical cantilever, f_0 , is in the 10- to 100-kHz range.

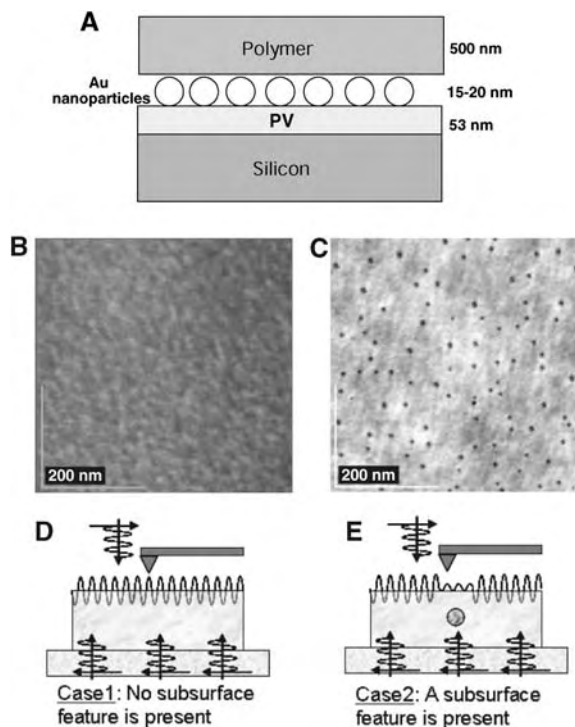


Fig. 2. (A) Schematic illustration of a model nanoparticle system for validation of SNFUH. Gold nanoparticles dispersed on a polymer-coated substrate (PV) are buried under a polymer layer ~ 500 nm thick. (B and C) A typical AFM topography image (B) shows a featureless top polymer surface, whereas the phase image of SNFUH (C) clearly reveals the buried gold nanoparticles with high definition. (D and E) Schematic explanation of images in (B) and (C). In (D), the standing wave is not perturbed because no subsurface scattering feature is present; in (E), the acoustic standing wave is perturbed as a result of subsurface scattering, which is monitored by the SPM tip.

acoustic wave scattering is monitored by the SPM acoustic antenna. The resulting cantilever deflection merely follows the perturbation to the surface acoustic standing wave, which represents the dissipative lag/lead in the surface response with respect to the tip reference frequency (i.e., the time-of-flight delay of the specimen acoustic waves reaching the sample surface). Extracting the spatial dependence of this phase term provides image contrast indicative of the relative elastic response of the buried structures, interfaces, and embedded defects to the specimen acoustic wave to create the resultant perturbation to the surface acoustic standing wave.

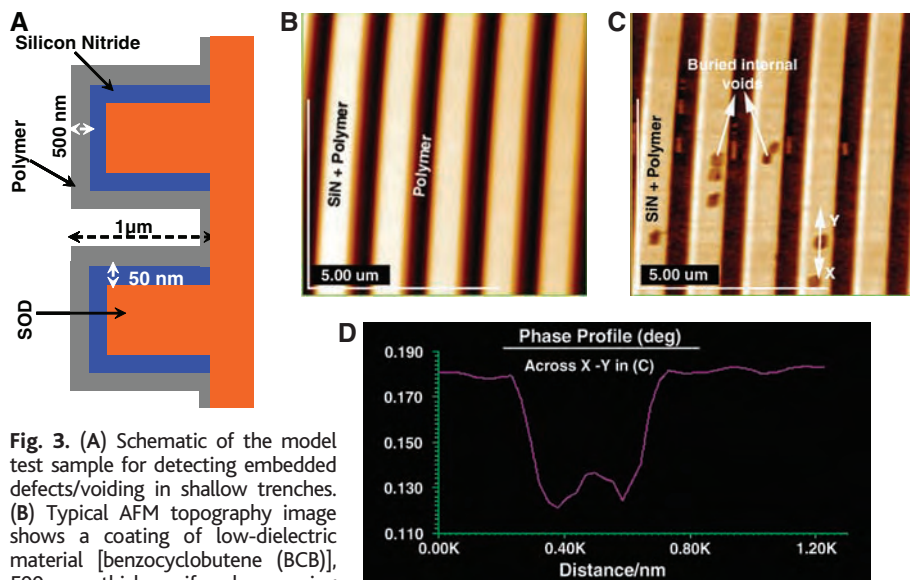
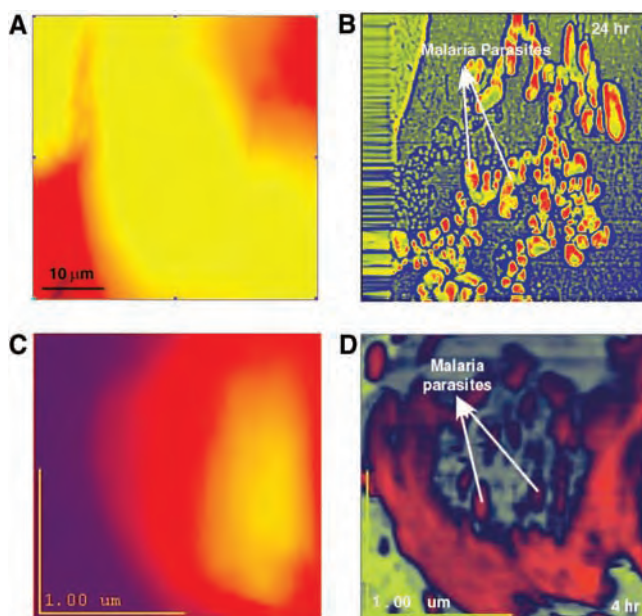


Fig. 3. (A) Schematic of the model test sample for detecting embedded defects/voiding in shallow trenches. (B) Typical AFM topography image shows a coating of low-dielectric material [benzocyclobutene (BCB)], 500 nm thick, uniformly covering the trenches. Trench width is ~ 400 nm and height is ~ 1 μm . (C) Phase image of SNFUH clearly reveals the surface elastic contrast and embedded voiding in polymer coating over nitride and hardening of it at the trench walls, a result of its curing. This is evident from the contrast at the trench walls. (D) The line profile across the void, marked across X-Y in (C). Remarkably high subsurface phase resolution is achieved.

Fig. 4. AFM topography images (A and C) and SNFUH phase images (B and D) of malaria-infected RBCs. In (A) and (B), obtained after 24 hours of incubation, the topography image shows typical surface features of RBCs with scan size of 10 μm by 10 μm , whereas the SNFUH phase image shows remarkable contrast from parasites inside the RBC at nanoscale spatial resolution. The images in (C) and (D) show early-stage parasite infection after 4 hours of incubation.



In a homogeneous specimen, the surface acoustic standing wave is merely the interference of the specimen and cantilever acoustic waves without any local perturbation (Fig. 2D). However, if a scattering feature is present below the specimen surface, the perturbation to the specimen acoustic wave results in local perturbation (Fig. 2E) to the surface acoustic standing wave that is registered by the SPM cantilever antenna. The contrast variation arises from the acoustic phase difference between the matrix and the feature, which in the case of acoustic wave propagation is directly related to the elastic modulus difference (7, 8). The lateral spatial

resolution is governed by the SPM probe interaction with the acoustic standing wave, which is proportional to the depth of the scattering features beyond the near-field regime. Within the near-field regime, the spatial resolution is limited principally by the SPM tip interactions, whereas resolution degradation will be commensurate with depth beyond the near-field regime because of far-field scattering and diffraction. Further, because the acoustic phase information is spatially recorded, it is possible to obtain (via modeling) depth distribution of phase and to convert the data into a 3D tomography map of the embedded features.

Some of the challenges in the next generation of microelectronics metrology include dimensionality and fatigue performance of electrical contacts and interconnects (28, 29), which are often buried and stacked. The current paradigm for electrical contact processing calls for an increase in the aspect ratio of metal contact lines, which in turn requires deposition of metal into damascene trenches and *vias* without leaving any unfilled volume (voids). The undesirable process defect voids result in increased resistivity and can cause serious open circuits and device failure. The major challenges in this critical microelectronics step include voiding, delamination, and cracking at the polymer-trench interface. Conventional techniques for characterization of voids and stresses in narrower trenches include destructive approaches such as cross-sectional scanning electron microscopy (SEM) or TEM, which are not only laborious and time-consuming but require the wafer to be sacrificed. Electrical testing is nondestructive but spatially insensitive, and it requires contact to the wafer. In the case of *via* chains, several metal levels must be fabricated before the electrical test can be completed. Clearly, a nondestructive subsurface imaging approach is warranted to identify and isolate such defects or delamination and thereby improve the process yield.

To demonstrate the efficacy of SNFUH in identifying underlying defects in narrower trenches, we fabricated shallow trench structures as shown in Fig. 3A. The trenches were etched in SOD (spin-on dielectric) with a 50-nm layer of low-pressure chemical vapor deposition (LPCVD) Si_3N_4 as a capping layer, and Si_3N_4 was then etched into the trenches (1 μm deep) by wet processing. A layer of polymer (benzocyclobutene) 500 nm thick was spin-coated, followed by thermal annealing to cure the polymer.

A conventional topography scan (Fig. 3B), 7.5 μm by 7.5 μm , shows uniform and contiguous polymeric coating on SiN and inside the trenches. On the other hand, the corresponding (simultaneously recorded) SNFUH phase image shown in Fig. 3C reveals phase contrast reminiscent of embedded voiding within the polymer and at the SiN-polymer interfaces. The dark contrast in the phase image in polymer-

coated SiN lines corresponds to voids at SiN-polymer interfaces (i.e., voiding underneath the contact). The contrast is due to the distinct viscoelastic response from the specimen acoustic wave from the voids. Interestingly, a notable hardening of the polymer in the trench and its sidewall is also evident in the phase image, which results from thermal annealing and possibly poor adhesion with SOD. Because it is nondestructive, SNFUH may be an ideal toolset for such subsurface metrology needs.

The efficacy of SNFUH in imaging of embedded or buried substructures in biology is demonstrated in Fig. 4, which depicts high resolution and remarkably high contrast arising from malaria parasites inside infected red blood cells (RBCs). The details of in vitro infection by malaria parasites are reported in (30); here, we demonstrate early-stage direct and real-space in vitro imaging of the presence of parasites inside RBCs without any labels or sectioning of cells, and under physiologically viable conditions. *Plasmodium falciparum* strain 3D7 was cultured in vitro by a modification of the method of Haldar *et al.* (31). Parasites were synchronized to within 4 hours by a combination of Percoll purification and sorbitol treatments, cultured to 10% parasitemia, and harvested at the indicated times.

SNFUH imaging was performed using the near-contact mode method for imaging soft structures. The SNFUH electronic module was used to bring the cantilever into near-contact mode, and then the sample was scanned over the RBCs while maintaining the near-field regime. An AFM topography image and a SNFUH phase image from infected RBCs are shown in Fig. 4, A and B, respectively. As expected, the AFM topography image shows the typical surface morphology of an infected RBC, whereas the SNFUH phase image shows remarkably high contrast from the parasite residing well inside the RBC. In addition to several other features reminiscent of membrane proteins and subcellular contents, multiple parasites are clearly evident. The morphology, spatial scale, and distribution of parasites are consistent with prior accounts of such infection (30, 32). To further demonstrate the capability of SNFUH for early-stage diagnosis of parasite infection, we examined RBCs incubated for only 4 hours; infection after such a brief period is difficult to validate by other noninvasive techniques such as fluorescence tagging. The images in Fig. 4, C and D, show that SNFUH is sensitive to early-stage parasite infection in RBCs, as reflected by image contrast consistent with parasite infection.

These representative examples of SNFUH development and applications demonstrate a versatile toolset for nondestructive, high-resolution, real-space imaging of diverse materials systems. We believe the SNFUH approach fills the critical gap in spatial resolution at the 10- to 100-nm scale for nondestructive sub-

surface imaging in physical sciences, engineered systems, and biology.

References and Notes

- H. N. Lin, *Appl. Phys. Lett.* **74**, 2785 (1999).
- M. R. VanLandingham *et al.*, in *Interfacial Engineering for Optimized Properties*, C. L. Briant, C. B. Carter, E. L. Hall, Eds., vol. 458 of *Materials Research Society Proceedings* (Materials Research Society, Pittsburgh, PA, 1997), pp. 313–318.
- M. R. VanLandingham *et al.*, *J. Adhesion* **64**, 31 (1997).
- B. Bhushan, L. Huiwen, *Nanotechnology* **15**, 1785 (2004).
- M. R. VanLandingham *et al.*, *J. Mater. Sci. Lett.* **16**, 117 (1997).
- K. Inagaki, G. A. D. Briggs, O. B. Wright, *Appl. Phys. Lett.* **76**, 1836 (2000).
- G. A. D. Briggs, *Acoustic Microscopy* (Clarendon, Oxford, 1992), p. 33.
- T. M. Nelson, R. W. Smith, *Adv. Mater. Process.* **162**, 29 (2004).
- G. S. Shekhawat *et al.*, *Appl. Phys. Lett.* **68**, 779 (1996).
- C. F. Quate, *Surf. Sci.* **299–300**, 980 (1994).
- W. Dickson, S. Takahashi, R. Pollard, R. Atkinson, *IEEE Trans. Nanotechnol.* **4**, 229 (2005).
- K. Lindfors, M. Kapulainen, R. Ryytty, M. Kaivola, *Opt. Laser Technol.* **36**, 651 (2004).
- B. C. Larson, W. Yang, G. E. Ice, J. D. Budai, J. Z. Tischler, *Nature* **415**, 887 (2002).
- X. Wang, Y. J. Pang, G. Ku, G. Stoica, L. H. V. Wang, *Opt. Lett.* **28**, 1739 (2003).
- K. Kostli, P. C. Beard, *Appl. Opt.* **42**, 1899 (2003).
- D.-Z. Huang, J.-B. Li, Z. Sheng, *Chin. J. Med. Imaging Technol.* **20**, 1815 (2004).
- International Technology Roadmap for Semiconductors (<http://public.itrs.net>).
- B. Altemus, G. S. Shekhawat, R. Geer, B. Xu, J. Castracane, *Proc. SPIE 4558* (2001).
- R. E. Geer, O. V. Kolosov, G. A. D. Briggs, G. S. Shekhawat, *J. Appl. Phys.* **91**, 4549 (2002).
- O. Kolosov, R. M. Castell, C. D. Marsh, G. A. D. Briggs, *Phys. Rev. Lett.* **81**, 1046 (1998).
- D. C. Hurley, K. Shen, N. M. Jennett, J. A. Turner, *J. Appl. Phys.* **94**, 2347 (2003).
- O. Hirotsugu, T. Jiayong, T. Toyokazu, H. Masahiko, *Appl. Phys. Lett.* **83**, 464 (2003).
- L. Muthuswami, R. E. Geer, *Appl. Phys. Lett.* **84**, 5082 (2004).
- M. T. Cuberes, H. E. Assender, G. A. D. Briggs, O. V. Kolosov, *J. Phys. D* **33**, 2347 (2000).
- L. Cheng, P. Fenter, M. J. Bedzyk, N. C. Sturchio, *Phys. Rev. Lett.* **90**, 255503-1-4 (2003).
- B. P. Tinkham, D. A. Walko, M. J. Bedzyk, *Phys. Rev. B* **67**, 035404-1-6 (2003).
- K. Shull, A. Kellock, *J. Polym. Sci. B* **33**, 1417 (1995).
- E. T. Ogama *et al.*, *IEEE International Reliability Physics Symposium, 40th Annual Proceedings* (IEEE, Piscataway, NJ, 2002), pp. 312–321.
- R. R. Keller, C. E. Kalnas, J. M. Phelps, *J. Appl. Phys.* **86**, 1167 (1999).
- E. Nagao, O. Kaneko, J. A. Dvorak, *J. Struct. Biol.* **130**, 34 (2000).
- K. Haldar, M. A. Ferguson, *J. Biol. Chem.* **260**, 4969 (1985).
- D. Gaur, D. C. Ghislaine, L. H. Miller, *Int. J. Parasitol.* **34**, 1413 (2004).
- Supported by NSF Major Research Instrumentation grant DMR-0420923, NSF Nanoscale Science and Engineering Center grant EEC-0118025, and based on U.S. Department of Energy Basic Energy Sciences grant DE-FG02-92ER45475. This work made use of the NUANCE center facilities at Northwestern University. We thank K. Shull and A. Hagman for polymer-nanoparticle samples, and K. Haldar and her group for assistance with the malaria-infected RBCs.

20 July 2005; accepted 22 August 2005
10.1126/science.1117694

A 5-Micron-Bright Spot on Titan: Evidence for Surface Diversity

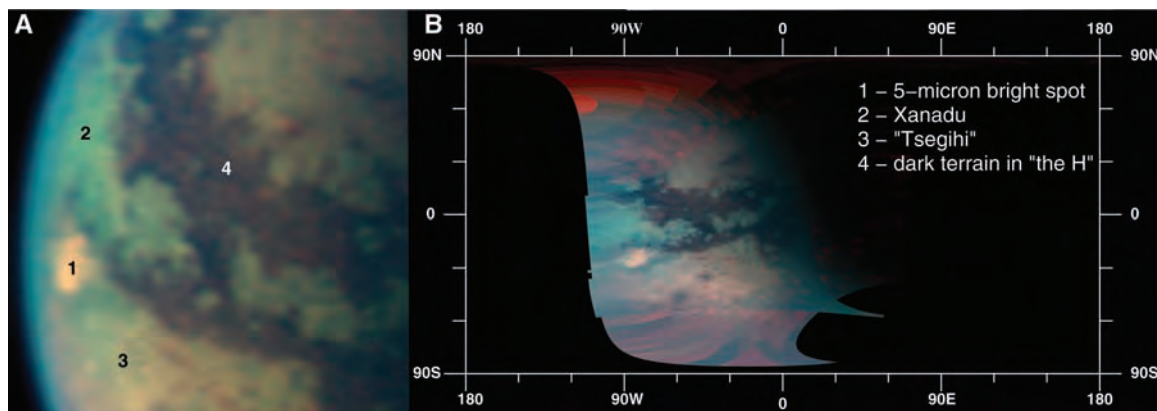
Jason W. Barnes,^{1*} Robert H. Brown,¹ Elizabeth P. Turtle,¹
Alfred S. McEwen,¹ Ralph D. Lorenz,¹ Michael Janssen,²
Emily L. Schaller,³ Michael E. Brown,³ Bonnie J. Buratti,²
Christophe Sotin,⁴ Caitlin Griffith,¹ Roger Clark,⁵ Jason Perry,¹
Stephanie Fussner,¹ John Barbara,⁶ Richard West,²
Charles Elachi,² Antonin H. Bouchez,⁷ Henry G. Roe,³
Kevin H. Baines,² Giancarlo Bellucci,⁸ Jean-Pierre Bibring,⁹
Fabrizio Capaccioni,¹⁰ Priscilla Cerroni,¹⁰ Michel Combes,¹¹
Angioletta Coradini,⁸ Dale P. Cruikshank,¹² Pierre Drossart,¹¹
Vittorio Formisano,⁸ Ralf Jaumann,¹³ Yves Langevin,⁹
Dennis L. Matson,² Thomas B. McCord,¹⁴ Phillip D. Nicholson,¹⁵
Bruno Sicardy¹¹

Observations from the Cassini Visual and Infrared Mapping Spectrometer show an anomalously bright spot on Titan located at 80°W and 20°S. This area is bright in reflected light at all observed wavelengths, but is most noticeable at 5 microns. The spot is associated with a surface albedo feature identified in images taken by the Cassini Imaging Science Subsystem. We discuss various hypotheses about the source of the spot, reaching the conclusion that the spot is probably due to variation in surface composition, perhaps associated with recent geophysical phenomena.

Large-scale relatively bright and dark regions are present on Titan's surface. Two bright areas particularly stand out: the continent-sized

Xanadu Regio centered at 110°W, 15°S and the sub-Saturnian mid-south-latitude bright region (now provisionally named "Tsegihi")

Fig. 1. Global image view (A) and cylindrical map view (B) of T5 (16 April 2005) data showing the spot. These color (but not true color) composites were created using data from the 1.57- μm atmospheric window as blue, from the 2.0- μm atmospheric window as green, and from the 5- μm atmospheric window as red. The area labeled 1 indicates the area from which we obtained bright spot spectra. 2 indicates Xanadu, 3 the sub-Saturnian mid-south-latitude bright region "Tsegih," and 4 the area representing dark terrain. Areas 1, 2, and 3 were chosen to have broadly similar emission angles and atmospheric contributions.



centered at 15°W, 40°S. Several groups (1–3) have hypothesized that dark organic haze particles settling out of the atmosphere might build up all over Titan's surface, only to be washed away during methane rainstorms; thus, the bright areas would be composed of dirty ice (4) and the dark areas would be covered by organics. Other Earth-based observations have showed evidence for lakes of liquid hydrocarbon (5) along with methane clouds (6). Hence, Titan may be the only object other than Earth that is known to have an active exchange of liquid between the atmosphere and surface.

Three Cassini instruments can see through the haze in Titan's atmosphere. The Visual and Infrared Mapping Spectrometer (VIMS) uses spectral image mapping to obtain images in 352 colors simultaneously (7). VIMS's wavelength range, 0.3 to 5.2 μm , includes spectral windows at 0.92, 1.06, 1.26, 1.57, 2.0, 2.7, and 5.0 μm , where neither haze nor atmospheric absorption completely obscures the surface. The Imaging Science Subsystem (ISS) is a visible/near-infrared (IR) camera with a charge-coupled device detector (8). ISS is capa-

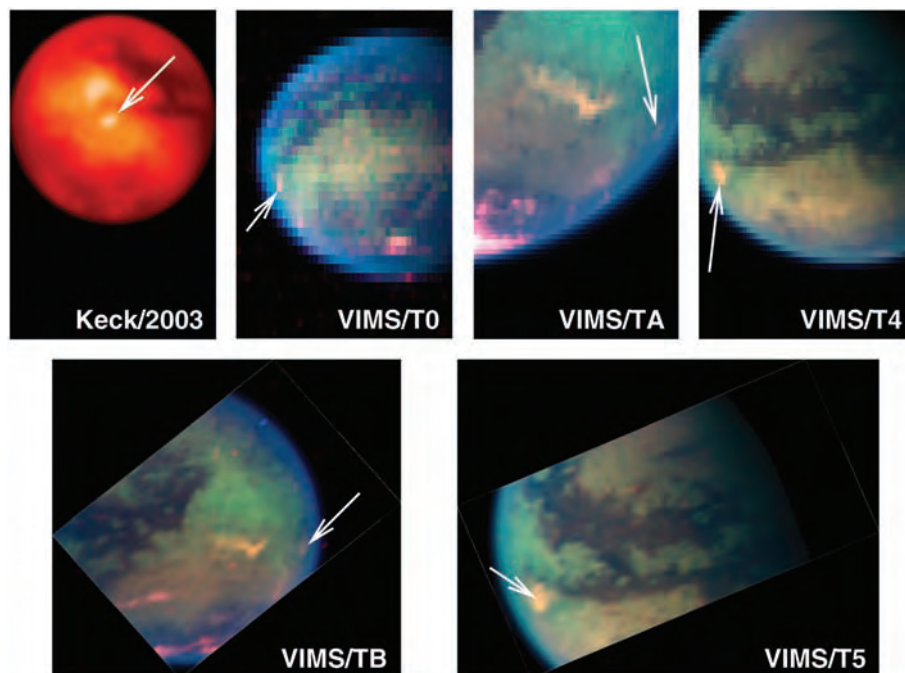


Fig. 2. Identifications of the 5- μm -bright spot from Keck AO ground-based imaging on 24 December 2003 and from VIMS during Cassini encounters on 3 July 2004 (T0), 26 October 2004 (TA), 13 December 2004 (TB), 31 March 2005 (T4), and 16 April 2005 (T5). North is at the top in all images. Keck data were taken through the K filter (1.95 to 2.30 μm) and color-mapped to produce the upper left image. The VIMS images were generated with 5 μm (VIMS channels 337 to 362 added together) as red, 2.0 μm as green, and 1.57 μm as blue. Spectral coverage for the T0 encounter was limited by bandwidth constraints; for the T0 image, we scaled the available data to simulate the full spectral window conditions that were used in the other flybys. The 5- μm -bright spot shows no spectral or spatial changes between T4 and T5, although the geometry of the other encounters is poor enough to not rule out changes in spatial coverage.

ble of observing Titan's surface through its 0.938- μm filter. Cassini's radar radiometer investigates spatial variation in surface properties with both active and passive modes. At short range, the radar is operated in active mode as a 2.17-cm synthetic aperture radar (9). At larger ranges, it can operate in passive mode, measuring the microwave flux from Titan's surface.

Here we present observations of an unusual bright region on Titan, southeast of Xanadu. The bright spot is located at 80°W, 25°S and became apparent in adaptive optics 1.6- μm

(10) and 2.0- μm imaging from the Keck Observatory. VIMS obtained its best views of the area on 31 March 2005 (T4) and 16 April 2005 (T5) (Fig. 1). A bright area consistent with this one is also present in data taken on 2 July 2004 (T0), 26 October 2004 (TA), and 13 December 2004 (TB), (Fig. 2). Thus, the spot was observed consistently over 9 months. The spot was near the sub-solar point during T5, but the spacecraft trajectory limited views of the spot to emission angles of over 60° at a spatial resolution of 30 km per pixel in the north/south direction

¹Lunar and Planetary Laboratory, University of Arizona, Tucson, AZ 85721, USA. ²Jet Propulsion Laboratory, California Institute of Technology, Pasadena, CA 91109, USA. ³Geological and Planetary Sciences, California Institute of Technology, Pasadena, CA 91125, USA. ⁴Laboratoire de Planétologie et Géodynamique, UMR CNRS 6112, Université de Nantes, France. ⁵U.S. Geological Survey, Flagstaff, AZ 86001, USA. ⁶NASA Goddard Institute for Space Studies, New York, NY 10025, USA. ⁷W. M. Keck Observatory, Kamuela, HI 96743, USA. ⁸Istituto di Fisica dello Spazio Interplanetario, Consiglio Nazionale delle Ricerche, Rome 00133, Italy. ⁹Institut d'Astrophysique Spatiale, Université de Paris-Sud, Orsay 91405, France. ¹⁰Istituto di Astrofisica Spaziale e Fisica Cosmica, Consiglio Nazionale delle Ricerche, Rome, Italy. ¹¹Observatoire de Paris, Meudon, France. ¹²NASA Ames Research Center, Moffet Field, Mountain View, CA 94035–1000, USA. ¹³Institute of Planetary Exploration, German Aerospace Center, Berlin 12489, Germany. ¹⁴Department of Earth and Space Sciences, University of Washington, Seattle, WA 98195–1310, USA. ¹⁵Department of Astronomy, Cornell University, Ithaca, NY 14853, USA.

*To whom correspondence should be addressed. E-mail: jbarnes@lpl.arizona.edu.

and 150 km per pixel in the east/west direction. Resolution was similar during T4. The spot's morphology was the same during both encounters. These observations are, therefore, consistent with a static feature.

The 5- μm -bright spot extends 450 km from north to south and 400 km from Titanian west to Titanian east. It is brightest in the mid-north. The spot is brighter than conventional bright terrain at all wavelengths, and it becomes progressively brighter than Xanadu beyond 1.6 μm (Fig. 3). In images created by co-adding all of the VIMS frames in the 5- μm spectral window, the spot outshines the sub-Saturnian mid-south-latitude bright region ("Tsegih") by 17% and outshines Xanadu by nearly a factor of 2. The spot's spectral signature more closely resembles that of "Tsegih" than that of Xanadu; even though the spot might spectrally be yet-brighter "Tsegih" terrain, Xanadu's sharply lower albedo at 5 μm is distinct. At 2.65 μm , the spot is of similar intensity relative to incoming solar flux (I/F) relative to other bright terrain, but is $\sim 15\%$ brighter than other terrain at 2.75 μm .

A thin, bright, semicircular feature bounded the 5- μm -bright spot to the south, as seen by ISS in December 2004 (TB). This feature ("the Smile") is 650 km long and up to ~ 90 km wide. The arc does not continue to the north, so it does not mark a recent circular impact structure. It could be a heavily eroded crater, although the old crater idea does not explain why "the Smile" is so bright. The feature's symmetry seems to imply structural control. The ISS image shows a crenulated margin, perhaps due to surface flows or erosion. ISS also observed this region in February 2005 (T3) and, within the limits of resolution, no difference in "the Smile" was detected.

"The Smile" is brighter than the rest of Xanadu (Fig. 4b). In the region where the 5- μm flux is strongest (the area within or bounded by "the Smile"), ISS shows a 300×500 km area of high albedo trending northeast-southwest. The 0.938- μm albedo of this area is comparable to that in Xanadu. Therefore, the 0.938- μm and 5.0- μm albedos of this area interior to "the Smile" are not correlated (Fig. 4C). In contrast, the albedos measured elsewhere on the surface of Titan by ISS and VIMS correlate strongly.

A moderately bright 0.938- μm area underlies the triangular tongue that is bright at 5 μm and stretches toward the southwestern edge of the H-shaped dark region that was first seen from Earth (11). But to the northwest, areas that are somewhat bright at 5.0 μm overlie a region that is dark at 0.938 μm . This variation probably reflects resolution differences between the two data sets. Thin, bright, radial fingers extend northward from "the Smile"'s center of arc into the dark region in the ISS view. The superposition of the bright fingers and dark background probably results in the moderate 5- μm brightness detected by VIMS. If this in-

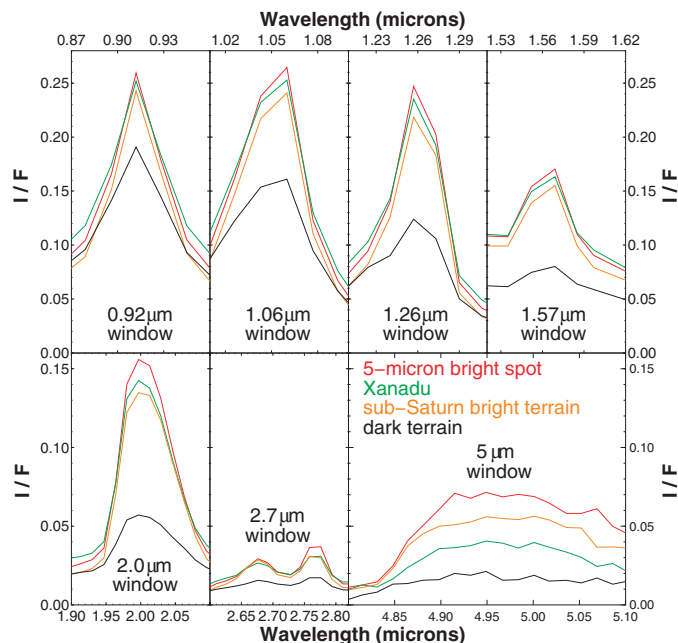


Fig. 3. Spectral comparison of the spot, Xanadu, the sub-Saturnian mid-south-latitude bright region ("Tsegih"), and dark terrains within Titan's different spectral windows. All Titanian bright terrain is not the same: Xanadu and "Tsegih" are distinctly different from one another. Although Xanadu is brighter than "Tsegih" at wavelengths shorter than 5 μm , it is dimmer at 5 μm , which may imply an icier composition. The bright spot more closely tracks Xanadu in its overall brightness, but like "Tsegih" is much brighter than Xanadu at 5 μm .

terpretation is correct, then the increased 5- μm flux is correlated with ISS bright terrain.

A low-resolution passive radiometry observation from T4 covers the study area (Fig. 4D) in one polarization, with a spatial resolution of about 250 km. A correlation of higher brightness temperature with lower near-IR albedo in the upper right corner of the map is prominent. This correlation appears to hold for most of Titan's surface at these spatial scales.

The spot cannot be specular reflection because the specular point for flat surfaces was located thousands of kilometers to the east. VIMS's observations span 12° to 57° in phase angle and show no variation in the spectral character of the spot; the much better-sampled ground-based Keck adaptive optics (AO) observations of the spot also show that its phase function matches the surrounding terrain between 0° and 70° .

The low density of craters on Titan (12, 9) implies a high resurfacing rate that may involve cryovolcanism (9). We performed radiative simulations that show the bright spot's 5- μm excess to be consistent with roughly gray-body thermal emission at a temperature of ~ 180 K. Some features of the ISS morphology are consistent with the idea that the 5- μm -bright spot represents a volcanic province: the bright optical albedo, crenulated margins, and possible linear flow features.

To test this hypothesis, we calculated brightness temperatures from passive microwave radiometry obtained by Cassini's radar during the T4 encounter. The microwave brightness temperature depends on polarization, incidence angle, composition, and physical temperature (13). The observations in Fig. 4D were made at incidence angles of around 57° , close to the Brewster angle for ices and hydrocarbons. At

this angle, vertically polarized radiation is perfectly absorbed or emitted by the surface, and thus (in the absence of subsurface scattering) the brightness temperature corresponds exactly to the physical temperature. Our observation with an antenna temperature of ~ 77 K had the polarization vector about 38° from vertical, which represents a sum of horizontal and vertically polarized brightness temperatures weighted ($\sim 62\%$) in favor of the vertical. Application of the orthogonal polarization, lower-resolution radiometer data (71 K) also taken on T4 suggests vertical brightness temperature $T_b(V) \sim 83$ K and horizontal brightness temperature $T_b(H) \sim 67$ K. The vertically polarized value is rather typical for other regions on Titan and is lower than the thermodynamic temperature of the surface because of subsurface scattering (which in effect partly reflects cold sky into the instrument in place of some surface emission). There is thus no evidence for elevated surface temperatures, which rules out the hot spot hypothesis.

If the spot represents a topographic high, sunlight would pass through less of Titan's atmosphere both incoming from the Sun and outgoing to Cassini. The reduced path length through the atmosphere would decrease both scattering by haze particles and absorption by atmospheric gases, resulting in a higher observed I/F for a surface of a given albedo. Because the optical depth of Titan's haze decreases with increasing wavelength, this hypothesis has difficulty explaining the spot's high 5- μm brightness. In addition, the lack of a strong negative brightness temperature anomaly associated with the feature in radiometry appears to argue against its being substantially elevated above surrounding areas. With a dry adiabatic lapse rate of ~ 0.6 to 0.8 K/km, even a generous 1 to 2 K temperature drop would

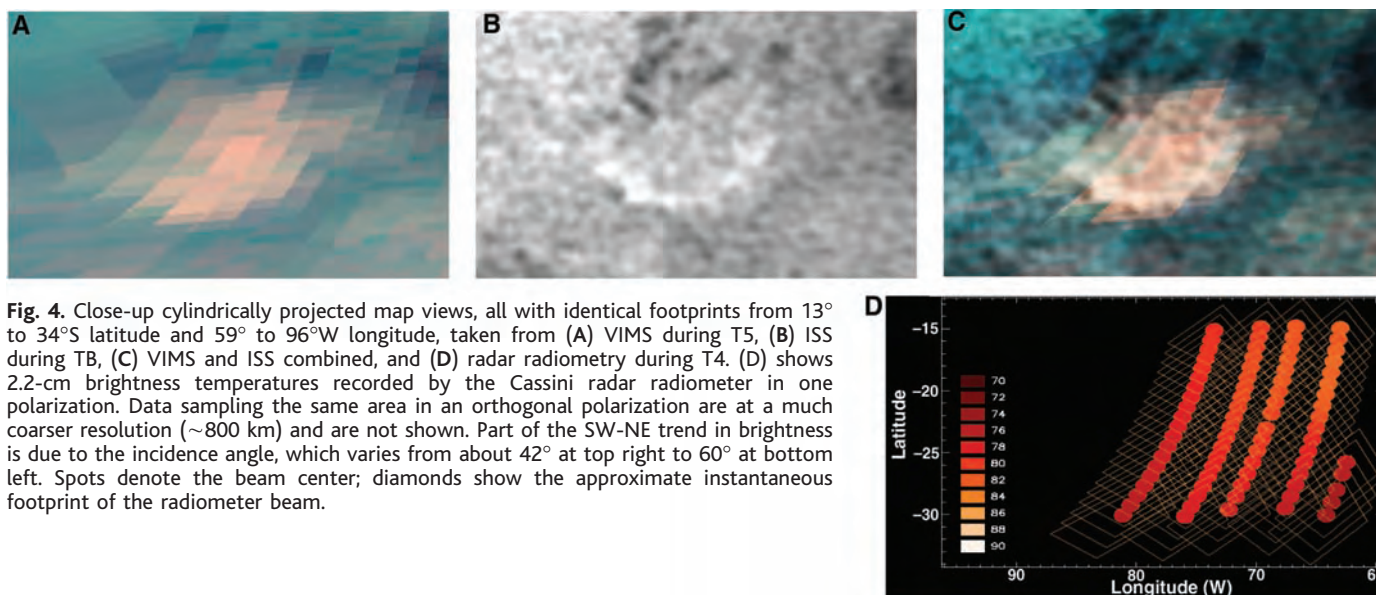


Fig. 4. Close-up cylindrically projected map views, all with identical footprints from 13° to 34°S latitude and 59° to 96°W longitude, taken from (A) VIMS during T5, (B) ISS during TB, (C) VIMS and ISS combined, and (D) radar radiometry during T4. (D) shows 2.2-cm brightness temperatures recorded by the Cassini radar radiometer in one polarization. Data sampling the same area in an orthogonal polarization are at a much coarser resolution (~800 km) and are not shown. Part of the SW-NE trend in brightness is due to the incidence angle, which varies from about 42° at top right to 60° at bottom left. Spots denote the beam center; diamonds show the approximate instantaneous footprint of the radiometer beam.

permit only 3 km of topography, which is not enough to account for the spot's brightness.

Two major lines of reasoning, however, argue against this feature being a cloud. First, the spot's spectrum does not match that of known clouds; second, the feature has persisted for much longer than known clouds. The uniformly high inferred albedo for the spot across VIMS's entire spectral range is consistent with cloud particles. If the 5- μm -bright spot is caused by methane condensate, it would have to be in the form of a persistent low-lying cloud or ground fog.

Keck and Cassini observations have found this particular spot to be bright and to maintain its spatial distribution for 4.5 years. Clouds seen in the past formed and dissipated on time scales between hours and days. With better spatial resolution and higher time resolution, ISS monitoring of this region during TB showed no apparent changes over tens of hours. If the spot is a cloud, it must be a cloud that is tightly controlled by the surface. It could be orographic, but on Earth and Mars, even though orographic clouds appear preferentially in certain places, they still appear, disappear, and change shape over time. The spot could correspond to fog overlying a lake, hot springs, or a volcanic field. However, the higher-altitude clouds that we have seen so far are much brighter than Xanadu when viewed by ISS, and although "the Smile" meets this criterion, the interior of the 5- μm -bright spot does not.

Finally, the 5- μm -bright region may be the result of a surface albedo marking. As such, it could represent an area with distinct crustal composition, an area in an unusual state of weathering, or a thin surficial coating. Because water ice is highly absorbing at 5 μm , the 5- μm -bright area cannot be more water-rich than either Xanadu or the sub-Saturnian mid-south-latitude bright region "Tsegihi." The strong negative deviation of Xanadu's spectrum at 5 μm

implies that it is Xanadu that has more water ice than either the bright spot or "Tsegihi." It is not obvious what composition might be both brighter than Xanadu at long wavelengths where water absorbs and brighter at short wavelengths where water strongly reflects. The area could be in an unusual state of weathering—either very young geologically or perhaps just recently cleaned by methane rainfall. Either might alter the chemistry of the topmost surface layer in a manner that could reproduce the observed spectrum, although it would seem that a recent methane cleaning would leave the area more icy, not less. Finally, the spatially localized nature of the 5- μm excess could be the result of a thin airfall deposit, perhaps emanating from vents in "the Smile" and blown northeast by prevailing winds. However, it is still difficult to conceive of a substance with the right spectral properties.

If the radiometric brightness temperatures $T_b(V) \sim 83$ K and $T_b(H) \sim 67$ K are interpreted as due to emission from a dielectric surface at 83 K (thus taking subsurface scattering crudely into account), the ratio of the two temperatures suggests a dielectric constant of ~ 3 . This value is rather higher than that typical for Titan as a whole, which exhibits polarization that is characteristic of dielectric constants of 2. The value would be consistent with the study area having an ice-rich composition, in contrast to the widespread value characteristic of porous ices or solid or liquid hydrocarbons. Pure ice appears inconsistent with the VIMS data. However, because the absorptivity or loss tangent of cold ice and hydrocarbons is very low ($< \sim 10^{-4}$), the microwave data probe depths of perhaps several meters. Hence, a thin frost or veneer of material only a few tens of microns thick could give the surface a very different near-IR reflectance from that expected from its bulk composition.

An intriguing possibility for the identity of the bright spot's reflecting material is CO_2 ice.

CO_2 ice reflects highly in the same short-wavelength Titanian atmospheric windows where water ice reflects, but is more highly reflective than water ice in the 5- μm window. Unfortunately, the most diagnostic wavelengths for carbon dioxide ice are not within Titan's spectral windows and thus are not amenable to remote sensing. Kress and McKay (14) recently predicted an abundance of CO_2 on Titan, based on chemical modeling of comet impacts early in Titan's history. In this scenario, the bright spot and "Tsegihi" could be either eroded layers of CO_2 or more recent overlying deposits. Observations in the coming years will shed additional light on this enigmatic feature.

References and Notes

- C. A. Griffith, T. Owen, R. Wagoner, *Icarus* **93**, 362 (1991).
- J. I. Lunine, *ESA SP-338: Symposium on Titan* (European Space Agency, 1992), pp. 233-239.
- P. H. Smith *et al.*, *Icarus* **119**, 336 (1996).
- C. A. Griffith, T. Owen, T. R. Geballe, J. Rayner, P. Rannou, *Science* **300**, 628 (2003).
- D. B. Campbell, G. J. Black, L. M. Carter, S. J. Ostro, *Science* **302**, 431 (2003).
- C. A. Griffith, T. Owen, G. A. Miller, T. Geballe, *Nature* **395**, 575 (1998).
- R. H. Brown *et al.*, *Icarus* **164**, 461 (2003).
- C. C. Porco *et al.*, *Space Sci. Rev.* **115**, 363 (2004).
- C. Elachi *et al.*, *Science* **308**, 970 (2005).
- H. G. Roe *et al.*, *Geophys. Res. Lett.* **31**, 17 (2004).
- M. Hartung *et al.*, *Astron. Astrophys.* **421**, L17 (2004).
- C. C. Porco *et al.*, *Nature* **434**, 159 (2005).
- R. D. Lorenz *et al.*, *Planet. Space Sci.* **51**, 353 (2003).
- M. E. Kress, C. P. McKay, *Icarus* **168**, 475 (2004).
- Some of the data presented herein were obtained at the W. M. Keck Observatory, which is operated as a scientific partnership among the California Institute of Technology, the University of California, and NASA. The observatory was made possible by the generous financial support of the W. M. Keck Foundation. This work was funded by the Cassini project. Authors from U.S. institutions were funded by NASA; authors from European institutions were funded by the European Space Agency.

7 July 2005; accepted 9 September 2005
10.1126/science.1117075

National Character Does Not Reflect Mean Personality Trait Levels in 49 Cultures

A. Terracciano,^{1*} A. M. Abdel-Khalek,² N. Ádám,³ L. Adamovová,⁴ C.-k. Ahn,⁵ H.-n. Ahn,⁶ B. M. Alansari,² L. Alcalay,⁷ J. Allik,⁸ A. Angleitner,⁹ M. D. Avia,¹⁰ L. E. Ayeart,¹¹ C. Barbaranelli,¹² A. Beer,¹³ M. A. Borg-Cunen,¹⁴ D. Bratko,¹⁵ M. Brunner-Sciarra,¹⁶ L. Budzinski,¹⁷ N. Camart,¹⁸ D. Dahourou,¹⁹ F. De Fruyt,²⁰ M. P. de Lima,²¹ G. E. H. del Pilar,²² E. Diener,²³ R. Falzon,¹⁴ K. Fernando,²⁴ E. Ficková,⁴ R. Fischer,²⁵ C. Flores-Mendoza,²⁶ M. A. Ghayur,^{27†} S. Gülgöz,²⁸ B. Hagberg,²⁹ J. Halberstadt,²⁴ M. S. Halim,³⁰ M. Hřebíčková,³¹ J. Humrichouse,¹³ H. H. Jensen,³² D. D. Jovic,³³ F. H. Jónsson,³⁴ B. Khoury,³⁵ W. Klinkosz,³⁶ G. Knežević,³⁷ M. A. Lauri,¹⁴ N. Leibovich,³⁸ T. A. Martin,³⁹ I. Marušić,¹⁵ K. A. Mastor,⁴⁰ D. Matsumoto,⁴¹ M. McRorie,⁴² B. Meshcheriakov,⁴³ E. L. Mortensen,³² M. Munyae,⁴⁴ J. Nagy,³ K. Nakazato,⁴⁵ F. Nansubuga,⁴⁶ S. Oishi,⁴⁷ A. O. Ojedokun,⁴⁸ F. Ostendorf,⁹ D. L. Paulhus,⁴⁹ S. Pelevin,⁴³ J.-M. Petot,¹⁸ N. Podobnik,⁵⁰ J. L. Porrata,⁵¹ V. S. Pramila,⁵² G. Prentice,⁴² A. Realo,⁸ N. Reátegui,¹⁶ J.-P. Rolland,⁵³ J. Rossier,⁵⁴ W. Ruch,⁵⁵ V. S. Rus,⁵⁶ M. L. Sánchez-Bernardos,¹⁰ V. Schmidt,³⁸ S. Sciculna-Calleja,¹⁴ A. Sekowski,³⁶ J. Shakespeare-Finch,^{57‡} Y. Shimonaka,⁵⁸ F. Simonetti,⁷ T. Sineshaw,⁵⁹ J. Siuta,⁶⁰ P. B. Smith,⁶¹ P. D. Trapnell,⁶² K. K. Trobst,¹¹ L. Wang,⁶³ M. Yik,⁶⁴ A. Zupancič,⁶⁵ R. R. McCrae^{1*}

Most people hold beliefs about personality characteristics typical of members of their own and others' cultures. These perceptions of national character may be generalizations from personal experience, stereotypes with a "kernel of truth," or inaccurate stereotypes. We obtained national character ratings of 3989 people from 49 cultures and compared them with the average personality scores of culture members assessed by observer ratings and self-reports. National character ratings were reliable but did not converge with assessed traits. Perceptions of national character thus appear to be unfounded stereotypes that may serve the function of maintaining a national identity.

Beliefs about distinctive personality characteristics common to members of a culture are referred to as national character (1) or national stereotypes (2–4). National stereotypes include beliefs about social, physical, and mental characteristics, but the present article focuses on personality traits. Several factors are thought to influence these beliefs. They may be generalizations based on observations of the personality traits of individual culture members. They may be inferences based on the national ethos, as revealed in socioeconomic conditions, history, customs, myths, legends, and values. They may be shaped by comparisons or contrasts with geographically close or competing cultures. Stereotypes are oversimplified judgments, but if they have some "kernel of truth" (5), national character should reflect the average emotional, interpersonal, experiential, attitudinal, and motivational styles of members of the culture.

There have been few attempts to examine the accuracy of national stereotypes (3, 5–7), perhaps because researchers lacked appropriate criteria. However, recent advances in personality psychology and cross-cultural research make it possible to compare perceived national character with aggregate personality data (that is, the means of a sample of assessments of individuals) across a wide range of cultures.

National character may be a social construction, but personality traits are rooted in biology. Most personality psychologists today agree that the dimensions of the five-factor model (FFM) of personality—neuroticism versus emotional stability, extraversion, openness to experience, agreeableness, and conscientiousness—account for the covariation of most personality traits (8), and behavioral genetics studies (9) have shown that traits from all five factors are strongly heritable. As products (in part) of the human genome, traits are universal: Cross-cultural

research suggests that the structure and development of personality traits is very similar in nations as dissimilar as India, Argentina, and Burkina Faso (10). In every culture examined, the five factors are hierarchically related to lower order traits or facets. For example, the extraversion factor in the Revised NEO Personality Inventory (NEO-PI-R) (11) is defined by warmth, gregariousness, assertiveness, activity, excitement seeking, and positive emotions facets.

Personality traits can be assessed with standardized instruments such as the NEO-PI-R, using either self-reports or observer ratings from knowledgeable informants. The reliability and validity of individual assessments made with the NEO-PI-R are well established (10, 11). Recent cross-cultural data also indicate that aggregate (or mean) NEO-PI-R scores can be validly used to describe cultures as a whole. In a study of self-report data from 36 cultures, culture-level scores were generalizable across age groups and gender, and aggregate scores showed meaningful patterns of convergent and discriminant validity with other culture-level variables such as individualism-collectivism (12). Geographically and historically related cultures (such as Germany and Austria or the United States and Canada) showed similar personality profiles (13). Most of these findings were replicated in a subsequent study using observer ratings from 51 cultures (10, 14), and aggregate self-reports were significantly correlated with aggregate observer ratings for most of the 30 NEO-PI-R facets. Assessed aggregate personality scores from these two studies can thus be used in a multimethod evaluation of the accuracy of perceptions of national character.

There is a substantial literature on the evaluation of the accuracy of stereotypes (3), showing that they may or may not reflect reality. For example, gender stereotypes depicting women as warm and men as assertive are widely held around the world (15). Cross-cultural studies using both self-reports and observer ratings have shown that women in fact score higher on measures of warmth, whereas men score higher on measures of assertiveness (10, 16). Assessed gender differences are small but are largely consistent with gender stereotypes (17, 18), so those views appear to have a basis in the characteristics of individuals.

The available literature provides less support for the accuracy of beliefs about national character. The perceptions of a panel of experts in cross-cultural psychology did not match beyond chance the assessed characteristics in a sample of 26 cultures (19). Church and Katigbak (20) identified raters who had lived in both the United States and the Philippines and asked them to compare the typical American with the typical Filipino on traits that paralleled the 30 NEO-PI-R facets. There was

considerable consensus among the judges, but their judgments did not correspond to differences observed when mean American self-reports were compared to mean Filipino self-reports. Another study using the NEO-PI-R found no support for popular stereotypes of northern and southern Italians (21).

Here, we examine whether national character, as described by culture members themselves (the in-group), are consistent with aggregate personality data. Aggregate scores from self-report and observer ratings on the NEO-PI-R provide the criteria, but measurement of perceived national character requires a new instrument.

We designed a short questionnaire, the National Character Survey (NCS), to describe the typical member of a culture (22). The NCS consists of 30 bipolar scales with two or three adjectives or phrases at each pole of the scale. For example, the first item asks how likely it is that the typical member of a culture is anxious, nervous, and worrying versus at ease, calm, and relaxed. Each five-point scale taps one of the 30 facets assessed by the NEO-PI-R, with six items for each of the five major dimensions of personality traits. Internal consistency and factor analysis of the NCS items (22) indicate

that the scales have acceptable psychometric properties and successfully define the dimensions of the FFM. To the extent that the FFM is a comprehensive model of personality, the NCS should capture the essential features of national character.

Data were gathered from 49 cultures or subcultures from six continents, using translations into 27 languages from Indo-European, Hamito-Semitic, Sino-Tibetan, Uralic, Malayo-Polynesian, and Altaic families. Most cultures corresponded to nations; however, where subcultures could be identified on the basis of history (e.g., England versus Northern Ireland) or language (e.g., French- versus German-speaking Switzerland), they were treated as separate samples. In each sample, we asked college students to complete the NCS to describe the typical member of their culture or subculture and then, as a common basis of comparison, the typical American.

Analyses of the NCS data in the full sample ($N = 3989$) and in selected subsamples supported the reliability, generalizability, and validity of the NCS as a measure of perceived national character (22). Interjudge reliability between single raters showed there is only modest agreement between individual judg-

ments of national character, with coefficients ranging from 0.09 to 0.30 (median, 0.17). This is roughly half the size of typical agreement between two judges on a single person they both know well (23). However, by aggregating the judgments of an average of 81 raters per culture, highly reliable means were obtained, with reliability coefficients ranging from 0.96 to 0.97 for the five factors, and from 0.89 to 0.97 (median, 0.94) for the 30 facets. These aggregate values correspond to the shared portion of individuals' perceptions. Men and women provided essentially the same profile of the typical member of their culture: When mean scores for female subsamples were correlated with mean scores for male subsamples matched on culture, correlations for the five factors ranged from 0.80 to 0.90 ($N = 49$; all P s < 0.001).

Additional analyses comparing NCS profiles across groups used T scores ($M = 50$, $SD = 10$) based on the grand means and standard deviations across all raters and samples for the 30 NCS items. Profile agreement is calculated as the intraclass correlation (ICC) across the 30 facets, using the double-entry method (24). Intraclass correlations are similar to Pearson correlations, but are sensitive to both

¹National Institute on Aging, NIH, DHHS, Gerontology Research Center, 5600 Nathan Shock Drive, Baltimore, MD 21224, USA. ²Department of Psychology, Faculty of Social Sciences, University of Kuwait, Post Office Box 68168, 71962, Kaifan, Kuwait. ³Faculty of Education and Psychology, Lóránd Eötvös University, 1075 Budapest, Kazinczy u. 23-25, Hungary. ⁴Institute of Experimental Psychology, Slovak Academy of Sciences, Dúbravská cesta 9, Bratislava, Slovak Republic, 813 64. ⁵Department of Education, Pusan National University, 30 Jangjeon-dong, Geumjeong-gu, Busan 609-735, Republic of Korea. ⁶Department of Psychology, Pusan National University, 30 Jangjeon-dong, Geumjeong-gu, Busan 609-735, Republic of Korea. ⁷Escuela de Psicología, Pontificia Universidad Católica de Chile, Vicuña Mackenna 4860, Macul, Santiago, Chile. ⁸Department of Psychology, University of Tartu, Tiigi 78, Tartu, Estonia, 50410. ⁹University of Bielefeld, Department of Psychology, Post Office Box 100131, Bielefeld, Germany, D-33501. ¹⁰Facultad de Psicología, Universidad Complutense de Madrid, Madrid, Spain. ¹¹Department of Psychology, York University, 4700 Keele Street, Toronto, ON, Canada, M3J 1P3. ¹²Department of Psychology, University of Rome, La Sapienza, Via Dei Marsi 78, 00185 Rome, Italy. ¹³Department of Psychology, University of Iowa, E11 Seashore Hall, Iowa City, IA 52242-1407, USA. ¹⁴Department of Psychology, University of Malta, Msida MSD 06 Malta. ¹⁵Odsjek za Psihologiju, Filozofski Fakultet u Zagrebu, I. Lucića 3, Zagreb, Croatia, 10000. ¹⁶Facultad de Psicología, Universidad Peruana Cayetano Heredia, Av. Armendáriz 497 Miraflores, Lima, Peru. ¹⁷Department of Psychology, University of Melbourne, Parkville VIC, 3010, Australia. ¹⁸Laboratoire de Psychologie Clinique des Faits Culturels, Université de Paris-X, 200, Avenue de la République, Nanterre, France, 92001. ¹⁹Department of Psychology, University of Ouagadougou, 03 B.P. 7021 Ouagadougou 03, Burkina Faso. ²⁰Department of Psychology, H. Dunantlaan, 2, Ghent, Belgium, B-9000. ²¹Faculdade de Psicologia, Ciências da Educação, Universidade de Coimbra, Coimbra, Portugal. ²²Department of Psychology, University of the Philippines, Diliman, Quezon City, 1101, Philippines. ²³Department of Psychology, University of

Illinois, 603 East Daniel Street, Champaign, IL 61820, USA. ²⁴Department of Psychology, University of Otago, Post Office Box 56, Dunedin, New Zealand. ²⁵School of Psychology, Post Office Box 600, Victoria University of Wellington, Wellington, New Zealand. ²⁶U Federal de Minas Gerais, Dept. de Psicologia, Sala 4042, Av. Antonio Carlos 6627, Belo Horizonte, Brazil. ²⁷Al Akhawayn University, Ifrane, Morocco. ²⁸Koç University, Sariyer 80910, Istanbul, Turkey. ²⁹Unit of Gerontology and Care for the Elderly, Lund University, Box 187, S-222 20 Lund, Sweden. ³⁰Faculty of Psychology, Atma Jaya Indonesia Catholic University, Jl. Jenderal Sudirman kav-51, Jakarta Selatan-12930, Indonesia. ³¹Academy of Sciences of the Czech Republic, Vevří 97, 602 00 Brno, Czech Republic. ³²Department of Health Psychology, Institute of Public Health, University of Copenhagen, Blegdamsvej 3, Copenhagen N, Denmark, DK-2200. ³³Institute for Psychiatry, Pasterova 2, Belgrade, Yugoslavia. ³⁴University of Iceland, Faculty of Social Science, Oddi, Sturlugata, 101 Reykjavík, Iceland. ³⁵Department of Psychiatry, American University of Beirut Medical Center, Post Office Box 11-0236, Riad El-Solh, Beirut 1107 2020 Lebanon. ³⁶Catholic University of Lublin, Department of Psychology, A1, Raclawickie 14, Lublin 20-950 Poland. ³⁷Department of Psychology, University of Belgrade, Cika Ljubina 18-20, 11000 Belgrade, Yugoslavia. ³⁸Faculty of Psychology, University of Buenos Aires, Buenos Aires, Argentina. ³⁹Department of Psychology, Susquehanna University, 514 University Avenue, Selingsgrove, PA 17870, USA. ⁴⁰Center for General Studies, Universiti Kebangsaan Malaysia, Selangor Darul Ehsan, Malaysia. ⁴¹Department of Psychology, San Francisco State University, 1600 Holloway Avenue, San Francisco, CA 94132, USA. ⁴²School of Psychology, Queen's University Belfast, Belfast BT7 1NN, Northern Ireland, UK. ⁴³Department of Psychology, International University Dubna, 19, Universitetskaya str., Dubna, Moscow area, Russia, 141980. ⁴⁴Center for Continuing Education, University of Botswana, Private Bag UB 0022, Gaborone, Botswana. ⁴⁵Department of Psychology, Iwate Prefectural University, 152-52 Sugo, Takizawa, Iwate, 020-0193 Japan. ⁴⁶Department of Organizational Psychology, Makerere University, Post

Office Box 7062, Kampala, Uganda. ⁴⁷Department of Psychology, University of Virginia, Post Office Box 400400, Charlottesville, VA 22904-4400, USA. ⁴⁸Department of Psychology, University of Ibadan, Ibadan, Nigeria. ⁴⁹Department of Psychology, University of British Columbia, Vancouver, Canada V6T 1Z4. ⁵⁰Psychiatric Hospital of Idrija, Pot Sv. Antona 49 Idrija, 5280 Slovenia. ⁵¹Escuela Graduada de Administración Pública, Universidad de Puerto Rico, Río Piedras, Puerto Rico. ⁵²Department of Psychology, Andhra University, Visakhapatnam 530 003, Andhra Pradesh, India. ⁵³Université Paris 10, STAPS Dept., 200 Avenue de la République, Nanterre, France, 92001. ⁵⁴Institute of Psychology, University of Lausanne, BFSH 2 Dorigny, Lausanne, Switzerland, CH-1015. ⁵⁵Psychologisches Institut, Zürichbergstrasse 43, 8044 Zürich, Switzerland. ⁵⁶Faculty of Arts, University of Ljubljana, Ljubljana, Slovenia. ⁵⁷School of Psychology and Counselling, Queensland University of Technology. ⁵⁸Department of Psychology, Bunkyo Gakuin University, 1196, Kamekubo, Oi-machi, Iruma-gun, Saitama, 356-8533, Japan. ⁵⁹Department of Psychology, Ramapo College of New Jersey, 505 Ramapo Valley Road, Mahwah, NJ 07430, USA. ⁶⁰Institute of Psychology, Jagiellonian University, Krakow, Poland. ⁶¹Department of Psychology, University of Sussex, Brighton, UK. ⁶²Department of Psychology, The University of Winnipeg, 515 Portage Avenue, Winnipeg, Manitoba, Canada R3B 2E9. ⁶³Department of Psychology, Peking University, Beijing, People's Republic of China. ⁶⁴Division of Social Science, Hong Kong University of Science and Technology, Clear Water Bay, Kowloon, Hong Kong. ⁶⁵Ministry for Health, Štefanova ulica 5, 1000 Ljubljana, Republic of Slovenia.

*To whom correspondence should be addressed. E-mail: terraccianoa@grc.nia.nih.gov (A.T.); mccraej@grc.nia.nih.gov (R.R.M.)

†Present address: Department of Psychology, San Diego State University, 5500 Campanile Drive, San Diego, CA 92182-4611, USA.

‡Present address: School of Psychology, University of Tasmania, Locked Bag 1342, Launceston, TAS, 7250 Australia.

the shapes of the profiles and differences in elevation, and are thus an appropriate metric for assessing profile similarity. With 30 profile elements, ICCs above 0.57 are significant at $P < 0.001$.

Several comparisons suggested that NCS means were robust. In Ethiopia and Italy, samples of adults were used as raters in addition to college students and yielded similar profiles (ICCs = 0.62 and 0.90, respectively). In some cultures, student data from multiple sites were available, and intraclass correlations between these different sites ranged from 0.76 to 0.94 (25). This is illustrated for Canada and the United States by the dotted lines in Fig. 1 (26).

Mean NCS scores for the 49 cultures are in table S1; the highest and lowest scoring cultures for each factor are listed in Table 1. It is perhaps not surprising that Australians see themselves as extraverts, German Swiss believe they are typically high in conscientiousness, and Canadians describe themselves as agreeable. But many of the other entries are nations with which most readers are not familiar, and it is difficult to judge the plausibility of these ratings. In any case, individual judgments of national character—including the reader's—have low reliability. The data suggest that aggregate values accurately reflect the

way in-group members perceive the personality of the typical member of their culture.

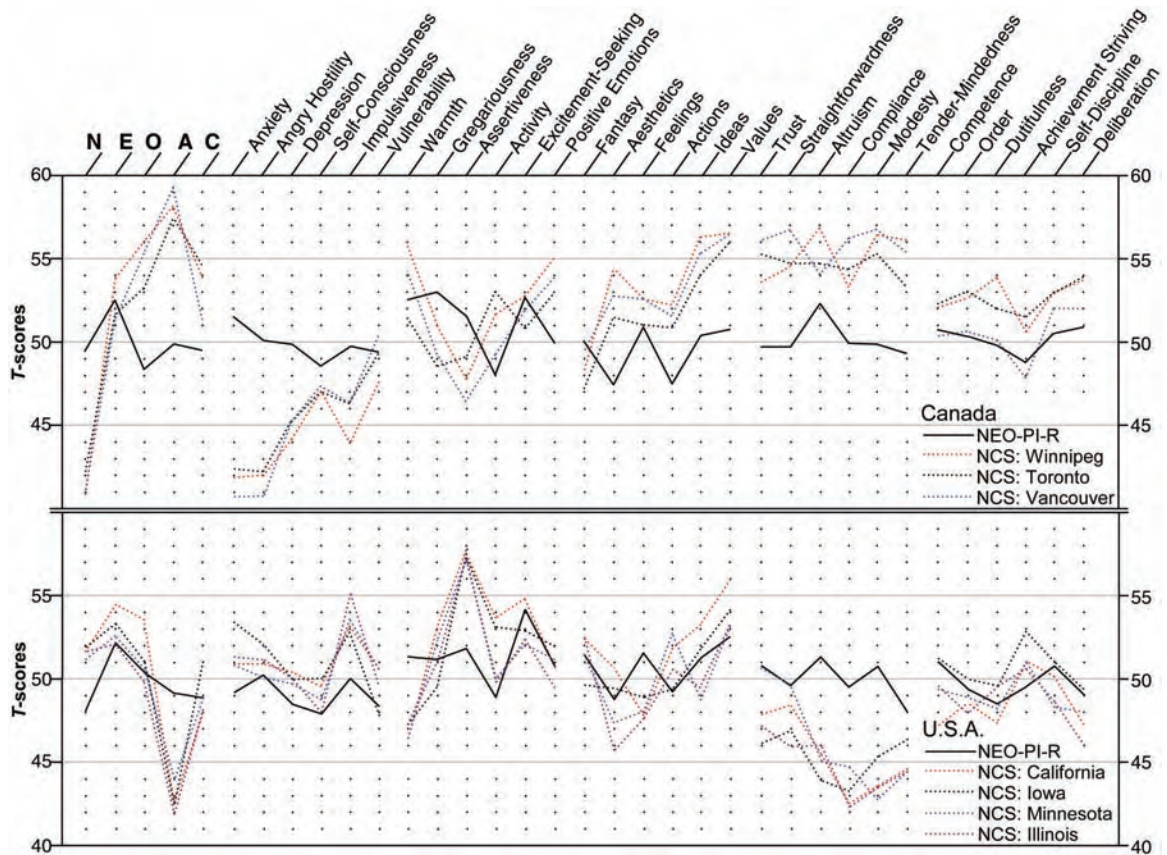
The primary question this study was designed to address is whether these in-group perceptions of national character accurately reflect aggregate judgments of individual personality traits. A first examination of the data shows one respect in which they are clearly different: There is a much greater range of variation across cultures in perceived traits than in assessed traits. For example, the typical German-speaking Swiss is thought to score 28 *T* score points higher on conscientiousness than the typical Indonesian, but the largest difference on observer-rated conscientiousness between any two cultures was only 8 *T* score points. Thus, if national stereotypes are accurate at all, they clearly exaggerate real differences.

We first examined agreement of trait profiles within cultures, correlating NCS facet scores with assessed mean facet values from NEO-PI-R observer ratings ($N = 11,479$) in 47 cultures (10) and self-reports ($N = 25,732$) in 30 cultures (12, 22). ICCs between NCS and the NEO-PI-R observer rating profiles ranged from -0.57 for England to 0.40 for Poland (median, 0.00), and there was a significant positive correlation in only four cultures (New Zealand, Australia, Poland, and Lebanon). Ex-

amples of these findings are shown in Fig. 1, in which the solid lines, representing mean observer-rated NEO-PI-R profiles, deviate markedly from the perceptions of national character, especially with regard to agreeableness facets. ICCs between NCS and mean NEO-PI-R self-report profiles ranged from -0.46 for Russia to 0.46 for Poland (median, -0.02), and only Poland and Japan showed significant positive correlations (table S1). Thus, only for Poland were the observer rating findings replicated. Overall, there is little support for the view that perceptions of national character profiles are accurate in any culture.

However, it is possible that agreement exists for some factors. To determine the degree of agreement for each trait, NCS domain and facet scores were correlated with NEO-PI-R observer ratings and self-reports across 47 and 30 cultures, respectively. For the five factors, correlations with observer ratings ranged from -0.23 to 0.13, and those with self-reports ranged from -0.34 to 0.30 (table S2), which indicates that there is no relation between aggregate NEO-PI-R data and the NCS on any of the five major dimensions. (This finding is illustrated in Table 1, where cultures scoring high versus low on the five NCS factors do not differ systematically on mean NEO-PI-R *T*

Fig. 1. *T* scores for NCS and NEO-PI-R factor and facet scales. On the left the scores for the five factors are plotted; toward the right are the 30 facets, grouped by the factor they define. Dotted lines show the NCS profile of the typical Canadian (top panel) and American (bottom panel) as perceived by students from three Canadian and four American sites, respectively. High profile similarity can be observed among the Canadian sites (ICCs = 0.89 to 0.92) and among the American sites (ICCs = 0.76 to 0.89), suggesting consensus on national character. Solid lines show mean observer-rated NEO-PI-R profiles. In both Canada (ICC = -0.03) and the United States (ICC = 0.23), in-group perceptions of national character across all sites do not reflect aggregate assessments of individual personality traits. The distinction between national character and mean trait levels can also be seen by comparing top and bottom panels: The NEO-PI-R profiles of the United States and Canada are similar



(ICC = 0.66), whereas there is no agreement between their national character ratings (ICC = -0.53). N, neuroticism; E, extraversion; O, openness to experience; A, agreeableness; C, conscientiousness.

scores.) There were 11 significant correlations at the facet level, 5 of which were negative. The median of the 70 correlations was 0.04. The only replicated effect was a significant negative correlation with openness to feelings: In cultures where people have a sensitive and rich emotional life, they perceive that their typical compatriot is emotionally impoverished. These analyses, too, provide little reason to trust national stereotypes (27).

Comparisons across cultures are always challenging, and several factors may have limited the association between NCS and NEO-PI-R profiles, including problems in translation, response biases such as acquiescence (a yea-saying tendency) (29), and the unfamiliarity of respondents in some cultures with the use of rating scales (10). Comparisons would have been more direct if the full NEO-PI-R had been used to assess national character. Yet, the mean NCS scores were reliable and generalizable across sites and types of rater and showed the hypothesized factor structure. Future studies might use more representative raters, although student and adult samples gave similar results when both were available.

In the case of gender differences, widely held stereotypes are consistent with—although they may exaggerate—assessed personality dif-

ferences between men and women (16–18). That kernel-of-truth hypothesis does not appear to apply to national character. Correspondence between perceived national character traits and the average levels of traits of individual members of each culture was found neither within nor across cultures. Perceptions of national character are not generalizations about personality traits based on accumulated observations of the people with whom one lives; instead, they appear to be social constructions that may serve different functions altogether. Correlations of NCS scores with culture-level variables might be informative about these functions. Whatever their origins, stereotypes may be perpetuated by information-processing biases in attention/perception, encoding, and integration of information (2, 30). They become cultural phenomena, transmitted through media, hearsay, education, history, and jokes.

However, national character also has a much darker side. When stereotypes of national or ethnic groups are unfavorable, they can lead to prejudice, discrimination, or persecution, of which history and the world today are full of tragic examples. The classic analysis of stereotypes depicted them as the product of authoritarian (31) or prejudiced (32) personalities; more recent approaches have consid-

ered them as the result of general cognitive processes (2). Although social scientists have long been skeptical about the accuracy of national stereotypes, the present study offers the best evidence to date that in-group perceptions of national character may be informative about the culture, but they are not descriptive of the people themselves.

References and Notes

1. D. Peabody, *National Characteristics* (Cambridge Univ. Press, New York, 1985).
2. C. N. Macrae, C. Stangor, M. Hewstone, *Stereotypes and Stereotyping* (Guilford Press, New York, 1996).
3. Y. T. Lee, L. Jussim, C. McCauley, *Stereotype Accuracy: Toward Appreciating Group Differences* (American Psychological Association, Washington, DC, 1995).
4. S. Madon et al., *Pers. Soc. Psychol. Bull.* **27**, 996 (2001).
5. J. C. Brigham, *Psychol. Bull.* **76**, 15 (1971).
6. C. McCauley, C. L. Stitt, *J. Pers. Soc. Psychol.* **36**, 929 (1978).
7. C. M. Judd, B. Park, *Psychol. Rev.* **100**, 109 (1993).
8. J. M. Digan, *Annu. Rev. Psychol.* **41**, 417 (1990).
9. T. J. Bouchard, *Science* **264**, 1700 (1994).
10. R. R. McCrae et al., *J. Pers. Soc. Psychol.* **88**, 547 (2005).
11. P. T. Costa Jr., R. R. McCrae, *Revised NEO Personality Inventory (NEO-PI-R) and NEO Five-Factor Inventory (NEO-FFI) Professional Manual* (Psychological Assessment Resources, Odessa, FL, 1992).
12. R. R. McCrae, in *The Five-Factor Model of Personality Across Cultures*, R. R. McCrae, J. Allik, Eds. (Kluwer Academic/Plenum, New York, 2002), pp. 105–125.
13. J. Allik, R. R. McCrae, *J. Cross Cult. Psychol.* **35**, 13 (2004).
14. R. R. McCrae et al., *J. Pers. Soc. Psychol.*, in press.
15. J. E. Williams, D. E. Best, *Measuring Sex Stereotypes: A Thirty Nation Study* (Sage, Newbury Park, CA, 1982).
16. P. T. Costa Jr., A. Terracciano, R. R. McCrae, *J. Pers. Soc. Psychol.* **81**, 322 (2001).
17. C. L. Martin, *J. Pers. Soc. Psychol.* **52**, 489 (1987).
18. J. K. Swin, *J. Pers. Soc. Psychol.* **66**, 21 (1994).
19. R. R. McCrae, *J. Pers.* **69**, 819 (2001).
20. A. T. Church, M. S. Katigbak, in *The Five-Factor Model of Personality Across Cultures*, R. R. McCrae, J. Allik, Eds. (Kluwer Academic/Plenum Publishers, New York, 2002), pp. 129–154.
21. A. Terracciano, R. R. McCrae, in *113th Annual Convention of the American Psychological Association* (Washington, DC, 2005).
22. Materials and methods are available as supporting material on Science Online.
23. R. R. McCrae et al., *J. Res. Pers.* **38**, 179 (2004).
24. D. Griffin, R. Gonzalez, *Psychol. Bull.* **118**, 430 (1995).
25. By contrast, distinct cultures within countries showed different profiles. In the UK, the profiles of England and Northern Ireland showed no resemblance (ICC = -0.01). Similarly, in the PRC, the profiles of China and Hong Kong showed no resemblance (ICC = -0.25). There is some resemblance between Czech and Slovakian (ICC = 0.43, $P < 0.05$), and Serbian and Croatian (ICC = 0.43, $P < 0.05$) profiles; the separation of those nations is relatively recent.
26. Additionally, we compared NCS scores from the Philippines to ratings made by bicultural raters in an earlier study (20). Because Church and Katigbak used comparative judgments, we created new NCS scores by subtracting Filipino ratings of the typical American from Filipino ratings of the typical Filipino. The correlation of these 30 difference scores with the Church and Katigbak ratings was 0.76, $P < 0.001$.
27. Different standards of evaluation across cultures might have affected the results—that is, raters from some cultures may have been more generous or critical in their ratings than raters from other cultures, distorting the comparison across cultures. On the assumption that such biases would affect ratings both of one's own compatriots and of Americans, we calculated difference scores by

Table 1. Cultures scoring highest and lowest on five National Character Survey (NCS) factors, with observer-rated Revised NEO Personality Inventory (NEO-PI-R) factor mean *T* scores.

Highest NCS scores		Lowest NCS scores	
Culture	NEO-PI-R <i>T</i> score	Culture	NEO-PI-R <i>T</i> score
<i>Neuroticism</i>			
Indonesia	50.0	The Philippines	48.3
Nigeria	47.8	Canada	49.5
Turkey	51.4	New Zealand	47.9
Poland	50.7	Australia	48.6
Japan	50.7	Burkina Faso	53.1
<i>Extraversion</i>			
Puerto Rico	51.6	Slovenia	49.5
Australia	53.8	Indonesia	45.4
Spain	50.4	French Switzerland	51.0
New Zealand	52.4	Japan	49.4
Serbia	49.3	Estonia	52.1
<i>Openness</i>			
Russia	49.7	P. R. China	50.1
India	48.8	Estonia	46.8
Nigeria	49.1	Chile	51.8
Kuwait	47.6	Turkey	48.2
Puerto Rico	49.7	Japan	51.2
<i>Agreeableness</i>			
Burkina Faso	51.3	Czech Republic	54.2
India	51.7	Lebanon	46.4
Canada	49.9	United States	49.1
Botswana	48.0	Argentina	50.6
Russia	50.3	Hong Kong	46.9
<i>Conscientiousness</i>			
German Switzerland	53.5	Spain	51.3
Sweden	45.7*	Turkey	51.4
Germany	52.3	Croatia	50.3
Burkina Faso	49.7	Chile	52.2
Estonia	50.0	Indonesia	49.6
Median	50.0		49.6

*Observer rating data were unavailable for Sweden; self-report data are shown (12).

subtracting each judge's rating of the typical American from his or her rating of the typical compatriot for each NCS item. Assuming that cultures agree on the typical American, this procedure in effect subtracts the bias plus a constant and leaves a potentially better estimate of national character. We standardized the differences as *T* scores, using difference score normative values from the worldwide sample, excluding the United States. The difference scores were highly correlated with NCS scores ($r_s = 0.65$ to 0.91 , $P < 0.001$) and provided essentially the same results. ICCs between difference scores and NEO-PI-R observer ratings ranged from -0.44 for England to 0.48 for Lebanon (median, 0.03). ICCs between difference scores and NEO-PI-R self-reports ranged from -0.47 for Russia to 0.53 for Poland (median, 0.01). For the five factors, correlations with observer ratings across cultures ranged from 0.08 to 0.23 , and those with self-reports ranged from -0.37 to 0.23 . These results suggest that the lack of correspondence between NEO-PI-R and NCS profiles is not simply due to different standards of evaluation in different cultures. A different issue concerns the reference-group effect (28), according to which self-reports and observer ratings of individuals are implicitly made by reference to the distribution of scores in the rater's culture. Such an effect would tend to make aggregate personality scores uniform for all cultures, and the failure to find correlations with NCS factors

would be due to a lack of variation in aggregate NEO-PI-R means. However, NEO-PI-R means in fact vary systematically across cultures and show strong correlations across methods and with other culture-level variables (12, 14). Thus, the reference-group effect cannot explain the failure to find correlations with NCS scales.

28. S. J. Heine, D. R. Lehman, K. P. Peng, J. Greenholtz, *J. Pers. Soc. Psychol.* **82**, 903 (2002).

29. F. van de Vijver, K. Leung, *J. Pers.* **69**, 1007 (2001).

30. D. L. Hamilton, T. L. Rose, *J. Pers. Soc. Psychol.* **39**, 832 (1980).

31. T. W. Adorno, E. Frenkel-Brunswick, D. J. Levinson, R. N. Sanford, *The Authoritarian Personality* [Norton, New York, 1969 (original work published 1950)].

32. F. H. Allport, *The Nature of Prejudice* (Houghton Mifflin, New York, 1954).

33. R.R.M. receives royalties from the Revised NEO Personality Inventory. This research was supported in part by the Intramural Research Program of NIH, National Institute on Aging. Czech participation was supported by grant 406/01/1507 from the Grant Agency of the Czech Republic and is related to research plan AV 020250504 of the Institute of Psychology, Academy of Sciences of the Czech Republic. S.G.'s participation was supported by the Turkish Academy of Sciences. Burkinabè and French Swiss participation was supported by a grant from the Swiss National Science Foundation to J.R. The data collection in Hong Kong was supported by

Research Grants Council Direct Allocation Grants (DAG02/03.HSS14 and DAG03/04.HSS14) awarded to M.Y. Data collection in Malaysia was supported by Universiti Kebangsaan Malaysia Fundamental Research Grant 11JD/015/2003 awarded to K.A.M. Portions of these data were presented at the 113th Convention of the American Psychological Association, August 2005, Washington, DC. For helpful comments on the manuscript, we thank Y. H. Poortinga; for their assistance on this project we thank F. Abal, L. de Almeida, S. Baumann, H. Biggs, D. Bion, A. Butković, C. Y. Carrasquillo, H. W. Carvalho, S. Catty, C.-S. Chan, A. Curbelo, P. Duffill, L. Etcheverry, L. Firpo, J. Gonzalez, A. Gramberg, H. Harrow, H. Imuta, R. Ismail, R. Kamis, S. Kannan, N. Messoulam, F. Molina, M. Montarroyos Calegaro, S. Mosquera, J. C. Munene, V. Najzrova, C. Nathanson, D. Padilla, C. N. Scollon, S. B. Sigurdardottir, A. da Silva Bez, M. Takayama, T. W. Teasdale, L. N. Van Heugten, F. Vera, and J. Villamil.

Supporting Online Material

www.sciencemag.org/cgi/content/full/310/5745/96/DC1
Materials and Methods

References

Tables S1 and S2
Appendix S1

11 July 2005; accepted 31 August 2005
10.1126/science.1117199

Transoceanic Migration, Spatial Dynamics, and Population Linkages of White Sharks

Ramón Bonfil,^{1*} Michael Mejer,² Michael C. Scholl,³
Ryan Johnson,⁴ Shannon O'Brien,¹ Herman Oosthuizen,²
Stephan Swanson,² Deon Kotze,² Michael Paterson^{2,†}

The large-scale spatial dynamics and population structure of marine top predators are poorly known. We present electronic tag and photographic identification data showing a complex suite of behavioral patterns in white sharks. These include coastal return migrations and the fastest known transoceanic return migration among swimming fauna, which provide direct evidence of a link between widely separated populations in South Africa and Australia. Transoceanic return migration involved a return to the original capture location, dives to depths of 980 meters, and the tolerance of water temperatures as low as 3.4°C. These findings contradict previous ideas that female white sharks do not make transoceanic migrations, and they suggest natal homing behavior.

Great white sharks (*Carcharodon carcharias*) occupy the apex of most marine food webs in which they occur. Their major centers of abundance are in the coastal waters of California–

Baja California, Australia–New Zealand, South Africa, and, formerly, the Mediterranean Sea (1–3). Management and conservation of this threatened species (4, 5) have been limited, partly because its space utilization and migrations and the linkages between populations were poorly understood and difficult to research until the development of sophisticated telemetry instruments and high-resolution genetic markers for the species (6–9). Long believed to primarily be shelf inhabitants, white sharks are now known to be more pelagic and to travel from California to Hawaii (6). Males are assumed to move between distant populations, whereas females have been assumed to be nonroving and philopatric (9).

We tagged white sharks off the Western Cape of South Africa between June 2002 and

November 2003 with pop-up archival satellite-transmitting (PAT) tags ($n = 25$), near-real-time satellite tags (from here onward, “satellite tags”) ($n = 7$), and acoustic tags ($n = 25$) in order to study their spatial dynamics (table S1). Using high-resolution photographic identification techniques, we have recorded the daily presence or absence of individual white sharks off Gansbaai (34°39'S, 019°24'E; Western Cape) since October 1997 (10).

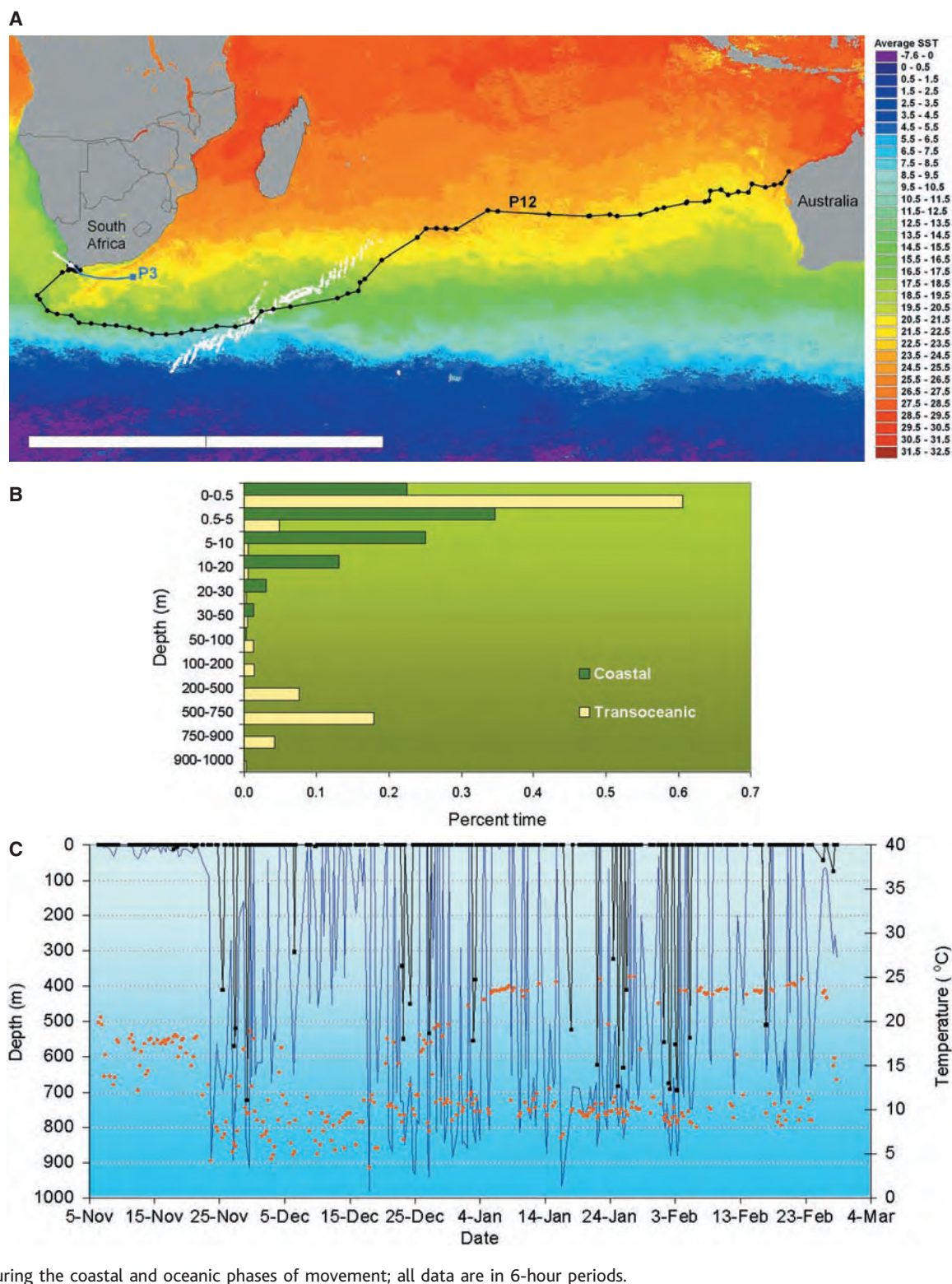
Electronic tagging and photographic identification records reveal complex spatial dynamics in white sharks, which we categorized into four behavioral patterns: rapid transoceanic return migrations, frequent long-distance coastal return migrations, smaller-scale patrolling, and site fidelity. A white shark performed a previously unknown fast transoceanic return migration spanning the entire Indian Ocean, swimming coast-to-coast from South Africa to Australia and back. This ~380-cm total length (TL; measured as a straight line from the tip of the snout to the end of the upper caudal lobe) female shark (number P12), PAT-tagged on 7 November 2003 off Gansbaai, traveled in 99 days to a location 2 km from shore and 37 km south of the Exmouth Gulf in Western Australia (22°01'05"S, 113°53'13"E; Fig. 1A). This shark's course of ~11,100 km (11) entailed a counterclockwise displacement of more than 750 km off the southern tip of Africa, followed by a remarkably direct path toward northwestern Australia, indicating that white sharks do not need oceanic islands as gateways for transoceanic migrations, as previously hypothesized (12). Shark P12 traveled at a minimum speed of 4.7 km hour⁻¹ during its migration to Australia (13), which is the fastest sustained long-distance speed known among sharks (14–17) and comparable to

¹Wildlife Conservation Society, 2300 Southern Boulevard, Bronx, NY, 10460, USA. ²Marine and Coastal Management Branch, Department of Environmental Affairs and Tourism, Private Bag X2, Roggebaai 8012, Cape Town, Western Cape, South Africa. ³White Shark Trust, Post Office Box 1258, Strand Street 6, Gansbaai 7220, Western Cape, South Africa; and Department of Zoology, University of Cape Town, Rondebosch 7700, Western Cape, South Africa. ⁴Department of Zoology and Entomology, University of Pretoria, Pretoria 0002, South Africa.

*To whom correspondence should be addressed. E-mail: rbonfil@wcs.org

†Present address: Sea Technology Services, Ground Floor, Foretrust House, Martin Hammerschlag Way, Cape Town, Western Cape, South Africa.

Fig. 1. Transoceanic migration of a white shark from South Africa to northwestern Australia and possible first leg of a second transoceanic-migrating shark. **(A)** Positions of (dots) and track followed by (black line) shark P12 during coastal and transoceanic movement; geolocation-estimated positions were corrected using SST data to derive positions shown (11). The first leg of another possible transoceanic migration to Australia (or an offshore movement toward the northeast coast of South Africa) is shown by the pop-up location of the PAT tag from shark P3 (blue line and square). Tagging and pop-up dates were as follows: for P12, 7 November 2003 and 28 February 2004; for P3, 14 April 2003 and 25 December 2003. SST is an average composite at 4 km resolution for daily Moderate Resolution Imaging Spectroradiometer data from 23 November 2003 to 28 February 2004. Southwest Indian Ridge shown as white depth contours (100 to 2000 m). The scale bar represents 5000 km; the white arrow marks the tag deployment location. **(B)** Differential time-at-depth patterns during the coastal and oceanic legs of shark P12's trip, showing a bimodal pattern with a strong preference for the depths of 0.0 to 0.5 m and 500 to 750 m during transoceanic travel. **(C)** Minimum (black line and squares) and maximum (bright blue line) depths and minimum temperature (orange dots) visited during the coastal and oceanic phases of movement; all data are in 6-hour periods.

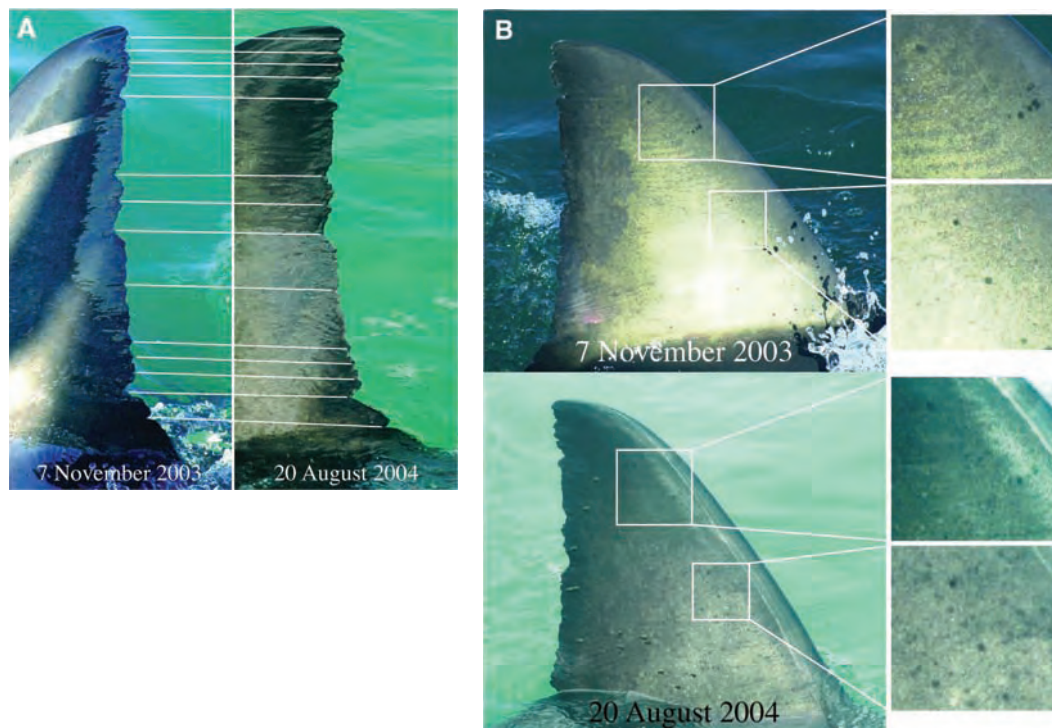


that of some of the fastest-swimming tunas (18, 19). Records obtained through photographic identification revealed the return of P12 from Australia back to its original tagging site on 20 August 2004 (Fig. 2 and fig. S1), evidencing site fidelity and an outstanding navigational ability. Shark P12 performed the fastest transoceanic return migration recorded

among marine fauna (14, 20), taking just under 9 months to complete a circuit of more than 20,000 km. Logged records from the photographic identification study show that P12 is a seasonal visitor (from June to December) to the Gansbaai area (table S2). It has been recorded during 38 different days spanning 1999–2004, suggesting that it is a

South African shark and that its transoceanic return migration could be common. A second PAT-tagged shark (unsexed, ~200- to 230-cm TL; number P3) traveled to an offshore location 242 km SE of Port Elizabeth, where its tag detached on 26 December 2003, in what might have been the first leg of a migration toward Australia (Fig. 1A).

Fig. 2. Photographic identification records of shark P12 at tagging (7 November 2003) and upon return to the tagging location at Gansbaai (20 August 2004) after its transoceanic migration to Western Australia. (A) Trailing edge of the first dorsal fin, showing a unique notch pattern allowing identification; the white lines connect corresponding notches in both photographs. (B) Right side of the first dorsal fin, with magnified details (left insets) showing a unique black pigmentation pattern aiding identification.



Transoceanic return migration is previously unknown in white sharks and only suspected in other chondrichthyans. Our results provide direct evidence of a physical link between two of the most important and widely separated white shark populations, and they confirm philopatry in white sharks. They also prove that female white sharks are capable of transoceanic migrations and indicate that the sex-biased dispersal of this species (9) is not necessarily based on differences in the proclivity of either sex to undertake transoceanic migrations, but is probably attributable to differences in how these migrants become reproductively integrated into the “recipient” population. In light of our data, the transmission of nuclear, and not mitochondrial, genetic material between South Africa and Australia (9) could be explained if (i) both sexes make transoceanic migrations, but only males reproduce in the recipient population, and/or (ii) females make transoceanic migrations and mate with males from the recipient population, only to return to their original location to give birth. Indeed, the migration of P12 from South Africa to Australia corresponds to what is thought to be the mating season in this region (21). An eventual return of this shark to give birth in South Africa would prove natal homing in white sharks, as has been suggested for other shark species (22, 23), and would support recent theories about the similarity of reproductive strategies among a wide range of marine taxa (24).

The mechanisms used by P12 to navigate to Australia and back remain unknown; aside from a few shallow seamounts on the South-

west Indian and Ninety East Ridges, there are no other topographic features that could be used for orientation on the route it followed (Fig. 1A). We analyzed the satellite-transmitted summary data to reveal the diving pattern of P12 and found that during eastward transoceanic migration, it made frequent deep dives, reaching record maximum depths (980 m) (25), experienced record ambient temperatures of 3.4°C, and spent 18% of the time at depths of 500 to 750 m (Fig. 1, B and C). This shark spent considerably more time (61%) just below the surface (0.0 to 0.5 m) while in oceanic waters than when in coastal waters (23%), swimming most of the time (66%) above 5 m during this trip. A strong preference for surface swimming during oceanic travel is a behavioral pattern previously unreported in white sharks (1, 2, 6, 26). We speculate that, like many other vertebrates (14), white sharks could be using visual stimuli such as celestial cues as an important navigational mechanism in addition to, or instead of, following gradients in Earth’s magnetic field as is commonly accepted behavior for sharks (27).

Great white sharks undertake long-distance return migrations along the South African coast with relative frequency, as revealed by the tracking of satellite tags and by PAT tag pop-up locations (Fig. 3 and fig. S2). They travel from high-abundance sites in the Western Cape (28, 29) to waters as far as >2000 km away off kwaZulu-Natal and beyond, using underwater routes along the continental shelf, then return to their original tagging sites off the Western Cape after 4 to 6 months. A 284-cm TL female (S1) was fitted with a satellite tag in Mossel

Bay (34°08’S, 22°07’E) on 24 May 2003 and completed the first tracked long-distance return migration for a chondrichthyan, moving in 65 days to waters northeast of Delagoa Bay (Mozambique) and outside the South African Economic Exclusive Zone, where white sharks are legally protected (Fig. 3). S1 returned to Mossel Bay 162 days after being tagged, and was photographed with its transmitter still attached. Shark S2, a 310-cm TL female double-tagged with satellite and acoustic tags in Mossel Bay on 31 May 2003, was tracked for 46 days to the Tugela Bank, then recorded by our acoustic-tag bottom monitors back in Mossel Bay 123 days after being tagged (Fig. 3). In total, 25% of tagged sharks that yielded information moved from the Western Cape to kwaZulu-Natal and beyond, and 12.5% showed return migrations (Fig. 3 and fig. S2). The high proportion of immature white sharks (table S1, Fig. 3, and fig. S2) moving to the rich environment of the Tugela Bank (30, 31) suggests that these long-distance coastal return migrations might be feeding-related events.

Records obtained from satellite and PAT tags reflect additional spatial dynamics patterns in white sharks, including smaller-scale patrolling behavior and site fidelity (Fig. 3 and figs. S3 and S4). These patterns and the return migrations described above suggest a wider and more complex range of behavioral patterns in white sharks than was previously thought to exist. The discovery of a trans-Indian Ocean return-migrating white shark after a relatively low tagging effort, in addition to its periodic absence from Gansbaai as evidenced through photographic records, implies that the Australian and South African pop-



Fig. 3. Northeastward long-distance return migrations of South African white sharks. The figure shows the tracks of two satellite-tagged sharks showing long-distance return migrations and crossing to Mozambique. Shark S1 (black trace) left Mossel Bay after tagging (24 May 2004); moved rapidly to Bird Island, residing within a limited area (385 km²) for 27 days; and continued northeast along the shelf edge, then in oceanic waters beyond the Agulhas Current, reaching Mozambique 65 days after tagging. Transmissions ceased 11 days later, to resume on Bird Island 62 days later, then at the original tagging location on 2 November 2003. Shark S2 (white trace), tagged on 31 May 2003 with satellite and acoustic tags, traveled steadily along the coast to the Tugela Bank in 37 days, where it ceased transmitting 9 days later and was recorded by acoustic bottom receivers back in Mossel Bay on 1 October 2004. The red star indicates the tagging location; the dashed line indicates projected movement during long periods without transmissions.

ulations maintain a physical link within a single generation and that this return migration might be more common than is presently known.

Our studies show that we do not have a full understanding of the ways in which identified populations are connected. The movement of a female to a region of Australia known for the presence of Australian white sharks and its return to South Africa, in conjunction with previous genetic studies, implies that earlier hypotheses about sex-biased dispersal might need to be modified. Males are currently considered to be the ones who move between populations (9), but our data suggest that the connectivity between populations could be facilitated also or exclusively by females. The return of females mating in Australia to give birth in South Africa would be consistent with genetic analyses; the finding of a rare male of South African “origin” in Australia (9) might reflect equally rare birthing in Australia by South African females.

The discoveries presented here and our lack of evidence of sex- or size-related patterns of space utilization in white sharks underscore the need for additional research. Multidisciplinary studies integrating population genetic analyses and electronic tagging, as well as the development of improved monitoring instruments, should be encouraged.

Long-distance and transoceanic migrations expose great whites to increased risk of mortality as they leave domestically protected waters in South Africa/Australia and travel into neighboring or remote countries, sometimes located across entire ocean basins. An increasing global demand for shark products (32), coupled with our findings, suggests that global protective measures, such as the recent listing of the white shark in CITES Appendix 2 (CITES, Convention on International Trade in Endangered Species of Wild Fauna and Flora), are warranted to ensure the effectiveness of local protective legislation currently in place in a handful of countries.

References and Notes

1. A. P. Klimley, D. G. Ainley, Eds., *Great White Sharks: The Biology of *Carcharodon carcharias** (Academic Press, San Diego, CA, 1996).
2. L. J. V. Compagno, *Sharks of the World. An Annotated and Illustrated Catalogue of Shark Species Known to Date. Vol. 2. Bullhead, Mackerel and Carpet Sharks (Heterodontiformes, Lamniformes and Orectolobiformes)*. FAO Species Catalogue for Fishery Purposes No. 1 (Food and Agriculture Organization of the United Nations, Rome, 2001).
3. A. Soldo, I. Jardas, *Periodicum Biologorum* **104**, 195 (2002).
4. L. J. V. Compagno, M. A. Marks, I. K. Fergusson, *Environ. Biol. Fish* **50**, 61 (1997).
5. C. Hilton-Taylor, Compiler, *2002 IUCN Red List of Threatened Species* (IUCN, Gland, Switzerland, 2000).

6. A. M. Boustany *et al.*, *Nature* **415**, 35 (2002).
7. B. A. Block, H. Dewar, C. Farwell, E. D. Prince, *Proc. Natl. Acad. Sci. U.S.A.* **95**, 9384 (1998).
8. R. L. Johnson *et al.*, paper presented at the meeting on Conservation Research of Great White Sharks, New York, 20 to 22 January 2004 (Wildlife Conservation Society, New York, 2004).
9. A. T. Pardini *et al.*, *Nature* **412**, 139 (2001).
10. Materials and methods are available as supporting material on Science Online.
11. The positions estimated from archived light-level data using geolocation algorithms provided by the manufacturer of the tags were corrected using satellite sea surface temperature (SST) data with the method described in the supporting online material.
12. G. Cliff, L. J. V. Compagno, M. J. Smale, R. P. Van Der Elst, S. P. Wintner, *S. Afr. J. Sci.* **96**, 365 (2000).
13. The widely accepted definition of migration is “the act of moving from one spatial unit to another” (14). This definition is general enough to be applicable to all animal taxa, independently of spatiotemporal scales, and includes at its core individual migration.
14. R. R. Baker, *Migration: Paths Through Time and Space* (Hodder and Stoughton, London, 1982).
15. S. A. Eckert, B. S. Stewart, *Environ. Biol. Fish* **60**, 299 (2001).
16. N. E. Kohler, P. A. Turner, *Environ. Biol. Fish.* **60**, 191 (2001).
17. I. G. Priede, *Fish. Res.* **2**, 201 (1984).
18. B. A. Block *et al.*, *Science* **293**, 1310 (2001).
19. T. Itoh, S. Tsuji, A. Nitta, *Fish. Bull. (Wash. D.C.)* **101**, 514 (2003).
20. D. Inagake *et al.*, *Bull. Nat. Res. Inst. Far Seas Fish* **38**, 53 (2001).
21. M. P. Francis, in (1), pp. 157–172.
22. R. E. Hueter, M. R. Huepel, E. J. Heist, D. B. Keeney, *J. Northw. Atl. Fish. Sci.* **35**, 239 (2005).
23. K. A. Feldheim, S. H. Gruber, M. V. Ashley, *Proc. R. Soc. London Ser. B* **269**, 1655 (2002).
24. P. Cury, *Can. J. Fish. Aquat. Sci.* **51**, 1664 (1994).
25. Previous reports of record diving depths of 1280 m for white sharks (2) are based on the capture of one specimen in a longline set at that depth; however, to our knowledge, there is no evidence that the shark was caught at 1280 m as opposed to anywhere else along the water column.
26. F. G. Carey *et al.*, *Copeia* **2**, 254 (1982).
27. T. P. Quinn, *Trends Ecol. Evol.* **9**, 277 (1994).
28. L. J. V. Compagno, D. A. Ebert, M. J. Smale, *Guide to the Sharks and Rays of Southern Africa* (Struik, Cape Town, South Africa, 1989).
29. R. L. Johnson, thesis, University of Pretoria, South Africa (2003).
30. S. T. Fennessy, *S. Afr. J. Mar. Sci.* **14**, 263 (1994).
31. S. T. Fennessy, *S. Afr. J. Mar. Sci.* **14**, 287 (1994).
32. S. C. Clarke, thesis, University of London, UK (2003).
33. We thank the Natal Sharks Board and particularly S. Dudley, G. Cliff, K. Cox, and W. Harrison for valuable fieldwork assistance and helpful discussions in the satellite tag study and S. Dudley for assistance in the design and supervision of the acoustic tag study; B. Mangold, C. Masterton, S. Parsons, P. Koen, D. Woodborne, and P. Fréon for the health maintenance of sharks; R. and J. Portway, L. Staveres, D. Reynolds, T. Keswick, and M. Rutzen for support and assistance with fieldwork; L. Drapeau for Geographic Information Systems assistance; Smit Marine for maintaining bottom receivers; M. N. Bester for supervision and D. Sadie for conception of the acoustic tag study; and the Roe Foundation, Wildlife Conservation Society, the South African Government, International Fund for Animal Welfare, World Wide Fund for Nature, and Professional Association of Diving Instructors—Aware for financial support.

Supporting Online Material

www.sciencemag.org/cgi/content/full/310/5745/100/DC1

Materials and Methods
SOM Text
Figs. S1 to Fig. S4
Tables S1 and S2
References

16 May 2005; accepted 21 July 2005
10.1126/science.1114898

Satellite Tagging and Cardiac Physiology Reveal Niche Expansion in Salmon Sharks

Kevin C. Weng,¹ Pedro C. Castilho,¹ Jeffery M. Morrisette,¹
Ana M. Landeira-Fernandez,^{1*} David B. Holts,² Robert J. Schallert,³
Kenneth J. Goldman,⁴ Barbara A. Block^{1†}

Shark populations are declining globally, yet the movements and habitats of most species are unknown. We used a satellite tag attached to the dorsal fin to track salmon sharks (*Lamna ditropis*) for up to 3.2 years. Here we show that salmon sharks have a subarctic-to-subtropical niche, ranging from 2° to 24°C, and they spend winter periods in waters as cold as 2° to 8°C. Functional assays and protein gels reveal that the expression of excitation-contraction coupling proteins is enhanced in salmon shark hearts, which may underlie the shark's ability to maintain heart function at cold temperatures and their niche expansion into subarctic seas.

Many sharks are threatened by fishing around the world (1), and biological knowledge is urgently needed to design management strategies. Sharks have been tracked using short-term acoustic telemetry (2) and towed satellite tags, which are attached to large, slow-moving basking and whale sharks (3, 4). Pop-up satellite archival tags (PATs) have also been used to track sharks (5, 6); however, geolocations have root mean square errors of 0.89° of longitude and 1.47° of latitude (7). In this study, we used a Smart Position Only Tag (SPOT), designed with a small Argos transmitter, that permits direct attachment to the shark's dorsal fin (Fig. 1). This tag enables the tracking of sharks with near-real-time positions for multiple years (table S1). SPOT tags greatly improve geopositioning for sharks. After applying a filter, 59% of our salmon shark positions having errors under 1 km, based on Argos accuracies (Fig. 1 and table S2).

The movements and behaviors of 48 salmon sharks (total length = 233 ± 9 cm, mean ± SD) were recorded by tagging sharks in Prince William Sound (PWS), Alaska, with two types of electronic tags. SPOT tags ($n = 38$ sharks) uplinked to Argos satellites provided track lengths of 351 ± 38 days (mean ± SE) and 8715 ± 747 km (13,335 total days) (Fig. 1 and fig. S1). The longest distance traveled by an individual was 18,220 km over 640 days (shark 37380). By double tagging some sharks with SPOT and PAT tags ($n = 21$)

and by tagging some individuals ($n = 10$) with PAT tags alone, we obtained 5048 days of behavioral and environmental data (mean length 163 ± 14 days). Archival records were obtained from three sharks recaptured after

tagging in the vicinity of their release location (table S1). The sharks provided 187,680 measurements of ocean pressure and temperature from the surface to a depth of 832 m, demonstrating their value as platforms for oceanographic observations (Fig. 2).

Salmon sharks undergo a striking seasonal migration from subarctic to temperate and subtropical regions, presumably to forage or give birth to their young (Fig. 1 and fig. S1) (8). During summer and autumn, the majority of tagged salmon sharks (all females) were foraging in PWS and the Gulf of Alaska (GOA). In winter, some sharks embarked on their migration to the subtropics, whereas others remained in GOA waters (overwintering). In spring, the migrating sharks' habitat extended as far south as Hawaii (22°N), a new location record for the archipelago (9), and from 170°W to the North American continental shelf, covering oligotrophic waters in the subtropical gyre (fig. S2) as well as the productive waters of the California Current.

Salmon sharks have a broad thermal niche, and their subarctic winter habitat demonstrates

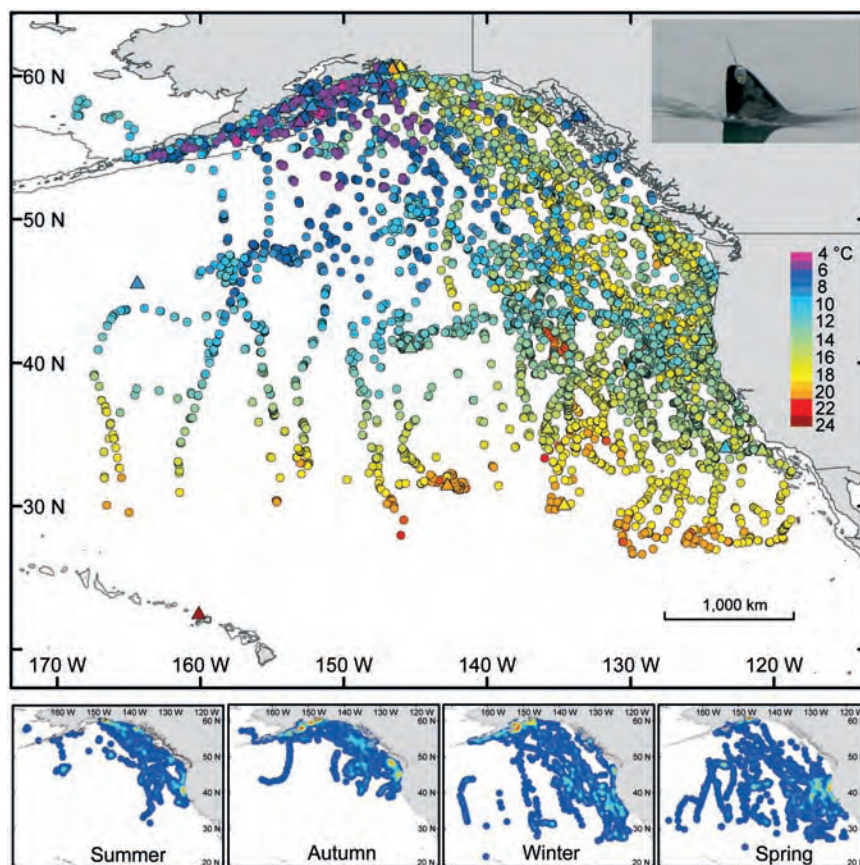


Fig. 1. Movements of salmon sharks in the eastern North Pacific. (Top) Salmon sharks occupy a broad region of the eastern North Pacific. Animals were tagged in Alaskan waters in July 2002, August 2003, and July 2004. Circles indicate SPOT positions and triangles indicate PAT satellite endpoint positions. (Inset) Photo of a salmon shark with a SPOT3 tag on the dorsal fin. (Bottom) Kernel density plots reveal extensive seasonal migrations. Salmon sharks used habitats in PWS and GOA most heavily in the summer and autumn, with some individuals overwintering in Alaskan waters. Sharks expanded their range southward in the winter and spring, encompassing a wide range of habitats from Hawaii to the North American coast.

¹Tuna Research and Conservation Center, Stanford University, Hopkins Marine Station, 120 Oceanview Boulevard, Pacific Grove, CA 93950, USA. ²National Marine Fisheries Service, 8604 La Jolla Shores Drive, La Jolla, CA 92037, USA. ³Monterey Bay Aquarium, 886 Cannery Row, Monterey, CA 93940, USA. ⁴Alaska Department of Fish and Game, 3298 Douglas Place, Homer, AK 99603, USA.

*Present address: Instituto de Bioquímica Médica, Rio de Janeiro, Brazil.

†To whom correspondence should be addressed. E-mail: bblock@stanford.edu

their tolerance of cold waters (Fig. 2). They inhabited waters from 2° to 24°C, spending much of their time (68 ± 6%) in waters cooler

than 10°C and 72 ± 3% of their time in waters shallower than 50 m (Fig. 3). The sharks ($n = 26$) often remained in subarctic waters during

winter, where they occupied depths from 0 to 368 m in an unstratified water column (Fig. 2A) with ambient temperatures of 2° to 8°C. PAT tags ($n = 13$) showed occupancy of these waters for mean durations of 53 ± 7 days and up to 96 days (690 total days), with $98 \pm 1\%$ of the time in water shallower than 150 m. Periods of submergence occurred, sometimes associated with temperature inversions, causing gaps in SPOT records (Fig. 2B). Salmon sharks are known to eat salmon (10) and herring (11). Whereas salmon are abundant in PWS during the summer and autumn, herring live there all year (12) and may be a prey species for sharks that overwinter. These data reveal that salmon sharks are major apex predators in Alaskan waters in all seasons, and this information could improve ecosystem models of PWS (13).

Upon migrating to the subtropical gyre, salmon sharks ($n = 19$) encountered warmer waters (18° to 24°C) with increased thermal stratification (Figs. 1 and 2). PAT data ($n = 4$, averaging 43 ± 9 days) indicate distinct bimodal diving behaviors, with one occupancy peak in the upper thermocline (100 to 200 m) at temperatures from 18° to 20°C and another below the thermocline (300 to 500 m) in 6° to 8°C waters. In these warm waters, salmon sharks remained submerged for long durations, possibly because of a physiological limitation, causing considerable gaps in SPOT records. Sharks that moved into the eastern Pacific along the continental shelf ($n = 12$) occupied water with temperatures of 7° to 18°C and foraged from the surface to 356 m.

For comparison, we tagged blue sharks ($n = 27$; total length 197 ± 23 cm, mean ± SD) in the eastern North Pacific (figs. S3 and S4 and table S3), producing track lengths averaging 114 ± 14 days (2970 total days). Blue sharks in the eastern North Pacific inhabit pelagic and neritic waters from 104° to 157°W and 4° to 37°N. Blue sharks carrying PAT tags ($n = 15$) spent $74 \pm 6\%$ of their time in waters of 14° to 27°C, with $67 \pm 5\%$ of their time above 50 m in the upper mixed layer. They encountered sub-10°C temperatures only on brief dives beneath the thermocline, which made up 6 ± 2% of their records (Fig. 3E). Over the range tracked, the occupancy of waters cooler than 10°C was significantly greater for salmon sharks than for blue sharks (Mann-Whitney test, $W = 30.5$, $P = 0.001$).

The distribution of salmon sharks and their prolonged occupation of subarctic waters indicate a capacity to sustain cardiac performance at cold temperatures. Salmon sharks are members of the family Lamnidae, renowned for their endothermic physiology (14). High metabolic rates combined with extensive counter-current heat exchangers (14) enable this species to maintain body temperatures up to 21.2°C above water temperature (15). As in all endothermic fishes, the oxygen demands of warm metabolically active tissues are supplied by a heart

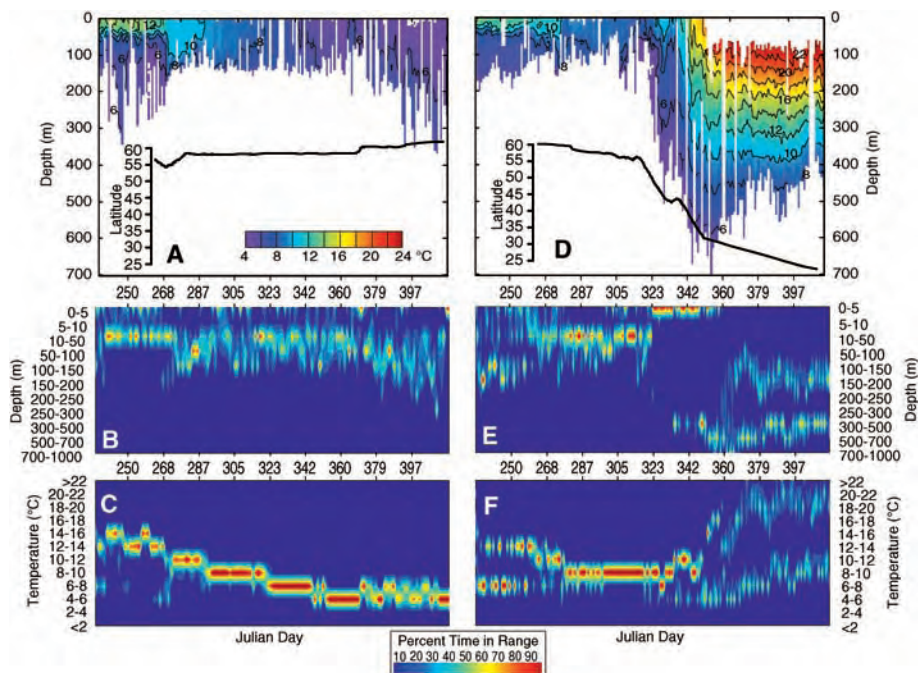


Fig. 2. Subarctic and subtropical depth and temperature preferences of salmon sharks. (A) Depth and temperature profiles of the water column along the track of a shark (41670) that overwintered in the GOA. The stratified summer water column cooled, and the thermocline dissipated in the autumn. Black lines show latitude. (B and C) Contour plots made from discrete measurements from PAT tags of (B) time-at-depth and (C) time-at-temperature show a preference for the shallow mixed layer through November, followed by deeper diving when an inversion developed in December and mixed layer waters cooled to 5° to 6°C. (D) The thermal profile slice along the track of a shark (41675) moving from Alaska to the subtropics shows an increase in temperature and strong thermal stratification. (E) Depth and (F) temperature preferences of the shark show a bimodal pattern in the warm subtropical gyre.

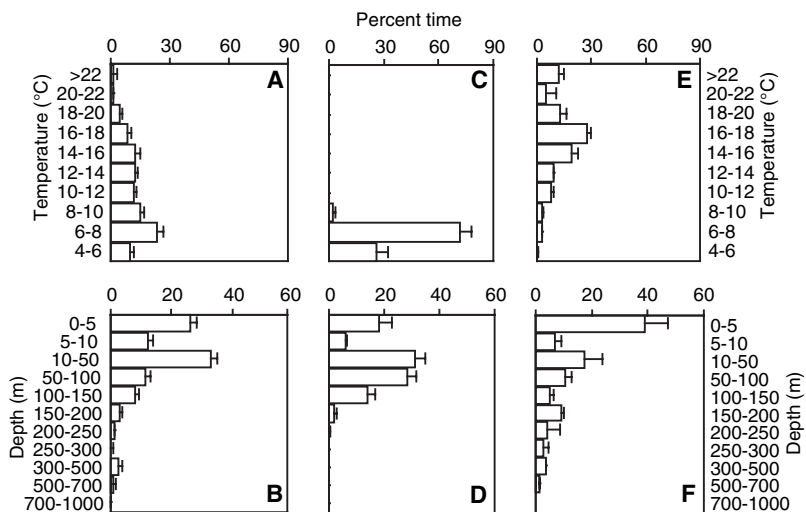


Fig. 3. Thermal and depth habitats of salmon sharks and blue sharks. (A) Thermal habitat for 22 PAT-tagged salmon sharks shows a broad thermal niche of 4°C to 24°C. Some sharks experienced temperatures that ranged as low as 2° to 4°C. (B) Salmon sharks spent $72 \pm 3\%$ of their time in the top 50 m. (C) PAT-tagged salmon sharks remaining in northern waters after the dissipation of the thermocline ($n = 13$) occupied 4° to 8°C waters and (D) occupied depth habitat predominantly shallower than 150 m. (E) Blue sharks ($n = 15$) preferred a warmer thermal environment, spending $44 \pm 7\%$ of their time in temperatures of 14° to 18°C, and had (F) depth preferences with greater time near the surface than salmon sharks. Error bars indicate SE.

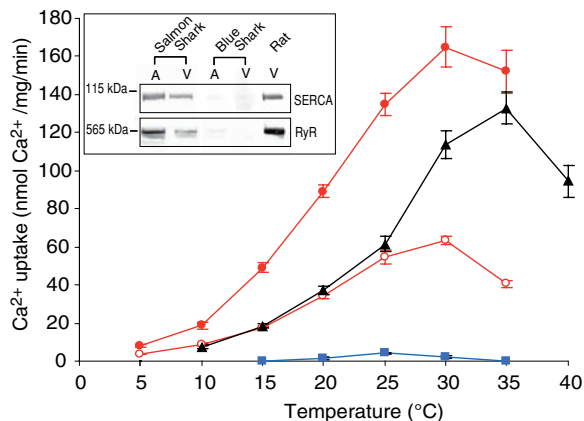


Fig. 4. Rate of SR Ca²⁺ uptake in salmon shark heart. Temperature dependence of Ca²⁺ uptake catalyzed by SERCA2 in microsomes from salmon shark atrium (red solid circles), salmon shark ventricle (red open circles), rat ventricle (black triangles), and blue shark atrium (blue squares). Values represent mean ± SE of experiments performed with preparations from at least four individuals. Absence of the appearance of error bars indicates that the error bars are smaller than symbol. (Inset) Immunoblot analysis of atrial (A) and ventricular (V) microsomes using a SERCA2-specific or RyR-specific polyclonal antibody.

operating at ambient temperature (16). We hypothesize that, similar to the *Thunnus* lineage (17), an increased expression of the proteins required for excitation-contraction coupling in the heart may underlie the ability to maintain cardiac contractility in the cold. This physiological trait may be a key specialization enabling thermal and geographic niche expansion into productive subarctic seas.

We measured the activity and expression of SERCA2, the sarcoplasmic reticulum (SR) Ca²⁺ adenosine triphosphatase (ATPase), which is a protein important for the maintenance of intracellular Ca²⁺ stores vital for beat-to-beat contractions. Salmon shark atrial SR vesicles have a high Ca²⁺ uptake rate, which is an order of magnitude greater than the rate for blue sharks (Fig. 4). SERCA2-dependent Ca²⁺ uptake could be measured at temperatures as cold as 5°C in salmon shark atrial and ventricular SR. The increase in the rate of Ca²⁺ uptake in the atrial tissues for each 10°C increase in temperature (*Q*₁₀ values, 15° to 25°C) were 2.6 ± 0.4 (mean ± SE) and 4.8 ± 0.02 for salmon shark and blue shark, respectively. Ca²⁺ uptake was negligible in blue shark ventricular SR, so for comparison, we measured Ca²⁺ uptake rates in rat ventricular SR. At temperatures below 25°C, the activity of the SERCA2 enzyme in salmon shark ventricle microsomes was equivalent to that of rat ventricle vesicle preparations. Activity in the salmon shark vesicles dropped below that of the rat vesicles above 25°C. *Q*₁₀ values (15° to 25°C) of ~3.3 for Ca²⁺ uptake in ventricular tissues were similar in salmon shark and rat.

Analysis of SR protein content showed high expression of SERCA2 and SR Ca²⁺ release channel (RyR2) proteins in salmon shark cardiac tissues (Fig. 4, inset) and in other sharks of the family Lamnidae (fig. S5). Densitometry indicated a 1.29 ± 0.72-fold greater SERCA2 expression in rat ventricle compared with salmon shark ventricle. The cold tolerance of salmon sharks may be directly related to this increased expression of SERCA2 and RyR2, which are crucial for maintaining rhythmic contractions of myocytes, cardiac output, and oxy-

genation of endothermic tissues. Enhanced SR Ca²⁺ uptake and increased expression of SERCA2 has been shown to be a cardioprotective mechanism in hibernating mammals that are also resistant to cardiac dysfunction at cold temperatures (18).

Direct satellite telemetry from the dorsal fins of sharks reveals subarctic-to-subtropical migrations of salmon sharks over multiple years. The species' cardiac specializations and endothermy underlie its remarkable capacity to occupy a subarctic niche. Satellite tracking technologies can be used to rapidly map shark habitats worldwide, an objective that is critical to their future protection.

References and Notes

1. J. Stevens, R. Bonfil, N. Dulvy, P. Walker, *ICES J. Mar. Sci.* **57**, 476 (2000).
2. F. G. Carey *et al.*, *Copeia* **1982**, 254 (1982).
3. S. A. Eckert, B. S. Stewart, *Environ. Biol. Fishes* **60**, 299 (2001).
4. I. G. Priede, *Fish. Res.* **2**, 201 (1984).
5. A. M. Boustany *et al.*, *Nature* **415**, 35 (2002).

6. D. W. Sims, E. J. Southall, A. J. Richardson, P. C. Reid, J. D. Metcalfe, *Mar. Ecol. Prog. Ser.* **248**, 187 (2003).
7. S. L. H. Teo *et al.*, *Mar. Ecol. Prog. Ser.* **283**, 81 (2004).
8. K. J. Goldman, J. A. Musick, *Fish. Bull.*, in press.
9. J. Randall, D. Greenfield, personal communication.
10. K. Nagasawa, *N. Pac. Anadrom. Fish Comm. Bull.* **1998**, 419 (1998).
11. B. Paust, R. Smith, *Salmon Shark Manual AK-SG-86-01* (Alaska Sea Grant College Program, Fairbanks, AK, 1986).
12. B. L. Norcross *et al.*, *Fish. Oceanogr.* **10**, 42 (2001).
13. L. Hulbert, in *Trophic Mass-Balance Model of Alaska's Prince William Sound Ecosystem for the Post-Spill Period 1994-1996*. T. A. Okey, D. Pauly, Eds. (Fisheries Centre, Univ. of British Columbia, Vancouver, ed. 2, 1999), pp. 42-45.
14. F. G. Carey, J. M. Teal, J. W. Kanwisher, *Physiol. Zool.* **54**, 334 (1981).
15. K. Goldman, S. Anderson, R. Latour, J. Musick, *Environ. Biol. Fishes* **71**, 403 (2004).
16. R. W. Brill, P. G. Bushnell, in *Tunas: Physiology, Ecology and Evolution*, B. Block, E. Stevens, Eds. (Academic Press, San Diego, 2001), pp. 79-120.
17. J. Blank *et al.*, *J. Exp. Biol.* **207**, 881 (2004).
18. A. Yatoni *et al.*, *Am. J. Physiol. Heart Circ. Physiol.* **286**, H2219 (2004).
19. This research is part of the Tagging of Pacific Pelagics program in the Census of Marine Life. Funding is from the Office of Naval Research, NSF IBN 0215272, the Alfred P. Sloan Foundation, and the Moore and Packard Foundation grants to B.B. P.C.C. is a postdoctoral fellow of the Conselho Nacional de Desenvolvimento Científico e Tecnológico (CNPq). We thank J. Ganong, D. Foley, and L. DeWitt for superb technical assistance and T. Murayama and Y. Ogawa for the use of their RyR antibody. Captain D. Branshaw of the Alaska Department of Fish and Game guided the field operations. We are indebted to D. Costa, G. Shillinger, C. Perle, J. Musick, S. Kohin, S. Teo, D. Kohrs, H. Dewar, A. Boustany, A. Walli, L. Hulbert, G. Strout, and M. Castleton.

Supporting Online Material

www.sciencemag.org/cgi/content/full/310/5745/104/DC1

Materials and Methods
Figs. S1 to S5
Tables S1 to S3
References

9 May 2005; accepted 4 August 2005
10.1126/science.1114616

EGFR Activation Mediates Inhibition of Axon Regeneration by Myelin and Chondroitin Sulfate Proteoglycans

Vuk Koprivica,¹ Kin-Sang Cho,² Jong Bae Park,¹ Glenn Yiu,¹ Jasvinder Atwal,³ Bryan Gore,³ Jieun A. Kim,¹ Estelle Lin,¹ Marc Tessier-Lavigne,³ Dong Feng Chen,² Zhigang He^{1*}

Inhibitory molecules associated with myelin and the glial scar limit axon regeneration in the adult central nervous system (CNS), but the underlying signaling mechanisms of regeneration inhibition are not fully understood. Here, we show that suppressing the kinase function of the epidermal growth factor receptor (EGFR) blocks the activities of both myelin inhibitors and chondroitin sulfate proteoglycans in inhibiting neurite outgrowth. In addition, regeneration inhibitors trigger the phosphorylation of EGFR in a calcium-dependent manner. Local administration of EGFR inhibitors promotes significant regeneration of injured optic nerve fibers, pointing to a promising therapeutic avenue for enhancing axon regeneration after CNS injury.

Failure of successful axon regeneration in the CNS is attributed not only to the intrinsic regenerative incompetence of mature neurons

but also to the environment encountered by injured axons (1-7). The inhibitory activity is principally associated with components of

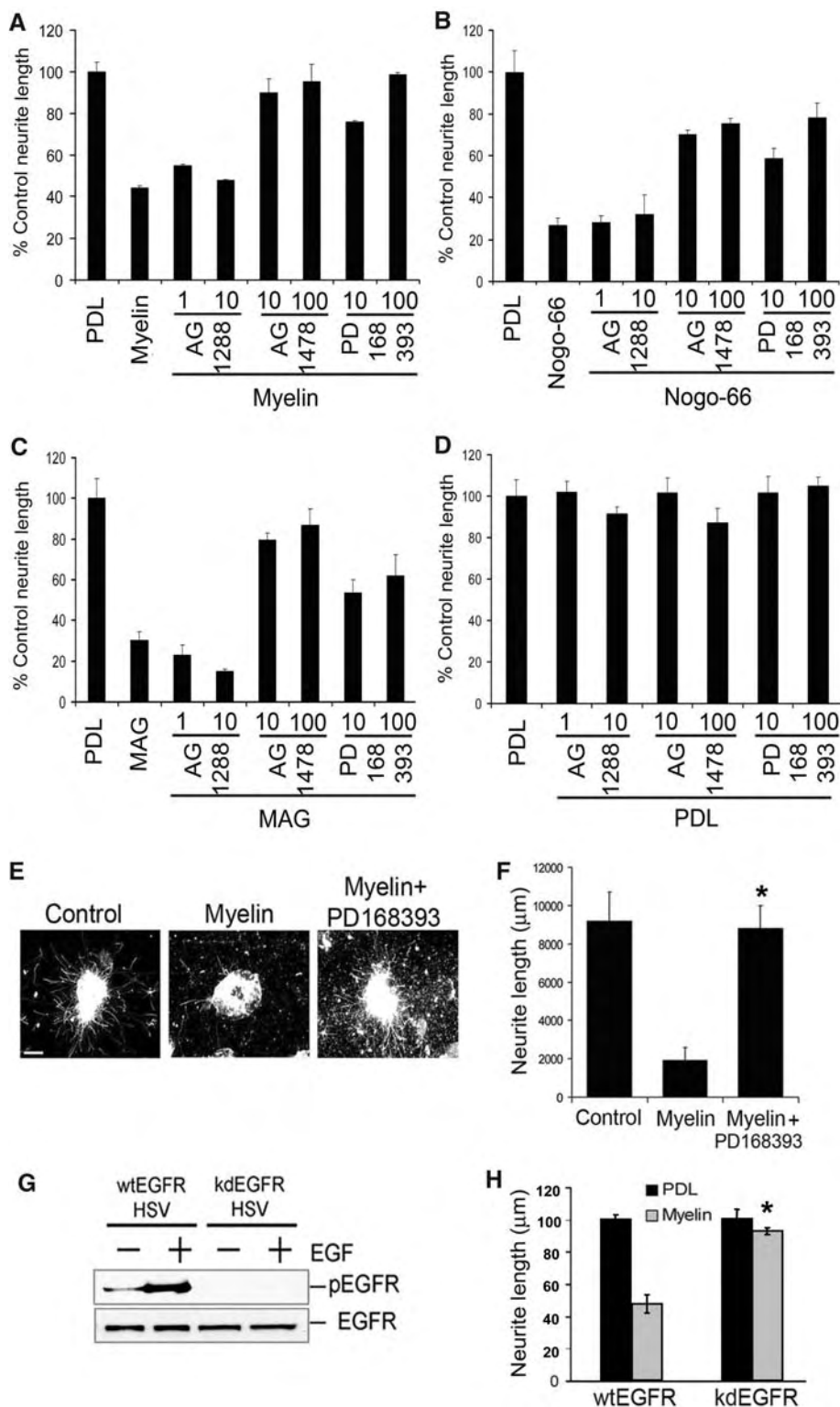


Fig. 1. EGFR kinase activity is required for myelin inhibition. (A to D) Quantitation of the effect of EGFR inhibitors on neurite outgrowth from p7-9 CGNs on myelin (A), Nogo-66 (B), MAG (C), or PDL (D). Data represent mean neurite lengths derived from at least three individual experiments, representing a total of about 500 neurons per condition. AG1478 and PD168393 treatments significantly enhanced neurite outgrowth on inhibitors [(A) to (C)] but not on PDL (D). The concentrations of each drug are as follows: AG1288: 1 and 10 μM; AG1478: 10 and 100 nM; PD168393: 10 and 100 nM. Statistical analyses were performed by analysis of variance (ANOVA) [myelin (A): $F = 64.8$, $df = 7$, $P < 0.0001$; Nogo-66 (B): $F = 20.5$, $df = 7$, $P < 0.001$; MAG (C): $F = 21.91$, $df = 7$, $P < 0.0001$; PDL (D): $F = 2.102$, $df = 6$, $P = 0.1767$], followed by Dunnett's posttest to compare outgrowth on each inhibitor with or without drug treatments. Both AG1478 and PD168393 were significant when compared with no treatment on inhibitors alone ($P < 0.001$, except for 10 nM PD168393 on MAG, where $P < 0.05$) [(A) to (C)]. None of the three drug treatments showed a significant change in outgrowth on PDL alone (D). Error bars show mean + SEM. (E and F) Effects of PD168393 on retinal neurite outgrowth inhibition by myelin. Retinal explants from P5-6 mice were cultured within a collagen matrix with and without myelin (10 μg/ml) in the presence or absence of PD168393 (10 nM) for 72 hours. Explants were fixed and stained with antibodies to tubulin (E). Scale bar, 200 μm. The mean total neurite lengths (+SEM, $N = 10$) are shown in (F). PD168393 significantly promoted outgrowth of explants when compared to myelin alone (*, Student's t test, $P < 0.0001$). (G) Wild-type (wtEGFR) and kinase-deficient EGFR (kdEGFR) HSV-infected CGNs were stimulated with 1-ng/ml EGF for 5 min and the lysates were immunoblotted with an antibody against pTyr1173 EGFR (pEGFR) and reprobed with antibodies to EGFR. (H) DRGs were infected with HSV viruses and plated on control and myelin substrates. Average neurite lengths from three different experiments (at least 100 neurons from each experiment) were obtained as above. kdEGFR significantly promoted DRG outgrowth on myelin when compared with wtEGFR (*, Student's t test, $P < 0.01$). Error bars show means ± SEM.

¹Division of Neuroscience, Children's Hospital, Boston, MA 02115, USA. ²Schepens Eye Research Institute, Department of Ophthalmology, Harvard Medical School, Boston, MA 02114, USA. ³Division of Research, Genentech, 1 DNA Way, South San Francisco, CA 94080, USA.

*To whom correspondence should be addressed. E-mail: zhigang.he@childrens.harvard.edu

CNS myelin and molecules in the glial scar at the lesion site (1-5). Recent studies have suggested that three myelin proteins—myelin-associated glycoprotein (MAG), Nogo-A, and oligodendrocyte myelin glycoprotein (OMgp)—collectively account for the majority of the inhibitory activity in CNS myelin (3-5). The inhibitory activity of MAG, OMgp, and the

extracellular domain of Nogo-A (Nogo-66) may be mediated by common receptor complexes that consist of the ligand-binding Nogo-66 receptor (NgR) and its signaling coreceptors p75/TROY and Lingo-1 (8-14). However, the intracellular mechanisms transducing these signals to the cytoskeleton remain unclear. For instance, it is known that MAG and per-

haps other myelin inhibitors are able to induce an elevation of intracellular calcium levels (15–17), but it is not known how intracellular calcium signaling leads to inhibition of axon regeneration.

In a systematic approach to identify signaling events required for the inhibitory activity of CNS myelin, we performed a small molecule screen to search for compounds with the ability to neutralize neurite outgrowth inhibitory activity associated with CNS myelin. We screened approximately 400 well-characterized small molecules in a neurite outgrowth assay using cerebellar granule cells (CGNs) on an immobilized myelin substrate. The majority of compounds tested did not have a noticeable effect on neurite outgrowth, and a small number of them were toxic (table S1). Most prominently, several EGFR kinase inhibitors showed a remarkable ability to counter the effects of myelin inhibition, suggesting the involvement of EGFR kinase activity in the inhibitory effects of myelin inhibitors.

To confirm our observations, we tested two well-characterized EGFR inhibitors, a competitive inhibitor AG1478, and an irreversible in-

hibitor PD168393 (18) in neurite outgrowth assays. Both inhibitors, but not a control compound AG1288, effectively promoted neurite outgrowth from both CGNs (Fig. 1, A to C) and dorsal root ganglion (DRG) neurons (fig. S1) when grown on an immobilized substrate of either whole myelin or individual myelin inhibitors. In contrast, none of the treatments affected neurite outgrowth on a control poly-D-lysine (PDL) substrate (Fig. 1D). Similarly, EGFR kinase inhibitors were able to block neurite outgrowth inhibition by myelin in retinal explant cultures grown in a collagen matrix laden with myelin (Fig. 1, E and F). Although retinal explants are mixtures of retinal ganglion cells (RGCs) and other cells, dissociated cultures contained primarily CGNs and DRG neurons. Thus, it is likely that EGFR inhibitors act directly on neurons to block their inhibitory responses to myelin inhibitors.

To complement our pharmacological results, we made recombinant herpes simplex viruses (HSVs) to transduce the expression of a mutant form of human EGFR in neurons (19, 20). The kinase deficient EGFR-K721A (kdEGFR) carries a point mutation in the kinase adenosine 5'-triphosphate-binding site

(19), and when overexpressed, can inhibit the activity of endogenous EGFR in a dominant-negative manner (Fig. 1G) (20). As expected, DRGs infected with the mutant but not with wild-type EGFR exhibited extensive neurite outgrowth on myelin (Fig. 1H). Taken together, these results suggest that EGFR kinase activity is required for myelin-dependent neurite outgrowth inhibition.

We next examined the expression of EGFR in the adult nervous system. Using in situ hybridization, we found that EGFR is expressed in most parts of the mature nervous system, including the cerebral cortex, cerebellum, most DRG neurons, and RGCs (fig. S2, A to C). Furthermore, immunostaining with antibodies to EGFR demonstrated the presence of EGFR protein in both cell bodies and neurites of cultured DRG neurons (fig. S2D) and retinal explants (fig. S2E).

To examine whether myelin inhibitors directly influence the activity of EGFR in myelin-responsive neurons, we treated serum-starved CGNs with recombinant soluble myelin inhibitors and assessed the phosphorylation of the endogenous EGFR receptor. By blotting neuronal lysates with antibodies directed against phosphorylated EGFR, we found that both Nogo-66 and OMgp triggered rapid EGFR phosphorylation (Fig. 2, A to B). However, neither control alkaline phosphatase (AP) protein nor the chemorepellant Semaphorin3A induced detectable levels of EGFR phosphorylation (Fig. 2B). Additional evidence for EGFR activation was obtained by observing that Nogo-66-dependent extracellular signal-regulated kinase 1/2 mitogen-activated protein kinase (ERK1/2 MAPK) activation occurred in an EGFR kinase-dependent manner (Fig. 2C).

How do myelin inhibitors activate EGFR in cultured neurons? Previously, we developed a truncated form of NgR that can bind to ligands but not its signaling coreceptors (9–11). When overexpressed, the truncated receptor can compete with the endogenous NgR for ligand binding, thus blocking the signaling pathways induced by myelin inhibitors (9–11). We found that expression of the truncated but not the full-length NgR efficiently blocked the EGFR phosphorylation triggered by Nogo-66 (Fig. 2D), suggesting that EGFR activation is NgR-complex dependent. Next, we performed cell surface binding and coimmunoprecipitation experiments but failed to detect either direct binding of EGFR to inhibitor ligands or a physical association with receptor components NgR or p75 (fig. S3). These results suggested that EGFR is not a likely receptor for myelin-derived inhibitors or part of the NgR receptor complex. It is known that in addition to activation by its cognate ligands, EGFR phosphorylation can also result from “trans-activation” by other signaling pathways (21–23). Failure to detect EGFR in the NgR receptor complex suggests

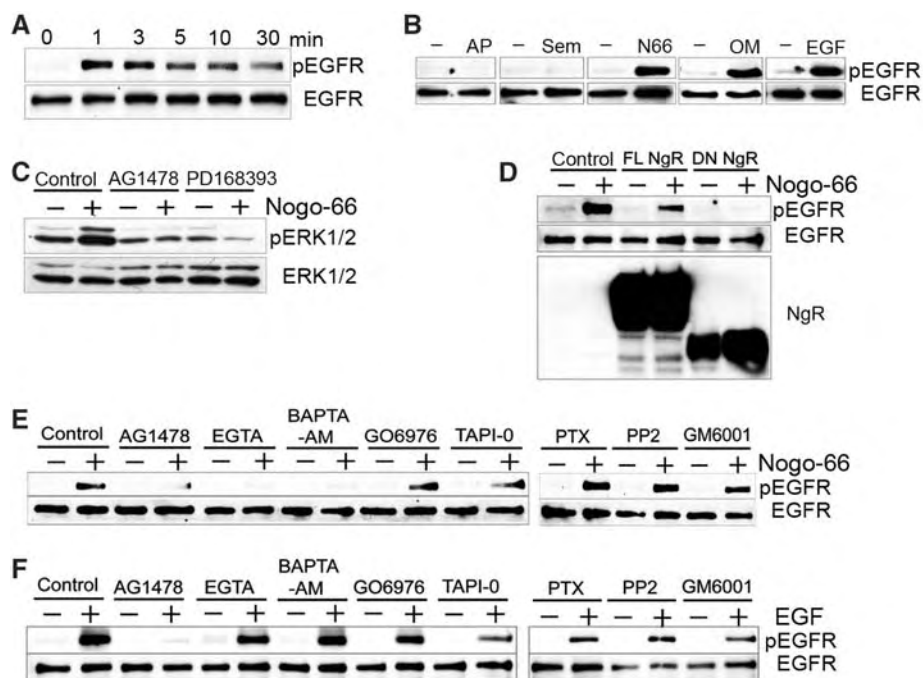


Fig. 2. EGFR activation by myelin inhibitors. (A) Serum-starved CGNs were stimulated with 5 nM AP-Nogo-66 for durations indicated. Lysates were blotted with an antibody to pEGFR, stripped, and reblotted with an antibody to EGFR, as in Fig. 1. (B) CGNs were stimulated with AP (5 nM), Semaphorin3A (Sem, 100 ng/ml), AP-Nogo-66 (N66, 5 nM), AP-OMgp (OM, 5 nM), and EGF (1 ng/ml) for 4 min, and the lysates were probed as above. (C) Nogo-66 activates ERK1/2 MAPKs in an EGFR-dependent manner. CGNs were preincubated (30 min) with AG1478 or PD16933 (both at 100 nM) and stimulated with Nogo-66 for 10 min. Lysates were blotted with antibodies against phospho-ERK1/2 and ERK1/2. (D) NgR-dependent EGFR activation. CGNs were infected with lentiviruses expressing full-length (FL NgR) or dominant-negative NgR (DN NgR) (10, 12) and stimulated with AP-Nogo-66 as in (B). The lysates were blotted with an antibody to pEGFR and an antibody to NgR. (E and F) CGNs were preincubated with AG1478 (100 nM), EGTA (3 mM), BAPTA-AM (5 μM), Go6976 (100 nM), TAPI-0 (1 μM), PTX (100 ng/ml), PP2 (10 nM), and GM6001 (100 nM) and stimulated with AP-Nogo-66 (5 nM) (E) or EGF (1 ng/ml) (F) for 5 min.

trans-activation of EGFR by means of signaling pathways downstream of the active NgR receptor. In support of this, we found that the extent of EGFR phosphorylation triggered by optimal concentrations of myelin inhibitors was comparable to that resulting from low concentrations (1 to 2 ng/ml) of epidermal growth factor (EGF) (Fig. 2B), reminiscent of what has been reported previously for EGFR trans-activation (22).

Several signaling molecules have been implicated in EGFR trans-activation, including calcium, protein kinase C (PKC), nonreceptor tyrosine kinases (Src and Pyk2), G protein-coupled receptors, and metalloproteases that generate EGF-like ligands (21–23). We examined whether any of these mechanisms are involved in NgR-dependent EGFR trans-activation by inhibiting specific signaling pathways pharmacologically. As shown in Fig. 2E, only the calcium chelators EGTA and 1,2-bis(2-aminophenoxy)ethane-*N,N,N',N'*-tetraacetic acid tetra(acetoxymethyl)ester (BAPTA-AM) substantially decreased EGFR phosphorylation resulting from Nogo-66 treatment. In contrast, a PKC inhibitor Go6976, metalloprotease inhibitors TAPI and GM6001, an Src inhibitor PP2, and pertussis toxin had no effect on Nogo-66-elicited EGFR phosphorylation. In further support of the idea of EGFR trans-activation, neither EGTA nor BAPTA-AM had any effect on EGF-induced EGFR phosphorylation (Fig. 2F). Moreover, treatment of cultured neurons with EGF or heparin-bound EGF triggered robust EGFR phosphorylation but did not inhibit neurite outgrowth (24), suggesting that EGFR activation may be a required, but not sufficient, signaling step in the response to myelin inhibitors.

In addition to myelin inhibitors, chondroitin sulfate proteoglycans (CSPGs) in the glial scar represent another major hurdle for regenerating axons. Consistent with previous observations that CSPGs induce an elevation in calcium levels in responding neurons (25), we found that EGFR inhibitors could neutralize the neurite outgrowth inhibitory activity of chicken brain-derived CSPG preparations in which the major components include neurocan, phosphacan, versican, and aggrecan (Fig. 3, A and B). Furthermore, soluble CSPGs added to serum-starved CGNs also elicited EGFR phosphorylation in a calcium-dependent manner (Fig. 3C). In contrast, neither growth cone collapse nor repulsive responses induced by Semaphorin3A were affected by EGFR inhibitors (Fig. 3, D to G). Because Semaphorin3A has previously been suggested to act independently of intracellular calcium (26), these results support the idea that EGFR might be a calcium-specific signaling molecule in axon guidance pathways.

We next examined whether EGFR inhibitors introduced at a CNS lesion site could promote axon regeneration in an optic nerve

crush model (27–29). Immediately after injury in adult mice, gelfoam soaked in a solution containing PD168393 or vehicle [dimethyl sulfoxide (DMSO)] was placed around the crush site of the nerve and replaced after

three days. The extent of axonal regrowth was assessed 2 weeks after injury by immunohistochemistry, which used antibodies to GAP-43 to detect regenerating axons. Although little regeneration was detected in DMSO-treated

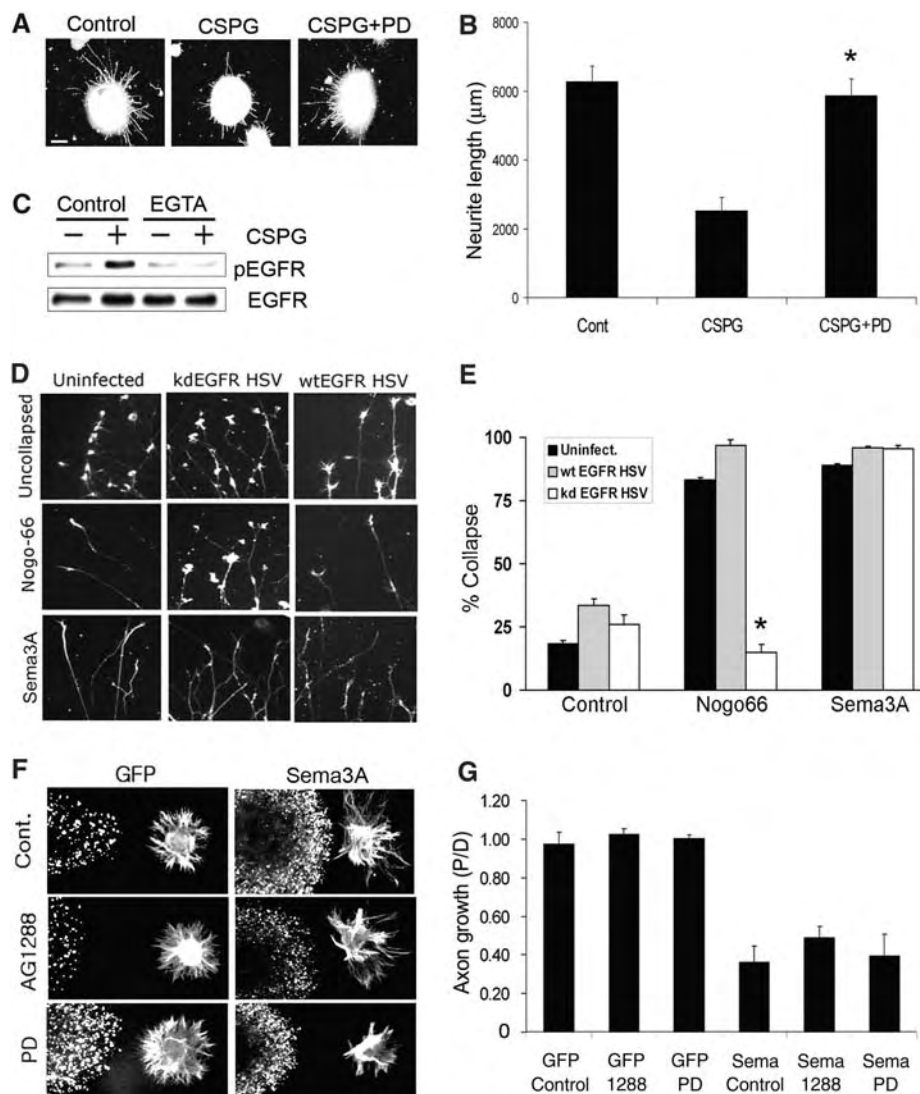


Fig. 3. Requirement of EGFR activity for CSPGs and Nogo-66 inhibition but not Semaphorin3A repulsion. (A) Retinal explants were grown in collagen gels with and without CSPGs (200 ng/ml, Chemicon) and PD168393 (100 nM) for 3 days, fixed and stained with antibodies to tubulin. Scale bar, 200 μ m. (B) Average total neurite lengths of retinal explants in the conditions described in (A). PD168393 significantly increased neurite length of explants when compared with CSPGs alone (*, Student's *t* test $P = 0.0015$). Error bars show means + SEM. (C) CSPGs activate EGFR in a Ca^{2+} -dependent manner. Serum-starved CGNs were stimulated with CSPGs for 5 min with and without 3 mM EGTA and the lysates were blotted. (D and E) Growth cone collapse after 30-min addition of AP-Nogo-66 (~5 nM) and Semaphorin3A (Sema3A) (100 ng/ml) to embryonic day 13 (E13) chick DRG cultures infected with or without HSVs expressing wtEGFR or kdEGFR. Representative growth cone morphology is shown in (D) and the average percentage of collapsed growth cones + SEM from quadruplicate experiments in (E). kdEGFR significantly decreased growth cone collapse in response to Nogo-66 when compared with wtEGFR (ANOVA, $F = 298$, $df = 8$, $P < 0.001$, using Dunnett's posttest). (F and G) EGFR inhibitors did not affect the repulsive activity of Semaphorin3A. E14 rat DRGs were embedded in collagen adjacent to 293 cells expressing Sema3A. AG1288 (10 μ M) and PD168393 (PD, 100 nM) were added at the same time, and cells were grown for 48 hours. Neurites were visualized by anti-tubulin staining. Representative images are shown in (F) and the quantitation from quadruplicate experiments in (G). Repulsive effects were quantified by comparing the ratio of proximal to distal neurite length (P/D) with respect to the 293 cell aggregates. No significant differences between AG1288 or PD168393-treated groups and their controls were detected by Student's *t* test. Error bars in (G) show means + SEM.

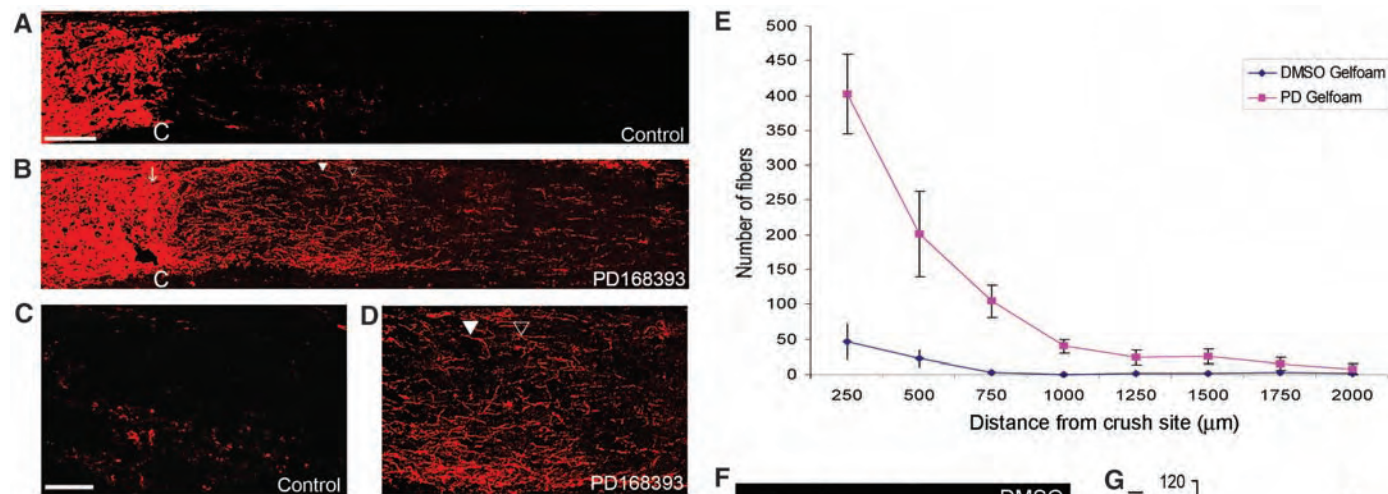


Fig. 4. PD168393 promotes optic nerve regeneration. (A to D) Representative images of optic nerves stained with antibodies to GAP43 from control [(A) and (C)] or PD168393-treated [(B) and (D)] mice. The injury site was identified visually and with lectin staining (marked by C). The images (C) and (D) are magnified views of the postcrush area. (C) The control nerve where few GAP-43 fibers are evident. (D) Numerous regenerating fibers, including some that have turned (filled triangle) as well as those that are straight (open triangle). Scale bar, 100 μm in (A) and (B) and 50 μm in (C) and (D). (E) Quantitation of regenerating fibers in control and PD168393-treated mice. Fibers were counted at 250-μm intervals from the crush site from three nonconsecutive sections and the number of fibers at a given distance was calculated as (27). There is a significant difference between DMSO and PD168393 treatment groups by ANOVA ($F = 63$, $df = 1$, $P < 0.001$, $n = 6$ for each group), with Bonferroni posttests at each distance indicating a significant difference between DMSO and PD168393 treatment

at 250 μm ($P < 0.001$) and 500 μm ($P < 0.01$). Error bars show means ± SEM. (F and G) Anti-tubulin stained RGCs in control and PD168393-treated retinas. Note large axon bundle (filled triangle) and retinal ganglion cell (open triangle) in (F). Scale bar, 10 μm. (G) Quantitation of surviving RGCs in control and PD168393-treated mice revealed no difference in survival between the two groups (Student's t test, $P = 0.349$). The results are plotted against the results from noncrushed controls. Error bars show means + SEM.

control mice (Fig. 4, A, C, and E), PD168393 treatment resulted in substantial axonal regrowth with a ninefold increase in the number of regenerating axons 0.25 mm beyond the injury site, as compared with control mice (Fig. 4, B, D, and E). To test the possibility that the observed axon regrowth after PD168393 treatment was a consequence of improved cell survival, we stained retinal sections with the antibody to the tubulin Tuj1, which stains RGCs in the retina, and counted surviving RGCs. No detectable effect of PD168393 on RGC survival was found (Fig. 4, F and G). The extent of axon regeneration observed after PD168393 treatment was comparable to that induced by a Rho inhibitor C3, but less than the combined effect of C3 and lens injury, a procedure that can enhance the regenerative capacity of RGC axons (28). We estimated that about 0.5% of RGC axons regenerated beyond the lesion site after PD168393 treatment. This low percentage of axon regeneration may be explained by previous observations that a small portion of postnatal RGCs retains rapid axonal growth ability (6). Independent experiments suggested that locally administrated AG1478 also induced significant regeneration of injured optic nerve fibers (fig. S3). In comparison with PD168393, the relatively weaker effects of AG1478 might reflect the reversible EGFR inhibition mechanism of this compound. These findings sug-

gest that local blockade of EGFR activity could alleviate inhibitory influences and promote the regeneration of lesioned CNS fibers in adult mice.

Taken together, our results suggest that EGFR activation might be a critical signaling event downstream of the intracellular calcium influx produced by myelin inhibitors and CSPGs. Interestingly, we found that Erlotinib (Tarceva), an EGFR inhibitor approved for the treatment of cancer (30), could also block neurite outgrowth inhibition by myelin inhibitors (fig. S5). Thus, such compounds might prove useful for promoting axon regeneration after brain and spinal cord injury.

References and Notes

1. M. E. Schwab, D. Bartholdi, *Physiol. Rev.* **76**, 319 (1996).
2. J. Silver, J. H. Miller, *Nat. Rev. Neurosci.* **5**, 146 (2004).
3. M. T. Filbin, *Nat. Rev. Neurosci.* **4**, 703 (2003).
4. A. W. McGee, S. M. Strittmatter, *Trends Neurosci.* **26**, 193 (2003).
5. Z. He, V. Koprivica, *Annu. Rev. Neurosci.* **27**, 341 (2004).
6. J. L. Goldberg, M. P. Klassen, Y. Hua, B. A. Barres, *Science* **296**, 1860 (2002).
7. H. M. Bomze et al., *Nat. Neurosci.* **4**, 38 (2001).
8. A. E. Fournier, T. GrandPre, S. M. Strittmatter, *Nature* **409**, 341 (2001).
9. K. C. Wang et al., *Nature* **417**, 941 (2002).
10. M. Domeniconi et al., *Neuron* **35**, 283 (2002).
11. K. C. Wang et al., *Nature* **420**, 74 (2002).
12. S. Mi et al., *Nat. Neurosci.* **7**, 221 (2004).
13. J. B. Park et al., *Neuron* **45**, 345 (2005).
14. Z. Shao et al., *Neuron* **45**, 353 (2005).

15. C. E. Bandtlow, M. F. Schmidt, T. D. Hassinger, M. E. Schwab, S. B. Kater, *Science* **259**, 80 (1993).
16. J. R. Henley, K. H. Huang, D. Wang, M. M. Poo, *Neuron* **44**, 909 (2004).
17. S. Shim et al., *Nat. Neurosci.* **8**, 730 (2005).
18. A. Levitzki, A. Gazit, *Science* **267**, 1782 (1995).
19. S. Felder et al., *Cell* **61**, 623 (1990).
20. A. M. Honegger, R. M. Kris, A. Ullrich, J. Schlessinger, *Proc. Natl. Acad. Sci. U.S.A.* **86**, 925 (1989).
21. E. Zwick, P. O. Hackel, N. Prenzel, A. Ullrich, *Trends Pharmacol. Sci.* **20**, 408 (1999).
22. J. Andreev et al., *J. Biol. Chem.* **276**, 20130 (2001).
23. L. B. Rosen, M. E. Greenberg, *Proc. Natl. Acad. Sci. U.S.A.* **93**, 1113 (1996).
24. V. Koprivica et al., data not shown.
25. D. M. Snow, P. B. Atkinson, T. D. Hassinger, P. C. Letourneau, S. B. Kater, *Dev. Biol.* **166**, 87 (1994).
26. H. Song et al., *Science* **281**, 1515 (1998).
27. M. Lehmann et al., *J. Neurosci.* **19**, 7537 (1999).
28. K.-S. Cho et al., *J. Cell Sci.* **118**, 863 (2005).
29. D. Fischer, D. V. Petkova, S. Thanos, L. I. Benowitz, *J. Neurosci.* **24**, 8726 (2004).
30. M. S. Tsao et al., *N. Engl. J. Med.* **353**, 133 (2005).
31. We thank G. Yiu, J. Flanagan, M. Greenberg, R. Meyer RL, J. Miotke, C. Stiles, and T. Schwarz for critically reading the manuscript and for discussions and Z. Wang for providing EGFR constructs. Supported by research grants from the National Institute of Neurological Diseases and Stroke, EJLB Foundation, and Patterson Fund (Z.H.) and the NIH (D.F.C.). Z.H. is a McKnight Scholar. V.K. is a recipient of NSF predoctoral fellowship. G.Y. is supported by an NIH training grant.

Supporting Online Material

www.sciencemag.org/cgi/content/full/310/5745/106/DC1
 Materials and Methods
 Figs. S1 to S5
 Table S1

31 May 2005; accepted 29 August 2005
 10.1126/science.1115462

Retinoic Acid Signaling Affects Cortical Synchrony During Sleep

Stéphanie Maret,¹ Paul Franken,^{1,2} Yves Dauvilliers,^{1,3}
Norbert B. Ghyselinck,⁴ Pierre Chambon,⁴ Mehdi Tafti^{1*}

Delta oscillations, characteristic of the electroencephalogram (EEG) of slow wave sleep, estimate sleep depth and need and are thought to be closely linked to the recovery function of sleep. The cellular mechanisms underlying the generation of delta waves at the cortical and thalamic levels are well documented, but the molecular regulatory mechanisms remain elusive. Here we demonstrate in the mouse that the gene encoding the retinoic acid receptor beta determines the contribution of delta oscillations to the sleep EEG. Thus, retinoic acid signaling, which is involved in the patterning of the brain and dopaminergic pathways, regulates cortical synchrony in the adult.

EEG oscillations in the delta frequency range (1 to 4 Hz) mark slow wave sleep (SWS) and represent widespread synchronized firing patterns of cortical and thalamocortical neurons (1). Activity in the delta range, quantified as power by the Fourier transform, is a measure of SWS depth and consolidation (2, 3). It is considered to be a reliable indicator of time spent awake (4) and has been proposed to reflect a homeostatic need for sleep (5).

In mice, the EEG characteristics of sleep are strongly affected by genetic factors (6). For instance, strain differences in the frequency of theta rhythms (5 to 9 Hz) are controlled by a single gene (7). In contrast to other inbred strains, DBA/2J (D2) mice show reduced delta activity during SWS, and the EEG is dominated by theta activity instead (6) (Fig. 1, A and B). Sleep is abnormally fragmented in D2 mice, and the rate at which SWS need accumulates is significantly reduced in this strain when compared with that in most other inbred strains (4). To better quantify the altered EEG pattern in D2 mice, we defined a theta/delta ratio (θ/δ); that is, power in the theta peak frequency range (6 to 7 Hz)/power in the delta peak frequency range (3 to 4 Hz) (fig. S1). In D2 mice, θ/δ was more than 5 standard deviations (SDs) higher when compared with that in B6 mice (1.5 ± 0.1 versus 0.9 ± 0.1 ; $P = 3 \times 10^{-7}$; $n = 7$ mice per strain) (Fig. 1C). In B6 \times D2 F₁ (heterozygous) mice, θ/δ was identical to that in B6 mice (1.0 ± 0.07 ; $n = 5$) and highly significantly different from that in D2 mice ($P = 1 \times 10^{-5}$), indicating a complete dominance of the B6 alleles. To map the underlying genes,

we recorded sleep in 25 BXD-recombinant inbred (RI) strains ($n = 110$; 4 to 6 mice per strain) (Fig. 1D). Analysis of variance in these strains indicated that 70% of variance was due to the additive effects of genes (broad sense heritability). Genomewide linkage analysis indicated a single, highly significant locus on chromosome 14 [best markers: D14Mit48, -99, -109; 0 to 3 cM according to the mouse consensus map, logarithm of the odds ratio for linkage (lod) score = 4.9, $P < 2 \times 10^{-6}$] (Fig. 1E) that explained more than 55% of the total variance in θ/δ , indicating the presence of an autosomal recessive gene. The θ/δ ratio was a robust EEG trait in that strain differences were not affected by 6 hours of sleep deprivation, and the same unique localization was found for θ/δ during recovery sleep (fig. S2).

To verify that a single gene was responsible for our phenotype in inbred mice, we screened a panel of 30 inbred strains with 10 Mit markers from our linkage region and identified D14Mit78 as a unique biallelic marker (either D2 or B6 type). Therefore, we recorded sleep in three other, unrelated inbred strains (LP/J, C3H/HeJ, and SPRET/Ei) with D2-type D14Mit78. The θ/δ ratios were similar to those in D2 mice (1.6 ± 0.1 , 1.8 ± 0.1 , and 1.5 ± 0.1 , respectively), providing additional evidence that a single gene in this region is segregating with the θ/δ trait. By using other polymorphic markers, we constructed a minimal chromosome 14 centromeric haplotype in four inbred strains of B6 phenotype [B6, AKR/J (AKR), BALB/cByJ (C), A/J (A)] and four of D2 phenotype (D2, LP, C3H, SPRET). A 350-kb region was identified as the smallest genomic region associated with θ/δ (Fig. 1F).

Among candidate genes in the region, a restriction fragment length polymorphism of the retinoic acid receptor beta (*Rarb*) showed a perfect match with D14Mit78. Although *Rarb* and D14Mit78 are placed 1.5 cM apart according to the mouse consensus map, D14Mit78 is located within the 5' region of the second *Rarb* promoter (P2). Retinoic acid, a vitamin A

derivative, activates a signaling pathway involving genes for retinoic acid receptors (*Rara*, *Rarb*, and *Rarg*) and retinoid-X receptors (*Rxra*, *Rxrb*, and *Rxrg*). These nuclear receptors form RAR-RXR heterodimers and play important roles during ontogenesis as ligand-dependent transcriptional regulators (8, 9). Retinoic acid receptors are highly expressed in the brain (10) where they are involved in the regulation of neural functions such as the control of locomotion (11) and long-term potentiation or depression (12), possibly through their effect on dopaminergic and cholinergic neurotransmission (11, 13, 14). On the basis of the tight linkage between D14Mit78 and θ/δ in inbred and RI strains and the fact that D14Mit78 is located within the *Rarb* locus, and given the role of the *Rarb* in the central nervous system (CNS) functioning, we further investigated the role of *Rarb* in shaping the sleep EEG.

Rarb extends over 650 kb with two major promoters directing the transcription of four transcripts (P1 for transcripts *Rarb1* and 3, P2 for transcripts *Rarb2* and 4) that differ only in their N terminal and 5'-untranslated region (5'-UTR). All four transcripts were amplified by reverse transcription polymerase chain reaction (RT-PCR) and sequenced in D2 and B6 mice to test for mutations or polymorphisms segregating with the θ/δ trait. In addition to D14Mit78, six previously unknown polymorphisms were identified. One was localized in the coding region but was silent, four were in the 5'-UTR of *Rarb1* and 3, and one was in the 3' region of all four transcripts. These polymorphisms were typed in 37 inbred strains and, except for the most proximal one, a (CT)_n, all others were either of B6 or D2 type, confirming the presence of only two *Rarb* variants (Fig. 1F).

EEG recordings were then performed in mice with a targeted deletion of the *Rarb1,3* ($n = 7$), *Rarb2* ($n = 7$), and *Rarb1-4* genes (all four transcripts; $n = 6$) and in their wild-type littermates ($n = 7$). Only *Rarb1-4* mutants had a significantly lower θ/δ ratio when compared with that in all other strains (Fig. 2A). We next produced hemizygous mice by crossing *Rarb* mutant mice with either D2 or B6 mice. A significant recovery of θ/δ was observed in D2 hemizygous mice, with maximal recovery in *Rarb1,3*-D2 hemizygotes (Fig. 2A). This finding adds further evidence that *Rarb* is the gene underlying the differences in θ/δ .

We verified whether *Rarb* polymorphisms between high- and low- θ/δ strains affect *Rarb* transcription in vivo. Using real-time RT-PCR, we quantified the relative expression of the three major *Rarb* transcripts (*Rarb1*, 2, and 3) in the brain of D2 and B6 mice ($n = 9$ per strain). All three *Rarb* transcripts were expressed at significantly higher levels in D2 mice (Fig. 2B), strongly suggesting that poly-

¹Center for Integrative Genomics, University of Lausanne, Génopode, 1015 Lausanne-Dorigny, Switzerland. ²Department of Biological Sciences, Stanford University, CA 94305-5020, USA. ³Service de Neurologie B, Hôpital Gui-de-Chauliac, 34295 Montpellier cedex 5, France. ⁴Institut de Génétique et de Biologie Moléculaire et Cellulaire (IGBMC) and Institut Clinique de la Souris (ICS), 67404 Illkirch cedex, France.

*To whom correspondence should be addressed. E-mail: mehdi.tafti@unil.ch

Fig. 1. Mapping of a gene regulating the relative contribution of theta and delta oscillations to the sleep EEG. (A) Eight-second EEG samples for SWS from representative C57BL/6J (B6) and DBA/2J (D2) mice. (B) EEG power spectra of SWS during the 12-hour light-period recordings (29). In D2 mice, the contribution of power in the theta (5 to 8 Hz) frequency range is larger than that of the delta (1 to 4 Hz) frequency range. (C) The θ/δ ratio in D2 mice is more than 5 SDs higher than in B6 mice; in contrast, the θ/δ ratio in heterozygous BXD-F₁ mice is similar to that in B6 mice, indicating that the D2 alleles are recessive. (D) The θ/δ ratios (+1 SD) in BXD-recombinant inbred strains used for mapping. Black and gray bars indicate those strains with the B6- or D2-type allele at the linked marker on chromosome 14, respectively. (E) Interval mapping of the θ/δ gene on chromosome 14. Permutation test ($n = 10000$) established a significant level for lod scores > 3.76 . The maximum lod score of 4.9 at marker D14Mit251 corresponds to an empirical genome-wide P value of 0.006 (Map Manager QTXb20). (F) Haplotype of the identified region on chromosome 14 over ~ 6 Mb. Numbers indicate the allele size for the Mit markers in the two groups of inbred strains (B6, C57BL/6J; C, BALB/cByJ; AK, AKR/J; A, A/J; D2, DBA/2J; C3H, C3H/He; LP, LP/J; Spr, SPRET/Ei). a and b (under *Il3ra*) indicate the presence or absence of a spontaneous loss-of-function mutation in the interleukin-3 receptor α chain. A and T (under *Rarb* (*Ex-2*)) indicate a single-nucleotide polymorphism in the second untranslated exon of the *Rarb* gene. This polymorphism and D14Mit78 clearly distinguish low- θ/δ (B6 type) and high- θ/δ (D2 type) groups. *Rarb* gene is represented on top with its 11 exons. Exon 1 starts with a variable (CT)_n sequence showing a strain distribution pattern similar to that of marker D14Gu103, indicating that the biallelic conserved region starts between (CT)_n and exon 2 and ends between D14Mit78 and D14Mit98 (~ 300 kb).

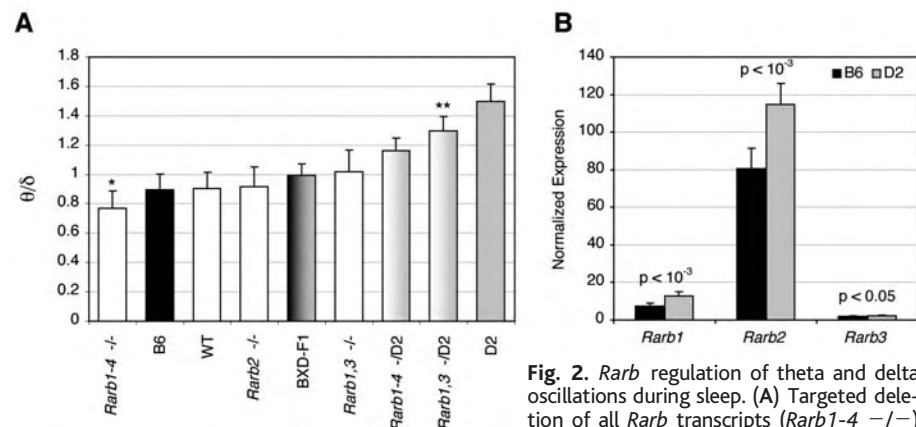
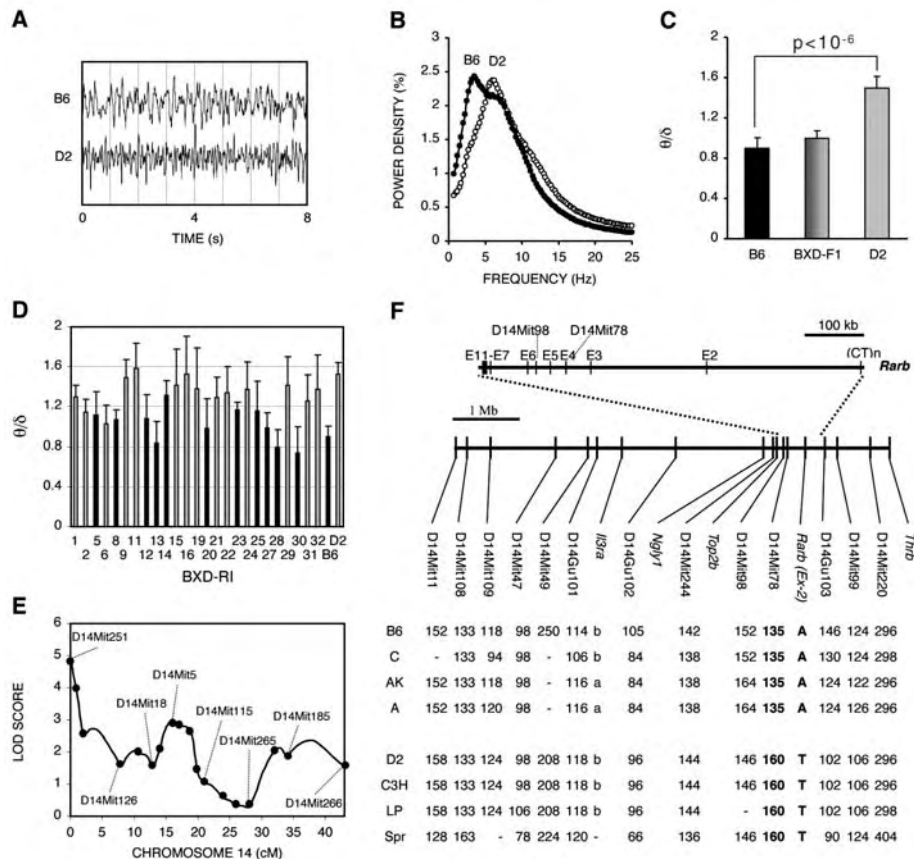


Fig. 2. *Rarb* regulation of theta and delta oscillations during sleep. (A) Targeted deletion of all *Rarb* transcripts (*Rarb1-4* $-/-$) but not *Rarb2* (*Rarb2* $-/-$) or *Rarb1* and 3 (*Rarb1,3* $-/-$) results in a significant decrease in θ/δ [* indicates a significant difference ($P < 0.05$) with all other strains]. The θ/δ ratio in hemizygous *Rarb* $-/B6$ mice is similar to that in B6 mice ($B6 = 0.9 \pm 0.1$, *Rarb1-4* $-/B6 = 1.0 \pm 0.1$, *Rarb1,3* $-/D2 = 1.1 \pm 0.2$), whereas in hemizygous *Rarb* $-/D2$ mice, there is a partial (*Rarb1-4* $-/D2$) or complete recovery (*Rarb1,3* $-/D2$) of the θ/δ ratio (** indicates a significant difference with heterozygous BXDF1 mice but no difference with D2 mice.) (B) Real-time quantitative RT-PCR measurements of *Rarb* transcripts in whole brain of B6 and D2 mice indicate a significant increase in expression in D2 strain (note that *Rarb1* is the second most abundant transcript, whereas *Rarb3* expression is very low). Values are normalized relative to those for the house-keeping gene ribosomal protein S9 and corrected for each transcript amplification efficiency (29).

morphisms in *Rarb* gene (as found in the 5'-UTR of *Rarb1,3*) affect its transcription. Subsequently, we measured the relative brain expression of *Rarb* transcripts in the other six

inbred strains and found that only *Rarb1* expression consistently varied with θ/δ (8.0 ± 1.4 , 8.9 ± 2.2 , and 6.7 ± 2.1 in low- θ/δ strains C, AK, and A, respectively; 11.3 ± 2.6 , $11.7 \pm$

1.6 , and 23.0 ± 2.5 in high- θ/δ strains C3H, LP, and SPRET, respectively; $n = 3$ to 4 mice per strain; $P < 0.05$ for all comparisons). The wild-derived SPRET/Ei strain has higher levels of expression for all *Rarb* transcripts as compared with that in all other inbred strains.

In summary, changes in the relative contribution of delta oscillations to the SWS EEG are linked to *Rarb* gene and more specifically to *Rarb1*. Vitamin A and its derivatives play essential roles during embryogenesis, particularly in the development of the CNS, as revealed by a large spectrum of abnormalities known as vitamin A-deficient syndrome (15). A major role for RARB receptors in the mesolimbic dopaminergic pathway, which is involved in the control of locomotion (11) and, possibly, in the neurobiology of Parkinson's disease, schizophrenia, Alzheimer's disease, and addiction, was suggested on the basis of *Rarb* mutant mouse models or hypothesized on the basis of human genetic linkage studies (11, 16). In all cases, RARB receptors are thought to influence complex behaviors by affecting either brain development and plasticity or dopaminergic neurotransmission. Sleep and the sleep EEG are developmentally regulated (17–19) and affect neuronal plasticity (20–22). Further, aging is accompanied by

profound changes in both sleep (23) and the sleep EEG (24, 25), with a major decrease in delta activity and increase in sleep fragmentation being the hallmarks of older age in humans (26). These changes parallel those of *Rarb* expression (27) in rats, suggesting a correlated tuning of both variables. We also hypothesize that both sleepiness and slow waves in the EEG induced by dopaminergic drugs (28) might be explained by the close interaction between the retinoic acid receptors and the mesolimbic dopaminergic pathway (11).

References and Notes

1. M. Steriade, D. A. McCormick, T. J. Sejnowski, *Science* **262**, 679 (1993).
2. D. Neckelmann, R. Ursin, *Sleep* **16**, 467 (1993).
3. P. Franken, D. J. Dijk, I. Tobler, A. A. Borbély, *Am. J. Physiol.* **261**, R198 (1991).
4. P. Franken, D. Chollet, M. Tafti, *J. Neurosci.* **21**, 2610 (2001).
5. S. Daan, D. G. Beersma, A. A. Borbély, *Am. J. Physiol.* **246**, R161 (1984).
6. P. Franken, A. Malafosse, M. Tafti, *Am. J. Physiol.* **275**, 1127 (1998).

7. M. Tafti et al., *Nat. Genet.* **34**, 320 (2003).
8. M. Mark, N. B. Ghyselinck, P. Chambon, *Annu. Rev. Pharmacol. Toxicol.*, in press.
9. S. Green, P. Chambon, *Trends Genet.* **4**, 309 (1988).
10. W. Krezel, P. Kastner, P. Chambon, *Neuroscience* **89**, 1291 (1999).
11. W. Krezel et al., *Science* **279**, 863 (1998).
12. M. Y. Chiang et al., *Neuron* **21**, 1353 (1998).
13. S. M. Farooqui, *Life Sci.* **55**, 1887 (1994).
14. W. A. Pedersen, B. Berse, U. Schuler, B. H. Wainer, J. K. Blusztajn, *J. Neurochem.* **69**, 4198 (1995).
15. J. G. Wilson, C. B. Roth, J. Warkany, *Am. J. Anat.* **92**, 189 (1953).
16. A. B. Goodman, *Proc. Natl. Acad. Sci. U.S.A.* **95**, 7240 (1998).
17. D. Jouvét-Mounier, L. Astic, D. Lacote, *Dev. Psychobiol.* **2**, 216 (1970).
18. M. G. Frank, H. C. Heller, *Am. J. Physiol.* **273**, R472 (1997).
19. M. G. Frank, H. C. Heller, *Am. J. Physiol.* **272**, R1792 (1997).
20. M. G. Frank, N. P. Issa, M. P. Stryker, *Neuron* **30**, 275 (2001).
21. H. Miyamoto, H. Katagiri, T. Hensch, *Nat. Neurosci.* **6**, 553 (2003).
22. J. H. Benington, M. G. Frank, *Prog. Neurobiol.* **69**, 71 (2003).
23. H. P. Roffwarg, J. N. Muzio, W. C. Dement, *Science* **152**, 604 (1966).

24. I. Feinberg, J. D. March, G. Fein, T. C. Floyd, J. M. Walker, *Electroencephalogr. Clin. Neurophysiol.* **44**, 202 (1978).
25. D. J. Dijk, D. G. Beersma, R. H. van den Hoofdakker, *Neurobiol. Aging* **10**, 677 (1989).
26. M. A. Carskadon, E. D. Brown, W. C. Dement, *Neurobiol. Aging* **3**, 321 (1982).
27. C. Feart et al., *Neurobiol. Aging* **26**, 729 (2005).
28. P. Bo, E. Ongini, A. Giorgetta, F. Savoldi, *Neuropharmacology* **27**, 799 (1988).
29. Materials and methods are available as supporting material on Science Online.
30. We thank B. Petit and B. Féret for technical assistance. Supported by the Swiss National Foundation for Scientific Research, the Centre National de la Recherche Scientifique (CNRS), the Institut National de la Santé et de la Recherche Médicale (INSERM), the Hôpital Universitaire de Strasbourg, the Collège de France, and the Institut Universitaire de France.

Supporting Online Material

www.sciencemag.org/cgi/content/full/310/5745/1117/DC1

Materials and Methods
Figs. S1 and S2
References

19 July 2005; accepted 1 September 2005
10.1126/science.1117623

Astrocytic Purinergic Signaling Coordinates Synaptic Networks

Olivier Pascual,¹ Kristen B. Casper,² Cathryn Kubera,¹ Jing Zhang,¹
Raquel Revilla-Sanchez,¹ Jai-Yoon Sul,¹ Hajime Takano,¹
Stephen J. Moss,¹ Ken McCarthy,² Philip G. Haydon^{1*}

To investigate the role of astrocytes in regulating synaptic transmission, we generated inducible transgenic mice that express a dominant-negative SNARE domain selectively in astrocytes to block the release of transmitters from these glial cells. By releasing adenosine triphosphate, which accumulates as adenosine, astrocytes tonically suppressed synaptic transmission, thereby enhancing the dynamic range for long-term potentiation and mediated activity-dependent, heterosynaptic depression. These results indicate that astrocytes are intricately linked in the regulation of synaptic strength and plasticity and provide a pathway for synaptic cross-talk.

After the discovery that neuronal transmitters evoke Ca²⁺ elevations in astrocytes (1, 2), several laboratories demonstrated that astrocytes release chemical transmitters, including adenosine triphosphate (ATP) (3), glutamate (4), and D-serine (5). Although gliotransmitters synchronize neuronal activity (6) and modulate synaptic transmission (7–10), the role of gliotransmission in synaptic networks is undefined, in part because neurons and astrocytes use similar chemical transmitters and receptors. Accumulating evidence supports the idea that gliotransmitters are released through soluble N-ethylmaleimide-sensitive

factor attachment protein receptor (SNARE) protein-dependent mechanisms (11–13). To investigate the role of gliotransmitters in synaptic networks, we generated transgenic mice in which the SNARE-dependant release of gliotransmitters was selectively impaired in astrocytes (14).

We expressed the cytosolic portion of the SNARE domain of synaptobrevin 2 (amino acids 1 to 96) selectively in astrocytes, a manipulation that blocks gliotransmission (15). We developed two lines of transgenic mice. In the first, GFAP:TA, the astrocyte-specific glial fibrillary acidic protein (GFAP) promoter drives the expression of the “tet-Off” tetracycline transactivator (tTA). The second, tetO:SNARE, contains a tet operator (tetO)-regulated SNARE domain and lacZ and enhanced green fluorescent protein (EGFP) reporter genes (Fig. 1A). Crossing lines yields mice in which SNARE, LacZ, and EGFP transgenes are expressed in GFAP-positive astrocytes, not in

neurons (Fig. 1B and E to J, and fig. S1), and in which transgene expression is suppressed by doxycycline (Dox) (Fig. 1, C and D, and fig. S1). We refer to these animals as dominant-negative SNARE (dn-SNARE) mice.

We determined if astrocyte-specific expression of the dn-SNARE domain affects synaptic transmission and plasticity by using acutely isolated hippocampal slices. The slope of Schaffer collateral-evoked field excitatory postsynaptic potentials (fEPSPs) was significantly larger ($P < 0.02$) in dn-SNARE mice expressing the transgene ($n = 10$ mice) compared to either dn-SNARE mice maintained on Dox to prevent transgene expression ($n = 9$ mice) or wild-type littermates (Fig. 2, A and B) with no change in the fiber volley (fig. S2). Thus, a SNARE-dependent process in astrocytes influences basal synaptic transmission.

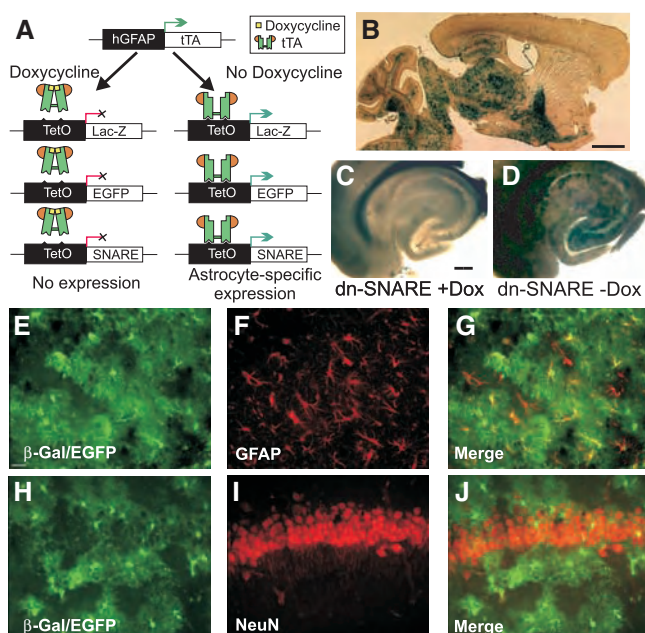
To ask whether astrocytes also modulate synaptic plasticity, we studied long-term potentiation (LTP). Theta-burst stimulation applied to wild-type brain slices potentiated fEPSP slope by $232 \pm 18\%$. The magnitude of LTP was significantly less ($P < 0.05$) in mice expressing dn-SNARE ($172 \pm 11\%$, $n = 10$ mice) (Fig. 2, C and D). Because the magnitude of LTP in wild-type mice was unaffected by maintenance on Dox, and yet this treatment prevented the change in LTP magnitude observed in dn-SNARE mice, we suggest that astrocytes control the available range for synaptic plasticity, by regulating the strength of basal synaptic transmission.

We evaluated potential roles for three gliotransmitters known to be released from astrocytes and asked whether they coordinately regulate baseline fEPSP slope and the magnitude of LTP. D-2-amino-5 phosphonopentanoate (D-AP5, 50 μ M, $n = 4$ mice) to block N-methyl-D-aspartate (NMDA) receptors, the

¹Department of Neuroscience, Conte Center for Integration at the Tripartite Synapse, University of Pennsylvania School of Medicine, Philadelphia, PA 19104, USA. ²Department of Pharmacology, University of North Carolina at Chapel Hill, Chapel Hill, NC 27599, USA.

*To whom correspondence should be addressed: email: pghaydon@mail.med.upenn.edu

Fig. 1. Astrocyte-specific expression of the dn-SNARE domain. (A) Two lines of animals were generated, hGFAP.tTA and tetO.SNARE. When these lines are crossed, Dox suppresses SNARE, EGFP, and lacZ expression. (B) β -galactosidase (β -Gal) expression on a parasagittal section of dn-SNARE mouse brain (scale bar, 1 mm). (C and D) Slices from dn-SNARE mice (\pm Dox) show transgene regulation by Dox as reported by β -Gal (scale bar, 200 μ m). (E) EGFP and β -Gal fluorescence and (F) GFAP immunoreactivity demonstrate expression of gene products in astrocytes. (G) Merged (E) and (F) images. (H to J) In hippocampal CA1, (H) EGFP and β -Gal transgenes are not expressed in neurons identified by (I) NeuN immunoreactivity. (J) Merged (H) and (I) images.



target of glial-derived D-serine and glutamate, did not change fEPSP slope (Fig. 2E) and blocked LTP (Fig. 2F). Because glial glutamate preferentially activates NR2B subunit-containing NMDA receptors (6), we tested ifenprodil (10 μ M, $n = 9$ slices), an NR2B subunit-containing NMDA receptor antagonist, and found actions on neither the fEPSP slope (Fig. 2E) nor LTP (Fig. 2G). The P2 receptor antagonists pyridoxal-phosphate-6-azophenyl-2',4'-disulfonic acid (PPADS) (50 μ M, $n = 5$ slices) and reactive blue-2 (RB-2) (2 μ M, $n = 4$ slices) had little effect on fEPSP slope (Fig. 2E), suggesting that ATP does not directly activate P2 receptors to mediate astrocytic potentiation of fEPSP and depression of LTP.

Released ATP can be converted into adenosine by ectonucleotidases (16). Because there is a tonic level of extracellular adenosine that acts through the A1 receptor to persistently suppress excitatory synaptic transmission (17–20), we asked whether adenosine mediated the effects of astrocyte-specific dn-SNARE expression. The A1 receptor antagonist

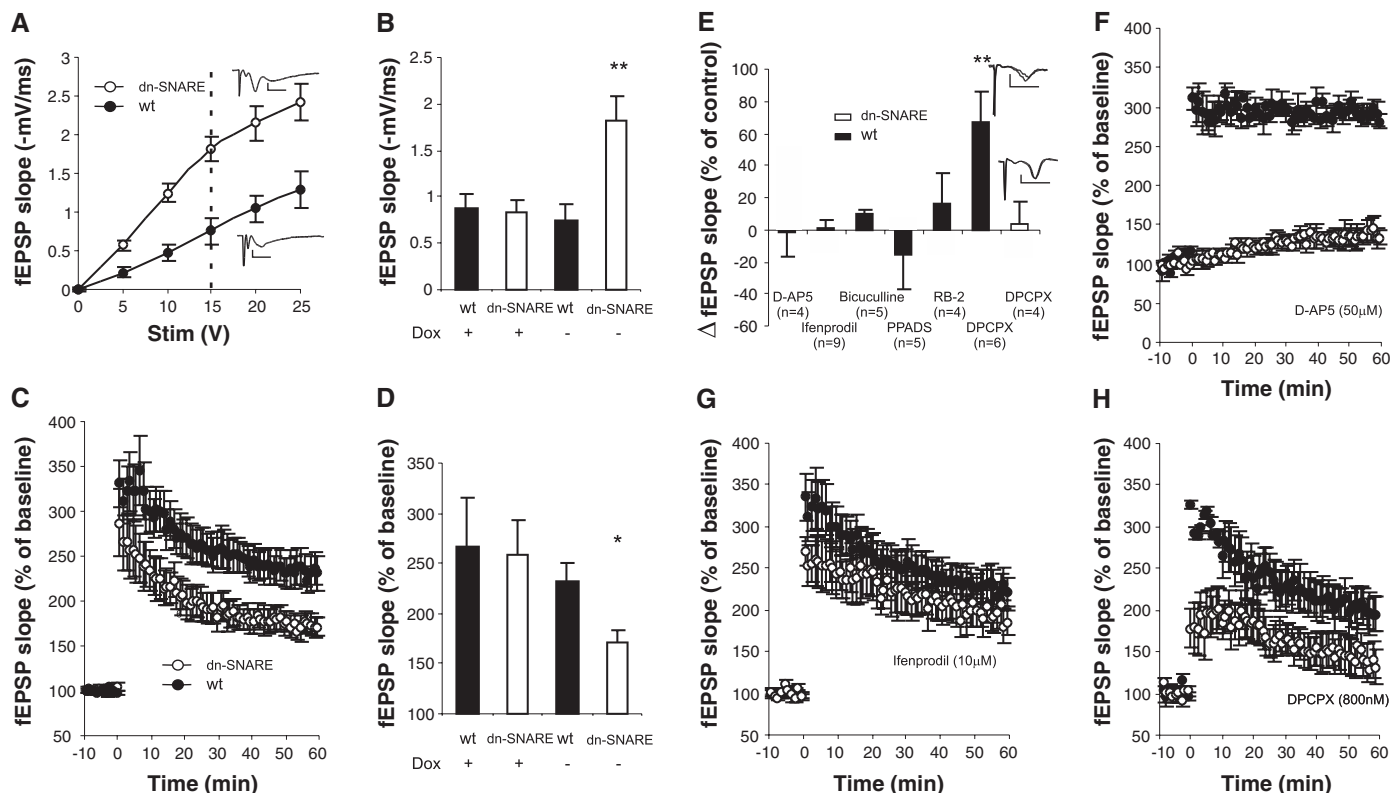


Fig. 2. Astrocytes regulate synaptic transmission and modulate plasticity through the control of extracellular adenosine. (A and B) Slope of Schaffer collateral CA1. fEPSP slope was larger in slices from dn-SNARE mice expressing this transgene ($-$ Dox, $n = 10$ mice) compared to dn-SNARE controls ($+Dox$, $n = 9$ mice) and wild-type (wt) littermates ($+Dox$, $n = 9$ mice; $-Dox$, $n = 10$ mice). **, $P < 0.02$; scale bars, 1 mV, 10 ms. Stim, the dashed line represents the stimulus voltage (Stim) used to evoke the individual example traces shown as inserts. (C and D) The magnitude of theta-burst LTP was smaller when dn-SNARE was expressed in astrocytes

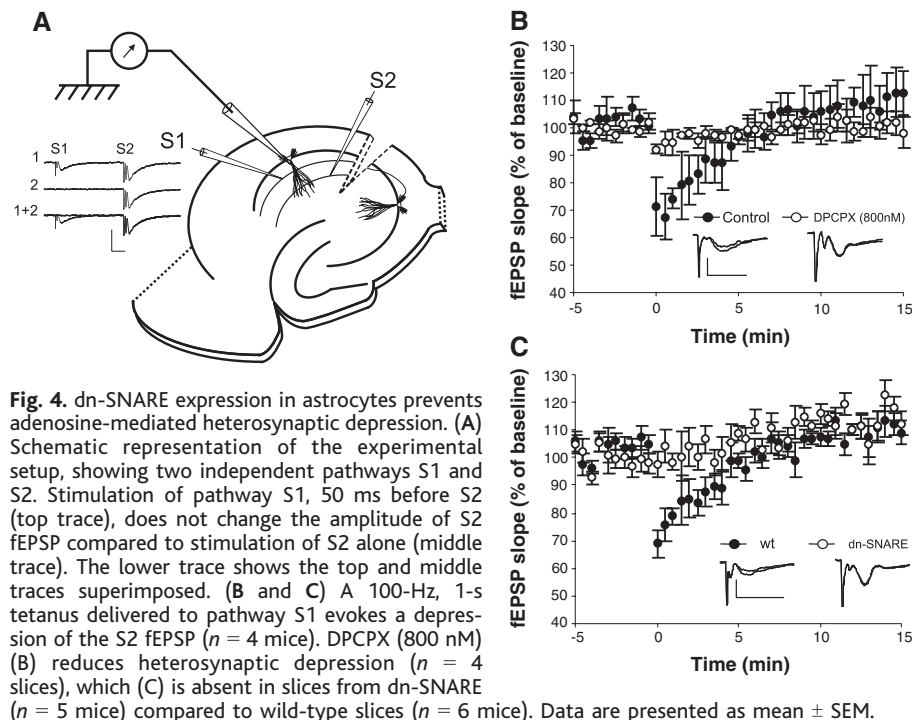
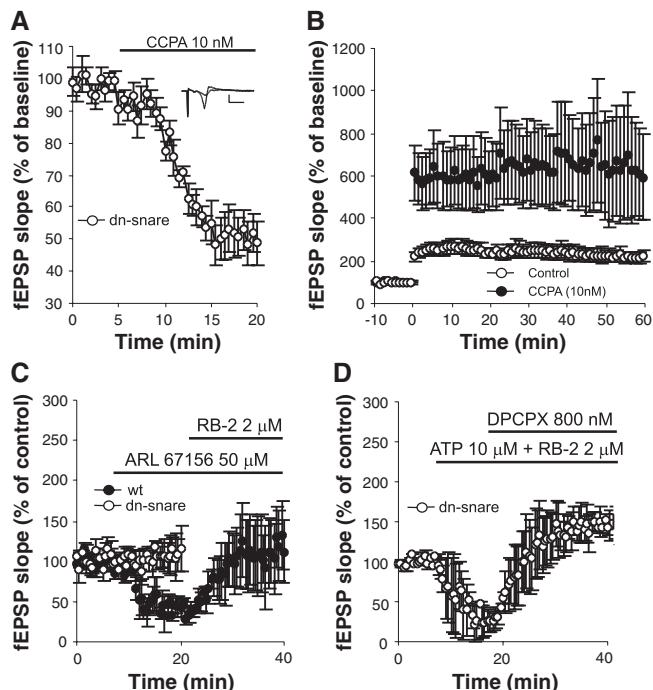
(dn-SNARE $-Dox$, $n = 10$ mice; dn-SNARE $+Dox$, $n = 9$ mice; wt $+Dox$, $n = 9$ mice; and wt $-Dox$, $n = 10$ mice). *, $P < 0.05$. (E) DPCPX (800 nM) augmented the slope of the fEPSP in slices from wild-type (**, $P < 0.05$) but not dn-SNARE ($-Dox$) mice. (F to H) The amplitude of theta-burst LTP in slices from wild-type animals was (F) blocked by D-AP5 (50 μ M, $n = 4$ slices), (G) essentially unchanged by ifenprodil (10 μ M, $n = 9$ slices) and (H) reduced to an extent similar to that observed in dn-SNARE mice ($-Dox$) by incubation in DPCPX (800 nM, $n = 6$ mice). Data are presented as mean \pm SEM.

8-cyclopentyl-1,3-dipropylxanthine (DPCPX) (800 nM) increased the fEPSP slope of wild-type slices by $67 \pm 19\%$ ($n = 6$ mice) (Fig. 2E) and decreased the amplitude of LTP ($n = 6$ slices) (Fig. 2H) to $146 \pm 20\%$, values similar to those measured in hippocampal slices obtained from dn-SNARE mice. In contrast, DPCPX (800 nM) had no effect on baseline synaptic transmission in slices from dn-SNARE

mice ($3 \pm 14\%$, $n = 4$ slices) (Fig. 2E). The A1 agonist 2-chloro-*N*⁶-cyclopentyladenosine (CCPA, 10 nM) reversed the actions of dn-SNARE expression by reducing the amplitude of the baseline fEPSP ($n = 7$ slices) (Fig. 3A) and augmenting the amplitude of LTP ($n = 7$ slices) (Fig. 3B).

There are two potential sources of astrocytic adenosine: loss from the cytosol through

Fig. 3. dn-SNARE expression in astrocytes reduces extracellular ATP, a source of adenosine that regulates synaptic transmission. (A and B) CCPA (10 nM) reverses the effects of dn-SNARE expression by (A) reducing the fEPSP slope and (B) augmenting theta-burst-induced LTP ($n = 7$ slices; scale bar, 1 mV, 10 ms). (C) The ectonucleotidase inhibitor ARL67156 (50 μ M) reduces fEPSP slope in wild-type slices ($n = 3$ slices), an action reversed by the P2 antagonist RB-2 (2 μ M). ARL67156 does not change the fEPSP slope of dn-SNARE slices ($n = 4$ slices), demonstrating an absence of background ATP when dn-SNARE is expressed in astrocytes. (D) ATP, in the presence of RB-2 to block P2-mediated actions, reduces fEPSP slope in dn-SNARE mice ($n = 4$ slices), an action reversed by DPCPX (800 nM). Data are presented as mean \pm SEM.



equilibrative transporters and accumulation resulting from ectonucleotidase-dependent hydrolysis of released ATP. Blockade of equilibrative nucleoside transporter 1 (ENT1) with S-(4-nitrobenzyl)-6-thioinosine (NBMPR, 100 nM), a highly selective ENT-1 antagonist (21), led to a further reduction in basal synaptic transmission (fig. S3), which is consistent with a role for ENT-1 in the uptake rather than the release of adenosine. We therefore studied the release of ATP from astrocytes as the potential source of adenosine accumulation, by using synaptic transmission as a sensitive assay for this nucleotide. Because P2 receptor antagonists do not change the magnitude of synaptic transmission (Fig. 2E), there is insufficient extracellular ATP under normal circumstances to activate synaptic P2 receptors. We asked whether the ectonucleotidase inhibitor ARL67156 (50 μ M) would lead to an accumulation of ATP that would modulate baseline fEPSP amplitude. Superfusion of ARL67156 caused an inhibition of synaptic transmission (Fig. 3C), an action that was reversed by the P2 antagonist RB-2 (2 μ M, $n = 3$ slices). If adenosine accumulation is mediated by the hydrolysis of ATP released from astrocytes, we would predict that the ARL67156-induced synaptic suppression would be absent in slices from dn-SNARE mice. Superfusion of ARL67156 did not significantly change ($9 \pm 22\%$) fEPSP slope in dn-SNARE slices, compared to a $-56 \pm 8\%$ reduction in wild-type slices (Fig. 3C). Luciferin/luciferase imaging of extracellular ATP detected significantly less ($P < 0.05$) extracellular ATP in slices from dn-SNARE mice (12 ± 7 counts s^{-1} , $n = 4$ mice) compared to wild-type (26 ± 8 counts s^{-1} , $n = 4$ mice). These results are consistent with dn-SNARE blocking a previously described vesicular mode of ATP release from astrocytes (22). We then asked whether exogenous ATP would restore A1 receptor-mediated, adenosine-induced synaptic depression. In the presence of RB-2, to block direct actions of ATP on P2 receptors, application of exogenous ATP to dn-SNARE ($n = 4$ slices) or wild-type ($n = 4$ slices) slices similarly induced a reduction in fEPSP slope that was reversed by the A1 antagonist DPCPX (Fig. 3D and fig. S4).

Tetanic stimulation of Schaffer collaterals causes an adenosine-mediated, heterosynaptic depression of neighboring unstimulated synapses (23). However, the source of the adenosine remains an enigma. Because stimulation of the Schaffer collaterals induces Ca^{2+} signals in astrocytes (24), which in turn evoke the release of gliotransmitters (6), and because heterosynaptic depression has been indirectly linked to a glial-dependent mechanism (25), we used the dn-SNARE mice to ask whether astrocytes mediate heterosynaptic depression. Two independent pathways (S1 and S2) were each stimulated at 30-s intervals

to monitor baseline synaptic transmission (Fig. 4A). In wild-type slices, tetanic stimulation of pathway S1 (100 Hz, 1 s) evoked homosynaptic LTP together with a heterosynaptic depression of the neighboring S2 pathway. The addition of an A1 antagonist (DPCPX, 800 nM) prevented heterosynaptic depression (Fig. 4B). To control for effects of enhanced baseline transmission that result in the presence of DPCPX, we switched from normal artificial cerebrospinal fluid (ACSF) to one containing 2.4 mM Ca²⁺ and 0.6 mM Mg²⁺, which enhanced synaptic transmission to 172 ± 8.9% (*n* = 3 slices) of that in control mice. We still found heterosynaptic depression to be intact (64.9 ± 8.2%, *n* = 3 slices) compared to ACSF controls (72.0 ± 8.6%, *n* = 3 slices). To determine whether astrocytes mediate adenosine-dependent depression, we repeated this study using dn-SNARE slices and found a virtual absence of heterosynaptic depression (Fig. 4C).

These studies place the astrocyte at center stage in the control of adenosine. Glial-released ATP, which is rapidly hydrolyzed to adenosine, leads to a persistent synaptic suppression mediated by A1 receptors. Because adenosine is implicated in the control of wake-to-sleep transitions (26, 27) as well as responses to hypoxia, the identification of the central role of the astrocyte in regulating this nucleoside offers mechanistic insights into these processes.

The kinetics of ATP hydrolysis and adenosine accumulation provide a synaptic network with unique spatiotemporal conditions to control synaptic transmission. Fast-acting

synaptic transmitters such as γ -aminobutyric acid and glutamate have high-affinity uptake systems in the vicinity of the synapse that constrain the time and distance over which a transmitter acts. Synaptic activation of an astrocyte to release ATP removes these constraints, because it takes ~200 ms before adenosine begins to accumulate (28). This provides time for ATP diffusion to distant sites, where it depresses synaptic transmission through accumulated adenosine, thereby providing a mechanism for cross-talk to distant synapses. In addition to activity-dependent actions, astrocytes, by persistently suppressing excitatory synaptic transmission, enhance the capability of synapses to express synaptic plasticity. Thus, the integration of synaptic activity by the astrocyte leads to a widespread coordination of synaptic networks. By suppressing excitatory transmission, astrocytes regulate the degree to which a synapse may be plastic, and during the induction of LTP, astrocyte-derived adenosine depresses neighboring unstimulated pathways.

References and Notes

1. A. H. Cornell-Bell, S. M. Finkbeiner, M. S. Cooper, S. J. Smith, *Science* **247**, 470 (1990).
2. A. Verkhratsky, H. Kettenmann, *Trends Neurosci.* **19**, 346 (1996).
3. P. B. Guthrie et al., *J. Neurosci.* **19**, 520 (1999).
4. V. Parpura et al., *Nature* **369**, 744 (1994).
5. M. J. Schell, M. E. Molliver, S. H. Snyder, *Proc. Natl. Acad. Sci. U.S.A.* **92**, 3948 (1995).
6. T. Fellin et al., *Neuron* **43**, 729 (2004).
7. A. Araque, V. Parpura, R. P. Sanzgiri, P. G. Haydon, *Eur. J. Neurosci.* **10**, 2129 (1998).
8. J. Kang, L. Jiang, S. A. Goldman, M. Nedergaard, *Nat. Neurosci.* **1**, 683 (1998).
9. T. A. Fiacco, K. D. McCarthy, *J. Neurosci.* **24**, 722 (2004).

10. A. Araque, R. P. Sanzgiri, V. Parpura, P. G. Haydon, *J. Neurosci.* **18**, 6822 (1998).
11. A. Araque, N. Li, R. T. Doyle, P. G. Haydon, *J. Neurosci.* **20**, 666 (2000).
12. P. Bezzi et al., *Nat. Neurosci.* **7**, 613 (2004).
13. L. Pasti, M. Zonta, T. Pozzan, S. Vicini, G. Carmignoto, *J. Neurosci.* **21**, 477 (2001).
14. Materials and methods are available as supporting material on Science Online.
15. Q. Zhang et al., *J. Biol. Chem.* **279**, 12724 (2004).
16. H. Zimmermann, N. Braun, *J. Auton. Pharmacol.* **16**, 397 (1996).
17. T. V. Dunwiddie, B. J. Hoffer, *Br. J. Pharmacol.* **69**, 59 (1980).
18. T. V. Dunwiddie, S. A. Masino, *Annu. Rev. Neurosci.* **24**, 31 (2001).
19. M. Kukley, M. Schwan, B. B. Fredholm, D. Dietrich, *J. Neurosci.* **25**, 2832 (2005).
20. K. A. Moore, R. A. Nicoll, D. Schmitz, *Proc. Natl. Acad. Sci. U.S.A.* **100**, 14397 (2003).
21. M. A. Ackley et al., *J. Physiol.* **548**, 507 (2003).
22. S. Coco et al., *J. Biol. Chem.* **278**, 1354 (2003).
23. O. J. Manzoni, T. Manabe, R. A. Nicoll, *Science* **265**, 2098 (1994).
24. J. T. Porter, K. D. McCarthy, *J. Neurosci.* **16**, 5073 (1996).
25. J. M. Zhang et al., *Neuron* **40**, 971 (2003).
26. T. Porkka-Heiskanen, L. Alanko, A. Kalinchuk, D. Stenberg, *Sleep Med. Rev.* **6**, 321 (2002).
27. R. Basheer, R. E. Strecker, M. M. Thakkar, R. W. McCarley, *Prog. Neurobiol.* **73**, 379 (2004).
28. T. V. Dunwiddie, L. Diao, W. R. Proctor, *J. Neurosci.* **17**, 7673 (1997).
29. We thank I. Levitan and T. Abel for constructive criticism on versions of this manuscript, T. Abel for his constant guidance, and R. Thresher, H. Bujard, and M. Brenner for constructs used to generate transgenic vectors. Supported by funds from the National Institute of Neurological Disorders and Stroke and the National Institute of Mental Health to K.M., S.J.M., and P.G.H.

Supporting Online Material

www.sciencemag.org/cgi/content/full/310/5745/113/DC1
Materials and Methods
Figs. S1 to S4

5 July 2005; accepted 7 September 2005
10.1126/science.1116916

Failure to Detect Mismatches Between Intention and Outcome in a Simple Decision Task

Petter Johansson,^{1*} Lars Hall,^{1*†} Sverker Sikström,¹ Andreas Olsson²

A fundamental assumption of theories of decision-making is that we detect mismatches between intention and outcome, adjust our behavior in the face of error, and adapt to changing circumstances. Is this always the case? We investigated the relation between intention, choice, and introspection. Participants made choices between presented face pairs on the basis of attractiveness, while we covertly manipulated the relationship between choice and outcome that they experienced. Participants failed to notice conspicuous mismatches between their intended choice and the outcome they were presented with, while nevertheless offering introspectively derived reasons for why they chose the way they did. We call this effect choice blindness.

A fundamental assumption of theories of decision making is that intentions and outcomes form a tight loop (1). The ability to monitor and to compare the outcome of our choices with prior intentions and goals is seen to be

critical for adaptive behavior (2–4). This type of cognitive control has been studied extensively, and it has been proposed that intentions work by way of forward models (5) that enable us to simulate the feedback from

our choices and actions even before we execute them (6, 7).

However, in studies of cognitive control, the intentions are often tightly specified by the task at hand (8–10). Although important in itself, this type of research may not tell us much about natural environments where intentions are plentiful and obscure and where the actual need for monitoring is unknown. Despite all its shortcomings, the world is in many ways a forgiving place in which to implement our decisions. Mismatches between intention and outcome are surely possible, but when we reach for a bottle of beer, we very seldomly end up with a glass of milk in our hands. But what if the world were less forgiving? What if it instead conspired to create discrepancies between the choices we make and the feedback we get? Would we always

¹Lund University Cognitive Science, Lund University, Kungshuset Lundagård, 222 22 Lund, Sweden. ²Department of Psychology, New York University, 6 Washington Place, New York, NY 10003, USA.

*These authors contributed equally to this work.
†To whom correspondence should be addressed.
E-mail: lars.hall@lucs.lu.se

be able to tell if an error were made? And if not, what would we think, and what would we say?

To examine these questions, we created a choice experiment that permitted us to surreptitiously manipulate the relationship between choice and outcome that our participants experienced. We showed picture pairs of female faces to 120 participants (70 female) and asked them to choose which face in each pair they found most attractive. On some trials, immediately after their choice, they were asked to verbally describe the reasons for choosing the way they did. Unknown to the participants, on certain trials, a double-card ploy was used to covertly exchange one face for the other (Fig. 1). Thus, on these trials, the outcome of the choice became the opposite of what they intended. Each subject completed a sequence of 15 face pairs, three of which were manipulated (M). The M face pairs always appeared at the same position in the sequence, and for each of these pairs, participants were asked to state the reasons behind their choice. Verbal reports were also solicited for three trials of non-manipulated (NM) pairs (11).

The experiment employed a 3-by-2, between-group factorial design, with deliberation time and similarity of the face pairs as factors. For time, three choice conditions were included: one with 2 s of deliberation time, one with 5 s, and one where participants could take as much time as they liked. Participants generally feel that they are able to form an opinion given 2 s of deliberation time (supporting online text). Nevertheless, the opportunity for participants to enjoy free deliberation time was included to provide an individual criterion of choice. For similarity, we created two sets of target faces, a high-similarity (HS) and a low-similarity (LS) set (fig. S1). Using an interval scale from 1 to 10, where 1 represents “very dissimilar” and 10 “very similar,” the HS set had a mean similarity of 5.7 (SD = 2.1) and the LS set a mean similarity of 3.4 (SD = 2.0).

Detection rates for the manipulated pictures were measured both concurrently, during the experimental task, and retrospectively, through a post-experimental interview (11) (supporting online text). There was a very low level of concurrent detection. With a total of 354 M trials performed, only 46 (13%) were detected concurrently. Not even when participants were given free deliberation time and a set of LS faces to judge were more than 27% of all trials detected this way. There were no significant differences in detection rate between the 2-s and 5-s viewing time conditions, but there was a higher detection rate in the free compared to the fixed viewing time conditions [$t(118) = 2.17, P < 0.05$]. Across all conditions, there were no differences in detection rate between the HS and the LS sets (Fig. 2A). In addition, there were no significant sex or age differences in detection rate. Tallying all forms of detec-

tion across all groups revealed that no more than 26% of all M trials were exposed.

However, these figures are inflated even so. The moment a detection is made, the outlook of the participants changes: They become suspicious, and more resources are diverted to monitoring and control. To avoid such cascading detection effects, it is necessary to discard all trials after the first detection is made. Figure 2B shows detection rates with this correction in place. The overall detection rate was significantly lower [$t(118) = 3.21, P < 0.005$], but none of our prior conclusions are affected by the use of this data set (the percentage of participants that detected the manipulation is shown in fig. S2).

Our experiment indicates that the relationship between intentions and outcomes may sometimes be far looser than what current theorizing has suggested (6, 9). The detection rate was not influenced by the similarity of the face pairs, indicating the robustness of the finding. The face pairs of the LS set bore very little resemblance to each other, and it is hard to imagine how a choice between them could be confused (fig. S1 and supporting online text). The overall detection rate was higher when participants were given free deliberation time.

This shows the importance of allowing individual criteria to govern choice, but it is not likely to indicate a simple subjective threshold. The great majority of the participants in the 2-s groups believed themselves to have had enough time to make a choice (as determined by post-test interviews), and there was no difference in the actual distribution of choices among the pairs from fixed to free deliberation time.

Next, we examined the relationship between choice and introspective report. One might suspect that the reports given for NM and M trials would differ in many ways. After all, the former reports stem from a situation common to everyday life (revealing the reasons behind a choice), whereas the latter reports stem from a truly anomalous one (revealing the reasons behind a choice one manifestly did not make).

We classified the verbal reports into a number of different categories that potentially could differentiate between NM and M reports. For all classifications, we used three independent blind raters, and interrater reliability was consistently high (supporting online text and table S1). We found no differences in the number of empty reports (when participants were unable to present any reasons at all) or in the

Fig. 1. A snapshot sequence of the choice procedure during a manipulation trial. (A) Participants are shown two pictures of female faces and asked to choose which one they find most attractive. Unknown to the participants, a second card depicting the opposite face is concealed behind the visible alternatives. (B) Participants indicate their choice by pointing at the face they prefer the most. (C) The experimenter flips down the pictures and slides the hidden picture over to the participants, covering the previously shown picture with the sleeve of his moving arm. (D) Participants pick up the picture and are immediately asked to explain why they chose the way they did.

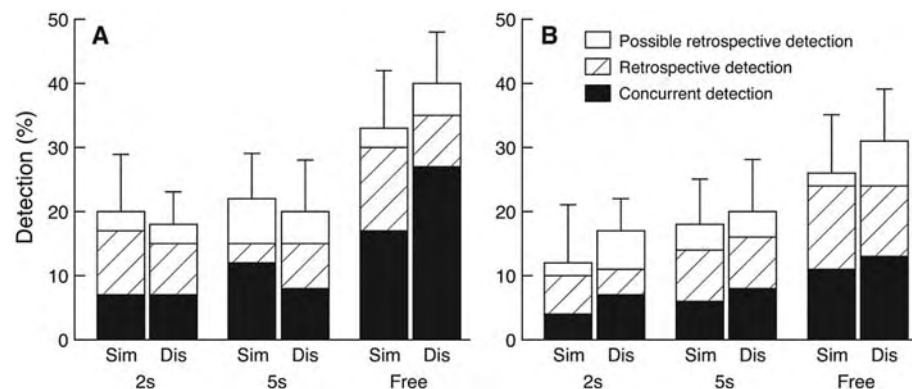
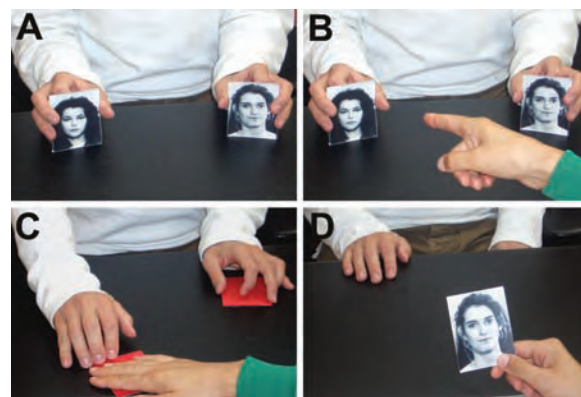


Fig. 2. Percent detection, divided into deliberation time and similarity, for (A) all trials and (B) trials corrected for prior detections. Sim, similar (HS); Dis, dissimilar (LS). Error bars indicate the standard deviation of the means.

degree to which reports were phrased in present or past tense (which might indicate whether the report is made in response to the present face or the prior context of choice). Neither did the length of the statements, as measured by number of characters, differ between the two sets (NM = 33, SD = 45.4; M = 38, SD = 44.4), nor the amount of laughter present in the reports (with laughter being a potential marker of nervousness or distress). We found significantly more dynamic self-commentary in the M reports [$t(118) = 3.31, P < 0.005$]. In this type of commentary, participants come to reflect upon their own choice (typically by questioning their own prior motives). However, even in the M trials, such reports occurred infrequently (5% of the M reports).

We rated the reports along three dimensions: emotionality, specificity, and certainty (using a

numeric scale from 1 to 5). Emotionality was defined as the level of emotional engagement in the report, specificity as the level of detail in the description, and certainty as the level of confidence in their choice the participants expressed. There were no differences between the verbal reports elicited from NM and M trials with respect to these three categories (fig. S3). Seemingly, the M reports were delivered with the same confidence as the NM ones, and with the same level of detail and emotionality. One possible explanation is that overall engagement in the task was low, and this created a floor effect for both NM and M reports. However, this is unlikely to be the case. All three measures were rated around the midline on our scale (emotionality = 3.5, SD = 0.9; specificity = 3.1, SD = 1.2; certainty = 3.3, SD = 1.1). Another possibility is that the lack of

differentiation between NM and M reports is an indication that delivering an M report came naturally to most of the participants in our task. On a radical reading of this view, a suspicion would be cast even on the NM reports. Confabulation could be seen to be the norm and truthful reporting something that needs to be argued for.

To scrutinize these possibilities more closely, we conducted a final analysis of the M reports, adding a contextual dimension to the classification previously used. Figure 3 shows the percentage of M reports falling into eight different categories. The “specific confabulation” category contains reports that refer to features unique to the face participants ended up with in a manipulated trial. As these reports cannot possibly be about the original choice (i.e., “I chose her [the blond woman] because she had dark hair”), this would indeed be an indisputable case of “telling more than we can know” (12). Equally interesting is the “original choice” category. These are reports that must be about the original choice, because they are inconsistent with the face participants ended up with (i.e., “I chose her because she smiled [said about the solemn one]”). Here, despite the imposing context of the manipulated choice, vestiges of the original intention are revealed in the M reports. Analogous to the earlier example of confabulation, this would be an unquestionable case of truthful report.

In summary, when evaluating facial attractiveness, participants may fail to notice a radical change to the outcome of their choice. As an extension of the well-known phenomenon of change blindness (13), we call this effect choice blindness (supporting online text). This finding can be used as an instrument to estimate the representational detail of the decisions that humans make (14). We do not doubt that humans can form very specific and detailed prior intentions, but as the phenomenon of choice blindness demonstrates, this is not something that should be taken for granted in everyday decision tasks. Although the current experiment warrants no conclusions about the mechanisms behind this effect, we hope it will lead to an increased scrutiny of the concept of intention itself. As a strongly counterintuitive finding, choice blindness warns of the dangers of aligning the technical concept of intention too closely with common sense (15, 16).

In addition, we have presented a method for studying the relationship between choice and introspection. Classic studies of social psychology have shown that telling discrepancies between choice and introspection can sometimes be discerned in group-level response patterns (12) but not for each of the individuals at hand. In the current experiment, using choice blindness as a wedge, we were able to “get between” the decisions of the participants and the outcomes with which they were presented.



Type	%		
Specific Conf.	13.3		She's radiant. I would rather have approached her at a bar than the other one. I like earrings! [M]
Detailed Conf.	17.3	She looks like an aunt of mine I think, and she seems nicer than the other one. [F]	
Emotional Conf.	9.3		Yes, well, [laughter] she looks very hot in this picture. [M]
Simple Conf.	10.8		Just a nice shape of the face, and the chin. [M]
Relational Conf.	21.3		I thought she had more personality, in a way. She was the most appealing to me. [F]
Uncertainty	11.6	Eh... I don't know. [F]	
Dynamic report	5.2		Oh, [short laughter] Why did I choose her? She looks very masculine! [M]
Original choice	11.2	Because she was smiling. [F]	

Fig. 3. Frequency distribution of the contents of the M reports aligned along a rough continuum from confabulatory to truthful report. Sample sentences (translated from Swedish) are drawn from the set of reports for the displayed face pair. Letters in brackets indicate whether the report was given by a male (M) or a female (F) participant. The specific confabulation (Conf.) category contains reports that refer to features unique to the face participants ended up with in an M trial. The detailed and emotional confabulation categories contain reports that rank exceptionally high on detail and emotionality (>4.0 on a scale from 1 to 5). The simple and relational confabulation categories include reports where the generality of the face descriptions precluded us from conclusively associating them with either of the two faces (i.e., everybody has a nose, and a personality). The category of uncertainty contains reports dominated by uncertainty (<2 on a scale from 1 to 5). The dynamic reports are reports in which participants reflect upon their own choice, and the final category contains reports that refer to the original context of choice.

This allowed us to show, unequivocally, that normal participants may produce confabulatory reports when asked to describe the reasons behind their choices. More importantly, the current experiment contains a seed of systematicity for the study of choice and subjective report. The possibility of detailing the properties of confabulation that choice blindness affords could give researchers an increased foothold in the quest to understand the processes behind truthful report.

References and Notes

1. K. R. Ridderinkhof, W. P. M. van den Wildenberg, S. J. Segalowitz, C. S. Carter, *Brain Cogn.* **56**, 129 (2004).
 2. K. R. Ridderinkhof, M. Ullsberger, E. A. Crone, S. Nieuwenhuis, *Science* **306**, 443 (2004).

3. M. Ullsperger, D. Y. Cramon, *Cortex* **40**, 593 (2004).
 4. M. E. Walton, J. T. Devlin, M. F. S. Rushworth, *Nat. Neurosci.* **7**, 1259 (2004).
 5. P. Haggard, S. Clark, *Conscious. Cogn.* **12**, 695 (2003).
 6. R. Grush, *Behav. Brain Sci.* **27**, 377 (2004).
 7. D. M. Wolpert, K. Doya, M. Kawato, *Philos. Trans. R. Soc. London Ser. B.* **358**, 593 (2003).
 8. J. G. Kerns et al., *Science* **303**, 1023 (2004).
 9. R. Hester, C. Fassbender, H. Garavan, *Cereb. Cortex* **14**, 986 (2004).
 10. H. C. Lau, R. D. Rogers, P. Haggard, R. E. Passingham, *Science* **303**, 1208 (2004).
 11. Materials and methods are available as supporting material on Science Online.
 12. R. E. Nisbett, T. D. Wilson, *Psychol. Rev.* **84**, 231 (1977).
 13. R. A. Rensink, *Annu. Rev. Psychol.* **53**, 245 (2002).
 14. D. J. Simons, R. A. Rensink, *Trends Cogn. Sci.* **9**, 16 (2005).
 15. D. C. Dennett, *The Intentional Stance* (MIT Press, Cambridge, MA, 1987).
 16. D. M. Wegner, *The Illusion of Conscious Will* (MIT Press, Cambridge, MA, 2003).

17. We thank D. de Léon, K. Holmqvist, P. Björne, P. Gärdenfors, T. Dickens, N. Humphrey, A. Marcel, Q. Rahman, E. Adams, N. Bolger, B. Cohen, and E. Phelps for useful comments and discussions. We also thank C. Balkenius for providing the illustrations for the article and P. Rosengren for invaluable advice concerning the use of card magic techniques. Supported by The New Society of Letters at Lund (P.J.), The Knowledge Foundation, The Erik Philip-Sörensen Foundation (L.H.), and the Swedish Research Council (S.S.).

Supporting Online Material
www.sciencemag.org/cgi/content/full/310/5745/116/DC1
 Materials and Methods
 SOM Text
 Figs. S1 to S3
 Table S1

2 March 2005; accepted 23 August 2005
 10.1126/science.1111709

Sexual Selection Can Resolve Sex-Linked Sexual Antagonism

Arianne Y. K. Albert* and Sarah P. Otto

Sexual selection is a potent evolutionary force. However, very few models have considered the evolution of female preferences for traits expressed in both sexes. Here we explore how female preferences coevolve with sexually antagonistic traits, which involve alleles that are beneficial to one sex but harmful to the other. We show that with a sexually antagonistic trait on the X chromosome (males XY, females XX), females evolve to prefer mates carrying alleles beneficial to daughters. In contrast, with a Z-linked trait (males ZZ, females ZW), females more often evolve mating preferences for mates carrying alleles beneficial to sons (that is, flashy displays).

Evolutionary biologists have long puzzled over how and why female preferences drive the evolution of exaggerated male traits. Generally, female preferences are thought to enhance a female's long-term fitness by increasing her offspring's fitness, either directly or through genetic associations between preference and trait loci (1, 2). Nearly all models assume that females do not initially express the male display trait, or else they assume that the fitness effects are the same in males and females (3). However, traits subject to sexual selection will often be sexually antagonistic, for example, with "sexy" male traits benefiting males but reducing female fitness (4-6). If a trait increases male reproductive success at the cost of female viability, females must then choose between having attractive sons (and unfit daughters) and having ugly sons (but unencumbered daughters). As long as females can detect the genotypic differences among males at sexually antagonistic loci, we expect mating preferences to evolve as described by the models explored here.

Theory predicts that sexually antagonistic loci are more likely to remain polymorphic on

the sex chromosomes (4, 5). Furthermore, recent empirical work suggests that many sexually selected traits in animals are located on the X chromosome (7, 8) and that most polymorphic sexually antagonistic traits are located on the X chromosome in *Drosophila* (5, 9). There is also evidence to suggest that a female's mate choice may result in a tradeoff in the fitness between her daughters and sons (10). Several recent theoretical examinations of the evolution of female preferences have explored sex linkage of the trait and/or preference (11-14). However, these models, with the exception of Reeve and Pfennig's (12),

assume that sexually selected traits have male-limited expression and therefore no fitness consequences when in females, and none has addressed sexual antagonism. Here we address the question of how female preferences evolve for traits that have contrasting fitness effects in each sex.

With sexual antagonism, chromosomal location should strongly affect the evolution of female preferences. Simply put, an X-linked male trait is never passed on from an attractive father to his sons, whereas his daughters suffer the cost of carrying the display trait (5, 9). Offspring in XY species therefore do not gain a fitness benefit from females preferring males with a more extreme X-linked display trait. In contrast, both males and females contribute a Z chromosome to sons in ZW species. Thus, females preferring a Z-linked display trait receive the fitness benefit of sexy sons, even though their daughters suffer a fitness cost (5, 9). This cost is lessened by the fact that daughters inherit only one of their father's Z chromosomes. With autosomal inheritance, these asymmetries in inheritance are absent.

To verify the verbal argument laid out above, we present the results of two-locus models that follow the fate of a newly arisen preference allele *p* in a population that is at a polymorphic equilibrium at a trait locus. We assume that

Table 1. Male and female fitness components in male heterogametic (XY) and female heterogametic (ZW) species.

	X-linked trait			Z-linked trait		
	<i>Male trait</i>					
		<i>T</i>	<i>t</i>	<i>TT</i>	<i>Tt</i>	<i>tt</i>
Female preference	<i>PP</i>	1	1 + <i>a_{pp}</i>	<i>P</i>	1 + <i>da_p</i>	1 + <i>a_p</i>
	<i>Pp</i>	1	1 + <i>a_{Pp}</i>	<i>p</i>	1 + <i>da_p</i>	1 + <i>a_p</i>
	<i>pp</i>	1	1 + <i>a_{pp}</i>			
Male viability		1 - <i>s_y</i>	1	1 - <i>s_z</i>	1 - <i>hs_z</i>	1
	<i>Female trait</i>					
		<i>TT</i>	<i>Tt</i>	<i>tt</i>	<i>T</i>	<i>t</i>
Female viability		1	1 - <i>hs_x</i>	1 - <i>s_x</i>	1	1 - <i>s_w</i>
	<i>Female preference</i>					
		<i>PP</i>	<i>Pp</i>	<i>pp</i>	<i>P</i>	<i>p</i>
Female cost		1 - <i> a_{pp} k</i>	1 - <i> a_{Pp} k</i>	1 - <i> a_{pp} k</i>	1 - <i> a_p k</i>	1 - <i> a_p k</i>

Department of Zoology, University of British Columbia, Vancouver, British Columbia V6T 1Z4, Canada.

*To whom correspondence should be addressed. E-mail: albert@zoology.ubc.ca

allele *T* is most fit in females (“female-benefit allele”) and allele *t* is most fit in males (“male-benefit allele”), with this tradeoff mediated by natural selection, sexual selection, or both. In the X-linked model, females with a *tt* genotype suffer a fitness disadvantage of $1 - s_x$ relative to *TT* females, where s_x is the strength of selection in females, and the fitness of *Tt* females is given by $1 - hs_x$, where *h* is a dominance coefficient. In the absence of sexual selection, males carrying the *T* allele have a relative fitness of $1 - s_y$ relative to males with the *t* allele (Table 1). Note that s_y can be positive or negative, allowing for natural selection either for or against the trait allele *t* in males. The mating preference of a female of genotype *i* at the preference locus is given by a_p , which describes the relative increase (or decrease) in the female’s probability of mating with males carrying allele *t* (Table 1) (3). We also allow for selection against the female preference by reducing fe-

male fitness by an amount proportional to her choosiness and a cost parameter, *k* (15). The fitness scheme in the Z-linked model is similar (Table 1). However, an additional parameter, *d*, is required to describe female preferences for heterozygous males when the preference locus is Z-linked. When both trait and preference loci are sex-linked, recombination occurs at a rate *r* between them; autosomal preference loci were also considered, in order to examine the influence of physical linkage on the results. Finally, both autosomal preference and trait loci were modeled. The analytical solutions for the polymorphic equilibria and the invasion rate of a new preference allele, *p*, are approximated assuming weak selection (s_x, s_y, a_p , and *k* are small).

There are three ultimate fates for sexually antagonistic genes: (i) the fixation of the allele with the higher fitness across both sexes, (ii) the evolution of sex-specific expression, or (iii) polymorphism (4, 5). A polymorphic equilib-

rium for an X-linked trait is maintained by sexually antagonistic selection in the X-linked model with allele *P* fixed as long as

$$2hs_x < (a_{pp} + s_y) < 2s_x(1 - h) \quad (1)$$

which requires that the male-benefit allele, *t*, be wholly or partially recessive in females ($h < 1/2$). As long as Eq. 1 holds, the model allows for the maintenance of polymorphism either by sexually antagonistic natural selection ($s_y > 0$) and/or by sexual selection opposing natural selection ($a_{pp} > 0$). Similar criteria for maintaining a polymorphic equilibrium at a Z-linked trait locus are presented in (15).

Performing a stability analysis, a new preference allele, *p*, invades a population that is polymorphic for an X-linked trait locus whenever it confers a stronger preference for males bearing the female-benefit allele, *T* ($a_{pp} < a_{pp}$). This result holds regardless of the physical location of the preference locus. Whereas recombination breaks apart genetic associations, it also places preference alleles on the same chromosome as the trait alleles that have been preferred and is therefore critical to the development of genetic associations. These two factors balance, causing the level of genetic associations to be fairly insensitive to the recombination rate.

In contrast to the X-linked case, when both the trait and preference loci are Z-linked, allele *p* can invade a population only when it confers a stronger preference for the male-benefit allele, *t* ($a_p > a_p$). Again, the recombination rate does not alter the range of conditions under which invasion occurs. However, when the trait locus is Z-linked and the preference locus is autosomal, *p* invades only when it increases the preference for the female-benefit allele, *T* ($a_{pp} < a_{pp}$), as in the X-linked case. Adding a cost of female preference to both the X- and Z-linked models just slows the spread of stronger preference alleles, as long as the costs are not too strong relative to selection acting on the trait locus (15).

Finally, if all of the loci are autosomal, there is no longer any selection for females to prefer traits that help only one sex, and the invasion of any particular preference allele depends crucially on the level of linkage (15). This is consistent with a previous model (16), which found that sexual selection could resolve a polymorphism of a male-limited trait either in favor of *T* or *t*.

To understand the selective forces at work, we performed a quasi-linkage equilibrium analysis (17). When females carrying a new allele *p* preferentially mate with males carrying *T*, for example, a positive genetic association develops between the *p* and *T* alleles. In the homogametic sex (either XX females or ZZ males), both cis and trans linkage disequilibrium are present and approximately equal in magnitude, but only cis disequilibrium can be

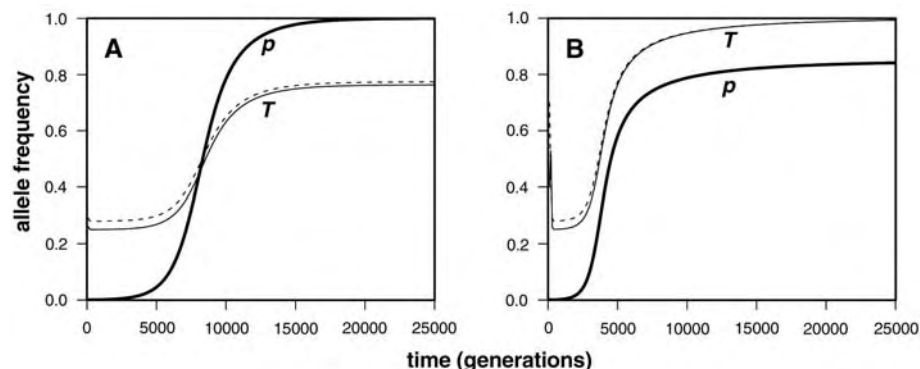


Fig. 1. Simulation results for the evolution of female preferences in male heterogametic species (XY). All simulations were started under conditions allowing a polymorphic equilibrium at an X-linked trait locus with *P* fixed. (A) A new allele *p* that prefers males carrying the female-benefit allele, *T*, is introduced and sweeps to fixation, leaving *T* polymorphic at a higher frequency and improving the fitness of daughters ($a_{pp} = 0.1, a_{pp} = 0, a_{pp} = -0.1$). (B) A preference allele favoring the *T* allele sweeps to high frequency, driving *T* to fixation. Sexual antagonism is thus completely resolved in favor of females ($a_{pp} = 0.1, a_{pp} = -0.1, a_{pp} = -0.2$). Both loci are X-linked, with $r = 0.5, h = 0.1, s_x = 0.2$, and $s_y = 0.2$. The frequency of *T* is shown in thin curves, and males are shown with dashed curves. The frequency of *p* is in bold, with indistinguishable curves for males and females.

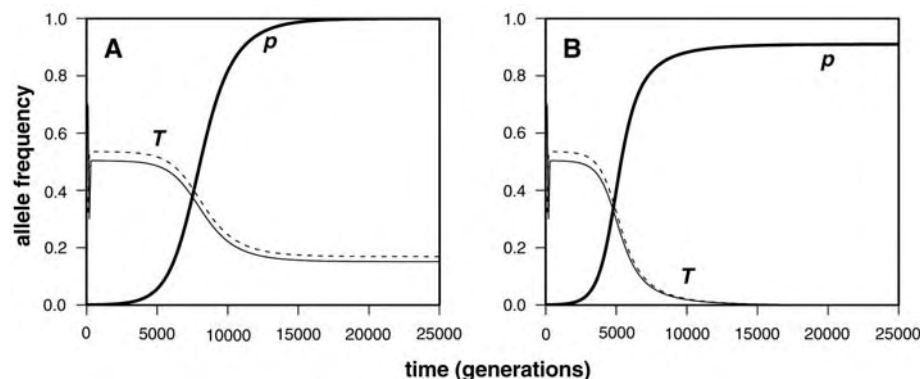


Fig. 2. Simulation results for the evolution of female preferences in female heterogametic species (ZW). (A) A new allele *p* that prefers males carrying the male-benefit allele, *t*, sweeps to fixation, driving *t* to high frequency and improving the fitness of sons ($a_p = -0.1, a_p = 0.08$). (B) A preference allele *p* favoring the *t* allele sweeps to high frequency, driving *t* to fixation ($a_p = -0.1, a_p = 0.2$). Sexual antagonism is thus completely resolved in favor of males. Both loci are Z-linked, with $r = 0.5, d = 0.5, h = 0.2, s_w = 0.224$, and $s_z = 0.3$. The curve types are the same as in Fig. 1.

present in the heterogametic sex (either XY males or ZW females when the preference is Z-linked). Consequently, the new preference allele rises by association with *T* in XX females (in whom *T* is favored) by twice the amount that it goes down in XY males (in whom *t* is favored), explaining the spread of female preferences for the trait favored in females among XY species. Conversely, when both the trait and preference are Z-linked, the new preference allele declines by association with *T* in ZZ males (in whom *t* is favored) by twice the amount that it goes up in ZW females (in whom *T* is favored), explaining why sexual selection does not favor preferences for the allele beneficial to daughters.

When the trait is Z-linked but the preference locus is autosomal, the situation is slightly more complex. Both sons and daughters now inherit two copies of the preference allele, but daughters inherit only one copy of the trait allele. Because daughters' trait alleles are only inherited from their father, stronger trans disequilibrium develops between the preference allele inherited from their mothers and the trait allele inherited from their fathers. The stronger genetic associations that develop in daughters than in sons again favor the spread of preferences for the female-benefit allele, *T*.

The conditions for the invasion of a new preference allele were determined assuming weak selection. How robust are these results to stronger selection? Simulations with selection coefficients on the order of 10 to 30% were explored; selection coefficients in this range are not uncommon (18). Invasion depends only on how the new preference allele changes female mating preferences and not on the strength of selection, confirming our analytical results (Figs. 1 and 2)

Our results point to a potentially large effect of the sex-determination mechanism on how female preferences evolve for sexually antagonistic traits. Over long time scales, evolutionary changes in female preferences will lead to the fixation of the trait alleles most fit in females in XY systems and ZW systems when the preference is autosomal, but the trait allele most fit in males in ZW systems with Z-linked preferences. Thus, sexually antagonistic selection is always resolved in favor of females in XY species (Fig. 1B), but in favor of males in ZW species when the preference is Z-linked (Fig. 2B). This process can occur very rapidly if the new allele has a strong effect on preferences.

Assuming the conditions of our model, we predict that the difference in fitness between daughters and sons should be greater for females that choose mates relative to females mating at random. Choosy females should produce daughters that are more fit than sons in XY systems and vice versa in ZW systems. Another prediction of our model is that female preferences can evolve more easily for male-benefit alleles in ZW species, which is con-

sistent with the greatly exaggerated displays observed in groups such as birds and butterflies (12). This prediction calls for phylogenetic analyses of the association between flashy displays and sex determination. Finally, our model predicts that sex-linked polymorphisms maintained by sexually antagonistic selection should disappear faster when sexual selection is present and as long as the females can detect the polymorphism. Once female preferences have resolved sexually antagonistic selection and become established within a species, they could cause the further evolution of flashy male displays at loci throughout the genome (11).

References and Notes

1. M. Andersson, *Sexual Selection* (Princeton Univ. Press, Princeton, 1994).
2. H. Kokko, R. Brooks, M. D. Jennions, J. Morley, *Proc. R. Soc. London Ser. B* **270**, 653 (2003).
3. M. Kirkpatrick, *Evolution* **36**, 1 (1982).
4. W. R. Rice, *Evolution* **38**, 735 (1984).
5. W. R. Rice, A. K. Chippindale, *J. Evol. Biol.* **14**, 685 (2001).
6. J. Seger, R. Trivers, *Nature* **319**, 771 (1986).
7. K. Reinhold, *Behav. Ecol. Sociobiol.* **44**, 1 (1998).
8. A. Lindholm, F. Breden, *Am. Nat.* **160**, S214 (2002).
9. J. R. Gibson, A. K. Chippindale, W. R. Rice, *Proc. R. Soc. London Ser. B* **269**, 499 (2002).

10. K. M. Fedorka, T. A. Mousseau, *Nature* **429**, 65 (2004).
11. I. M. Hastings, *Proc. R. Soc. London Ser. B* **258**, 83 (1994).
12. H. K. Reeve, D. W. Pfennig, *Proc. Natl. Acad. Sci. U.S.A.* **100**, 1089 (2003).
13. J. A. Andrés, E. H. Morrow, *J. Evol. Biol.* **16**, 219 (2003).
14. M. Kirkpatrick, D. W. Hall, *Evolution* **58**, 683 (2004).
15. Information on recursions and stability analyses, including details of the cost and autosomal models, is available as supporting material on Science Online.
16. S. P. Otto, *Evolution* **45**, 1443 (1991).
17. M. Kirkpatrick, T. Johnson, N. Barton, *Genetics* **161**, 1727 (2002).
18. J. G. Kingsolver *et al.*, *Am. Nat.* **157**, 245 (2001).
19. We are indebted to M. Drapeau and T. Long for discussions that inspired this model. We thank T. Vines, D. Schluter, M. Kirkpatrick, A. Agrawal, and the SOWD group for comments and discussions. A.Y.K.A. was supported by a Natural Sciences and Engineering Research Council of Canada (NSERC) postgraduate scholarship, and S.P.O. was supported by an NSERC discovery grant.

Supporting Online Material

www.sciencemag.org/cgi/content/full/310/5745/119/DC1

Materials and Methods

Tables S1 and S2

References

26 May 2005; accepted 7 September 2005
10.1126/science.1115328

Arabidopsis H⁺-PPase AVP1 Regulates Auxin-Mediated Organ Development

Jisheng Li,^{1*} Haibing Yang,^{1*} Wendy Ann Peer,³ Gregory Richter,²
Joshua Blakeslee,³ Anindita Bandyopadhyay,³
Boosaree Titapiwantakun,³ Soledad Undurraga,¹
Mariya Khodakovskaya,¹ Elizabeth L. Richards,³ Beth Krizek,⁴
Angus S. Murphy,³ Simon Gilroy,² Roberto Gaxiola^{1†}

The transport of auxin controls developmental events in plants. Here, we report that in addition to maintaining vacuolar pH, the H⁺-pyrophosphatase, AVP1, controls auxin transport and consequently auxin-dependent development. AVP1 overexpression results in increased cell division at the onset of organ formation, hyperplasia, and increased auxin transport. In contrast, *avp1-1* null mutants have severely disrupted root and shoot development and reduced auxin transport. Changes in the expression of AVP1 affect the distribution and abundance of the P-adenosine triphosphatase and Pinformed 1 auxin efflux facilitator, two proteins implicated in auxin distribution. Thus, AVP1 facilitates the auxin fluxes that regulate organogenesis.

The phytohormone auxin [principally indole acetic acid (IAA)] plays a fundamental role in the formation of all plant organs, and gradients of auxin have been shown to be essential to polarity of development (1, 2). Because IAA is a weak acid (pK_a 4.75, where K_a is the acid dissociation constant), a chemiosmotic model describes polar auxin uptake and efflux driven by a plasma membrane H⁺ gradient (3). In the acidic apoplast, an enrichment of the lipophilic protonated species of IAA facilitates its entry into the cell. The same gradient motivates efflux of anionic (non-lipid soluble) IAA⁻

retained in the neutral cytoplasm by means of polarly localized efflux complexes (4). Thus, the transporters responsible for setting cytoplasmic and apoplastic pH are likely to have key roles in driving this polar flux of auxin.

Plants have three distinct membrane H⁺-pumps capable of generating pH gradients (5). The P-type H⁺-adenosine triphosphatase (P-ATPase) is a single-subunit protein that energizes transport across the plasma membrane (PM) by extruding H⁺ from the cell (6). The vacuolar H⁺-ATPase (V-ATPase) complex, encoded by at least 26 genes, acidifies

the vacuole and other intracellular trafficking compartments and is known to be required for embryonic development and cell expansion (7, 8). H⁺-pyrophosphatases (H⁺-PPases) are single-subunit proteins that also generate

proton gradients in endomembrane compartments with the use of pyrophosphate (PP_i) instead of ATP (9). The *Arabidopsis* genome contains one type I H⁺-PPase, *AVP1* (10), and one type II, *AVP2/AVPL1*, which shares 35% amino acid identity with *AVP1* (11). *AVP1* has been traditionally viewed as a vacuolar H⁺-pump and has not previously been implicated in hormone transport or developmental regulation.

However, we observed that alterations in *AVP1* expression produce plants with morphogenetic variations typical of hormonal defects. Thus, the *AVP1* overexpressing plants (*AVP1OX*) *AVP1-1* and *AVP1-2* had more

rosette leaves (3 and 16, respectively; table S1) and significantly greater leaf area (60 and 40%, respectively, $P < 0.05$) than wild-type plants (Fig. 1B and fig. S1) as a result of increased cell numbers (figs. S2 and S3). Furthermore, *AVP1-1* and *AVP1-2* exhibited enhanced root growth (Fig. 1C) and dry weight (2.6 and 9.4 heavier, $P < 0.01$; table S2) compared with wild-type plants. Thus, *AVP1* appears to function in both shoot and root development.

To further assess the role of *AVP1* in organ development, we analyzed *avp1* loss-of-function mutants. *avp1-1* is a recessive mutant with a transferred DNA insertion in the predicted fifth exon of the *AVP1* gene. This lesion impairs full-length transcription (fig. S4). Consistent with *avp1-1* being a knockout allele, the 81-kD *AVP1* protein was not detected in Western blots of microsomal fractions isolated from *avp1-1* homozygotes. (Fig. 1G). However, a faint band at ~84-kD was observed in the *avp1-1* microsomal fraction, consistent with detection of *AVP2/AVPL1*, which is ~3 kD larger than *AVP1* (11). Immunoblot analysis with an antibody raised against the V-ATPase B subunit detected the expected 60-kD band in both wild-type and *avp1-1* plants (Fig. 1G).

Homozygous *avp1-1* seedlings showed altered root and shoot development: Cotyledons were either normal (~1%), cup-shaped (~1%), or heart-shaped (~98%) similar to *cup-shaped cotyledon* mutants (12) (Fig. 1A). Only 30% of the *avp1-1* plants initiated flower development, and none developed fully (Fig. 1, D to F). Most formed small cuplike structures (Fig. 1E) that had no floral organs or occasionally contained a small pistil (<10%) (13).

Consistent with the increase in leaf size due to increased cell number seen in *AVP1OX*, rosette leaf size in *avp1-1* was ~20% that of the wild-type leaf size (Fig. 1D). However, the average size of *avp1-1* mesophyll cells was unchanged from that of the wild-type cells (Col-0 = 782 ± 196 μm², $n = 476$; *avp1-1* = 741 ± 343 μm², $n = 251$, $P > 0.05$, Student's *t* test, errors are SD), suggesting a reduction in cell number in this mutant. Vascular patterning and mesophyll cell organization along the leaf blade were also disordered, resulting in thicker leaves with uneven margins (Fig. 1D and fig. S5). No abnormalities in cell organization were visible in shoot apical meristems in *avp1-1* during early development (fig. S6), but disrupted growth later became evident (Fig. 1, D and E).

The *Arabidopsis* root tip is a highly ordered structure with a well-defined root cap, three columella cells layers, and a layer of peripheral or tip cells covering the apical meristem (14) (Fig. 1H). However, the cells of the *avp1-1* root apex were small, the columella was reduced to two layers, and the root

¹Department of Plant Science, University of Connecticut, Storrs, CT 06268, USA. ²Biology Department, Pennsylvania State University, University Park, PA 16802, USA. ³Horticulture Department, Purdue University, West Lafayette, IN 47907, USA. ⁴Department of Biological Sciences, University of South Carolina, Columbia, SC 29208, USA.

*These authors contributed equally to this work.
†To whom correspondence should be addressed.
E-mail: roberto.gaxiola@uconn.edu

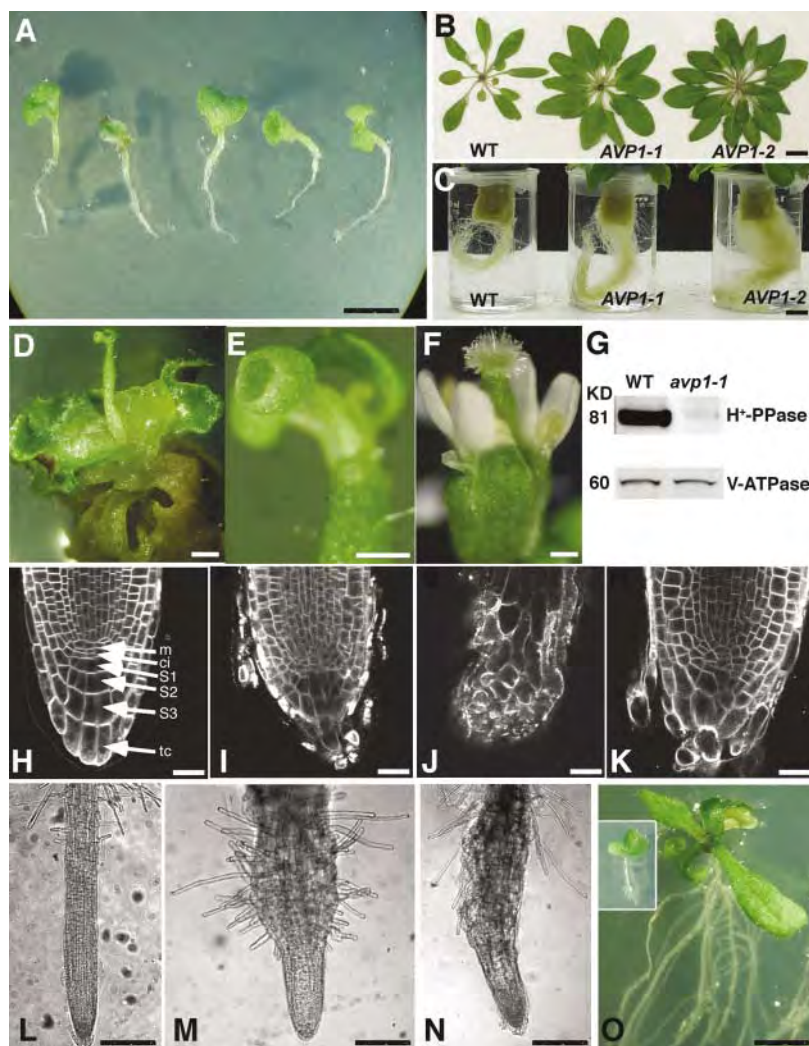


Fig. 1. Phenotypes associated with *AVP1* gain- and loss-of-function mutants. (A) Seven-day-old *avp1-1* plants grown on plates. Scale bar, 2.5 mm. (B) Rosettes from 45-day-old, soil-grown Col-0 (WT) and *AVP1OX* plants. (C) Root systems from 50-day-old, hydroponically grown Col-0 and *AVP1OX* plants. Scale bar in (B) and (C), 1 cm. (D) A 70-day-old *avp1-1* plant grown on plates. (E) *avp1-1* inflorescence. Scale bar in (D) and (E), 1 mm. (F) Wild-type flower. Scale bar, 0.5 mm. (G) Immunoblots of Col-0 and *avp1-1* membrane proteins probed with antisera to *AVP1* and V-ATPase. (H and I) Root apices from 7-day-old Col-0 (H) and *avp1-1* (I). m, meristem; ci, columella initial; S1 to S3, stories of columella cells; tc, tip cells. (J) A 35-day-old *avp1-1* plant apex. (K) Root of *AVP1*-RNAi plant 7 days after induction. Scale bar for (H) to (K), 20 μm. (L and M) Six-day-old roots from Col-0 (L) and *avp1-1* (M) grown on plates. (N) A 6-day-old Col-0 root grown with 25-μM NPA. Scale bar for (L) to (N), 200 μm. (O) *avp1-1* mutant is complemented with *pINDEX3-AVP1* construct after 12 days of induction. Plant at day 1 (inset). Scale bar, 0.5 cm.

cap was reduced and deformed (Fig. 1I), eventually collapsing (Fig. 1J), as reported in the auxin-related *pin4* and *tt4* mutants (15, 16). Disrupted cell elongation was also evident in the upper portions of *avp1-1* roots (Fig. 1, L and M) which exhibited swelling similar to wild-type roots treated with the auxin-efflux inhibitor *N*-1-naphthylphthalamic acid (NPA) (Fig. 1N).

Comparison with *AVP1* RNA interference (RNAi) lines and complementation confirmed that the *avp1-1* phenotypes were due to a lesion in the *AVP1* gene. Thus, *AVP1* RNAi lines exhibited impaired shoot development and disordered root cell patterns similar to *avp1-1* (Fig. 1K and fig. S7). Further, wild-type shoot and root phenotypes were restored in dexamethasone (DEX)-treated homozygous *avp1-1* seedlings (Fig. 1O, inset) carrying a DEX-inducible *AVP1* cassette (Fig. 1O and fig. S8). These observations strongly suggest that the organogenesis-related phenotypes seen in *avp1-1* are attributable to the lesion in *AVP1*.

The phenotypes of both gain- and loss-of-function *AVP1* mutants suggest that *AVP1* functions in organ development. In situ hybridization revealed that *AVP1* is expressed in all shoot meristems as well as the endodermal/pericycle ring of mature roots, developing leaves, sepals, petals, stamens, and carpels (Fig. 2, A to J). The reported expression patterns of the CAMATA and VOZ transcription factors (17) predicted to bind a 38-base pair cis-acting region of the *AVP1* promoter are also consistent with these *AVP1* expression patterns.

To better understand how a H^+ -PPase could impact developmental programs, we analyzed the subcellular distribution of *AVP1*. In addition to vacuolar membrane (tonoplast) localization, immunolabeling revealed a punctuate *AVP1* signal throughout wild-type and *AVP1-2* young roots (Fig. 2, K and L). This signal was absent in *avp1-1* (Fig. 2M) and strongly increased in cortical cells above the elongation zone in *AVP1OX* roots (Fig. 2, K and L, insets). Western blots of wild-type and *AVP1OX* root microsomal fractions separated by discontinuous sucrose density gradients detected *AVP1* signal in tonoplast, endosome, and PM fractions (Fig. 3, A and B). The PM and the endosomal *AVP1* signals in *AVP1OX* roots were 60 and 80% greater than Col-0, respectively (Fig. 3, A and B). Microsomal fractions from *AVP1OX* plants also exhibited increased PM P-ATPase protein abundance (~70%) and activity (~100%) (Fig. 3, C and D), whereas the decreased P-ATPase activity observed in *avp1-1* seedlings (Fig. 3D) was consistent with a reduced P-ATPase signal detected in immunofluorescence imaging of *avp1-1* root tips (Fig. 3F).

The phenotypes of *AVP1* gain- and loss-of-function mutants are consistent with altera-

tions in auxin-mediated development but apparently do not reflect altered auxin synthesis. Total free auxin levels in *AVP1OX* and *avp1-1* whole seedlings were comparable to those in the wild-type seedlings (13). However, the increased lateral root proliferation and rates of gravitropic bending observed in *AVP1OX* (fig. S10) are consistent with enhanced cellular auxin uptake and efflux (18). Consistent with this interpretation, free auxin levels in hypocotyls of *AVP1OX* were $\sim 60 \pm 17\%$ those of the wild type. Altered auxin uptake was also suggested when we observed that *avp1-1* seedlings treated with either IAA or the synthetic auxin naphthalene acetic acid (NAA) formed calli rather than the hairy root systems usually seen in auxin-treated wild-type plants (Fig. 4A and fig. S11).

To further investigate the effects of *AVP1* activity on auxin distribution, we used the synthetic auxin-responsive *DR5::GUS* reporter (19). Wild-type seedlings transformed with *DR5::GUS* exhibited GUS signal in root apices, vascular tissue, and cotyledonary margins (Fig. 4, B and D) (2). In contrast, the *DR5::GUS* signal in *avp1-1* roots was restricted to the meristem with no signal in the stele (Fig. 4C). Notably, a strong *DR5::GUS* signal was observed in the abnormally developed vascular systems in the *avp1-1* fused cotyledons (Fig. 4E). These aberrant

DR5::GUS patterns and altered vascular development observed in *avp1-1* roots and cotyledons, respectively, further suggested to us that alterations in auxin transport and accumulation were occurring when *AVP1* expression was altered (20).

To directly test this hypothesis, basipetal transport of IAA from the shoot tip to both the root-shoot junction and the root tip was assayed in *AVP1* overexpression and loss-of-function mutants. Auxin transported to *AVP1-1* root tips was 46% greater than in wild-type plants ($P < 0.05$) (Fig. 4F); transport to the root-shoot junction was approximately 20% less than in wild-type plants ($P < 0.05$), suggesting a higher rate of auxin transport in *AVP1OX* seedlings. Conversely, transport of auxin to the root tip and the root-shoot junction was significantly reduced in *avp1-1* seedlings (27 and 50%, respectively, of transport in the wild-type seedlings; $P < 0.05$) (Fig. 4F). These data are consistent with the *DR5::GUS* patterns and suggest that auxin transport is responsive to *AVP1* levels.

PM-localized H^+ -PPases are unlikely to function directly in apoplastic acidification (21). However, the altered P-ATPase abundance and activity seen with *AVP1OX* and *avp1-1* plants could alter apoplastic pH and affect intracellular proton homeostasis and gradients and so alter the driving forces for auxin

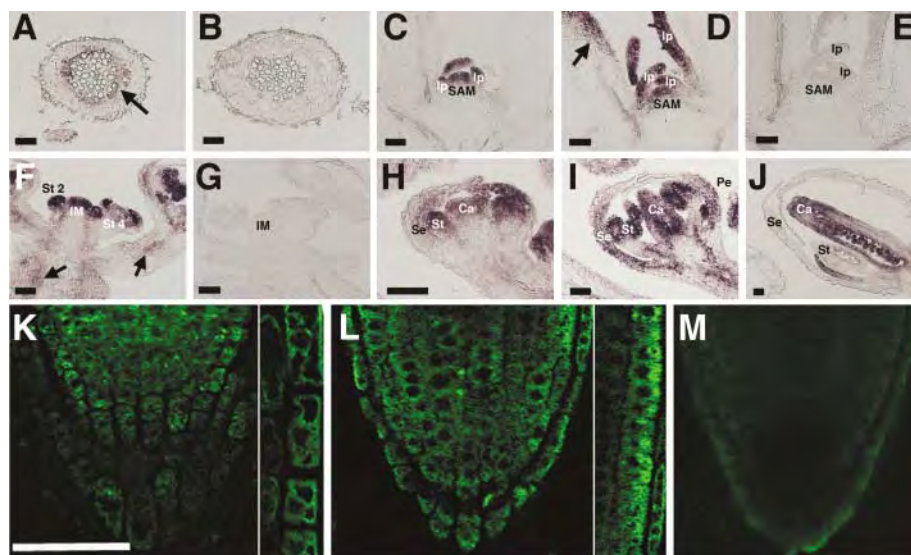


Fig. 2. *AVP1* expression patterns at the messenger RNA and protein levels. [(A), (C), (D), (F), (H) to (J)] *AVP1* antisense probe. [(B), (E), (G)] *AVP1* sense probe. Scale bar, 50 μ m. (A) *AVP1* is expressed in the parenchyma cells surrounding the vasculature in roots. (B) No signal was detected with *AVP1* sense probe. (C) *AVP1* is expressed in the shoot apical meristem and young leaf primordia at 13 days but restricted to the adaxial side of older leaves (D). (E) No signal was detected with *AVP1* sense probe. (F) *AVP1* is expressed in inflorescence meristems, floral primordia, and procambium cells (arrows). (G) No signal was detected with *AVP1* sense probe. (H) Longitudinal section of a stage 6 flower. (I) *AVP1* expression remains high in petals, anthers, and carpels in stage 10 flowers. (J) At stage 12, *AVP1* is only detected in petals and carpel. SAM, shoot apical meristem; lp, leaf primordia; St 2, stage 2 floral meristem; St 4, stage 4 flower; IM, inflorescence meristem; Se, sepal; Pe, petal; St, stamen; Ca, carpel. (K to M) Confocal immunohistochemical images of 5-day-old seedlings. Scale bar, 50 μ m. (K) *AVP1* localization is punctuate in Col-0 root tip and at the plasma and vacuolar membranes in epidermal cells (inset). (L) *AVP1* signal is increased in *AVP1-2* root tip and epidermal cells (inset). (M) *AVP1* signal is not observed in *avp1-1* root tips.

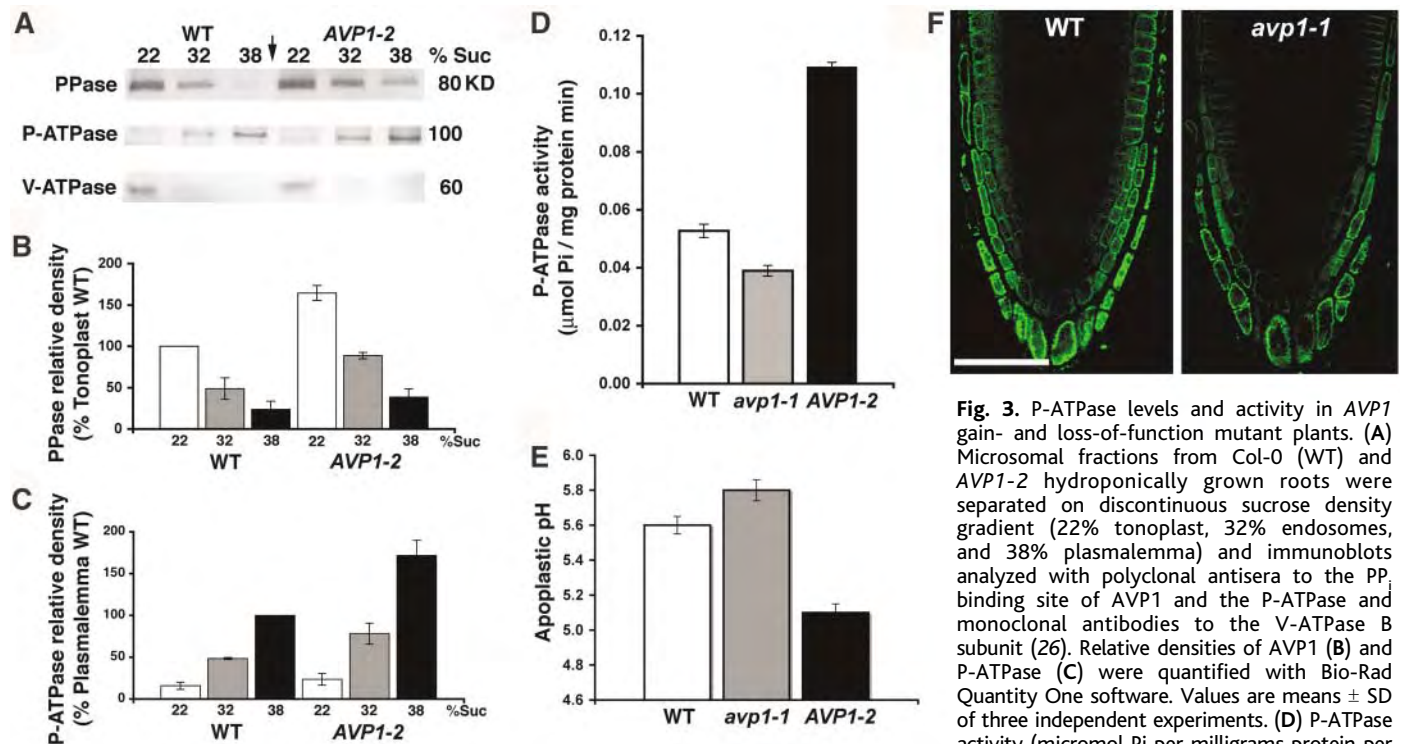


Fig. 3. P-ATPase levels and activity in *AVP1* gain- and loss-of-function mutant plants. (A) Microsomal fractions from Col-0 (WT) and *AVP1-2* hydroponically grown roots were separated on discontinuous sucrose density gradient (22% tonoplast, 32% endosomes, and 38% plasmalemma) and immunoblots analyzed with polyclonal antisera to the PP_i binding site of AVP1 and the P-ATPase and monoclonal antibodies to the V-ATPase B subunit (26). Relative densities of AVP1 (B) and P-ATPase (C) were quantified with Bio-Rad Quantity One software. Values are means \pm SD of three independent experiments. (D) P-ATPase activity (micromol Pi per milligrams protein per minute) of microsomal fractions from Col-0, *avp1-1*, and *AVP1-2*. Data are means \pm SD of three independent experiments. (E) Apoplastic pH was determined at the root elongation zone from Col-0, *avp1-1*, and *AVP1-2* 6-day-old seedlings with the use of Oregon Green. Values represent means \pm SD of five measurements from ≥ 10 individual plants. (F) P-ATPase immunohistochemical localization at the plasma membrane in 5-day-old Col-0 and *avp1-1* root tips. Scale bar, 50 μ m.

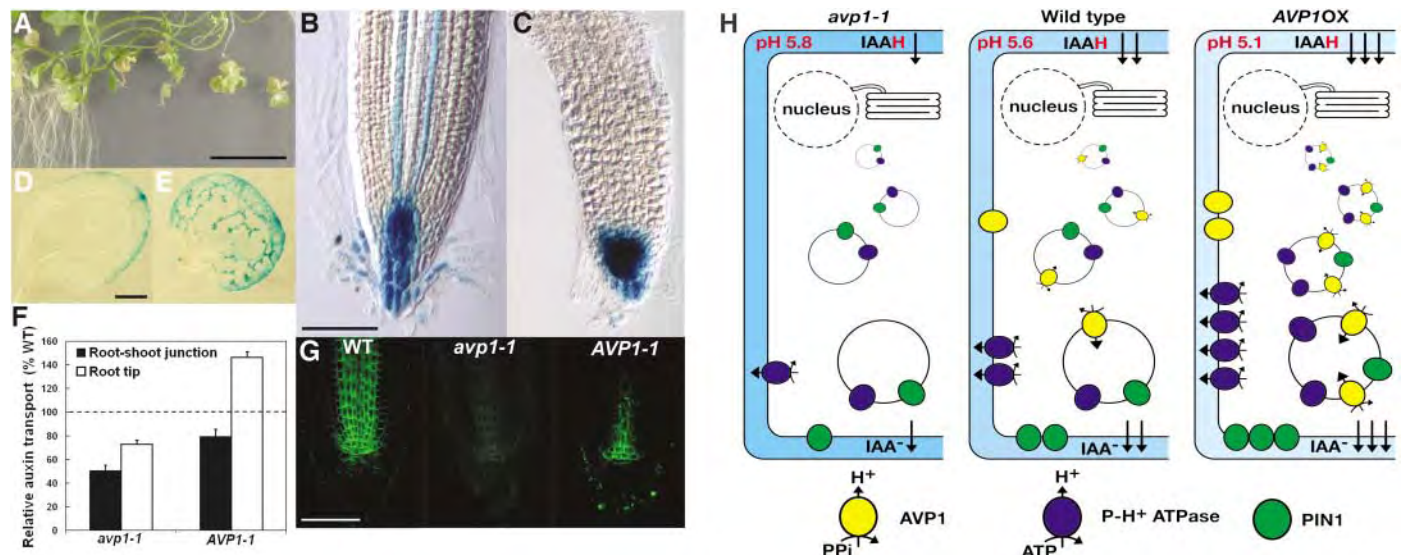


Fig. 4. Auxin transport, PIN1 localization and trafficking model in *AVP1* gain- and loss-of-function seedlings. (A) Shoot and root development of 53-day-old Col-0 (WT) and *avp1-1* plants with 5 μ M IAA. Scale bar, 1 cm. GUS staining in 6-day-old roots of Col-0 *DR5::GUS* (B) and *avp1-1DR5::GUS* (C). GUS staining in 6-day-old cotyledons of Col-0 *DR5::GUS* (D) and *avp1-1DR5::GUS* (E). Scale bar in (B) to (E), 50 μ m. (F) Basipetal IAA transport from shoot apex to root-shoot junction and root tips of 5-day-old *avp1-1* and *AVP1-1* seedlings. Values are percentage of Col-0 control, and means \pm SD of two assays of 10 seedlings each. PIN1 (G) localization in root tips of 5-day-old Col-0, *avp1-1*, and *AVP1-1*. Scale bar, 50 μ m. *AVP1* function regulates trafficking of H⁺-ATPase and PIN1. (H) Loss of *AVP1* function results in decreased H⁺-ATPase and PIN1 abundance on the PM; overexpression results in increased abundance; H⁺-ATPase and PIN1 traffic in the same vesicles (23). Resultant changes in pH alter chemiosmotically driven auxin flux through the cells (arrows). In *avp1-1*, auxin levels do not fall below the threshold required for increased PIN1 redistribution (16).

transport. Vacuolar, cytosolic, and apoplastic pH were therefore measured in root elongation zone cells of wild-type, *AVP1OX*, and *avp1-1* seedlings to test whether alterations in *AVP1*

expression might directly or indirectly influence pH homeostasis. The apoplastic pH was significantly more acidic in *AVP1OX* (pH 5.1 \pm 0.05) and more alkaline in *avp1-1* (pH 5.8 \pm 0.06)

than in wild-type plants (pH 5.6 \pm 0.05) ($P < 0.05$, Student's *t* test) (Fig. 3E). No difference in cytosolic pH was detected (fig. S9A). However, the vacuolar pH of the *avp1-1*

seedlings was more alkaline than that in wild-type seedlings ($P < 0.05$, Student's t test) (fig. S9B). The observed changes in P-ATPase activity and cell wall acidification suggest an explanation for at least some of the observed *avp1-1* and *AVPIOX* phenotypes. Thus, altered apoplastic acidity in *avp1-1* and *AVPIOX* would be expected to result in consequent changes in chemiosmotic motivation of polar auxin transport. Furthermore, because at normal apoplastic pH (5.5), only ~16% of the extracellular IAA is protonated, even a small change in pH would be expected to have a pronounced effect on IAA uptake.

In addition to apoplastic acidification, other regulatory factors involved in auxin transport might be affected by altered AVP1 activity. Alterations in speciation and distribution of flavonoids are thought to regulate auxin transport (16). Altered flavonoid accumulations were observed in *avp1-1* but appeared to be a response to altered auxin accumulations and PM P-ATPase activity (22) rather than a factor contributing to altered auxin transport (fig. S12).

The Pinformed 1 (PIN1) facilitator component of the auxin efflux carrier is also essential for polar auxin transport from the shoot tip to the root tip (4) and correlations between PIN-dependent auxin efflux, auxin gradients, and primordia development have been documented in organ formation (1). PIN1 has been shown to dynamically cycle together with P-ATPases between the PM and endomembrane compartments in a manner that is sensitive to auxin efflux inhibitors, the membrane trafficking inhibitor brefeldin A, and levels of auxin itself (4, 23, 24). PIN2 is also dynamically cycled, but by a different mechanism. To determine whether AVP1 activity influences subcellular localization of auxin efflux carriers, PIN1 and PIN2 were immunolocalized in root tips. PIN2 localization and abundance were similar to those in the wild-type plants (fig. S13). PIN1 distribution was also similar to that in the wild-type plants (23, 24) in *avp1-1*, but the signal intensity was decreased, suggesting decreased

plasma membrane abundance. In *AVPIOX*, the PIN1 signal intensity increased, but was restricted to the apical portion of the vascular cylinder (Fig. 4G). *PIN1* expression in *avp1-1*, as determined by quantitative real-time fluorescence polymerase chain reaction, was not different from expression in wild-type plants; however, it was decreased in *AVPIOX* (13). The *AVPIOX* results are consistent with auxin-responsive reduction of *PIN1* expression in nonvascular tissues and increased PM stabilization of PIN1 and P-ATPases observed in root apical tissues (16, 24). Furthermore, the decreased PIN1 signal observed in *avp1-1* cannot be attributed to reduced auxin transport to the root, as this is expected to result in an increased PIN1 signal (16). Instead, this result suggests that loss of AVP1 activity directly affects PIN1 trafficking or stability. A direct role in the increased PM abundance of PIN1 seen in *AVPIOX* vascular tissues also cannot be ruled out.

The data presented here indicate that although classically thought of as a tonoplast resident proton pump responsible for acidifying the vacuole, AVP1 also contributes to the regulation of apoplastic pH and to auxin transport, likely by mediating the trafficking of the PM P-ATPase and associated proteins, including PIN1 (Fig. 4H). Changes in intracellular auxin levels are also known to alter the expression of *P-ATPase* genes (25), establishing a feedback loop where AVP1 activity can regulate both targeting and level of the PM proton pump. Thus, in addition to its established role in the maintenance of vacuolar pH, our data reveal a previously unrecognized role for AVP1 in facilitating auxin transport and the regulation of auxin-related developmental processes.

References and Notes

1. I. Bllilou *et al.*, *Nature* **433**, 39 (2005).
2. S. Sabatini *et al.*, *Cell* **99**, 463 (1999).
3. T. L. Lomax, R. J. Mehlhorn, W. R. Briggs, *Proc. Natl. Acad. Sci. U.S.A.* **82**, 6541 (1985).
4. J. J. Blakeslee, W. A. Peer, A. S. Murphy, *Curr. Opin. Plant Biol.* **8**, 1 (2005).

5. H. Sze, X. Li, M. G. Palmgren, *Plant Cell* **11**, 677 (1999).
6. R. Serrano, *FEBS Lett.* **325**, 108 (1993).
7. S. Padmanaban, X. Lin, I. Perera, Y. Kawamura, H. Sze, *Plant Physiol.* **134**, 1514 (2004).
8. G. Strompen *et al.*, *Plant J.* **41**, 125 (2005).
9. R. G. Zhen, E. J. Kim, P. A. Rea, in *The Plant Vacuole*, R. A. Leigh, D. Saunders, Eds. (Academic Press Limited, San Diego, CA, 1997), vol. 25, pp. 298–337.
10. V. Sarafian, Y. Kim, R. J. Poole, P. A. Rea, *Proc. Natl. Acad. Sci. U.S.A.* **89**, 1775 (1992).
11. N. Mitsuda, K. Enami, M. Nakata, K. Takeyasu, M. H. Sato, *FEBS Lett.* **488**, 29 (2001).
12. M. Aida, T. Ishida, H. Fukaki, H. Fujisawa, M. Tasaka, *Plant Cell* **9**, 841 (1997).
13. J. Li *et al.*, data not shown.
14. L. Dolan *et al.*, *Development* **119**, 71 (1993).
15. J. Friml *et al.*, *Cell* **108**, 661 (2002).
16. W. A. Peer *et al.*, *Plant Cell* **16**, 1898 (2004).
17. N. Mitsuda, T. Hisabori, K. Takeyasu, M. H. Sato, *Plant Cell Physiol.* **45**, 845 (2004).
18. W. Boerjan *et al.*, *Plant Cell* **7**, 1405 (1995).
19. T. Ulmasov, J. Murfett, G. Hagen, T. Guilfoyle, *Plant Cell* **9**, 1963 (1997).
20. R. Aloni, K. Schwalm, M. Langhans, C. Ullrich, *Planta* **216**, 841 (2003).
21. J. M. Davies, C. P. Darley, D. Sanders, *Trends Plant Sci.* **2**, 9 (1997).
22. I. R. Baxter *et al.*, *Proc. Natl. Acad. Sci. U.S.A.* **102**, 2649 (2005).
23. N. Geldner, J. Friml, Y. D. Stierhof, G. Jurgens, K. Palme, *Nature* **413**, 425 (2001).
24. T. Paciorek *et al.*, *Nature* **435**, 1251 (2005).
25. I. Frias *et al.*, *Plant Cell* **8**, 1533 (1996).
26. Materials and methods are available as supporting material on Science Online.
27. We thank G. R. Fink for critical reading of the manuscript, J. Celenza for *cyc1At-CDB-GUS* construct, G. Hagen for the *DR5::GUS Arabidopsis* line, K. Noonan for assistance with the cartoon artwork, and H. Sze and R. Serrano for the V-ATPase and P-ATPase sera, respectively. This work was supported by grants from National Research Initiative U.S. Department of Agriculture Cooperative State Research, Education, and Extension Service no. 2001-35100-10772, University of Connecticut Research Foundation, Storrs Agricultural Experimental Station Hatch to R.A.G.; NSF 0132803 and USDA 01-35304-12290 to A.S.M.; Department of Energy grant 98ER20312 to B.K.; NSF (MCB 02-12099, DBI03-01460) and NASA (NAG2-1549) to S.G., and a NASA graduate student fellowship to G.L.R.

Supporting Online Material

www.sciencemag.org/cgi/content/full/310/5745/121/DC1

Material and Methods

Figs. S1 to S13

Tables S1 to S3

References

6 June 2005; accepted 29 August 2005

10.1126/science.1115711

Turn a new
page to...

www.sciencemag.org/books

Science
Books et al.
HOME PAGE

- ▶ the latest book reviews
- ▶ extensive review archive
- ▶ topical books received lists
- ▶ buy books online

RNA Release and Purification

The MELT (multi-enzymatic liquefaction of tissue) Total RNA Isolation System is a hands-free technology for the rapid digestion of fresh or frozen tissue. Up to 10 mg of tissue can be digested at room temperature in less than 15 minutes using a novel formulation that includes a potent ribonuclease inhibitor and a cocktail of powerful catabolic enzymes. Following digestion, the RNA can be purified using a streamlined process based on Ambion's MagMAX magnetic bead procedure. The MELT System provides highly intact RNA from a variety of tissue types. The MELT reagents irreversibly inactivate ribonucleases, allowing storage of digested tissue for more than a week at room temperature without significant loss in RNA integrity. The step of breaking open the cell architecture to release the RNA is typically achieved by mechanical disruption methods such as tissue grinding with a machine or mortar and pestle—the MELT system is a simpler alternative that is amenable to high throughput tissue processing.

Ambion For information 800-888-8804 www.ambion.com

Protein Structure and Interactions

Two new deuterated (heavy) cross-linking reagents and their hydrogen-containing (light) analogs can be used to yield low-resolution, three-dimensional structure information and protein complex information by integrating cross-linking techniques with the power of mass spectrometry. In this strategy, heavy and light cross-linking agents are reacted simultaneously with the target protein or protein complex. The deuterium incorporated at discrete positions in the cross-linking reagent allows both protein cross-linking and labeling to occur in a single step, simplifying identification of peptides resulting from the coupling reactions.

Pierce For information 800-874-3723 www.piercenet.com

Nano Flow Sensor

This noninvasive Nano Flow Sensor reports flow rate in the nanoliter through low microliter per minute range. Using proprietary thermal anemometry technology, it directly measures the mass flow rate of liquids in an isolated flow channel and displays it on an LCD readout. It features high sensitivity, fast response, high accuracy, and low drift.

Upchurch Scientific For information 800-426-0191 www.upchurch.com

Silica Spheres

The ÅngströmSphere line of uniform micron-sized silica spheres is available in the size range from 0.05 µm to 2 µm. The spheres are supplied in dry form with no surface modification or in dispersions of water or alcohols or other materials. Custom sizes and surface modifications can be synthesized on request. Applications include chromatography, filler for high-performance polymeric systems, nanocomposite filler, ceramic and glass forming, biomedical, particle size standards, light diffusers, inorganic diffractive pigments, photonic crystals, and more.

Fiber Optic Center For information 800-473-4237 www.focenter.com

BioRobot Universal System

The BioRobot Universal System is an automated solution for systems biology, providing a wide range of ready-to-run applications in 96-well format. Fully automated protocols are available for the purification of DNA and RNA, and for polymerase chain reaction (PCR) and reverse transcription (RT)-PCR setup, with protein and sequencing applications available soon. The system enables automated purification of pure RNA from a range of sample types, including blood, tissues, and cells, plus RT-PCR setup. The system also enables purification of high-quality genomic DNA from up to 192 buccal swab samples and reliable PCR setup.

Qiagen For information 800-426-8157 www.qiagen.com

Ultrapure Water

A cost-effective new laboratory water purification system can convert pretreated (distillation, deionization, reverse-osmosis) water to ultrapure (Type I) water. The Synergy UV system is suitable for low-volume laboratory needs such as buffers and solutions for many techniques, including chromatography, electrophoresis, spectrophotometry and spectroscopy, cell culture media, and molecular biology reagent preparation. After connecting the system to a pretreated water supply, it is simple to install the single purification cartridge.

Routine maintenance usually consists of changing the cartridge every 10 months and the ultraviolet (UV) lamp every 2 years. The UV lamp reduces total organic carbon to less than 5 parts per billion. Various filters and cartridges are available to match individual requirements.

Millipore For information 800-MILLIPORE www.millipore.com/H2O



Literature

Macromolecular Crystallography Products is a product guide designed to help researchers find custom-tailored solutions in the areas of crystal screening, crystallization optimization, cryo-crystallography, and phasing. These high-quality reagents eliminate much of the trial and error associated with nucleation and crystal growth. Jena Bioscience crystallization screening reagents are designed for efficient and flexible screening of crystallization conditions for proteins, peptides, nucleic acids, macromolecular complexes, and water-soluble small molecules. Also available are products designed for efficient crystal

screening in cryogenic conditions and products for the screening of heavy atoms in applications in which phase determination is required.

Axxora For information 800-550-8332 www.axxora.com

For more information visit **GetInfo**,
Science's new online product index at
<http://science.labvelocity.com>

From the pages of GetInfo, you can:

- Quickly find and request free information on products and services found in the pages of *Science*.
- Ask vendors to contact you with more information.
- Link directly to vendors' Web sites.

Newly offered instrumentation, apparatus, and laboratory materials of interest to researchers in all disciplines in academic, industrial, and government organizations are featured in this space. Emphasis is given to purpose, chief characteristics, and availability of products and materials. Endorsement by *Science* or AAAS of any products or materials mentioned is not implied. Additional information may be obtained from the manufacturer or supplier by visiting www.science.labvelocity.com on the Web, where you can request that the information be sent to you by e-mail, fax, mail, or telephone.